UNIVERSITY OF EAST ANGLIA

Targeting the p53/MDM2 Protein-Protein Interaction

by

Sarah Anne Goffin

A thesis submitted in partial fulfillment for the degree of Doctor of Philosophy

in the

School of Pharmacy

January 2016

Declaration of Authorship

I, SARAH ANNE GOFFIN, declare that this thesis titled, *Targeting the p53/MDM2 Protein-Protein Interaction* and the work presented in it are my own. I confirm that:

- This work was done wholly or mainly while in candidature for a research degree at this University.
- Where any part of this thesis has previously been submitted for a degree or any other qualification at this University or any other institution, this has been clearly stated.
- Where I have consulted the published work of others, this is always clearly attributed.
- Where I have quoted from the work of others, the source is always given. With the exception of such quotations, this thesis is entirely my own work.
- I have acknowledged all main sources of help.
- Where the thesis is based on work done by myself jointly with others, I have made clear exactly what was done by others and what I have contributed myself.

Signed: _____

Date: _____

Submitted Work Within this Thesis

Paper 1

Cominetti, M. M. D. and Goffin, S. A. and Raffel, E.
and Turner, K. D. and Ramoutar, J. C. and OConnell,
M. A. and Howell, L. A. and Searcey, M. Identification of a new p53/MDM2
inhibitor motif inspired by studies of chlorofusin
Bioorganic and Medicinal Chemistry Letters, **2015** *Article in Press*

Paper 2

Goffin, S. A. and Gandhi, D. and Angulo, J. and Howell, L. A.
and Searcey, M. STD NMR Initial Growth Rates
Approach in Protein-Protein Interactions: Unveiling the
"Three-Fingered Pharmacophore" required for p53-MDM2 Inhibition
Chemical Communications, **2015** *Submitted*

UNIVERSITY OF EAST ANGLIA

Abstract

School of Pharmacy

Doctor of Philosophy

The p53/MDM2 protein-protein interaction is the most widely characterised protein-protein interaction to date. As of 2014, there are over 20 compounds that have been shown to the p53-MDM2 protein-protein interaction, however many compounds have not progressed into clinical trials due to their high hydrophobicity.

Herein we describe the synthesis, molecular modelling, physical characterisation and biological testing of novel inhibitors of the p53/MDM2 protein-protein interaction based on the natural product chlorofusin.

The first focus is a combinatorial library generated in the Searcey laboratory of known p53/MDM2 protein-protein interaction inhibitors with the desire to generate novel analogues and study their interactions with the protein through NMR spectroscopy and molecular modelling. These compounds were tested by in a fluorescence polarisation assay and also in cell lines overexpressing MDM2 as well as p53-null cells as a comparator. This generated two novel compounds shown to have activity selectively for the p53/MDM2 protein-protein interaction.

The second chapter focuses on simplified substitutions of the azaphilone (the chromophore portion of chlorofusin, a natural product inhibitor of the p53-MDM2 protein-protein interaction): initially with simple fused bicyclic carboxylic acids and later using click chemistry substitutions. Interestingly, *in vitro* studies showed that the click analogues retained activity or activity improved when the peptide portion was removed and hence further studies of the click amino acid analogues were generated. This library generated one analogue that was active *in vitro* as well as selectively in MDM2-overexpressing cell lines.

The third chapter focusses on the azaphilone chromophore present in the natural product chlorofusin. The Sonogashira precursor used to generate azaphilone analogues was synthesised using a methodology adopted by Porco *et al* and subsequent analogues were generated using a novel double-Sonogashira approach followed by functionalisation published by Boger *et al*. Once the azaphilone was synthesised, metholodogies were trialled

in order to condense the azaphilone with the chlorofusin peptide in order to create analogues containing both the peptide and small molecule portions of chlorofusin. In addition, molecular modelling was attempted to generate novel binding analogues.

Acknowledgements

There are so many people that I would like to thank I will try to be concise...

Firstly to my supervisors Mark and Lesley for all of their assistance and support over the last few years and for never giving up on me, as well as Maria O'Connell, Richard Bowater, Jesus Angulo and Onur Atasoylu for the biology, NMR and computational modelling respectively.

Richard Steel, Sunil Sharma, Estelle Payerne, Alex Roberts, Jess Di Gesso, Jenna Bradley, Jon Cowan, Tony Blake and Paul McDermott for all of their assistance with the biological testing and the organic synthesis. Also to my wonderful lab group including Michael Austin (although I can't say I'll miss the music!), Michael Stephenson and Lydia Kriticos!

To my wonderful mum and my extended family who have always supported me, in particular my awesome big brother Ian, his amazing wife Amanda and my beautiful nieces Carmen and Jasmine. Also to my amazing friends, especially Laurence Bennett, Lucy Hann, Natalie Craske, Sarah Taylor, Heidi Sweeney, Chris Wilson, Luke Ferry, Gemma Marsh, Cristina Adriana, Ivana Knyght and Maria Christou for always being so kind and supportive to me and such a welcome distraction when I got stressed out!

Also to the amazing students that I have had the pleasure of working with over the years: Riel Santiago, Daivik Gandhi, Ross Kelly, Ewan Raffel and Hamara Amjad. I hope that you all succeed in your future ventures.

Finally to my honourable mentions: to the support and assistance of the Cook, Soper and Bloomfield families for all of their moral support and assistance, in particular to Colin, whom I had to give him an honourary mention to for putting up with me during the process and remaining a dear friend to this day! But my FINAL mention goes to Benjamin Wraight: thanks for giving me my smile back and being a genuinely awesome human being!

Contents

List of Figures

List of Schemes

List of Tables

Abbreviations

Abl	Abelson
AML	Acute myeloid leukaemia
APCI	Atmospheric-pressure chemical ionisation
ARF	Alternative reading frame
ASPP1	Apoptosis-stimulating of p53 protein 1
ASPP2	Apoptosis-stimulating of p53 protein 2
BAK	Bcl-2 antagonist killer
BAX	Bcl-like protein X
Bcl-2	B-cell lymphoma 2
Bcl-X	B-cell lymphoma X
Bcr	Break point cluster
BH3	Binding homology 3
Boc	^{t}-butyloxycarbonyl
CDI	1,1'Carbonyldiimidazole
CML	Chronic myeloid leukaemia
DBU	1,8-Diazabicyclo[5.4.0]undec-7-ene
DEAD	Diethylazodicarboxylate
DEPT	Distortionless enhancement by polarisation transfer
DIC	N,N'-diisocarbodimide
DIPA	diisopropylamine
DIPEA	Diisopropylethylamine
DMAP	Dimethylaminopyridine
DMF	N,N'-dimethylformamide
EDCI	1-ethyl-3-(3-dimethylaminopropyl)carbodiimide
EI	Electron ionisation

ELISA	Enzyme-linked immunosorbance assay
ESI	Electrospray ionisation
FA	Fluorescence anisotropy
Fmoc	Fluorenylmethyloxycarbonyl
FP	Fluoresence polarisation
HDM2	Human double-minute 2
HDMX	Human double-minute X
HMBC	Heteronuclear multiple-bond correlation spectroscopy
HOAt	1-hydroxy-7-azabenzotriazole
HOBt	Hydroxybenzotriazole
HMQC	Heteronuclear multiple quantum coherence
HPLC	High performance liquid chromatography
HSQC	Heteronuclear single quantum coherence
HTRF	Homogeneous time resolved fluorescence
HTS	High throughput screen
IR	Infa-red spectroscopy
ITC	Isothermal titration calorimetry
LCMS	Liquid chromatography mass spectrometry
MALDI	Matrix-associated laser dissociation ionisation
Mcl-1	Myeloid cell leukaemia 1
Mcl-X	Myeloid cell leukaemia X
MDM2	Murine double-minute 2
MDMX	Murine double-minute X
mp	Melting point
Ms	Mesyl
MTS	(3-(4,5-dimethylthiazol-2-yl)-5-(3-carboxymethoxyphenyl)-2-(4-sulfophenyl)-2H-tetrazolium)
MTT	3-(4,5-dimethylthiazol-2-yl)-2,5-diphenyltetrazolium bromide
NMP	N-methylpyrrolidone
NMR	Nuclear magnetic resonance
NOESY	Nuclear Overhauser effect spectroscopy
NOXA	NADPH oxidase activator
p53	protein 53

PBS	Phosphate-buffered saline
Ph	Philadelphia chromosome
pRb	protein retinoblastoma
PUMA	p53 upregulated modulator of apoptosis
RING	really interesting new gene
ROESY	Rotating-frame Overhauser effect spectroscopy
SAR	Structure-activity relationships
SpR	Surface plasmon resonance
STD	Saturation transfer difference
TAT	Transactivating domain
THC	Tetrahydrocannabinol
TR FRET	Time-resolved förster resonance energy transfer
USP1	Ubiquitin-specific protein 1
WSC	Water-soluble carbodiimide
WST	Water soluble tetrazolium salts
wt	Wild type

Dedicated to Carmen Lee-Bennett, a scientist of the future

Chapter 1

Introduction

p53 is an important transcription factor, which ensures the destruction or repair of cells containing damaged DNA. p53 also codes for MDM2, which prevents the over-activity of p53 (which could lead to premature ageing through unnecessary destruction of cells). When MDM2 is overexpressed, damaged DNA is allowed to replicate and therefore cancerous cells can be generated.

This introduction will cover the general causes of cancer and therapies available, as well as give examples of different protein-protein interactions and their role in disease progression. The introduction will then go on to focus on the p53/MDM2 protein-protein interaction and inhibitors that have been discovered to date.

1.1 What is Cancer?

Cancer is a multifactorial disease in which cells are permitted to undergo rapid, uncontrolled cellular proliferation.[1] This generally occurs when damaged DNA is able to replicate by bypassing checkpoints present in the cell cycle.

1.1.1 Epidemiology, Aetiology and Pathophysiology

In 2012, 14.1 million people were diagnosed with cancer worldwide and 8.2 million people died as a result of cancer in the same year.[2] At present, it is predicted that 46% of men and 54% of women diagnosed with cancer between 2010 and 2011 will survive 10 years or greater.[3] The most common cancers constituting over half of all cases worldwide are breast (15%), lung (13%), prostate (13%) and bowel (13%).[2] 36% of cancers diagnosed in the UK between 2009 and 2011 were diagnosed in patients aged 75 and over.[4] Cancer

types also vary greatly with age: children (both male and female from birth to 14 years old) are more prone to leukaemias,[5] males (50 years and over) are more likely to suffer from cancers of the prostate[4] and women (25 years and over) are more likely to suffer from breast cancer.[6]

Figure **1.1** shows the 5- and 10-year survival statistics for men and women (aged 15 to 99) in England and Wales between 2010 and 2011 (the most recent published data available via Cancer Research UK).[3] The highest survival rates were associated with testicular cancer (99% at 1-year and 98% at 5- and 10-years), malignant melanoma (97% at 1-year reducing to 89% at 10-years) and breast cancer (96% at 1-year and 78% at 10-years). The lowest survival rates were associated with brain cancer (40% at 1-year reducing to 13% at 10-years), lung cancer (32% at 1-year reducing to 5% at 10-years) and pancreatic cancer (21% at 1-year survival reducing to 1% at 10-years).[3]

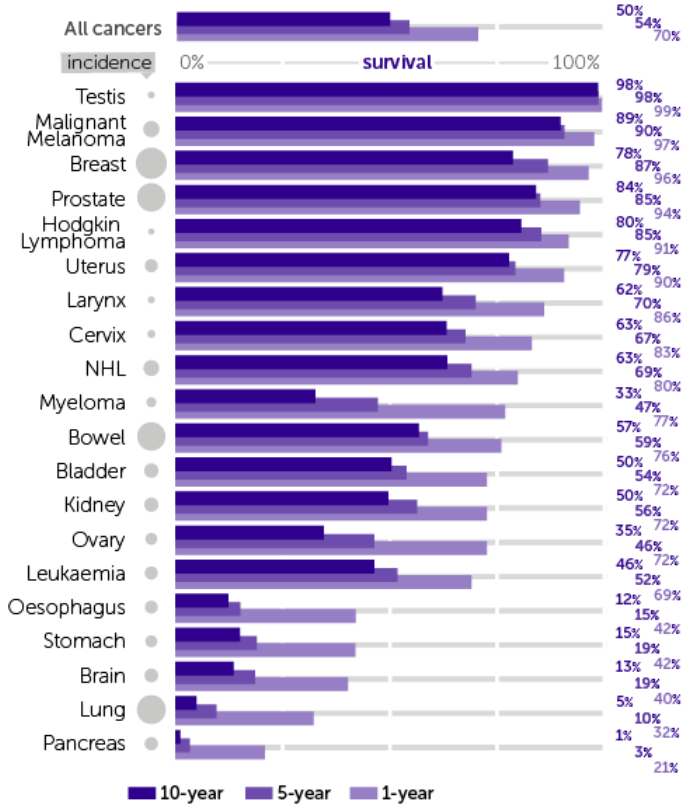

FIGURE 1.1: Age-Standardised One-, Five- and Ten-Year Net Survival, Selected Cancers, Adults (Aged 15-99), England and Wales, 2010-2011[3] (data freely accessible to the public)

1.1.1.1 Causes of Cancer

Cancer can be caused by a variety of different agents, either which directly cause DNA damage or that lead to uncontrolled cellular proliferation.[1] DNA can be damaged by a variety of different substances: tobacco smoke (either through passive smoking or first-hand cigarette smoke) attributed to 101,000 new cases in the UK in 2010 and 64,300 deaths in the UK in the same year.[7] Smoking is most prevalent in areas of social deprivation (32.1% of males and 24.3% of females from lower economic backgrounds).[8]

Alcohol and toxic metabolites can also damage DNA,[9] with alcohol and toxic metabolites being linked to approximately 12,500 cancer cases in the UK in 2010.[9] The most common cancers related to alcohol are those of the upper digestive tract, including the oral cavity (20.6%) and pharynx (30.4%).

Ultraviolet radiation has been attributed to 3.5% of all cancers and increased exposure to sunbeds and increased travel overseas has led to an increase in incidence in malignant melanoma over the past 30 years.[10] It is approximated that 85.9% of malignant melanoma cases in the UK in 2010 were correlated to UV radiation exposure. Radiation from ionising sources including X-rays contributed to 1.8% of all cancers in the UK in 2010.[11] Radiotherapy and radon had the highest number of cases (1,380 for each), background radiation (1,170 cases), followed by nuclear medicine (19 cases).

Although infection is a less likely attributing factor for cancer, it has still been linked to 3.1% of all cancer cases in the UK in 2010.[12] It is more common in females (3.7% in females versus 2.5% in males), with the top infective agents being human papilloma virus (2,690 cases), *Helicobacter pylori* (2,560 cases), Epstein Barr virus (1,210 cases), hepatitis B and C (620 cases), HIV /Kaposis sarcoma virus and human herpes virus 8 (approximately 25 cases).

Other factors that can attribute to the development of cancers include genetic predisposition (2% to 3% of cancers diagnosed in the UK annually are considered to be the result of a faulty gene)[2] and high body weight (being overweight or obese is believed to cause 5% of total cancers in the UK annually, whilst a diet lacking in fruit and vegetables has been shown to attribute to 9% of total cancers in the UK each year).[2]

1.1.2 Cancer Treatment Options

The most common form of cancer therapy is surgery, in which cancerous tissue (and some surrounding healthy tissue) is excised from the patient, however this is not always plausible if the cancer is in a difficult-to-target area. It is also important to note that

excision of affected tissue can have further implications dependent on the tissue being removed, such as malabsorption due to resection of the bowel (as the bowel becomes much shorter so there is less surface area for absorption of nutrients into the body).

Other factors to consider in surgical treatment include cost to the NHS due to the requirement of inpatient hospital stay (for example, laparoscopic resection costs between £250 and £300 per patient, which could equate to £2.1 million per year for the total number of patients requiring surgery),[13] which can also increase the risk of venous thromboembolism and opportunistic infections such as hospital-acquired pneumonia.

Radiotherapy is the second most common form of cancer treatment and diagnostics, in which X-rays are used to destroy tumour cells. Radiotherapy utilisation is most common in breast (10% of all cancers), lung (7.6% of all cancer cases) and prostate (7.2% of all cancer cases). The total percentage of patients receiving radiotherapy (across all cancers) was 52.3% in the year 2005.[14] Although this method negates the requirement for surgery in some cases, radiation from this process can itself lead to the development of cancers.[11]

Chemotherapy is often used as an adjunctive therapy and works by the premise of targeting rapidly-dividing cells.[15] Although this is still a mainstay of treatment, with agents such as the antitumour antibiotic doxorubicin and the vinca alkaloid vincristine still commonly used today (both shown in figure **1.2**).

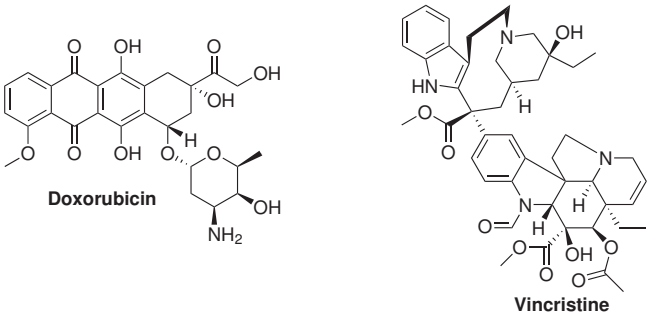

FIGURE 1.2: Structures of doxorubicin and vincristine

The greatest disadvantage of classic chemotherapy agents is their myriad of adverse effects: as they selectively target rapidly-dividing cells (instead of tumour cells specifically), other rapidly-dividing cells such as hair follicles are targeted as a consequence, resulting in hair loss.[16] It is therefore plausible, as in the case of radiotherapy, that treatment using these agents can lead to the development of cancers in later life, hence the need for the development of novel, less cytotoxic agents that maintain potency.[17] In order to prevent resistance, many of these cytotoxic therapies are used in combination

(such as paclitaxel, PEGylated doxorubicin hydrochloride and topotecan for the treatment of advanced ovarian cancer).[18] The purpose of using a combination is that it is less likely that tumour cells will have inherent resistance to multiple therapies and therefore combination therapies are more likely to lead to full cancer remission without recurrence. As chemotherapy is used as an adjunct therapy, trials published in the literature are usually in combination with another form of treatment such as hormone therapy. For example, Gelmon *et al* published a review of randomised controlled trials published between 1985 and 2000 to examine the 15-year survival of breast cancer patients who received treatment with polychemotherapy and/or hormonal therapy in the early stages of the disease.[15] The findings of this study were that 6 months of treatment with an anthracycline in addition to FAC (fluorouracil, doxorubicin, cyclophosphamide) or FEC (fluorouracil, epirubicin, cyclophosphamide) reduced cancer incidence by 38% for women under 50 years of age, whilst the addition of adjuvent treatment with tamoxifen over 5 years reduced cancer incidence by 31% in a separate patient sample of women under 50 years of age (although this was only the case for patients with an oestrogen-receptor positive status). This data was collated with data gathered from meta-analyses, which generated overall statistics of 57% and 45% reduction in the number of cases of oestrogen-receptor positive breast cancer in those receiving adjuvent tamoxifen and those without respectively.[15]

Although classical chemotherapy agents are still commonly used in the clinic, novel compounds have begun to emerge in the treatment of a variety of cancers.[19] The first in a novel group of anticancer agents, imatinib (figure **1.3**), worked by a novel mechanism of action by which an unnatural tyrosine kinase was inhibited.[20] What was most interesting and unique about this approach was that this kinase was produced by a mutation in the Philadelphia chromosome, in which the genes for BCR-Abl are combined and produce said tyrosine kinase. Since imatinib, other agents such as trastuzumab (a Her2/Neu receptor antagonist) have been developed, promising increased tolerability in patients and selectivity for cancer cells.

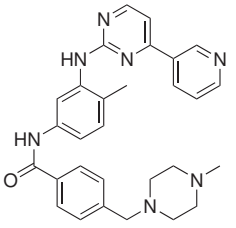

FIGURE 1.3: Structure of imatinib

Using the lessons learned from molecular therapeutics and the development of imatinib, there has been a shift in therapeutic drug development towards agents which play a

modulatory role in the pathways involved in cancer: a great step forward in the way that cancer treatment has been perceived. As a result, newer cancer therapies have a more targeted effect and therefore have an improved side effect profile. At present, there is a great deal of investigation of protein-protein interactions in the treatment of cancer as well as a plethora of other illnesses, as they have specific modulatory roles within cells and therefore would produce targeted effects if stimulated or inhibited.

1.2 Protein-Protein Interactions

Protein-protein interactions (PPIs) are of growing interest to the medicinal chemistry community due to their ability to modulate outcomes (such as cellular apoptosis) within cells, hence allowing greater control than classical drug targets such as enzymes or receptors.[21] These interactions are prevalent throughout the body and are able to control a wide range of biological systems, such as the regulation of inflammation[22] or the development of new nerves.[23]

Unfortunately, difficulty arises because protein interactions are dynamic and the state in which they are interacting is transient. Also, the interfaces between proteins where interactions occur are large, flat and hydrophobic (general interaction area equates to 1500 to 3000 $\mathring{A}^2$, as opposed to 300 to 1000 $\mathring{A}^2$ for small molecule interactions with proteins).[24] As a result, binding pockets can be hidden deep within the protein and may only be exposed upon binding of a complementary ligand.

Despite the known difficulties in targeting, it has not deterred researchers from exploiting these interactions. There are three main examples of protein-protein interactions that have been successfully targeted by either cell-penetrating peptides or small molecules are mentioned below. The third example serves as the focus of this research.

1.2.0.1 The Bcl-2 Family (Example 1)

Figure 1.4 illustrates the interaction of the different members of the Bcl-2 family and the downstream consequences for the cell.

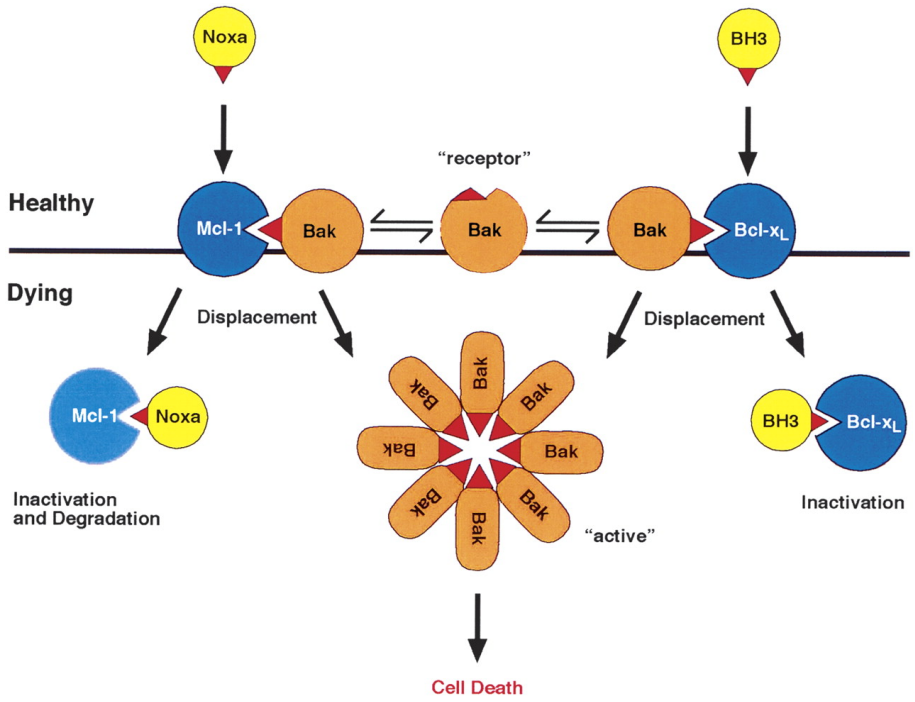

FIGURE 1.4: Diagram showing the interaction of different proteins in the Bcl-2 family and subsequent downstream effects[25] (open access article)

The Bcl-2 family of proteins encompasses fifteen pro-apoptotic (three important members being Bcl-2-like protein X, BAX, Bcl-2-associated death promoter, BAD and Bcl-2-antagonist/killer, BAK)[25,26] and five or six anti-apoptotic proteins (one of these being Myeloid Cell Leukaemia-1, Mcl-1), as shown in table **1.1**. The pro-apoptotic proteins only contain a Binding Homology 3 (BH3) region. When unbound, these BH3 proteins move to the mitochondria, recruit a series of caspases and cause perforation of the cell membrane, initiating apoptosis. When the BH3 proteins are in their α-helical conformation they can bind to their anti-apoptotic partners and therefore apoptosis does not occur. In conclusion, BH3 binding status determines whether or not a cell will apoptose, which is important in the prevention of damaged or cancerous cells replicating which could otherwise lead to the development of cancers.

Bcl family member	Pro/Anti-apoptotic	BH1 domain present	BH2 domain present	BH3 domain present	BH4 domain present	TM domain present
BCL-2	**Pro**	**Yes**	**Yes**	**Yes**	**Yes**	**Yes**
BCL-X_L	**Pro**	**Yes**	**Yes**	**Yes**	**Yes**	**Yes**
BCL-W	**Pro**	**Yes**	**Yes**	**Yes**	**Yes**	**Yes**
A1	**Pro**	**Yes**	**Yes**	**Yes**	**Yes**	**No**
MCL-1	**Pro**	**Yes**	**Yes**	**Yes**	**Yes**	**Yes**
BOO	**Pro**	**Yes**	**Yes**	**Yes**	**Yes**	**Yes**
BAX	**Anti**	**No**	**Yes**	**Yes**	**Yes**	**Yes**
BOK	**Anti**	**No**	**Yes**	**Yes**	**Yes**	**Yes**
BCL-X_S	**Anti**	**Yes**	**Yes**	**No**	**No**	**Yes**
BAK	**Anti**	**No**	**Yes**	**Yes**	**Yes**	**Yes**
BCL-G_L	**Anti**	**No**	**Yes**	**No**	**Yes**	**No**
BFK	**Anti**	**No**	**Yes**	**No**	**Yes**	**No**
BAD	**Anti**	**No**	**Yes**	**No**	**No**	**No**
BIK	**Anti**	**No**	**Yes**	**No**	**No**	**Yes**
BID	**Anti**	**No**	**Yes**	**No**	**No**	**No**
HRK	**Anti**	**No**	**Yes**	**No**	**No**	**Yes**
BIM	**Anti**	**No**	**Yes**	**No**	**No**	**Yes**
NOXA	**Anti**	**No**	**Yes (2 copies)**	**No**	**No**	**No**
PUMA	**Anti**	**No**	**Yes**	**No**	**No**	**No**
BMF	**Anti**	**No**	**Yes**	**No**	**No**	**No**

TABLE 1.1: Table showing the different members of the Bcl-2 family, their role in survival and the binding homology (BH) and transmembrane (TM) domains present in each protein (adapted from Strasser *et al*, 2005)[27]

Evidence for the importance of these proteins in cancer was reported by Zhou*et al*, who discovered that Mcl-1 is overexpressed in chronic myeloid leukaemia.[28] Further work published by Quinn *et al* in 2011 also indicated Mcl-1 overexpression in breast, lung, ovarian, central nervous system, prostate, melanoma and renal cancers. The high prevalence of Mcl-1 in a variety of cancers increases its viability as a therapeutic target. Also, homology between Bcl-2 and Mcl-1 means that current Bcl-2 inhibitors can be optimised to aid binding into the pocket (the homology is illustrated in figure **1.7**, which indicates the binding modes of a Bcl-2 inhibitor in different members of the Bcl-2 family).

ABT-737 was the first inhibitor discovered that acted against the Bcl-2/Mcl-1 protein-protein interaction. It was discovered through a high throughput screen and parallel synthesis, utilising fragment-based drug discovery, as shown in figure **1.5**.[26]

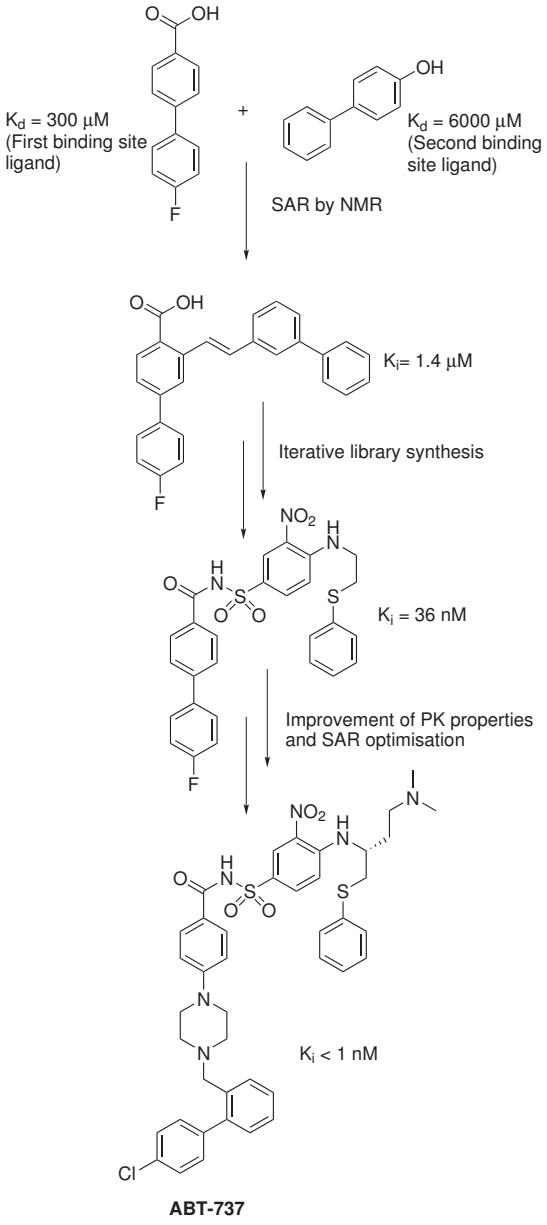

FIGURE 1.5: Fragment-based design of Bcl-2 inhibitors, followed by optimisation of potency and pharmacokinetics to produce ABT-737

ABT-737 was considered to be a dual inhibitor, as it also inhibited the Bcl-X interactions with BAD, BAK and BAX proteins (the key binding interactions common to both ABT-737 and the BH3 domain are illustrated in figure **1.6**. ABT-737 was able to mimic key π-π-stacking and hydrophobic interactions present within the hydrophobic groove,

with the bichlorophenyl binding in the lower groove with the thiophenyl group binding in the upper groove of Bcl-2 anti-apoptotic proteins, as shown in figure **1.7**.

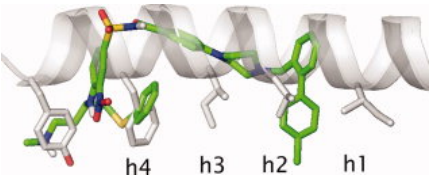

FIGURE 1.6: Superimposed image of the BH3 domain and ABT-737[29] (reproduced with permissions)

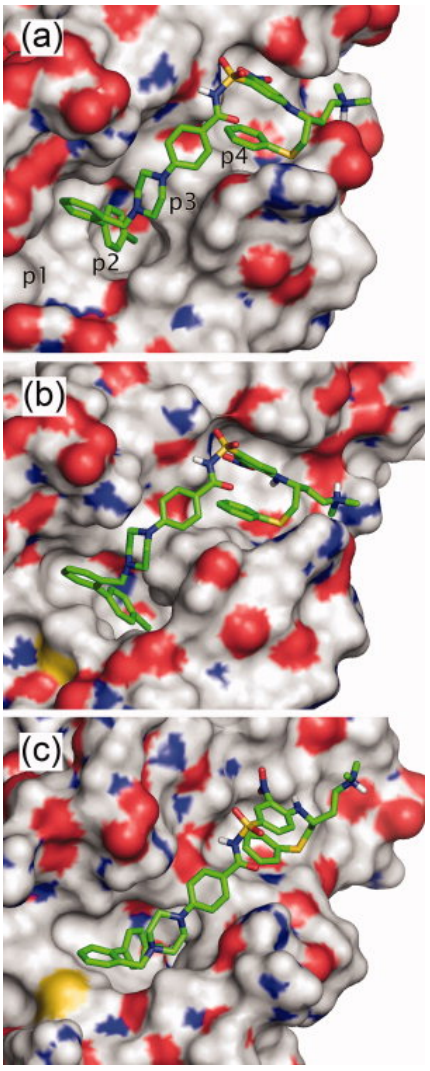

FIGURE 1.7: Docking model of ABT-737 within A. the Bcl-xL hydrophobic pocket B. the Bcl-2 hydrophobic pocket and C. the Mcl-1 hydrophobic pocket[29] (reproduced with permissions)

ABT-737 was found to inhibit the Bcl-2/Mcl-1 interaction with an IC_{50} value of less than

10 nM as determined by isothermal titration calorimetry (ITC). Despite pre-clinical success, ABT-737 was not orally bioavailable and contained undesirable functional groups, such as a nitro group which would be readily reduced *in vivo*[30] (although the antibiotic nitrofurantoin is a nitroaromatic that is used clinically for urinary tract infections, despite its known rare hepatotoxicity resulting from the nitro group).[31] As a result, this compound required further optimisation to improve its pharmacological properties.

The first bioavailable inhibitor of the Bcl-2 pro-apoptotic proteins (ABT-263, also referred to as Navitoclax, shown in figure **1.8**) was reported by Tse *et al* in 2008.[32]

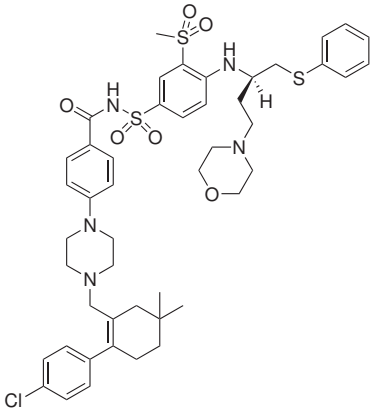

FIGURE 1.8: Structure of ABT-263 (Navitoclax): a Bcl-2 inhibitor discovered by Tse and coworkers[32]

ABT-263 was found to mimic the hydrophobic interactions generated by BAD (a pro-apoptotic protein). Preclinical animal models showed tumour regression in xenografts within 2 hours of treatment. The clinical studies of this compound are currently ongoing.

Although ABT-263 was a highly potent inhibitor, it was dose-limiting due to thrombocytopenia. As a result, further work was undertaken to minimise side effects, resulting in the generation of ABT199,**1.9** which is currently in phase I clinical trials.[33] The crystal structures of the Bcl-2 inhibitors are shown in figure **1.9**.[34]

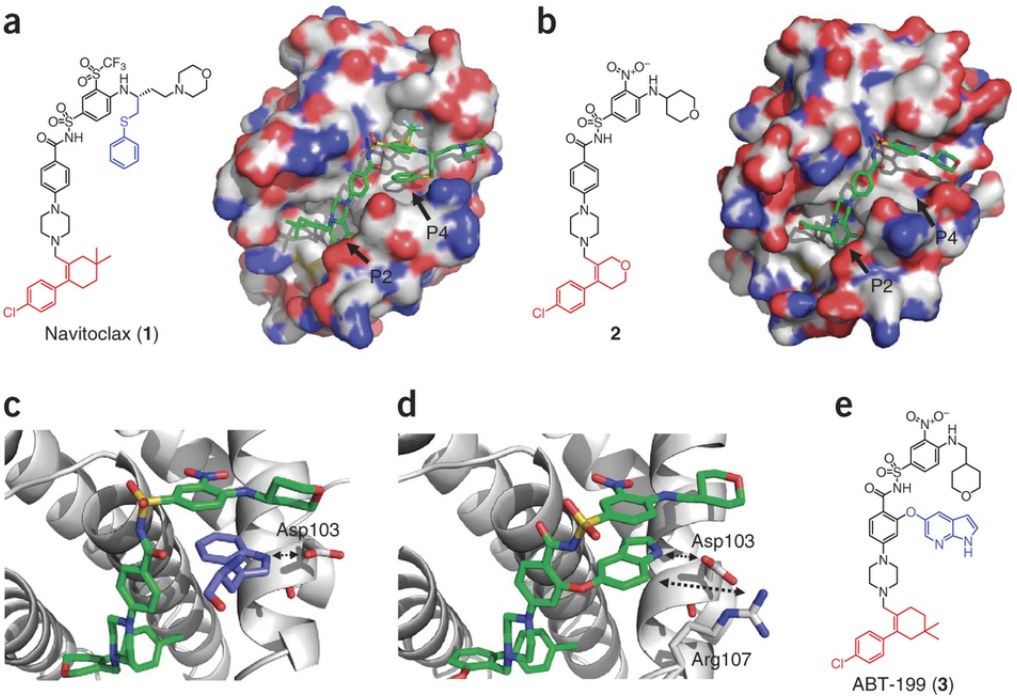

FIGURE 1.9: A. Cocrystal structure of ABT-263 (Navitoclax) within Bcl-2 (where P2 and P4 indicate the two hydrophobic hotspots on Bcl-2), B. cocrystal structure of an analogue of ABT-263 in Bcl-2 (where P2 and P4 indicate the two hydrophobic hotspots on Bcl-2), C. ribbon representation of Bcl-2 bound to ABT-263 (indicating key hydrogen bonding interactions between Asp103 and the imidazole moiety of ABT-263) D. ribbon representation of Bcl-2 bound to intermediary 2 (indicating key hydrogen bonding interactions between the imidazole of intermediary 2 and Arg107 and Asp103 present within Bcl-2) and E. structure of final optimised compound ABT-199 (reproduced with permissions)

At present, there are no inhibitors that act at the Mcl-1 protein. Work is currently being undertaken by Nguyen and coworkers in the design of novel inhibitors against Mcl-1,[35] as the overexpression shown in the CHO cell lines presents itself as a viable target in the treatment of cancer.[28]

1.2.0.2 The Nrf2/Keap1 Binding Partners (Example 2)

Figure **1.10** illustrates the Nuclear factor erythroid 2-related factor 2/Keap1: Kelch-like ECH-associated protein 1 (Nrf2/Keap1) protein-protein interaction.

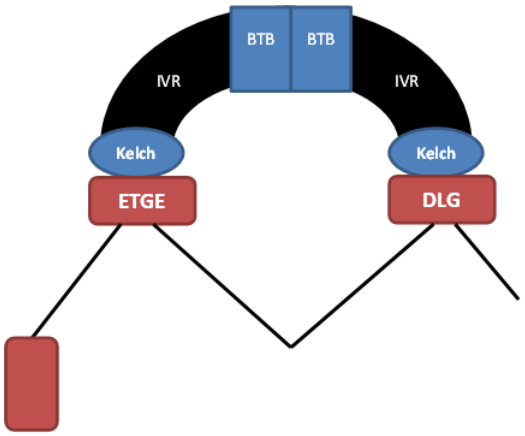

FIGURE 1.10: Diagram showing the binding of the Nrf2 protein to the two Keap1 Kelch domains (adapted from Kansanen *et al*, 2013)[22]

Keap1 is a highly cysteine-rich protein, which is able to oxidise at postions C151, C273 and C288, causing a conformational change and permitting binding to Nrf2.[36] Nrf2/Keap1 is a protein-protein interaction involved in the inflammatory response and has also been implicated in cancer[37] (as cancer can be resultant from prolonged inflammation),[38] however the interaction's role in cancer is still not fully understood. Nrf2 binds to 2 key subunits on Keap1 (known as Kelch domains),[39] forming a beta-hairpin structure. Inhibition of this interaction has been shown to reduce the inflammatory response,[40] however its role in the treatment of cancer is somewhat more complex. In 2013, Searcey *et al* published a high affinity binding sequence consisting of the Transactivation domain (TAT) found in HIV to improve cellular permeability and a 14mer sequence of Nrf2.[41] This high-affinity binder was fluorescently tagged as used as a probe against Keap1 to discover novel inhibitors of the Nrf2/Keap1 protein-protein interaction through fluorescence polarisation.

High throughput fluorescence polarisation assays were also undertaken by Munoz and coworkers in 2013 and Silvia and coworkers in the same year.[42,43] Munoz and coworkers discovered the inhibiting compound (SRS)-5 (figure **1.11**, which had a K_d of 1 μM), whilst the 2D-FIDA assay undertaken by Marcotte and coworkers discovered the compounds Cpd15 and Cpd16 (figure **1.12**), with ED_{50} values of 118 μM and 2.7 μM respectively.

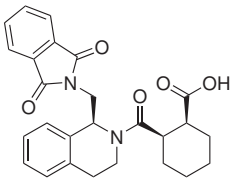

FIGURE 1.11: Structure of (SRS)-5[43]

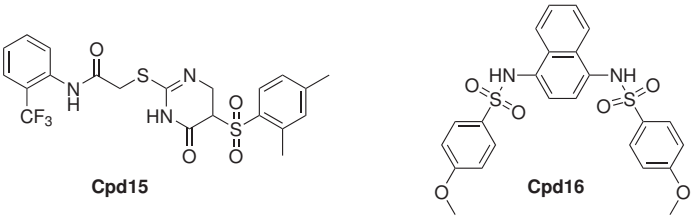

FIGURE 1.12: Structures of Cpd15 and Cpd16 produced by Sun and coworkers[44]

In 2014, Sun and coworkers discovered a potent inhibitor of the Nrf2/Keap1 protein-protein interaction.[44] Initially, a static structural analysis of the binding pocket of Keap1 was analysed using the protein databank entry 1X2R, which utilised the Nrf2 sequence LDEETGEFI. This peptide motif contained side chains capable of forming hydrogen bonds (in addition to the hydrogen bonds that can be formed by all peptide backbones), as demonstrated in figure **1.13**.

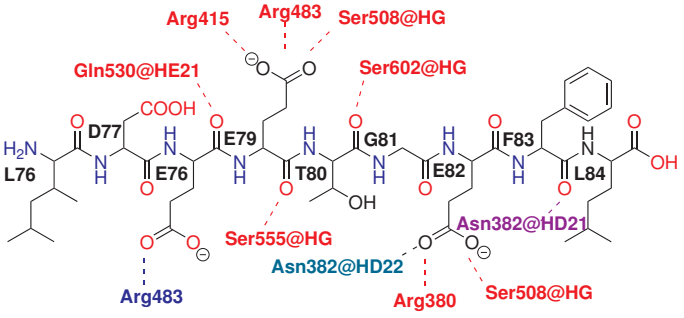

FIGURE 1.13: Diagram showing hydrogen-bonding interactions between the Nrf2 binding sequence and Keap1, as well as their relative intensities as calculated through molecular modelling. The amino acid sequence of NRF2 is labelled in bold. Atom and amino acid colours indicate the significance of the dipole interaction (red labels are over 80% importance, purple labels interact with between 60% and 80% importance, blue labels interact with between 40% and 60% importance whilst green labels interact with between 20% and 40% importance (adapted from Jiang *et al*, 2014)[44]

Using this information, combined with the previously described inhibitor Cpd16, Sun and coworkers undertook a fragment-based approach to determine optimal binding

within the pocket. It was hypothesised that the addition of carboxylic acids to Cpd16 could improve hydrogen bonding within the Keap1 binding pocket. Compound 2, the optimised form of Cpd16, is shown in figure **1.14**.

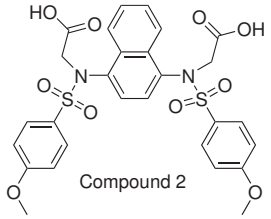

FIGURE 1.14: Structure of Compound 2, the optimised form of Cpd16 produced by Sun and coworkers[44]

Cpd16, FITC-labeled Nrf2 binding sequence and the newly designed compound 2 was tested in a Bio-Layer Interferometry (BLI) assay, in which the interference of white light by a substance (in this case a protein) against a biosensor chip is analysed. Any changes in the interaction state of the proteins will alter the interference with white light, which can then be detected by a spectrophotometer. The BLI assay indicated that the optimised compound 2 had a K_d of 3.59 nM, in comparison to Cpd16 (1690 nM) and the FITC-labeled Nrf2 binding sequence (15.8 nM). EC_{50} values were also determined for these three compounds using fluorescence polarisation, with values of 395 nM, 1460 nM and 28.6 nM for 9mer Nrf2, Cpd16 and compound 2 respectively.

In order to determine the downstream effects of compound 2, quantitative realtime polyerase chain reaction (qRT-PCR) studies were undertaken. The RNA levels of HO-1, NQO-1 and GCLM RNA levels were examined, as these are known downstream targets of Nrf2. In each case, levels of these targets increased with increasing concentration of compound 2.

Although compound 2 showed promising biological data, the compound had poor cell permeability, which would be caused by the carboxylates present at biological pH (pH 7.2), as the presence of the negative charge on the carboxylates prevents movement through the cell membrane. Follow-up work to this would be to improve the cell permeability of the Nrf2-Keap1 inhibitors. At present, there is still a great deal of investigation and optimisation of inhibitors against this interaction.

1.2.0.3 The p53/MDM2 Binding Partners (Example 3)

Figure **1.15** displays an overview of the protein 53/Murine-Double-Minute 2 (p53/MDM2) protein-protein interaction. The p53/MDM2 interaction has been the most well-studied

to date and studies by Lane and coworkers showed for the first time that these type of reactions are "druggable".[45]

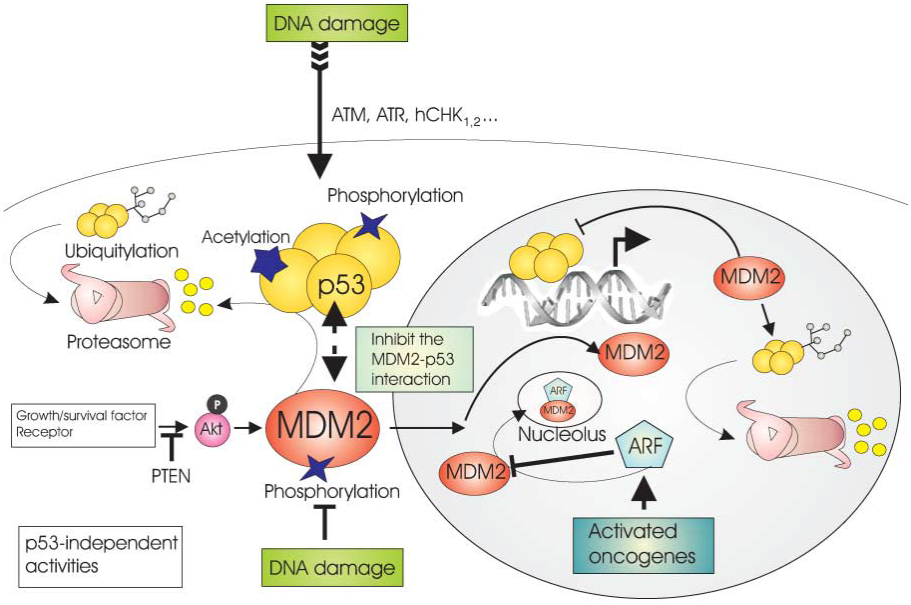

FIGURE 1.15: Intracellular pathways affected by the binding of p53 to MDM2[46] (reproduced with permissions)

Following are the details of the proteins involved with this interaction as well as downstream effects and inhibitors that have been shown to inhibit this interaction.

1.2.1 An Introduction to p53

Figure **1.16** illustrates the genetic construct of protein 53 (p53). p53 was first coined as the "guardian of the genome by Sir David P Lane in 1992, as it led to the repair or apoptosis of damanged DNA and therefore preserved the integrity of the genome.[47] p53 contains 393 amino acids consisting of a transactivation domain and a proline-rich domain towards the N-terminus, a DNA binding domain in the central region, an oligomerisation region that causes p53 to form a homotetramer and a regulatory region that controls p53 levels within the cell.[48] p53 normally resides in the nucleus of the cell, where it scans for damaged DNA and triggers the cell into apoptosis or DNA repair.

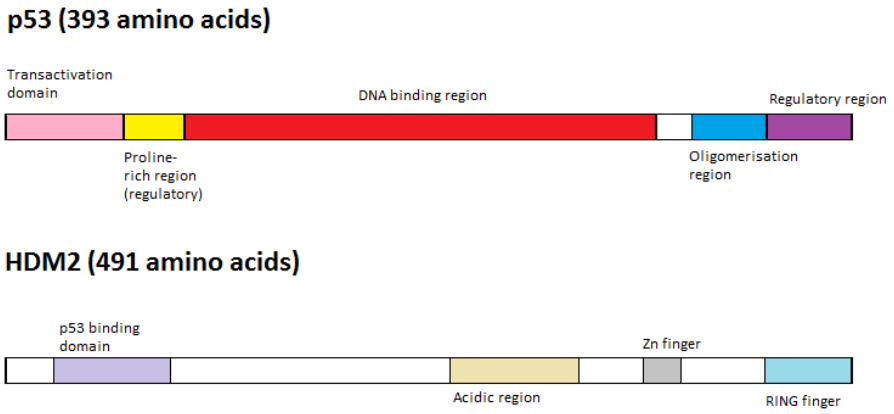

FIGURE 1.16: Constructs of both p53 and MDM2, indicating key binding and regulatory regions present within each sequence (adapted from Petrenko *et al*, 2003)[46]

Tetrameric p53 is exported into the cytoplasm for degradation by MDM2, but monomeric p53 is thought to have its own separate pathway of degradation, although the exact mechanism of this is still undergoing investigation. The monomeric pathway is thought to be masked during the formation of tetrameric p53.[49]

p53 is an important tumour suppressor protein that ensures that cells that are damaged by cellular stress (including single- or double-stranded DNA breaks, hypoxia, faulty spindle formation during anaphase of mitosis, reduction in ribonucleotides, teratogenic substances and so on) are either repaired or apoptosed.[50] As to the pathway chosen, it is generally considered that higher levels of p53 are associated with apoptosis of the cell. Under normal conditions, p53 levels in the cell are low. p53-induced apoptosis is a result of downstream induction of **p**53 **u**pregulated **m**odulator of **a**poptosis (PUMA) and Phorbol-12-myristate-13-acetate-induced protein 1 (also known as NOXA),[51] which are pro-apoptotic proteins. These signalling proteins translocate to the mitochondria to bind to the anti-apoptotic proteins Bcl-2, Bcl-X, Bcl-W (in the case of PUMA),[52] Mcl-1 and Bcl-2A1 (in the case of NOXA).[53] When inhibition of the anti-apoptotic proteins reaches a certain threshold, apoptosis occurs. In addition to the binding to anti-apoptotic proteins by downstream PUMA and NOXA, translocation of p53 to the mitochondria can lead to the direct activation of pro-apoptotic members of the Bcl-2 family, causing apoptosis. The final mode of cell death is through downstream signalling of p21 (a downstream tumour suppressor) caused by elevated p53 levels. Elevated p21 leads to opsonization of damaged cells by macrophages and senescence.[54] In addition, the p21cif1/waf1 complex inhibits the action of cyclin-dependent kinases (Cdks).[55]

Additional proteins are involved in the promotion of p53 binding to pro-apoptotic partners. Apoptosis-stimulating of p53 protein 1 (ASPP1) and apoptosis-stimulating of p53

protein 2 (ASPP2) are cofactors that promote the binding of p53 to either BAX or p53-inducible protein, both of which are pro-apoptotic.[56] The RNAi iASPP1 has been shown to inhibit apoptosis and is overexpressed in breast cancer and AML and has been linked to a resistance to treatment in ovarian cancers.[57] iASPP1 has also been found in melanomas, but not overexpressed.[58]

Alternative reading frame (ARF) protein is a protein responsible for the production of p53. ARF is also capable of binding MDM2, which could contribute to increased p53 stabilisation in the nucleus by prevention of MDM2 shuttling.[59] *In vitro*, it has been shown that ARF binding to MDM2 does not affect MDM2s ability to bind p53 and therefore both the ARF-MDM2 and ARF-MDM2-p53 complexes have been formed.[60] ARF also causes MDM2 localisation in the nucleolus.

Ubiquitin-specific protein 1 (USP1) has a rather more complex relationship with p53: USP1 causes deubiquitination of Inhibitors of DNA binding (IDs).[61] These IDs then prevent binding of E2A and basic-helix-loop-helix (bHLH) transcription factors, leading to uncontrolled proliferation through inhibition of cell cycle arrest by p53 and downstream p21 activation in osteosarcoma models.

C-Abl is also a p53 modulator and in its non-oncogenic role acts to antagonise MDM2 and therefore lead to increased stability of p53.[62] Although oncogenic Bcr-Abl is also able to cause accumulation of p53, it utilises the p53/MDM2 negative feedback loop to prevent p53 from carrying out its tumour suppressor activities.

p53 is mutated in over 50% of cancers (usually within its DNA binding domain): two common mutations include E177R, which prevents the binding of p53 to DNA and S46A, which prevents p53 from inducing apoptosis in HSC-2 human oral squamous cell carcinomas.[63,64]

1.2.2 An Introduction to MDM2

Murine-Double-Minute 2 (MDM2) or its human homologue Human-Double-Minute 2 (HDM2) promotion is initiated by p53. MDM2 is an E3 ubiquitin ligase consisting of 491 amino acids.[48] MDM2 contains a region specifically for binding tetrameric p53, an acidic region that is capable of interacting with ribosomal protein L5 and ARF tumour suppressor protein. It also contains a zinc finger and a Really Interesting New Gene (RING) finger, which is thought to cause nuclear export of p53.

MDM2 is able to target the retinoblastoma protein (pRB) for degradation through either ubiquitin-dependent or ubiquitin-independent pathways.[65] The associated retinoblastoma proteins, p107 and p130, cause the recruitment of Mdm2 but are not ubiquitinated

by Mdm2.[66] p107 inhibits muscle differentiation and also inhibits Myo-D dependent transactivation.[67,68]

MDM2 is capable of activating or inhibiting E2F-1.[69,70,71] Interestingly, E2F1 was up-regulated following treatment of cells using doxorubicin, but downregulated by nutlin-3-treated cells. Normal melanocytes retain E2F1 levels upon nutlin-3, but do not gain features of senescence. Loss of MDM2 function also appeared to downregulate E2F1 through p53-modulation and proteasome-independent mechanisms. p73, a homologue of p53, can activate the p53 response element and cause apoptosis through E2F1-associated pathways.[72]

MDM2 is overexpressed in 7-8% of cancers. This leads to uncontrolled entry into S phase and polyploidy, resulting in hyperproliferation of cancerous cells. A key point mutation leading to MDM2 overexpression and permanent reduction in p53 activity is 309T to G (SNP309).[71]

1.2.3 The p53/MDM2 Protein-Protein Interaction

Figure **1.17** illustrates an X-ray crystal structure of the p53/MDM2 protein-protein interaction, shown diagrammatically by two different methods. When damaged DNA is detected by p53 in the nucleus, p53 levels rise and the DNA in question is either repaired or the cell is apoptosed, depending on the degree of damage and factors affecting the downstream pathway chosen such as the threshold levels of p53 in the cell.

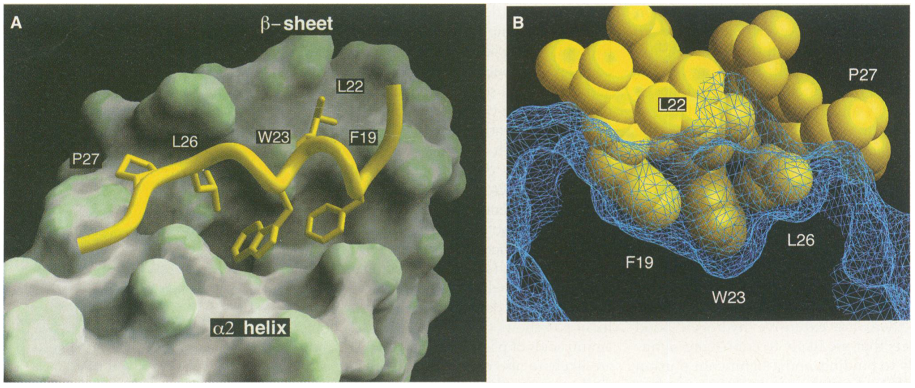

FIGURE 1.17: X-ray crystal structure of the p53 transactivation domain bound to MDM2, indicating the key binding amino acids Phe[19], Trp[23] and Leu[26] (reproduced with permissions).[73]

During this process p53 also transcribes MDM2, which is a negative modulator of p53 to prevent p53 from overworking and leading to high levels of apoptosis. When MDM2 binds to α-helical tetrameric p53 via the MDM2 hydrophobic pocket (containing Phe[19]-,

Trp^{23}- and Leu^{26}-binding regions, as shown in figure **1.17**), p53 is then triggered for ubiquitinylation and degradation by MDM2, thus ceasing the action of p53 within the nucleus.

Malignancy occurs when MDM2 is overexpressed, as this leads to rapid p53 degradation and prevents p53 from carrying out its tumour suppressor functions within the cell. This process is found in 7-8% of all cancers.[72] As a result, compounds attempting to (re)activate p53 or suppress the action of MDM2 are currently being investigated as cancer therapeutics.

1.3 Inhibitors of the p53/MDM2 Interaction Currently in Clinical Trials

Table **1.2** indicates the current p53/MDM2 protein-protein interaction inhibitors (all of which are small-molecule MDM2 antagonists) currently in clinical trials either as monotherapy or as combination therapies with cytarabine or doxorubicin, both of which are classical chemotherapy agents.

Compound	**Status in Phase I Trials**	**Clinical Trials ID**	**Company**
RG7112 (also known as RO5045337)	Phase I trial in advanced solid tumours, solid tumours, haematological neoplasms and liposarcomas (all completed)	NCT00559533 NCT01164033 NCT00623870 NCT01143740	Roche
RG7112 (also known as RO5045337) with cytarabine	Phase I in AML (completed)	NCT01635296	Roche
RG7112 (also known as RO5045337) with doxorubicin	Phase I in soft tissue sarcoma (completed)	NCT01605526	Roche
RO5503781	Phase I in advanced malignancies (recruiting)	NCT01462175	Roche
RO5503781 with cytarabine	Phase I in AML (recruiting)	NCT01773408	Roche
MI-773 (also known as SAR405838)	Phase I in malignant neoplasms (recruiting)	NCT01636479	Sanofi
DS-3032b	Phase I in advanced solid tumour lymphoma (recruiting)	NCT01877382	Daiichi Sankyo

TABLE 1.2: Table of all inhibitors of the p53/MDM2 interaction currently in clinical trials [year 2014][45]

It is thought that all inhibitors working at the p53/MDM2 interface are competitive blockers that bind in the same region as p53, disrupting key hydrophobic and π-π stacking interactions produced by the Phe^{19}, Trp^{23} and Leu^{26} of p53. As this inhibition is competitive and these inhibitors are to only be used in cancers with overexpressed MDM2, it means that there is still sufficient levels of MDM2 to undertake normal p53 modulation, whilst maintaining levels of p53 required for normal DNA replication and cell division to take place. The following describes the development of p53/MDM2 protein-protein interaction inhibitors, their synthetic pathways key structural properties and their biological data. This information is key to gaining a full understanding of

how these inhibitors work, their advantages and limitations, as well as further information on the future development of improved inhibitors and how this impacts the research completed within this thesis.

1.4 Most Potent Small Molecule Inhibitors of the p53/MDM2 Interaction and their Development

There are four main classes of small molecule inhibitor that act on the p53/MDM2 protein-protein interaction: these are the nutlins, the spiro-oxindoles, the pyrrolidines and the piperidones.[45] Figure **1.18** summarises the chemical structures, biochemical data and company responsible for the discovery and development of the top four small-molecule p53/MDM2 inhibitor classes.[74] Each of these classes of compounds are explained in detail below, as well as associated small molecules that were designed from the optimisation of these key compounds. The nutlins, spiro-oxindoles and pyrrolidines are currently in clinical trials (RG7112, Mi-773 and RO5503781 respectively in table **1.2**, although the exact structure and biochemical data of RO5503781 have yet to be disclosed); whilst the piperidinones are currently in preclinical trials. As the structure of RO5503781 has not been disclosed, its most potent published predecessor in its class, RG7388, is discussed in respect to the pyrrolidines and their structure-activity relationships.

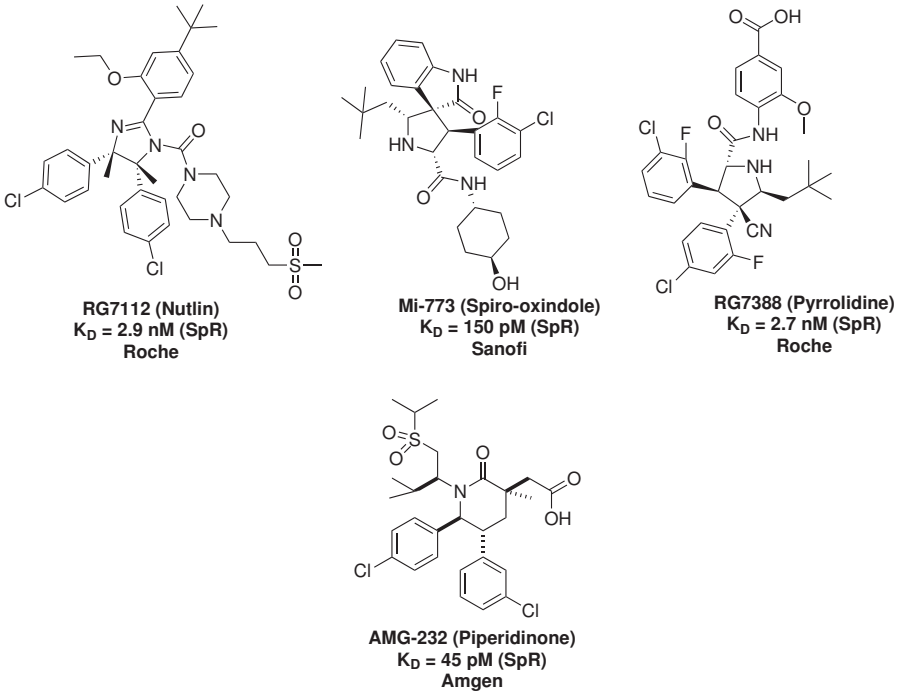

FIGURE 1.18: Top four inhibitors of the p53/MDM2 interaction (SpR = surface plasmon resonance)[74]

1.4.1 Main Techniques used to Determine p53/MDM2 Inhibition

There are three main techniques used to determine inhibition of the p53/MDM2 interaction: surface plasmon resonance (SpR), fluorescence polarisation (FP) and enzyme-linked immunosorbance assay (ELISA). Surface plasmon resonance is a technique in which plane polarised light intercepts an electronically-conducting surface at the interface with a media with a different refractive index. The two interfaces are the media (high refractive index) and a buffer with a low refractive index. When incident light covering a range of angles intercepts the surface, energy is absorbed and plasmons are produced, which reduces the intensity of the reflected light. At points of interaction at the surface, more energy is absorbed and hence less energy is reflected. This reduction in intensity of the reflected light is then measurable and can be quantified to indicate the degree of interaction.[75]

Fluorescence polarisation (FP) is a technique that analyses the ratio of the intensity of plane polarised light intercepting from and emitted by a molecule containing a fluorescent tag.[76] The degree of plane polarised light depends on the rate of tumbling of a molecule in solution, which decreases with size (that is, a complex will tumble slower than untagged fluorescent peptide). If a competitive inhibitor is introduced, the amount of unbound fluorescently-tagged ligand increases, causing a reduction in polarisation.

The last main method (although largely superceded by FP due to cost and assay runtime) is ELISA. This technique relies on biotinylated peptide, which has affinity for the streptavidin-coated plate.[77] Binding is proceeded by washing, incubation with inhibitor and secondary binding partner, further washing to remove any unbound components, followed by addition of antibodies that attach to the secondary binding partner and metabolise a substrate if binding is present. If inhibitor is present, the secondary binding partner and inhibitor will be washed away and therefore there will be little to no metabolism of substrate and therefore low absorbance in the detected range by a spectrophotometer. Other techniques used within the literature are discussed in their relevant section.

1.4.2 The Discovery of the Nutlins: an Imidazoline-Based Library

The nutlins were the first class of p53/MDM2 protein-protein interaction inhibitors to be synthesised. The nutlin library of compounds was initially investigated through high throughput screening by Pazgier and coworkers.[78] They are based on a 4,5-dihydroimidazoline structure. The top hit compound, racemic nutlin-3, was found to have a K_d value of 263 nM using surface plasmon resonance.[79]

Further research showed that one enantiomer (nutlin-3a, figure **1.19**) was 150 times more active than its alternative stereochemistry enantiomer (nutlin-3b), with a K_i of 40 nM as determined by fluorescence polarisation assays and an IC_{50} of 90 nM by competition surface plasmon resonance alongside recombinant p53 ligand (compared to nutlin-3b, which was found to have an IC_{50} of 13.6 μM in the same assay).[73] Nutlin-3a was more potent as the stereochemistry permitted greater π-π-stacking interactions within the hydrophobic pocket, as the conformation allowed the compound to overlap better with the key wildtype-p53 interactions with MDM2.

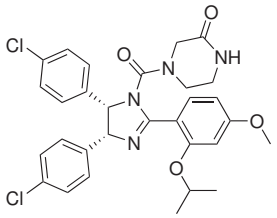

FIGURE 1.19: Nutlin-3a, the original nutlin found to inhibit the p53/MDM2 interaction

Nutlin-3a was then tested in cell lines HCT116 (wt p53, key binding sequence SQETFSDLWKLLP) and SJSA-1 (overexpressed MDM2), which were stained with in bromodeoxyuridine (BrdU), to determine effects in the cell cycle. In both cases, 24 hours

following 4 μM nutlin-3a treatment, there were increased levels of G_1 and G_2/M activity in the cell cycle, with a significant reduction of S-phase activity, which is the point at which DNA replication occurs. Investigation of gene expression in the presence of nutlin-3a led to significant increases in the transcription of p53 and p21 (an associated tumour suppressor protein in the downstream pathway of p53).[45]

Additional cytotoxicity assays were undertaken to determine the effect of nutlin-3a on apoptosis through transferasemediated deoxyuridine triphosphate nick end labeling (TUNEL). As cells undergo damage and apoptosis, the labeling becomes more extensive and this can be quantified using flow cytometry and fluorescence microscopy.[80] Using TUNEL, it was determined that 45% of SJSA-1 cells exposed to nutlin-3a became TUNEL-positive 48 h after incubation (at 24 h there were insignificant levels of TUNEL-positive cells).

In progressing from single cells to animal systems in preclinical studies of nutlin-3a, it was also determined that nude mice xenografts implanted with SJSA-1 cells had their tumour growth inhibited by 81% at 10 mg/kg inhibitor (the maximum tolerated dose).

Solution-phase NMR-based studies combined with X-ray crystal structures showed that the disubstituted benzene ring occupied the Phe^{19} pocket, whilst the two chlorophenyl rings inhibit the Trp^{23} and Leu^{26} pockets.[81] The piperidone-like moiety does not affect binding, however it works to improve aqueous solubility, as the compound is otherwise very lipophilic.

Although nutlin-3a showed great promise as an inhibitor, it was not a candidate for clinical trials due to its poor pharmacokinetic properties (its high lipophilicity made penetration into the desired tissues and drug formulation for drug delivery was difficult) and therefore analogues of nutlin-3a were investigated, which retained or improved potency whilst also improving aqueous solubility.

1.4.2.1 Nutlins Optimisation: The Design of RG7112

In 2011, further SAR studies were undertaken on nutlin-3a to improve the potency of the nutlins and improve binding to MDMX, a secondary binding partner of both p53 and MDM2.[82] This optimisation led to the development of RG7112 (figure **1.18**). RG7112 was the first p53/MDM2 interaction inhibitor to make it into Phase I clinical trials in advanced solid tumours, early-stage solid tumours, haematological cancers and liposarcomas; as well as acute myeloid leukaemia (AML) in combination with cytarabine.[83]

RG7112, the most potent nutlin generated to date (shown in figure **1.18**), was developed through the optimisation of nutlin-3a, in which the key binding modality was

the projection of the chlorophenyl groups into the Trp^{23} and Leu^{26} binding pockets of MDM2.[83]

During the development of RG7112, the methoxy group present on nutlin-3a was susceptible to degradation and produced phenol as a breakdown product of metabolism. Substitution of the methoxy with a *t*-butyl functionality prevented the production of phenol as a toxic metabolite.[84] Another key modification was the introduction of methyl functionalities to prevent the degradation of the imidazoline core to imidazole, which was completely inactive against MDM2. The isopropoxy functionality was replaced with an ethoxy to reduce the molecular weight and hence produce a more "druggable" compound (that is, a compound with desirable pharmacokinetics and potent pharmacodynamics permitting the formulation of the drug into a medicine). Finally, as the amide side chain was solvent-exposed, it was hypothesised that this could be used for solubilisation in aqueous media and therefore a variety of different polar substitutents were investigated. The most active compound, RG7112, contained a piperidine side chain linked to a methylsulfoxy by a propyl linker. The IC_{50} of RG7112 as determined by competition SpR was 2.9 nM (compared to 90 nM for nutlin-3a as determined by competition SpR).

Despite the high potency of the nutlin class, resistance to RG7112 and other nutlins governed by mutations within the binding pocket and lid region of MDM2 has resulted in a need for further development of inhibitors.[85] Interestingly, a recent paper has explored the cross-reactivity of nutlin-3a between both the anti-apoptotic Bcl family and the p52/MDM2 interaction,[86] which could reduce the likelihood of resistance as well as increase its effectiveness in cancers. Using the X-ray crystal structure PDB-1YCR and nutlin-2 as a small molecule template, the stage was set for the design of novel small molecules that could inhibit this interaction.

1.4.3 The Spiro-oxindoles

In 2006, Ding and coworkers used structure-based design to produce the spiro-oxindole library of p53/MDM2 protein-protein interaction inhibitors (figure **1.20**), the most potent of which had an IC_{50} value of 86 nM as determined using an FP assay.[87]

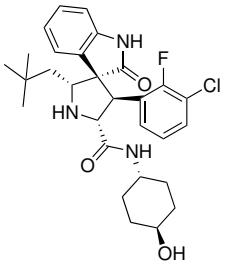

FIGURE 1.20: Mi-773, a spiro-oxindole

The spiro(cyclic)-oxindoles have an aromatic ring fused to a lactam, haveing resemblance to the structure of tryptophan, which is present at position 23 of the p53 peptide.[88] Structure-based design also considered Leu[22] in the analogue design, as it was proposed that additional hydrophobic interactions could be generated at this position within MDM2. Substitution at the C3 position (adjacent to the lactam ketone) and secondary amide moieties permits the generation of libraries. Starting from the spiro-oxindole core with a ketone in position 3, analogues can be generated through the following routes: (i) by reacting the starting compound with an amino acid or primary amine, it is possible to form an imine, which can react with activated alkenes to form multiple heterocycles. (ii) The imine can also react with a nucleophile to introduce a chiral centre at position 3. (iii) Direct reaction with a nucleophile can produce oxo-spiro-oxindoles or alternatively, (iv) prior reaction with a Michael donor, followed by nucleophilic attack can remove the heteroatom and instead produce a diastereotopic cyclic system.

The synthetic strategy for this class of inhibitors was examined due to the similarity in the central core to the isoquinolin-1-ones synthesised in this thesis (as both contain a lactam functionality fused to an aromatic ring) and therefore it was originally proposed that similar synthetic strategies may be permitted in this thesis. Figure **1.21** illustrates the design of the spiro-oxindole library based on the tryptophan present in wt p53. The initial lead compound Mi-5 was designed through structure-based design and tested in an FP assay, producing an IC_{50} of 8.7 μM against the p53/MDM2 protein-protein interaction. Further computational studies deduced that chlorinating the aromatic core and introducing a *t*-butyl group could maximise interactions within the hydrophobic pocket. The optimised compound, Mi-17, produced an IC_{50} of 86 nM in the FP assay. Optimisation of Mi-17 produced Mi-63, which produced an IC_{50} of 3 nM in the FP assay, almost 30 times more potent than Mi-17, proving that the strategy to improve interactions was successful. The limitation of Mi-63 was that it was only approximately 10% orally bioavailable. Mi-219 was then synthesised, which had improved bioavailability and retained activity, with an IC_{50} of 5 nM and 65% oral bioavailability in rats. Molecular modelling of Mi-219 indicated that the chlorophenyl side chain bound within the Phe[19]

pocket, whilst the *t*-butyl group projected into the Leu^{26} and the fluorochlorophenyl side chain resides in the Trp^{23} pocket. Although Mi-219 was very drug-like, further optimisation was undertaken. The most active diastereomer of Mi-219 was isolated and further optimised to improve pharmacokinetic properties to produce Mi-888. Mi-888 produced a K_i of 0.44 nM and IC_{50} of 80 nM by WST-8 assay using SJSA-1 (MDM2 overexpressed) cells. It has also been shown that Mi-888 was able to achieve complete tumour regression in mice models with overexpressed MDM2.[89] Interestingly, pharmacological studies have shown that Mi-888 increases the level of autoubiquitinylation of MDM2 in human B-cell lymphomas, which is not the case with the nutlin library.[90]

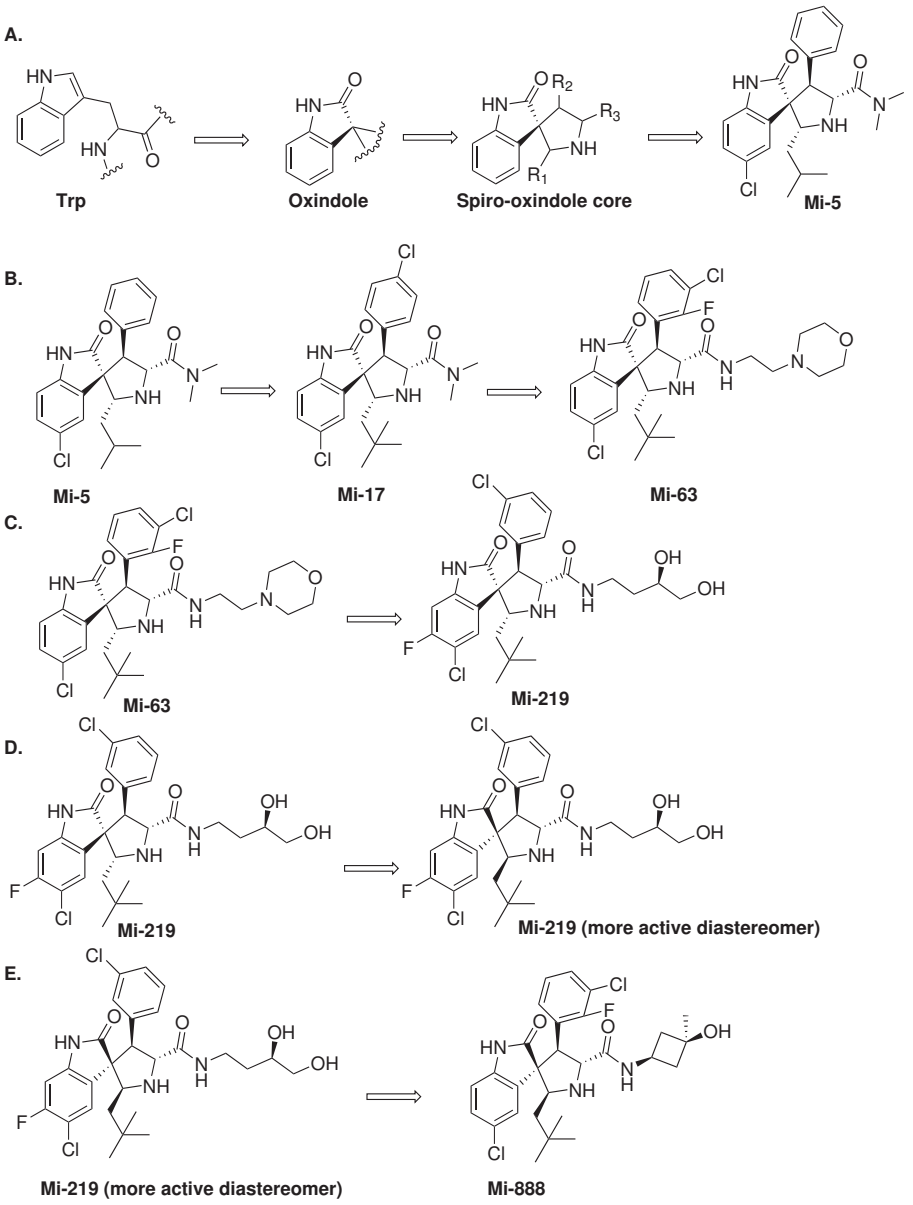

FIGURE 1.21: Design and optimisation of the spiro-oxindoles A. design of the oxindole core based on tryptophan and generation of the first lead compound B. Optimisation of substituents to improve potency C. Increase in aqueous solubility and potency D. Improvements in oral bioavailability E. Further pharmacokinetic optimisation to produce Mi-888

Whilst Ascenta Therapeutics were in the process of developing Mi-888,[89] a rival company, Sanofi, synthesised Mi-773 (figure **1.18**), which is currently in clinical trials (although there is less published data regarding SAR and biological data available for Mi-773).[45] As well as spiro-oxindoles being tested for activity against the p53/MDM2 interaction, the spiro-oxindoles have also showed promise as antimalarial therapy against *Plasmodium falciparum* (NITD609).[91]

The structure-based design approach was used within this thesis (although different synthetic routes were undertaken), although the starting point for inhibitor development within this thesis was either the isoquinolin-1-one scaffold or chlorofusin. The majority of inhibitor development within this thesis focused on increasing potency, however further work was undertaken to improve aqueous solubility and cell permeability of the isoquinolin-1-one library, discussed in 'Chapter 2'.

1.4.4 The Pyrrolidines

Figure **1.22** illustrates the pyrrolidine, RG7388, which is the most potent published pyrrolidine in the literature for which the structure has been disclosed. The original notion for the design of the pyrrolidine series by Graves *et al* in 2013 was the use of a 5-membered ring system instead of a six-membered system (as is present in the spiro-oxindole core), as the 5-membered ring permitted a greater deal of flexibility and was postulated to adapt into the hydrophobic pocket to improve the fit.[92] Inspiration for the pyrrolidine library was greatly driven by the development of RG7112, which also contains a 5-membered ring core. The pyrrolidine library was synthesised as a racemic mixture through non-stereoselective methods, separated by chiral HPLC and tested in HTRF binding assays and MTT proliferation in wt p53 (SJSA-1) and mutant p53 (SW480) cell lines.[92] RG7388 had an IC_{50} of 6 nM by HTRF and 30 nM in MTT assays, with a selectivity 344 times more potent against wt p53 cells over cells containing mutant p53.

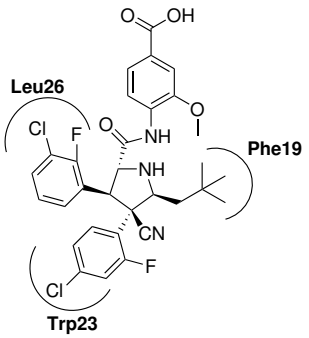

FIGURE 1.22: RG7388, a pyrrolidine-based inhibitor currently in clinical development and its binding epitope within MDM2[93]

Examination of the binding motif of the pyrrolidines showed that RG7388 formed π-π stacking interactions with the Trp^{23} through its 2-fluoro-4-chlorophenyl ring. The 2-fluoro-3-chlorophenyl ring aligned with the Leu^{26} pocket, whilst the neopentyl group

was found to occupy the Phe^{19} pocket (see figure **1.22**). The carbonyl within the pyrrolidine was also able to form hydrogen bonds with His^{96} (PDB entry 4JRG). Currently, these compounds are in clinical development but the data has yet to be published.[93]

1.4.5 The Piperidinones

Another novel HTS lead compound, compound **11** (figure **1.23**), was determined through high throughput screening by Fox *et al* in 2012.[94] The lead compound produced an IC_{50} of 2.42 μM in serum-based homogenous time-resolved fluorescence (HTRF) and 960 nM in 15% human serum HTRF.

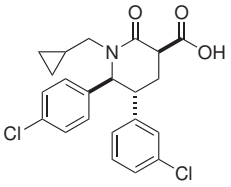

FIGURE 1.23: Structure of the initial Amgen lead piperidinone (compound 11)[95]

Simplification of compound **11** and removal of the additional side chain functionality towards the Phe^{19} pocket was used to develop the piperidinone analogues. The halogenated phenyl rings were retained for binding into the tryptophan and leucine pockets, although different halogens and substitution patterns were examined. A carboxylic acid moiety was introduced adjacent to the piperidone to improve aqueous solubility and a variety of N-alkyl side chains explored. Cyclopropyl substitution was most potent, with the final compounds producing IC_{50} values of 340 nM (in serum-free HTRF) and 370 nM (in 15% human serum HTRF).

Further exploration of the piperidinones led to the design of AM-8553 (figure **1.24**), which contained the piperidinone core, but a much less rigid structure than the Amgen lead.[96] Additional alcohol groups were also added to the compound to improve aqueous solubility. AM-8553 was tested by SpR, producing an K_d of 400 pM by SpR and an IC_{50} of 70 nM as determined in the 5-ethynyl-2-deoxyuridine (EdU) proliferation assay, which works to introduce labeled EdU onto damaged DNA, which can then be quantified using a spectrophotometer.

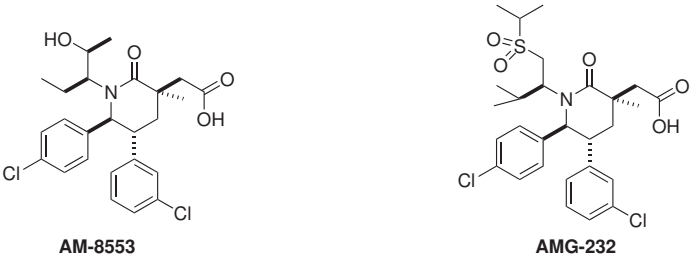

FIGURE 1.24: Structure of the lead piperidinone AM-8553 and the optimised compound AMG-232[74]

Initial replacement of the alcohol group with a variety of nitrile substituents or substitution with different alcohol functionalities resulted in analogues which may have retained potency, however cellular activity was severely affected in the case of secondary alcohols. Sulfonamides were also substituted in place of the secondary alcohol. Sun and coworkers discovered that reversing the sulfonamide retained activity but did not confer any advantage in terms of metabolic stability.[74] In the case of sulfone deriviatives, however, it was found to improve hepatic clearance in rat models. This final compound, AMG-232, was taken into preclinical studies (figure **1.24**). Further pharmacokinetic analyses in mice showed favourable data (with improved hepatic clearance compared to the previous analogues) but clinical trials data has yet to be published.

1.4.6 Key Features of the Top p53/MDM2 Small Molecule Inhibitors and Further Development

There are key features common to many of the different p53/MDM2 small molecule inhibitors. The majority of the small molecules contain either a monocyclic aromatic (figure **1.25**) or fused bicyclic core. The monocyclics are predominantly 5-membered aromatic rings containing an imidazole, thiophene, or furan functionality, which provides the central core with rigidity. Three of the top inhibitors also contain a 5-membered core but are non-aromatic (figure **1.18**, with the exception being the spiro-oxindole, which is a 5-membered ring fused to a 6-membered aromatic ring). RITA (figure **1.25**), although a linear molecule lacking a central core, contains both furan and thiophene functionalities. As there appear to be a variety of these 5-membered aromatics in the literature, it was proposed that these could potentially be incorporated into the side chains of the analogues synthesised within this thesis.

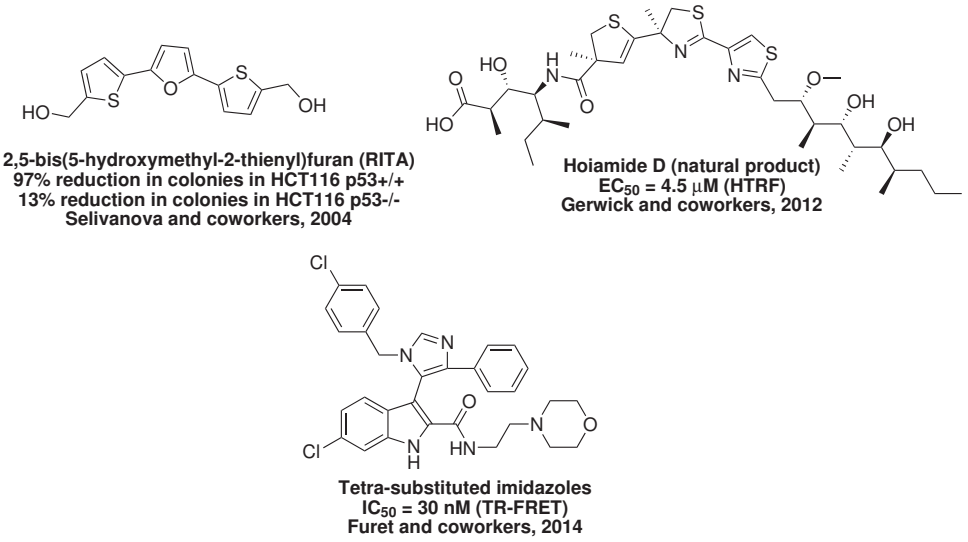

FIGURE 1.25: Selection of small molecule p53/MDM2 inhibitors containing a 5-membered aromatic core[97,98,99]

Many of the small molecule inhibitors, both monocyclic and bicyclic, contain a form of lactam in their central core (figure **1.26**), which provides compounds with a degree of rigidity and is also relatively stable to degradation, as the lactam can resonate its charge through its bonds. Isoindolinones contain a five-membered ring,[100] piperidinones contain a six-membered lactam ring, whilst benzodiazepinediones and thiobenzodiazepinediones contain a seven-membered lactam ring.[101,102,103] As the lactam functionality can be produced synthetically by a variety of reactions (one of which being the Castagnoli reaction),[104] and is common to many of these small molecule inhibitors, it was decided that this would be incorporated into the first library to be explored within this thesis: the isoquinolin-1-ones.

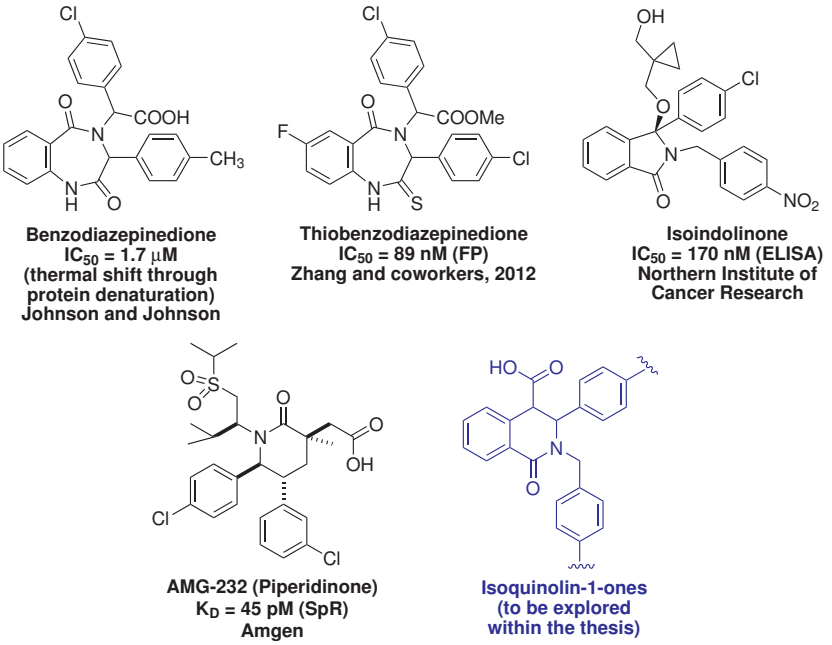

FIGURE 1.26: Selection of small molecule p53/MDM2 inhibitors incorporating a lactam functionality

Leading on from the monocyclic and bicyclic cores are the polycyclic molecules that have been shown to inhibit the p53/MDM2 interaction (figure **1.27**). α-Mangostin and gambogic acid have been shown to inhibit the p53/MDM2 interaction, as tested using a yeast hybrid screen.[105] The activity of these compounds was dependent on the p53 status in MCF-7 cell lines. Both compounds were shown to have high degrees of interaction at Gly^{58}, Asp^{68}, Val^{75} and Cys^{77} of the MDM2 pocket, but gambogic acid alone was able to form hydrogen bonds with Gln^{72} and Phe^{55}.[105]

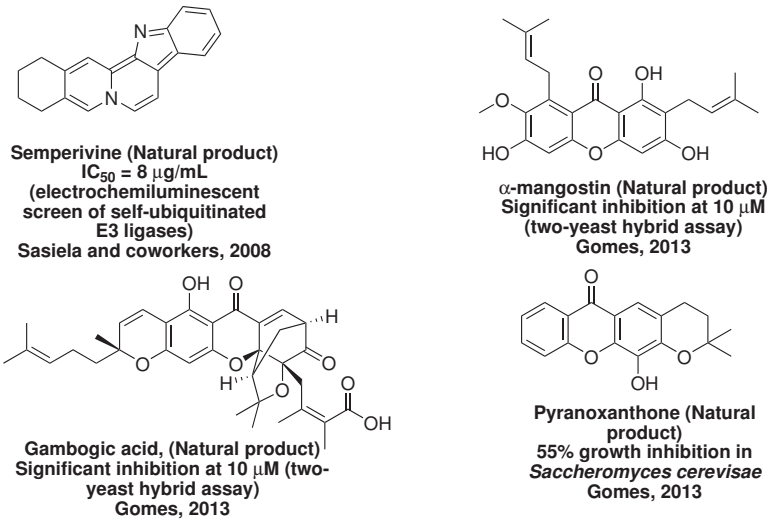

FIGURE 1.27: Examples of small molecule p53/MDM2 inhibitors containing a polycyclic planar core[106,105]

Arguably, the most important aspect of binding into the hydrophobic pocket is the presence of halogenated aromatics, in particular chlorophenyl groups. Hardcastle and coworkers demonstrated this concept with his most potent isodolinone (figure **1.28**). Hardcastle and coworkers showed that when the most potent isoindolinone chloro groups were substituted with with methoxy or ethoxy groups, activity was abolished.[100]

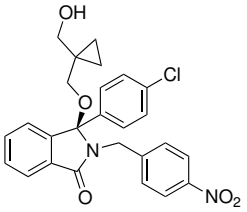

FIGURE 1.28: Most potent isoindolinone as determined by Hardcastle and coworkers[100]

Figure **1.29** shows the binding epitopes for the top four classes of p53/MDM2 inhibitors. The literature shows that the Leu^{26} pocket is large enough to accomodate an aromatic ring, whilst further work has been undertaken to form hydrogen bonds with His^{96} and hydrophobic interactions with the Val^{93} present within the MDM2 hydrophobic pocket.[107,108]

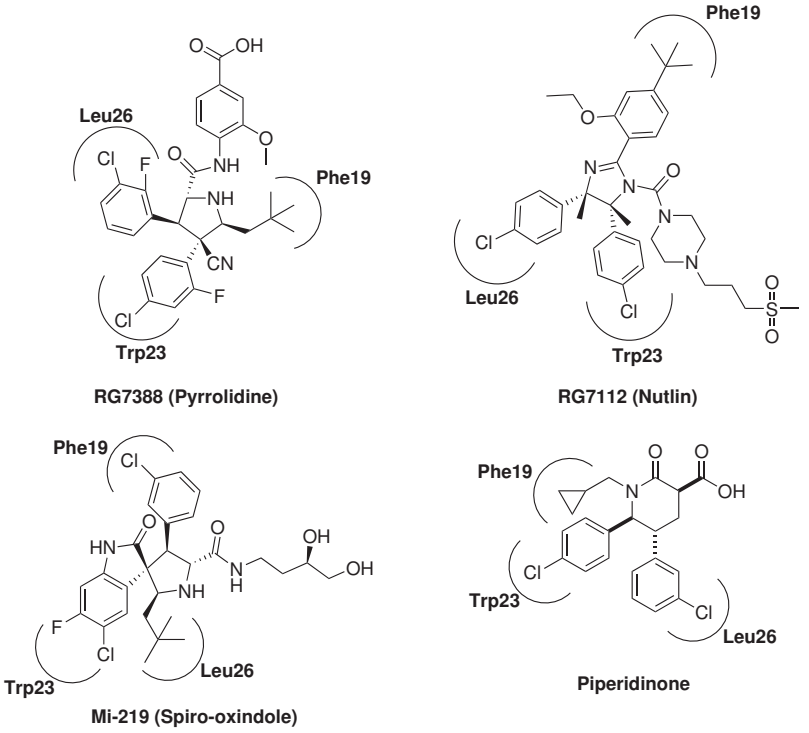

FIGURE 1.29: Binding epitopes of the top four classes of p53/MDM2 inhibitor

1.4.7 Peptide-Based Inhibitors

In addition to the research on small molecule inhibitors, there has been copious research on the used of peptide-based inhibitors, including stapled peptide and helical mimetics. Peptide-based inhibitors pose the advantage of the possibility of high specificity, potency and low levels of toxicity.[109] Initial work on peptide-based inhibitors started in 2000 by Furet *et al.*[110] Initial studies involved the binding of monoclonal antibodies to p53 regions to determine the key binding sequence. Peptides were sequenced haveing structural similarity to the p53 sequence with an acetylated N-terminus to permit entry into cells. Although the initial hexapeptide TFSALW was shown to bind to HDM2, it had a very weak binding affinity (IC_{50} = 700 μM). Further screening was undertaken on phage display libraries and examined by ELISA, which led to the discovery of a potent octapeptide Ac-FMDYWEGL-$CONH_2$ (IC_{50} = 8.95 μM). This peptide sequence was further optimised by substitution of aspartic acid with R-aminoisobutyric acid (Aib), tyrosine with 6-Cl- β,β-pentamenthylene-β-mercaptopropionic acid (Pmp-6-Cl),[111] and glycine with 1-aminocyclopropanecarboxylic acid (Ac_3c),[110] which resulted in an IC_{50} of 5 nM by ELISA.

In 2009, Lu *et al* further explored the use of peptide-based inhibitors using phage display. Phage display was carried out against biotinylated GST-tagged MDM2 and MDMX and

PMI (TSAFAEYWNLLSP)[78] was shown to be a high affinity binder. PMI had a K_d of 3.3 nM (MDM2) and 8.9 nM (MDMX) as analysed by isothermal titration calorimetry and surface plasmon resonance respectively. In the binding assays, p53(15-29) and p53(17-28) were used as comparators, where the numbers in brackets indicates the section of amino acids in the p53 sequence used in each assay.

Peptide-based inhibitors suffer from rapid degradation by enzymes. To overcome this problem an alternative strategy is to use D-amino acids. These are far more stable to proteolytic degradation, as enzymes present in the body are only capable of processing L-amino acids due to their stereospecificity. Using chemical ligation and mirror image phage display, DPMI-α (TNWYANLEKLLR) and DPMI-γ (DWWPLAFEALLR) were discovered. SpR analysis indicated K_d values of 219 nM for DPMI-α and 53 nM for DPMI-γ. Unfortunately, these peptides were unable to penetrate into cells and therefore showed no cytotoxicity in HCT116 p53 +/+ and HCT116 p53 -/-. Addition of an arginine-rich cell-penetrating peptide (TAT) led to nonspecific cytotoxicity in p53 +/+ and p53 -/- cells. This outcome has also been shown in other cell-penetrating peptides attached to p53-like sequences, in which tumour necrosis was induced without p53 activation. However, encapsulation of the peptide in liposomes with cyclic-RGD peptide (a fluorescent, cell-permeable peptide which shows whether or not the liposomes release into the cell) showed that the DPMI-alpha sequence was active in human glioblastoma and nude mice xenographs.

A second peptide, pDI (LTFEHAWAQLTS), was also discovered as a high affinity binder using ELISA against GST-MDM2 and GST-MDMX proteins.[112] pDI had an IC_{50} of 0.01 μM for MDM2 and 0.1 μM for MDMX. Peptide inhibition was also demonstrated using Western blot, showing a gradual decrease in the MDM2 and MDMX bands with increasing concentration of peptide.

Despite extensive work on peptide-based inhibitors against the p53/MDM2 interaction, there are currently no inhibitors in clinical trials. The reason that peptide research is of particular interest within this thesis is because chlorofusin, a peptide-based natural product, was used as the lead compound for analogues in chapters 3 and 4, whilst analogues of the chlorofusin peptide are the primary focus of 'Chapter 3'.

1.4.7.1 Helical β-peptide Inhibitors

Another way of reducing proteolytic degradation is to use β-peptides: these have an additional carbon spacer between the carboxylic acid and the amino group. Figure **1.30** illustrates the difference in secondary structure and binding of α- and β-p53 into the hydrophobic pocket of MDM2. The diagram illustrates that all of the key interactions

between p53 and MDM2 are maintained regardless of whether they are α- or β-peptides, however the decreased proteolysis of the β-peptides makes them more promising as drug molecules.

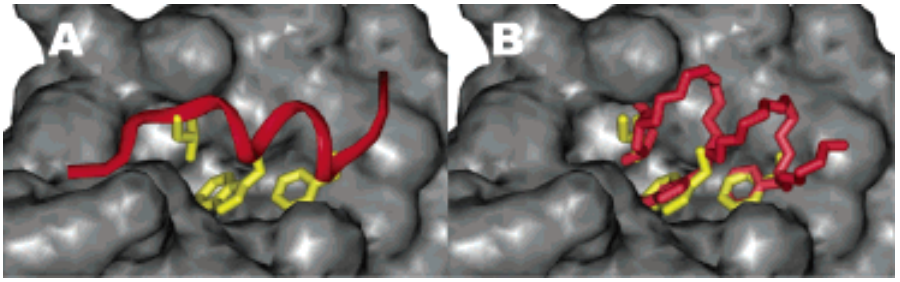

FIGURE 1.30: Differences in crystal structure between (A) the native p53 α-helix and (B) an ideal modified β-helix[113] (reproduced with permissions)

In 2004, Schpartz *et al* synthesised different variations of β53.[113] Firstly, the Phe[19], Trp[23] and Leu[26] interactions were mimicked by the corresponding β-amino acid of p53. Secondly, the p53 amino acids were replaced by β-alanine, as a drop in activity upon replacement with alanine would indicate importance for activity. The formation of the 14mer β53 helix was examined by circular dichroism, showing that between 30% and 50% of the peptide adopted the β-helix for sequences β53-1, β53-3 and β53-4 (each of which contain the key Phe[19], Trp[23] and Leu[26] amino acids, but in different positions). β53-1 and β53-3 showed inhibition of the p53-hMDM2 interaction by fluorescence polarisation, with IC_{50} values of 94.5 μM and 1589 μM respectively. Direct titration of fluorescently-tagged β53-1 to hDM2 produced a K_d of 368 nM.

1.4.7.2 Stapled Peptides

The p53 α-helix is only present when bound to MDM2 and remains disordered in solution at all other times.[114] One strategy of increasing the potency against MDM2 is to staple the peptide, so that p53 is always in the helical conformation (and hence permanently able to bind to MDM2), as shown in figure **1.31**.

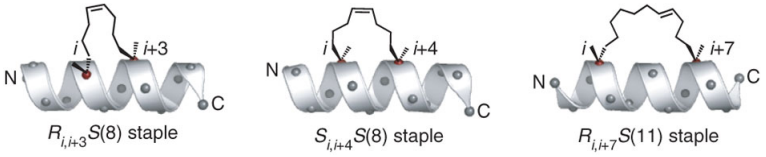

FIGURE 1.31: Three examples of different α-helical stapled peptides[114] the i, i+3, i+4 and i+7 refer to positions at which the staple (in this case, an olefin-based staple) can be attached to rigidify the peptide secondary structure (reproduced with permissions)

The staple generally consists of a hydrocarbon linker, which forms the staple through olefin metathesis at the attachment points indicated as i or i + n (where n is the distance from the inital attachment). Aryl staples have also been used as it was thought that these could further improve rigidity. The staple also has the added advantage of reduced proteolysis and can also increase cellular uptake.[115] SAH-p53-8 was synthesised by Walensky and coworkers: the sequence was based on p53 trasactivation domain, with replacement at S20 and P27 to contain olefinic side chains to form the staple. Interestingly, this sequence was shown to be active in nutlin-resistant cells.[116]

1.4.7.3 Peptide Helical Mimetics

As an alternative to α-helical peptide synthesis, α-helical mimetics have been studied, an example of which is shown in figure **1.32**. Again, the peptide helical mimetics are more stable to degradation than α-peptides.

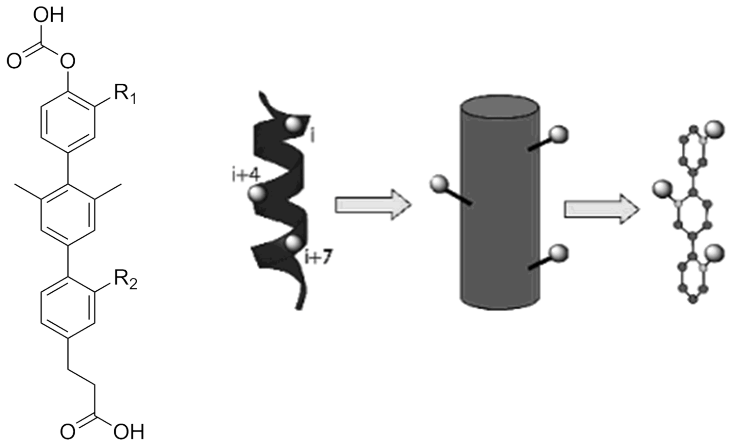

FIGURE 1.32: General structure of a peptide helical mimetic and the positions of i, i+4 and i+7. R1 and R2 indicate the positions at which lipophilic substituents (such as methyl and t-butyl) are introduced[117] (reproduced with permissions)

In 2005, Chen *et al* synthesised and examined terphenyl-based α-helical mimetics.[117] The terphenyl helix mimetics utilized Suzuki coupling to form the oligomerr. Carboxylic acid functionality was later introduced to improve aqueous solubility. The terphenyl analogues have substitution at the i, i+4 and i+7 positions to mimic the Phe^{19}, Trp^{23} and Leu^{26} interactions with the hydrophobic pocket. The terphenyl helix mimetics were initially tested in an ELISA assay, with the most potent inhibitors producing IC_{50} values between 10 μM and 20 μM, which are a great deal higher than the small molecules that have been synthesised against the p53/MDM2 interaction. The two most potent compounds were then introduced into HCT116 p53+/+ cells and caused 10-fold p53

activation at 10 μM, however there are currently no peptide helical mimetics currently in preclinical or clinical trials.

1.4.8 Chlorofusin: A Natural Product Inhibitor of the p53/MDM2 Interaction with Peptide and Small Molecule Properties

The Searcey lab has a great interest in using nature as an inspiration for the design and synthesis of drug molecules. The first natural product inhibitor of the p53/MDM2 interaction, chlorofusin (figure **1.33**), was of particular interest to the Searcey group due to its unnatural cyclic peptide and chromophore moietites.[118]

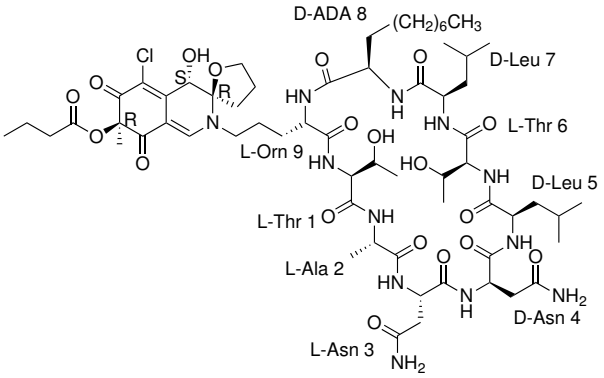

FIGURE 1.33: Structure of chlorofusin, indicating the amino acids and stereochemistry

Chlorofusin was first isolated in 2001 by Duncan *et al* from the *Fusarium sp. Microdocium caespitosum*, a type of marine sponge.[119] Initial structural work was carried out with a combination of ESI mass spectroscopy, ^{1}H-NMR, ^{13}C-NMR, COSY, NOESY and ROESY. ESI+ revealed masses corresponding to $(M+H)^{+}$ and $(M+Na)^{+}$, resulting in masses of 1363.7 Da and 1385.7 Da respectively.[118] There was also evidence of a chlorine atom due to isotopes present on the ESI spectra (a 3:1 ratio which corresponded to ^{35}Cl and ^{37}Cl). The ^{1}H-NMR data, ^{13}C-NMR data and 2D experiments permitted the assignment of the amino acid macrocycle, revealing an unnatural amino acid at position 8, aminodecanoic acid. The chromophore was assigned using a combination of ^{13}C-NMR and ^{1}H-NMR, revealing 8 quarternary carbons and a complex splitting pattern towards the aliphatic end of the spectrum. The initial screening was done using a DELFIA-modified ELISA assay, producing a K_d 4.7 μM and IC_{50} of 4.6 μM.

A follow-up paper was published by Duncan *et al* in 2002, detailing the modality of binding of chlorofusin to MDM2.[119] The binding of MDM2 to the N-terminus was studied using surface plasmon resonance. The MDM2 protein was immobilised onto the carboxymethlated dextran surface of the sensor chip through covalent bonding. MDM2

quantification was done using the Bradford method, Chlorofusin was passed over the surface of the chip containing either MDM2 or a ubiquitin control at varying concentrations. The data suggested that that chlorofusin initially binds to MDM2 rapidly, leading to a conformational change in the protein, after which there is a second, slower binding step. At present, this is the limit of our knowledge of the mode of chlorofusin binding to MDM2, as at present there are no crystal structures published.

In 2003, two papers were published on the chlorofusin peptide, one involving the first synthesis of the chlorofusin peptide (and diastereomers in an attempt to determine stereochemistry) on solid phase by Searcey *et al*[120] and one on the assignment of the asparagine stereochemistry by Boger *et al* completed using solution-phase chemistry.[121] The synthesis published by Searcey *et al* utilised Fmoc solid phase peptide synthesis with side-chain immobilisation on Rink Amide MBHA resin, followed by head-to-tail synthesis, followed by cyclisation.[120] The starting amino acid was Fmoc-Asp-ODMab, as the DMab group could be easily removed in the presence of hydrazine to uncover the free carboxylic acid, which could then cyclise with the terminal amine of asparagine in the presence of HOBt and DIC. All amino acids were purchased enantiomerically pure with the exception of 2-aminodecanoic acid. 2-Aminodecanoic acid was synthesised initially as a racemate and the enantiomers of the peptide sequence were separated by semi-preparative reverse phase HPLC, as the structural conformation at the time was unclear.

The 2003 paper published by Boger *et al* explored the total synthesis of chlorofusin and assignment of the asparagines at positions 3 and 4 in solution phase. Instead of synthesising the peptide in solid phase as per Searceys protocol, Boger synthesised the peptide in fragments using Boc, Fmoc, benzyl, SES and CBZ protection. The fragments were coupled together using HOAt and EDCI until the full cyclic peptide was produced. Four separate variants were synthesised by this method, each containing either 3-L-Asn or 3-D-Asn and 4-L-Asn or 4-D-Asn. ^{1}H-NMR and ^{13}C-NMR analyses compared to the natural product permitted the absolute stereochemical configuration of 3-L-Asn and 4-D-Asn.

In 2007, Yao *et al* examined the stereochemical assignment of the azaphilone chromophore of chlorofusin.[122] Retrosynthesis of the chlorofusin natural product initially separated the ornithine side chain from an isochromene. The isochromene was further analysed by ring opening of the furan side chain, hydrolysis of the butyl ester and ring opening to produce a Sonogashira precursor.

A variety of different azaphilone analogues were synthesised and condensed onto the ornithine side chain, each synthesised as a racemate. The compounds were separated by chiral HPLC and analysed by X-ray single crystal analysis. The analysis suggested

that the stereochemical configuration of the azaphilone was (4S,8R,9S). This was then challenged by Boger *et al* in the same year, who also analysed the different diastereomers against the natural product peptide.[123] Again, analysis was done by ^{1}H-NMR, ^{13}C-NMR, COSY, ROESY, HMQC, HMBC and it was shown that the stereochemical assignment of (4R,8S,9R) was a near-identical match to the natural product, whereas the assignment proposed by Yao *et al* showed distinct comparisons with the natural product.

In 2007, the first analogues of chlorofusin were synthesised by Searcey *et al.*[77] Using the methodology detailed in his 2003 paper, the cyclic peptide portion was analysed. This time, however, it was possible to synthesise enantiomerically pure Fmoc-Ada-OH using diethylacetoamidomalonate and 1-bromooctane, followed by hydrolysis and enzymatic resolution. Analogues of the peptide were synthesised as well as simple aromatic substitution in place of the natural azaphilone. ELISA assay was undertaken, but no hits were determined within the assay. Interestingly, although the stereochemistry was unimportant for activity, the whole molecule was required in order for binding to occur.

In conclusion, the structure of chlorofusin and its activity has been finalised and at present no analogues based on the whole chlorofusin molecule have been shown to be active against the p53/MDM2 interaction. Also, evidence for chlorofusins binding modality in the hydrophobic pocket of MDM2 is limited and at present there are no published crystal structures of this binding. Although inhibitors have already been explored, there is still scope for a wider variety of inhibitors to be investigated that have yet to be mentioned within the literature, which is one of the main purposes of this thesis.

1.5 Research Motivations and Objectives

Despite great strides in the development of novel inhibitors, there is still a need for optimisation due to resistance to treatment as well as solubility problems associated with targeting a hydrophobic pocket competitively. The focus of this thesis is to develop novel inhibitors of the p53/MDM2 interaction based on four different synthetic strategies. The first strategy was to synthesise small molecule combinatorial libraries for rapid analogue generation and screening. The second and third strategies used the natural product chlorofusin, which is fascinating due to its separate chromophore and peptide components, which both appear to be important for binding. This thesis focusses on utilising both the chromophore and the peptide separately, hence the second chapter focusses on simplefied chromophores linked to the peptide and chlorofusin analogues based on click chemistry, as the azide group is stable to proteolytic degradation, the azide serves as a bioisostere of the amide group and click chemistry permits the generation of a wide

variety of binding partners and hence a variety of analogues. The final synthetic chapter focusses on generating analogues of the azaphilone chromophore, with the potential to conjugate onto the native chlorofusin peptide.

Chapter 2

Synthesis, Characterisation and Biological Testing of Novel Isoquinolin-1-one Inhibitors of the p53/MDM2 Interaction

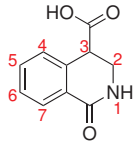

FIGURE 2.1: Structure of an isoquinolic acid and position numbering

The first compounds to be explored in this thesis are the isoquinolinones: they are highly amenable to rapid analogue generation through combinatorial means and have been previously shown to have activity against the p53-MDM2 protein-protein interaction in ^{15}N-HSQC studies undertaken by Rothweiler and coworkers.[124] It also bears similarity to the piperidinones, another class of p53-MDM2 inhibitors containing a 6-membered lactam functionality. The nature of the key reaction used to synthesise isoquinolin-1-ones, the Castagnoli reaction and its various incarnations have been well-documented in the literature.[125] This series of compounds can also be analysed not only for extensive structure-activity relationships, but to also serve as model compounds for molecular modelling studies and how different enantiomers may interact differently within the hydrophobic pocket.

2.1 The Castagnoli Reaction and its Evolution

The classical Castagnoli reaction was first detailed by Neal Castagnoli Jr and Mark Cushman in 1971.[125] The premise of the reaction is the condensation of a Schiff base with an acid anhydride. The anhydride used by Castagnoli in his initial studies was succinic anhydride. The Schiff base was produced by the condensation of a primary amine with an aldehyde. Both the imine formation and the subsequent Castagnoli reaction were heated to reflux and the imine formation also incorporated the use of Dean Stark apparatus to collect the water formed in the reaction, which prevented hydrolysis of the newly-formed imine. The imine proceeded to ring-open the anhydride through nucleophilic attack and reclose the ring through the formation of a γ-lactam. Although this method was successful, heating to reflux and the involvement of Dean Stark apparatus did not make this technique amenable to combinatorial synthesis, however Cushman adapted this work to produce tetrahydrocannabinols (THC),[126] topoisomerase I poisons see scheme **2.4**,[127] corydalic acid methyl esters[128] and nicotine analogues.[129]

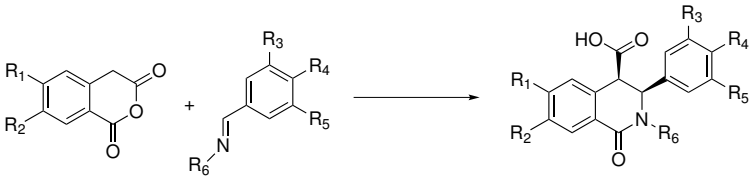

FIGURE 2.2: General scheme for the synthesis of topoisomerase I poisons[127]

The method used to synthesise the topoisomerase I poisons was undertaken at room temperature using homophthalic anhydride in chloroform. The compound produced then precipitated out of the organic solution and was then filtered and washed with further chloroform. If an alcohol was present on the side chain, a silyl group was used to protect during the synthesis, which was later removed when the isoquinolone structure was formed, as the alcohol could esterify in the presence of an acid anhydride.

The yields were moderate, ranging from 24% up to 64% depending on the analogue.

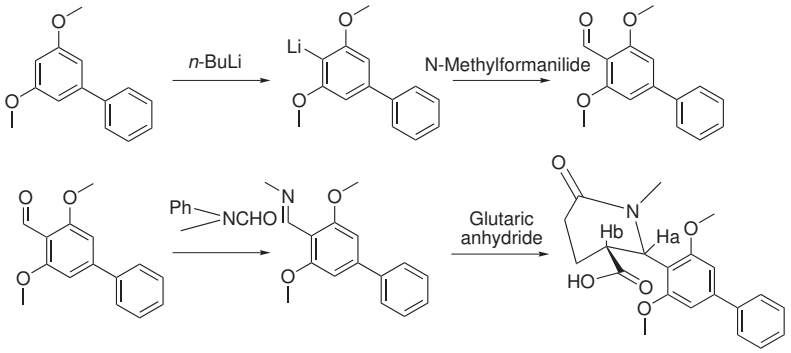

SCHEME 2.1: Synthesis of an example tetrahydrocannabinol analogue, produced by lithiation in the presence of *n*-butyllithium and subsequent formylation in the presence of N-methylformanilide. The final step resulted in an 86% yield of the final THC compound[126]

Scheme **2.1** shows the scheme for the synthesis of tetrahydrocannabinol. The tetrahydrocannabinols were synthesised through the formation of 2,6-dimethoxy-*n*-amylbenzaldehyde following lithiation of olivetol dimethyl ether and subsequent lithium exchange with N-formylanilide. The aldehyde was then reacted with methylamine to form the desired Schiff base. The imine was then refluxed in xylene with glutaraldehyde to form the desired piperidones, which were then separated by fractional distillation. The final racemic compound was isolated in 86% yield, whilst the major diastereomer was isolated in 45% yield and characterised through ^{1}H-NMR spectroscopy.

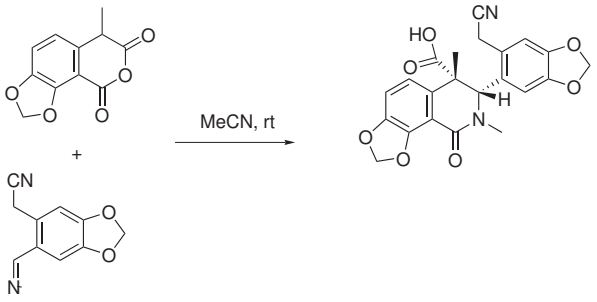

FIGURE 2.3: Synthesis of corydalic acid analogues

In the case of corydalic acid, the components were stirred at room temperature in acetonitrile for 1.5 hours, as in scheme **2.3**. The reaction produced excellent yields of circa 94% and was adapted to generate a library of analogues.

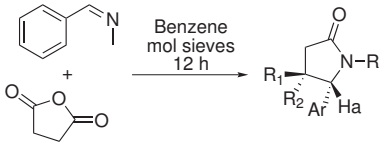

SCHEME 2.2: Synthesis of an example methylnicotine analogue[129]

Methylnicotine analogues were synthesised through the nucleophilic attack on succinic anhydride by a Schiff base in the presence of dry benzene for 12 h. The reaction produced excellent yields of circa 92% and the reaction was used to generate a wide variety of analogues.

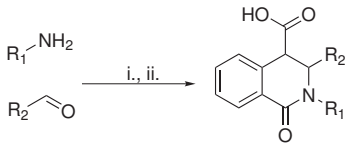

FIGURE 2.4: Modified Castagnoli reaction as a two-step, one-pot reaction i. $MgSO_4$, CH_2Cl_2, rt, 2-4 h ii. homophthalic anhydride, rt, overnight

Since the first published procedure variants of this have permitted the production of large combinatorial libraries, as imine formation can be undertaken in the presence of magnesium sulphate at room temperature (see scheme **2.4**).[104]

The use of alternative anhydrides such as homophthalic anhydride permitted the second step of the reaction to be carried out at room temperature, as these anhydrides were more reactive.[130] Generally, these reactions are undertaken in methylene chloride and, in many cases, the resulting product precipitates out of the methylene chloride and can be purified by recrystallization, or simply through washing with hot ethyl acetate. In some cases, where the product was soluble in methylene chloride, the compound was purified by column chromatography.

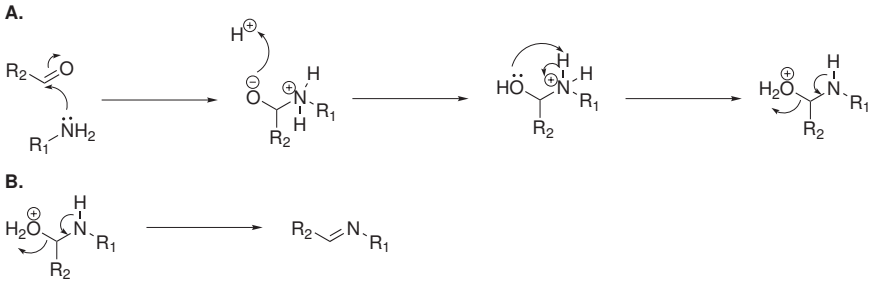

FIGURE 2.5: Mechanism of imine formation between an aldehyde and a primary amine A. addition of the aminde to the aldehyde B. elimination of water to form the imine

Imine formation occurs between a primary amine and an aldehyde under anhydrous conditions (see scheme **2.5**). The reaction can be acid-catalysed, which causes protonation of the ketone, increasing electrophilicity and increasing the likelihood of nucleophilic attack by the amine. In this case, an acid catalyst was not required.

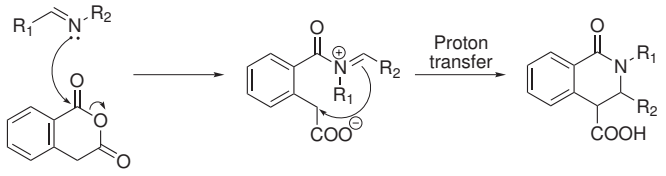

FIGURE 2.6: Mechanism of Schiff base nucleophilic attack on homophthalic anhydride. The R2 and hydrogen can adopt two different conformations, which will determine whether or not the material is cis or trans

The imine/Schiff base undertakes nucleophilic attack on the ketone carbon, causing ring opening, as shown in scheme **2.6**. The intermediate is then able to undergo proton transfer to reclose the ring. This methodology is stereoselective, but the individual enantiomers, in any case, require chiral preparative HPLC to isolate each enantiomer.[124]

The aim of this chapter is to synthesise a racemic library of isoquinolin-1-ones to be screened by fluorescence polarisation against the p53/MDM2 protein-protein interaction (preparation of the protein was undertaken with the assistance of Dr. Richard Steel, Dr. Tony Blake and Dr. Alex Roberts, whilst preparation of SDS PAGE gels for analysis were undertaken with the assistance of Dr. Jess Di Gesso and Dr. Jenna Bradley). Compounds that were shown to inhibit the p53/MDM2 interaction were then tested for antiproliferative activity using MTS (the preparation of cells and plating of cells was undertaken with the assistance of Dr. Maria O'Connell). The reason for using fluorecence polarisation was that it is a rapid technique (preparation and data collection can be done in an hour compared to a day as is the case of in an ELISA assay). Also, reagents for the FP assay were readily available and low cost compared to other assays (for example, antibodies required for ELISA are costly). The rationale for the MTS assat was to determine cell permeability as well as antiproliferative activity in p53-null, wt p53 and overexpressed MDM2 cell lines.

Subsequently, the diastereomers and enantiomers would be synthesised separately to examine any differences, firstly to determine if it was active and the degree of activity and secondly, to examine the binding epitope using a combination of STD NMR (preparation of samples and processing of data was undertaken under the supervision of Dr. Jesus Angulo) and molecular modelling (image generation was undertaken with the assistance of Dr. Onur Atasoylu). STD NMR was selected as this technique allows

for accurate visualisation of the binding epitope generated by experimental data, which gives a greater idea of binding compared to 15N-HSQC (for example).

2.2 Synthesis of Isoquinolin-1-one Analogues

Isoquinolin-1-ones contain a γ-lactam functionality, bearing similarity to the isoquinoline core of a condensed azaphilone. The advantage of the synthesis of the isoquinolin-1-one is that it is facile and the product generally precipitates out, only requiring purification by hot ethyl acetate washing, however this was only feasible when the compounds were highly insoluble in organic solvents. The methods undertaken here are diastereotopically-selective but not diastereotopically-specific (the trans conformation appears to be the dominant diastereomer in the literature as it is more thermodynamically stable), however there are procedures in the literature that allow for selection over different diastereomers, for example through the use of silica-supported perchloric acid to isolate the cis conformation only or refluxing in acetic acid to isolate the trans conformation only.[131]

The general procedure for the synthesis of this library is the formation of an imine by reacting an aldehyde and an amine under anhydrous conditions in the presence of magnesium sulphate. The resultant Schiff base then acts as a nucleophile and attacks homophthalic anhydride at the aryl carbonyl, producing an isoquinolin-1-one with a carboxylic acid in the 3-position (see figure **2.6**). This can be further functionalised by reacting with a primary amine to form an amide bond, which could in theory be used to improve aqueous solubility, as demonstrated in the 2008 publication by Rothweiler *et al*.[124]

2.3 Design of Isoquinolin-1-one Analogues

Evidence proposed by Huang *et al* in 2012 and Wang *et al* in the same year suggested an importance of halogens for their directing effects into the hydrophobic pockets. This data, combined with previously reported isoquinolin-1-ones bearing aromatic substituents to allow for π-π stacking, were used to synthesise a wide variety of analogues (at the R1 and R2 positions on the isoquinolin-1-one product indicated on **2.6**) as well as comparators to allow for structure-activity relationship analysis.[132,133]

The first generation library consisted of benzyl substituents on the R_1- and R_2- positions to serve as an initial comparator (See figure **2.14**). This was then developed further by producing monosubstituted aromatics such as methyl, ethyl, methoxy, ethoxy and halogens in the ortho, meta, and para position on the aromatic groups in positions 1- and

2- of the isoquinolin-1-one. Following on from this, di- and tri- substituted aromatics were screened in a fluorescence polarisation assay.

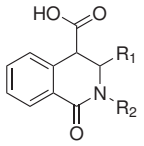

FIGURE 2.7: General structure of the isoquinolinone scaffold in the generated analogues

Table **2.1**, table **2.2**, table **2.3** and table **2.4** display the yields of the different isoquinolin-1-ones synthesised, the ratio of diastereomers, the key ^{1}H-NMR characterisation of the major diastereomers present and the mass spectrometry data observed. The letter 'A' refers to all compounds synthesised in this chapter and the compounds were numbered sequentially.

No.	**R1**	**R2**	**% Yield**	**Cis-to-Trans Ratio**	**δ_H(diastereotopic protons) in ppm**	***J*-value in Hz**	**MS**
A01	2,5-diOMePh	Bn	30	1:0	4.52 to 4.54 and 5.38 to 5.39	6.09	440.1
A02	2,4-diMePh	Bn	4	1:0	4.52 to 4.54 and 5.10 to 5.12	6.25	408.1
A03	4-OEtPh	Bn	20	1:0	4.64 to 4.66 and 4.90 to 4.91	6.00	416.5
A04	4-EtPh	Bn	16	0:1	4.07 and 5.22	0*	385.9
A05	2-OH,5-NO_2Ph	Bn	29	1:2	3.86 and 5.54	0*	419.1
A06	4-ClPh	Bn	9	1:1	3.92 and 3.96 (trans); 4.70 to 4.72 and 5.00 to 5.01	0*, 8.07	392.1
A07	4-BrPh	Bn	2	Not examined	Not examined	Not examined	458.0
A08	2-FPh	Bn	9	1:1	4.15 and 5.18; 4.72 to 4.74 and 5.06 to 5.08	0*	376.1 and 398.1
A09	3-Ph	Bn	8	1:0	4.69 to 4.70 and 4.97 to 4.98	6.76 and 4.51	358.1
A10	3-Pyr	Bn	58	0:1	4.16 and 5.40	0*	359.1
A11	4-Pyr	Bn	29	0:1	4.17 and 5.36	0*	359.1

Table 2.1: Table of all synthesised first generation isoquinolin-1-ones

No.	**R1**	**R2**	**% Yield**	**Cis-to-Trans Ratio**	**δ_H(diastereotopic protons) in ppm**	***J*-value in Hz**	**MS**
A12	3-Thio	Bn	2	1:0	4.62 to 4.63 and 5.09 to 5.10	8.09	364.1
A13	3-PhOPh	4-MeBn	16	0:1	4.04 and 5.25	0*	464.1
A14	2,4-diMePh	4-MeBn	31	1:0	4.52 to 4.54 and 5.08 to 5.10	6.68	399.9
A15	4-OEtPh	4-MeBn	22	1:0	4.58 to 4.59 and 4.86 to 4.87	7.35 and 5.88	415.9
A16	4-EtPh	4-MeBn	23	0:1	4.05 and 5.17	0*	400.1
A17	4-ClPh	4-MeBn	2	0:1	4.08 and 5.25	0*	404.1059
A18	4-Cl,3-CF_3Ph	4-MeBn	32	0:1	4.17 and 5.46	0*	474.1
A19	4-BrPh	4-MeBn	4	0:1	4.07 and 5.23	0*	450.9
A20	2-FPh	4-MeBn	8	0:1	2.25 and 4.12	0*	389.9
A21	3-Thio	4-MeBn	37	1:3	4.15 and 5.28	0*	377.9
A22	2,4-diMePh	4-OMeBn	41	1:0	4.51 to 4.59 and 5.08 to 5.10	7.19 and 6.16	416.1
A23	2-OH-5-NO_2Ph	4-OMeBn	22	0:1	4.03 and 5.50	0*	449.3
A24	2-NO_2Ph	4-OMeBn	31	0:1	4.15 and 5.88	0*	433.4
A25	2-FPh	4-OMeBn	45	0:1	4.13 and 5.30	0*	388.9
A26	3-Pyr	4-OMeBn	66	0:1	4.17 and 5.33	0*	468.2

TABLE 2.2: Table of all synthesised first generation isoquinolin-1-ones

No.	**R1**	**R2**	**% Yield**	**Cis-to-Trans Ratio**	**δ_H(diastereotopic protons) in ppm**	***J*-value in Hz**	**MS**
A27	3-PhOPh	4-FBn	28	0:1	4.06 and 5.29	0*	468.2
A28	2,5-diOMeBn	4-FBn	53	1:0	4.55 to 4.56 and 5.39 to 5.40	5.84	465.9
A29	2,4-diMeBn	4-FBn	11	1:0	4.56 to 4.58 and 5.11 to 5.13	6.65	403.9
A30	4-OEtPh	4-FBn	33	0:1	4.06 and 5.29	0*	420.1
A31	4-EtPh	4-FBn	19	0:1	4.07 and 5.22	0*	404.1
A32	2-OH-5-NO_2Ph	4-FBn	25	0:1	4.06 and 5.50	0*	436.9
A33	2-NO_2Ph	4-FBn	51	0:1	4.17 and 5.92	0*	420.9
A34	4-ClPh	4-FBn	43	0:1	4.08 and 5.31	0*	410.1
A35	4-Cl,3-CF_3Ph	4-FBn	50	0:1	4.13 and 5.49	0*	478.2
A36	4-BrPh	4-FBn	30	0:1	4.04 and 5.26	0*	454.0449
A37	2-FPh	4-FBn	47	0:1	4.05 and 5.35	0*	478.2
A38	3-Ph	4-FBn	62	0:1	4.04 and 5.41	0*	376.1
A39	3-Pyr	4-FBn	49	0:1	4.15 and 5.41	0*	376.9
A40	4-Pyr	4-FBn	52	0:1	4.18 and 5.35	0*	376.9
A41	3-Fur	4-FBn	36	0:1	4.07 and 5.16	0*	366.2
A42	4-IPh	4-FBn	4	0:1	4.09 and 5.25	0*	502.0312
A43	3-BrPh	4-FBn	48	0:1	4.13 and 5.35	0*	456.1

TABLE 2.3: Table of all synthesised first generation isoquinolin-1-ones continued

No.	**R1**	**R2**	**% Yield**	**Cis-to-Trans Ratio**	**δ_H(diastereotopic protons) in ppm**	***J*-value in Hz**	**MS**
A44	3,4-diBrPh	4-FBn	55	0:1	4.12 and 5.34	0*	534.0
A45	2-ClPh	4-FBn	23	0:1	4.03 and 5.57	0*	432.1
A46	3-PhOPh	4-ClBn	52	0:1	3.98 and 5.32	0*	484.3
A47	4-ClPh	4-ClBn	71	0:1	4.11 and 5.30	0*	426.0658
A48	4-Cl,3-CF_3Ph	4-ClBn	57	0:1	4.10 and 5.49	0*	494.0
A49	4-BrPh	4-ClBn	29	0:1	4.09 and 5.28	0*	470.0153
A50	3-Ph	4-ClBn	37	0:1	4.11 and 5.28	0*	392.1
A51	3-BrPh	4-ClBn	47	0:1	4.16 and 5.34	0*	469.9
A52	4-NO_2Ph	4-ClBn	29	0:1	4.19 and 5.49	0*	437.1
A53	4-ClPh	4-BrBn	14	0:1	4.10 and 5.31	0*	470.0153
A54	4-BrPh	4-BrBn	19	0:1	4.06 and 5.29	0*	563.9
A55	3-Ph	4-BrBn	38	0:1	4.09 and 5.26	0*	515.9
A56	4-IPh	4-BrBn	5	0:1	4.10 and 5.25	0*	607.9
A57	3-BrPh	4-BrBn	49	0:1	4.16 and 5.34	0*	505.9
A58	4-IPh	4-IBn	24	0:1	3.94 and 4.33	0*	426.1
A59	4-BrPh	3,4-diClBn	29	5:1	4.83 to 4.84 and 5.13 to 5.15	6.17	505.9
A60	3-Ph	3,4-diClBn	29	1:0	4.12 to 4.13 and 5.35 to 5.36	1.20	448.0

TABLE 2.4: Table of all synthesised first generation isoquinolin-1-ones continued

2.4 Discussion of the Isoquinolin-1-ones Generated

^{1}H-NMR revealed that the diastereotopic protons in the trans conformation did not undergo splitting, whereas cis-oriented protons were split into doublets. This phenomenon value is explained with the Karplus equation (equation 2.1).[134]

$$J(\phi) = Acos^2\phi + Bcos\phi + C \tag{2.1}$$

The Karplus equation states the effect that the degree of torsion within a bond affects the J-coupling value. ϕ refers to the angle of torsion whilst J refers to the J-coupling value whilst A, B and C are parameters that vary depending on the constituent atoms within the molecule. As angle ϕ exceeds 90°, J tends towards 0 (as cos90 = 0 whilst higher angles will result in the A and B terms cancelling out).

Despite previous published data suggesting that the trans conformation was more energetically stable,[124] the characterisation data illustrated that the diastereomer synthesised was highly dependent on the substituents of the amine and the aldehyde: an unsubstituted benzylamine precursor predominantly led to the production of the cis isomer, with the exception of pyridine- and nitro- containing analogues. The inclusion of halogenated benzylamine precursors in the synthesis generally led to a predominant trans isomer, with the exception of the dichlorobenzylamine precursor analogues. Also, all of the methoxybenzylamine precursor analogues produced the trans conformation, with the exception of one compound. Interestingly, the majority of the analogues synthesised contained predominantly one diastereomer, with the exception of **A06** (4-chlorophenylbenzaldehyde and methylbenzylamine precursors) and **A08** (2-fluorophenylbenzaldehyde and dichlorobenzylamine precursors).

In addition to the ^{1}H-NMR characterisation which indicated both the structure and the conformation, this was also teamed with COSY, ^{13}C-NMR and HSQC experiments to determine the spatial relations between carbons and hydrogens (see Appendices 'A', 'B', 'C' and 'D' for the model spectra for **A34** and how the data was interpreted). LCMS was also used to determine that compounds were of the correct molecular weight, as well as to examine isotope patterns (for example the 3:1 ratio of chlorine isotopes). IR spectroscopy was used for completeness to determine the presence of the carboxylic acid and the amide carbonyls.

In terms of the percentage yield for the generation of analogues there was a great deal of variability. Low yields were attributed to low levels of precipitation (as the mixture remaining after precipitation was not further purified). It is also possible that alternative

diastereomers remained in the mixture and did not precipitate and were therefore not isolated.

In the case of compounds in which there was no precipitation, the product was isolated through column chromatography, which proved troublesome as many of the compounds present in the mixture had similar Rf values in different solvent systems (the two normal-phase systems used were ethyl acetate:hexane and methylene chloride:methanol).

2.5 *In vitro* Screening of Compounds Using Fluorescence Polarisation

2.5.1 Principle of Fluorescence Polarisation

Fluorescence anisotropy can be used in a type of biochemical *in vitro* assay to determine binding of ligands to macromolecules. Readings are taken due to a difference in the rotation of plane-polarised light, caused by a change of rotation speed by a fluorescently-tagged binder is measured, which can also be explained as a difference in signal intensities along different degrees of polarisation. This principal has been adopted to examine ligand binding as disruption of the fluorescently-tagged compound-protein complex causes a decrease in anisotropy.

When a fluorescently-tagged binder is tumbling freely in solution, it tumbles rapidly: this means that when the binder is intercepted by plane-polarised light, the light will scatter and only a small amount of plane-polarised light is detected (giving a low anisotropy). When the fluorescently-tagged binder attaches to another macromolecule (such as a protein) the speed of tumbling greatly slows down, hence when the complex is hit by plane-polarised light then a much higher percentage of light remains polarised after interception. This phenomenon can be explained mathematically, as shown in equation **2.2** and equation **2.3**.

$$FP = \frac{I_{\text{II}} - I_{\perp}}{I_{\text{II}} + I_{\perp}} \tag{2.2}$$

$$FA = \frac{I_{\text{II}} - I_{\perp}}{I_{\text{II}} + 2I_{\perp}} \tag{2.3}$$

The above equations are mathematical representations of fluorescence polarisation (FP, equation **2.2**) and fluorescence anisotropy (FA, equation **2.3**) analysis, where I_{II} refers

to the fluorescence intensity parallel to the excitation plane and $I_{\perp}$ refers to the fluorescence intensity perpendicular to the excitation plane. Although FP and FA are used interchangeably, the FA also takes into account twice the perpendicular light emitted from the sample and therefore incorporates a greater degree of rotation in the FA equation.[76]

The assay can be used to examine direct binding, competitive binding and enzymatic conversion, the former two of which are adapted in the assay firstly to illustrate direct binding of the fluorecently-tagged probe to the protein and the displacement of the probe through the introduction of a potential inhibitor.[135]

As this is a difference-based assay it would be correct to assume that a larger difference in size between the fluorescently-tagged binder and the macromolecule will result in a larger minimum and maximum anisotropy difference. One challenge of attempting this is that the HDM2 portion of the protein used within this assay is relatively small (14.2 kDa). This means, although there is a detectable and reproducible difference, the difference in the minimum and maximum anisotropy values are smaller than if it was a larger protein.

Another limitation of this methodology is, if the inhibitor being tested bears any intrinsic fluorescence or absorbance in the region that is being analysed then the assay can produce false positives or negatives and hence a second form of testing is required to confirm results. Alternatively, the fluorophore can be changed to a fluorophore that is red-shifted and therefore will not interfere with the assay.

It is also important to note that each varying concentration of protein was repeated in triplicate to ensure reproducibility, although there is still the possibility of inter-batch variation (that is, where new containers of protein were used). Inter-batch variation was caused by using new reagents and different batches of the fluorescently-tagged peptide and protein, however this was also examined during the process of the biological experiments (wt p53 inhibition was examined on two different days to examine the effect on the IC_{50} and K_i values). Inter-batch variation was found not to have a profound effect on final IC_{50} and K_i values.

This methodology has been adapted for the examination of protein-protein interactions, as the procedure is much more rapid than ELISA (hence its application in high throughput screening), the reagents are much cheaper and also readily available (for example, there is no need to source expensive antibodies).

2.5.2 Synthesis of Components for Fluorescence Polarisation

In order to undertake the FP assay, the fluorescently-tagged peptide and the protein were synthesised in-house. The techniques used to synthesise these components are described below. The fluorescently-tagged peptide used in the assays described in this thesis was first published by Czarna *et al.*:[136] it was chosen due to its higher affinity for HDM2 than wt p53, which reduced the quantity required per run of the assay.

2.5.2.1 Synthesis of the Fluorescently-Tagged Peptide for Fluorescence Polarisation, A65

Fmoc solid phase synthesis (scheme **2.3** is a well-documented series of reactions utilised in order to synthesise long polymer chains, in particular peptides, through a series of deprotection and coupling reactions. Solid phase synthesis involves the synthesis of polymers on a solid support, which is acid-labile in the case of Fmoc (or base-labile in the case of Boc), so that cleavage from the resin does not occur prematurely. There is a wide variety of different resins available, which can produce different carboxy termini: in this case, MBHA Rink Amide resin was used, as the carboxy terminus is unimportant for binding and amides are easier to prepare than carboxylic acids, as an amide can be prepared using a standard coupling and be monitored using the Kaiser test, whereas an initial ester formation cannot be monitored and requires the preparation of a symmetrical anhydride to increase reactivity.

The first example of solid phase peptide synthesis was determined by Merrifield in 1963.[137] It involved the formation of a tetrapeptide through attachment of amino acids onto a modified polystyrene solid support with acid-labile protection of the amine. Deprotection of the amine occurred in the presence of TFA and washes were completed using DMF to remove any residual reagents and prevent side reactions. Cleavage of the peptide from the resin is undertaken using HF, as the linker is acid-labile to prevent premature cleavage. This method is effective and is still used today, however the presence of TFA and HF means that the reaction cannot be automated, as TFA and HF could react with the vials or the equipment. As an alternative, Fmoc-driven synthesis has generally superseded Boc solid phase synthesis, although there may still be instances in which Boc synthesis maybe preferred, such as the incorporation of specialised unnatural amino acids.

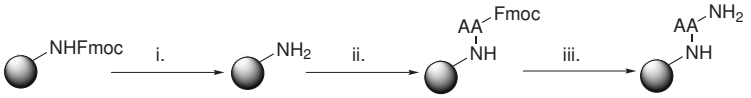

SCHEME 2.3: General example scheme for Fmoc solid phase peptide synthesis used to generate peptides within this thesis. i. Fmoc deprotection of the Rink Amide MBHA using 40% and 20% piperidine in DMF. ii. Attachment of the first amino acid using HOBt, HBTU, DIPEA, AA and DMF. iii. Fmoc deprotection of the amino acid using 40% and 20% piperidine in DMF

The principle of Fmoc-driven synthesis involves the use of the fluorenylomethoxycarbonyl (Fmoc) group, which is a base-labile amine-protecting group. Fmoc can be efficiently removed in the presence of either piperidine or piperazine, with the latter conferring an additional benefit of reduced racemisation during synthesis.[138] This deprotection can be determined through Kaiser testing, in which the ninhydrin component is able to form a complex with the free amine, resulting in deep blue resin beads, for which the reaction scheme is shown in scheme **2.4**.[139,140] The primary amine reacts with a hydroxyl group to form a complex, which is then decarboxylated and undergoes further rearrangement. The resultant intermediate is hydrolysed and a second molecule of ninhydrin reacts, forming Ruhemann's purple, which is the deep blue colour observed if primary amines are present. The Kaiser test is the most commonly used test to determine coupling reaction completion, however it is important to note that this is destructive and therefore each test will be to the detriment to the overall yield. To prevent side chain reactions during the process, reactive side chains are protected with acid-labile groups, which would not deprotect prior to cleavage from the resin.

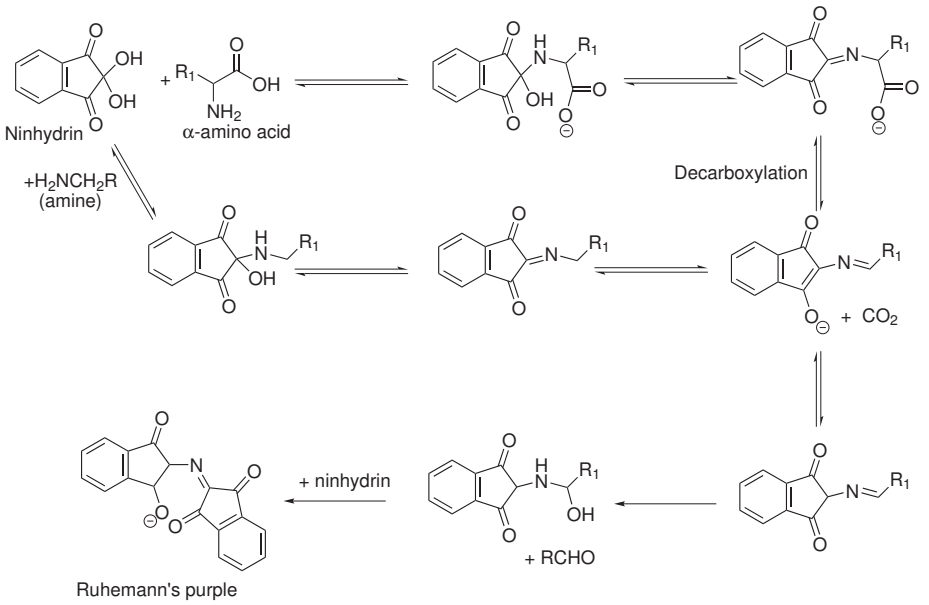

SCHEME 2.4: Scheme for the generation of the Ruhemann's purple complex generated from the reaction of ninhydrin with a primary amine

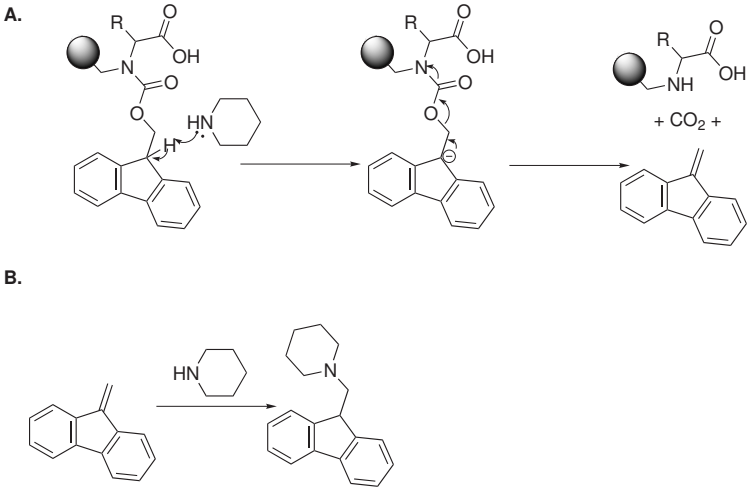

SCHEME 2.5: Fmoc deprotection in the presence of piperidine. A. Deprotonation in the presence of piperidine results in a negative charge, which leads to cleavage of the carbamate and decarboxylation. B. a second molecule of piperidine reacts with the decarboxylated Fmoc group

Scheme **2.5** illustrates the mechanism for Fmoc deprotection. In the presence of base (usually piperidine or piperazine), the Fmoc group becomes deprotonated. The resultant negative charge feeds into the carbamate, resulting in cleavage of the bond and release of the free amine, carbon dioxide and an aromatic intermediate that can further react with another molecule of base.

Following Fmoc deprotection (and subsequent washing with copious amounts of DMF to prevent premature Fmoc removal of the next amino acid), amino acids are attached sequentially, using HOBt, HBTU and DIPEA to form amide bonds for peptides synthesised within this thesis. Each coupling was undertaken with 5 equivalents of all reagents (except for DIPEA, for which 10 equivalents were used). Each coupling was reacted for 30 minutes, after which a Kaiser test was undertaken to determine if there was any unreacted free amine, which would indicate an incomplete coupling. If the coupling was incomplete, the reagents were refreshed and a second coupling was undertaken, as this would force the reaction towards completion.

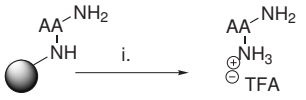

SCHEME 2.6: General example scheme for cleavage of the peptide from the resin i. 95:2.5:2.5 TFA:H_2O:TIPS

The finished peptide was washed five times with DMF, then three times with CH_2Cl_2 then three times with 1:1 MeOH:CH_2Cl_2. The peptide on resin was then treated with 95%:2.5%:2.5% TFA:H_2O:TIPS for 3 h to cleave the peptide from the solid support, with the TIPS and H_2O scavenging free radicals to quench any side reactions caused during side chain deprotection. The cleaved peptide was drained off and the resin washed three times with neat TFA to wash off any residual peptide and the peptide was concentrated *in vacuo*. The organic impurities were removed through precipitation of the peptide using cold diethyl ether and subsequently filtered. Purification was then performed using reverse-phase preparative HPLC.

The peptide described by Czarna, LTFEHAQWYLTS-$CONH_2$, was synthesised in house on solid phase and 5(6)-FAM attached via the N-terminus. Upon purification, the two diastereomers were separated through semi-preparative HPLC and it appeared that the minority isomer (the less intense peak by HPLC) was 10-fold more active than the alternative stereoisomer. The most potent stereoisomer produced a K_D for HDM2 comparable to the literature (1.44 nM experimentally-derived versus 5.40 nMin the literature).[136]

2.5.2.2 Expression of the HDM2 Protein for Fluorescence Polarisation

Due to the complexity of proteins, it is necessary for these to be synthesised biosynthetically to ensure correct folding, so that the structure of the hydrophobic pocket is maintained. The sequence of the protein was encoded and inserted into a bacterial

plasmid. In order to produce sufficient plasmid to cause protein expression, the His-HDM2 (pET14b) plasmid was first transfected into cloning cells (JM109), which rapidly produced large quantities of the plasmid. Following transfection, the bacteria was cultured and grown overnight, lysed, and then treated with a commercially-available DNA miniprep kit to isolate the plasmid (see 'Experimental' section). Prior to transfection into expression cells (BL21(DE3)PLysS), the plasmid was sent for sequencing to ensure that no mutations occurred during bacterial growth.

Transfection was performed on BL21(DE3)PLysS cells. This particular cell line contains an enzyme that helps to lyse the cells during the centrifugation process, which aids the release of the protein. The cells were grown overnight (20 mL) and a sample taken for a large-scale growth in 2 x 3 L of media, as the fresh media encouraged growth. The production of protein is undertaken at an optical density (OD) of 0.6, as this is when the bacteria are growing in the log phase and production of the protein would be rapid. At this point, Isopropylβ-D-1-thiogalactopyranoside (IPTG) is added, which stimulates the *lac* operon (which is usually inhibited) to become active and start producing the protein. IPTG is a type of sugar subunit and causes displacement of the *lac* repressor, which serves the general purpose in bacteria of preventing protein expression under normal conditions.

Following overnight culture growth, it was found that growing the bacteria overnight at room temperature was more effective than growing at 37°C for 5 h (which is also standard protocol). Overnight growth at room temperature allows bacteria to grow more slowly, hence reducing the rate for competition for nutrients and therefore appeared in this case to produce protein more effectively. The bacteria was then lysed and centrifuged. The lysate was then passed through a nickel-affinity column (as the protein is His-tagged and therefore will adhere to the column in low concentrations of imidazole and elute from the column in high concentrations of imidazole). The fractions, non-bound eluent and the cell lysate were analysed by 15% SDS-page. Pure fractions were then dialysed and concentrated through spin filtration using a 5 kDa filter, as the protein was only 14.2 kDa and the low porosity was necessary to prevent the protein passing through. The final protein concentration was determined using nanodrop using the Beer-Lambert law (equation **2.4**), in which A is the absorbance of the protein, ϵ indicates the extinction coefficient of the protein, c is the concentration of protein in the sample and l is the pathlength that the light travels through the sample:

$$A = \epsilon c l \tag{2.4}$$

This produced a concentration of 44.1 μM of HDM2 protein in buffer (10 mM PBS, 10% glycerol, 10 mM β-mercaptoethanol, dd H_2O).

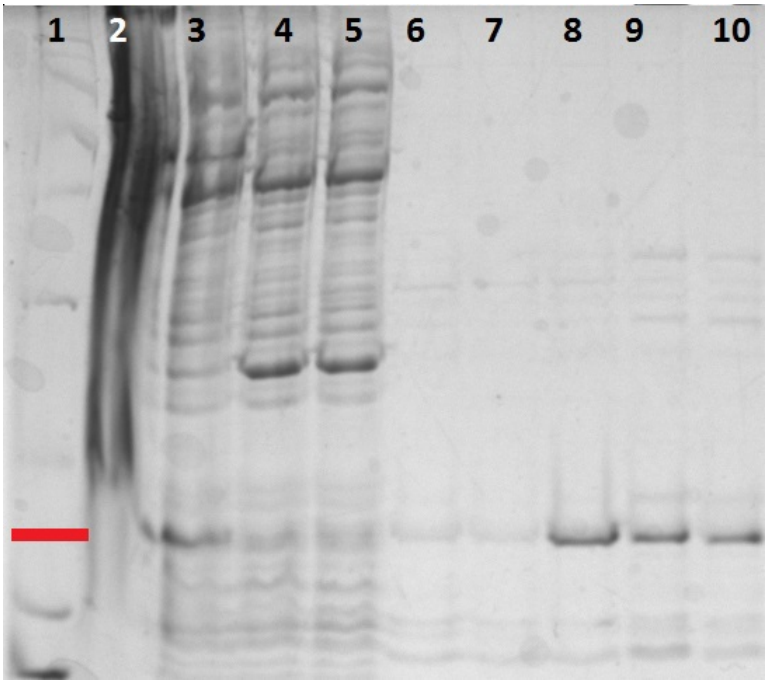

FIGURE 2.8: Gel image of His-HDM2 purification on a nickel-affinity column lane 1. gel ladder (red line indicates 14.2 kDa) lane 2. Undiluted pellet lane 3. Cell lysate lane 4. and lane 5. Not bound 6. lane and lane 7. wash fractions lanes 8., 9. and 10. eluted fractions

Figure **2.8** illustrates the SDS-PAGE gel used to analyse the purification of the protein. The ladder was used in the first lane to determine the presence of the desired molecular weight. The undiluted pellet was added to determine if any of the protein remained following lysis of the cell and centrifugation. The crude cell lysate determined whether or not the protein was present in the sample prior to application to the column. The unbound lysate was added to determine if the protein in question bound to the column. Wash fractions and elution fractions were added to determine firstly the presence of the protein and secondly, whether or not the protein was pure.

2.5.3 Setup of the Fluorescence Polarisation Assay

2.5.3.1 Preliminary runs to determine the working concentration of HDM2 for the FP assay

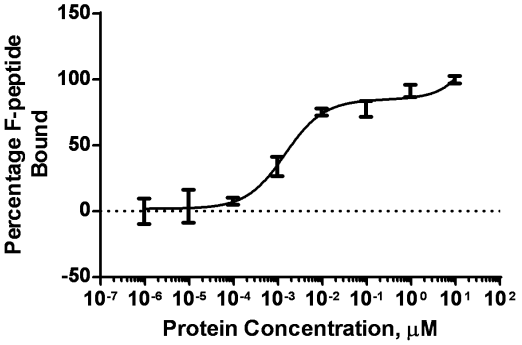

FIGURE 2.9: Binding curve for the FAM-LTFEHAQWYLTS-$CONH_2$, K_D = 1.448 nM (95% CI 0.7608 nM to 2.135 nM), mean +/- SEM, n = 3, 10−2 to 10^{-6} μM HDM2 (17-125), 10 nM F-LTFEHAQWYLTS-$CONH_2$

Figure **2.9** illustrates the initial triplicate runs of the fluorescently-tagged peptide incubated with various concentrations of the HDM2 peptide. HDM2 was titrated at 10-fold dilutions ranging from 956 fM to 9.56 μM. The fluorescently-tagged peptide remained constant at 10 nM. The buffer used was PBS-0.05% Tween-20 (the Tween-20 acting as a surfactant and preventing protein adhering to the sides of the wells) at pH 7.4.

As the concentration of the protein increases, there is less of the free fluorescently-tagged peptide present and therefore there is a high anisotropy value. The sigmoidal curve is due to the saturation of the fluorescently-tagged peptide at high concentrations of protein.

2.5.3.2 Preliminary run to determine experimental K_D of positive control inhibitor

Figure **2.10** shows the displacement of the fluorescently-tagged peptide following the inclusion of a p53/MDM2 protein-protein interaction inhibitor, in this case, wildtype (wt) p53 (amino acids 15-27). As more inhibitor is introduced, this causes higher levels of free fluorescently-tagged peptide, therefore resulting in a low anisotropy at high concentrations of inhibitor.

The calculated IC_{50} and K_i values are given alongside 95% confidence intervals, which are the range of values in which the actual value is expected to be found, as shown in

equation **2.5**. μ refers to the mean, SE refers to the standard error of the mean whilst 1.96 is a coefficient used with two-way equations (where the actual value lies within a Normal distribution).

$$95\%CI = \mu \pm 1.96SE \tag{2.5}$$

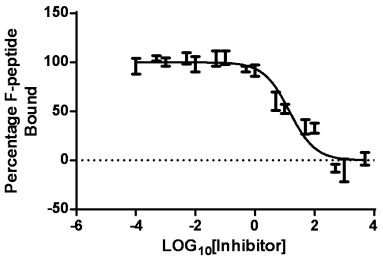

FIGURE 2.10: Inhibition curve of wt p53, IC_{50} = 14.45 μM (95% CI (9.194 μM to 22.72 μM) Ki = 1.819 μM (95% CI 1.157 μM to 2.860 μM), mean +/- SEM, n = 3, 10 nM HDM2 (17-125), 10 nM F-LTFEHAQWYLTS-$CONH_2$

Originally, the untagged version of the Czarna peptide was tested, however it was soon determined that the untagged peptide produced a background fluorescence (due to the high concentrations of aromatic side chain within the peptide), which caused interference with the assay at high concentrations and therefore it was not possible to obtain an accurate inhibition curve. As a result, wildtype (wt) p53 (amino acids 15-27) was used as the control compound as interference was not observed at higher concentration.

In order to determine the robustness of the assay and suitability for high throughput screening, a Z-prime was carried out, in which 24 replicates of tagged compound-protein and 24 replicates of tagged compound-protein-inhibitor are screened and placed into the following equation,[141]

$$Z' = \frac{3(\sigma_p + \sigma_o)}{|\mu_p - \mu_o|} \tag{2.6}$$

In equation **2.6** σ refers to the standard deviation of anisotropy whilst μ refers to the mean anisotropy. The subscript 'p' refers to the positive control (using 100 μM wt p53 within the well) whilst the subscript 'o' refers to the negative control (DMSO in place of inhibitor). If the assay is robust, the Z value should be between 0.5 and 1, meaning that the values are precise and there is no overlap in the positive and negative controls. The Z' value for this assay is 0.57, which demonstrates that this assay has excellent reproducibility. The graphical representation of this data is shown in figure **2.11**.

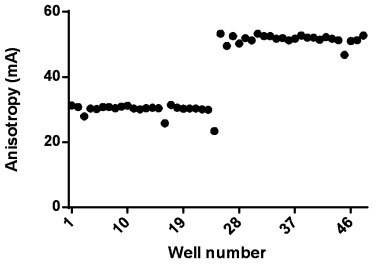

FIGURE 2.11: Z test for robustness; wells 1-23: 100 μM wt p53, 10 nM HDM2 (17-125), 10 nM F-LTFEHAQWYLTS-$CONH_2$; wells 24-46: 10 nM HDM2 (17-125), 10 nM F-LTFEHAQWYLTS-$CONH_2$

2.5.4 *In vitro* Screening of Inhibitors Against the p53/MDM2 Protein-Protein Interaction

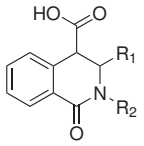

FIGURE 2.12: General structure of the isoquinolinone scaffold in the generated analogues

No.	**R1**	**R2**	**IC_{50} (95% CI) in μM**	**K_i (95% CI) in μM**	**R^2**
A34	4-ClPh	4-FBn	56.61 (25.13 to 127.5)	7.125 (3.163 to 16.05)	0.9142
A36	4-BrPh	4-FBn	19.75 (9.801 to 20.77)	2.486 (1.724 to 3.584)	0.9172
A42	4-IPh	4-FBn	57.74 (31.41 to 106.2	7.286 (3.954 to 13.36)	0.9449
A47	4-ClPh	4-ClBn	61.22 (26.88 to 139.5)	7.706 (3.383 to 17.55)	0.9214
A51	4-BrPh	4-ClBn	21.25 (11.59 to 38.96)	2.675 (1.459 to 4.904)	0.9525
A53	4-ClPh	4-BrBn	27.06 (11.23 to 65.16)	2.357 (1.414 to 8.202)	0.9242
A54	4-BrPh	4-BrBn	6.555 (2.618 to 16.41)	0.8251 (0.3296 to 2.066)	0.8816
Nutlin-3a	-	-	0.6067 (0.494 to 0.745)	0.0771 (0.0627 to 0.0946)	0.9935

TABLE 2.5: Table of the top hit compounds as demonstrated in the FP assay, including the positive control Nutlin-3a

Table **2.5** illustrates the most active compounds as shown by the FP assay, with nutlin-3a compared as a "gold standard" positive control (as it is the first and most well-known p53/MDM2 interaction inhibitor). All compounds synthesised were screened at 100 μM and therefore active compounds were determined to have an IC_{50} of less than 100 μM. The results showed that the halogenated compounds were the most active and that the fluorine substituent on position R2 was more active than chlorine, however the top hit compound displayed a bromine substituent on both R1 and R2. The importance of the halogen group was in agreement with the previously reported literature, suggesting that halogens aid ligand binding into receptors and pockets present within macromolecules.[132] Fluorine also serves as a bioisostere of hydrogen and is also capable of forming hydrogen bonds.[142] Also it was interesting to note that all of the hits were para-substituted, suggesting that the para permits the most effective binding interactions. The compounds found to be active in the FP assay were taken forward for futher studies in cells.

2.6 MTS Cytotoxicity Screening of Compounds

2.6.1 Principle of the MTS Assay

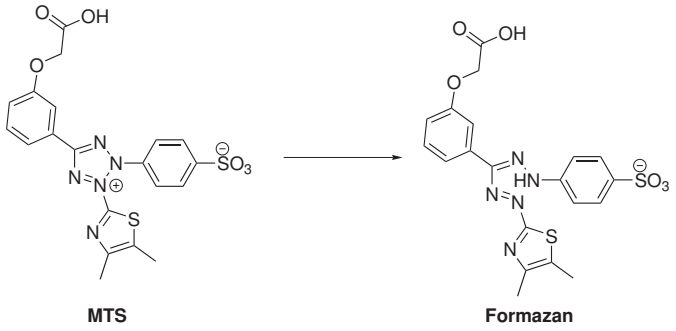

FIGURE 2.13: Structures of MTS and formazan

Scheme **2.13** shows the conversion of MTS to Formazan in the MTS assay. The MTS assay determines antiproliferative activity. MTS (3-(4,5-dimethylthiazol-2-yl)-5-(3-carboxymethoxyphenyl)-2-(4-sulfophenyl)-2H-tetrazolium) is metabolised to formazan in healthy cells by the mitochondria, which has an absorbance maxima between 490 nm and 500 nm, which is detectable by a spectrophotometer. If the cells that the compound are incubated with are dead, there is no production of formazan and therefore the absorbance changes.

Positive and negative controls are undertaken, using media without cells and cells without an inhibitor to determine whether or not there is cell death. The outer wells of the plate contain water to prevent media evaporating during the incubation period. Initially, a blanket screen was undertaken in triplicate at 100 μM inhibitor concentration to determine if the compounds were cytotoxic, after which an IC_{50} value was determined through screening of the cells at various concentrations of inhibitor (starting at 100 μM in the well, reducing in 1 in 2 dilutions to a final concentration of 781 nM). The absorbances were processed in GraphPad Prism and the IC_{50} values determined.

2.6.2 Growth of Cells for the MTS Assay and Cell Lines Chosen

The MTS assay needed to determine if a compound is cytotoxic and iIf a compound is selective for the p53/MDM2 protein-protein interaction. In order to produce the desired outcomes, three different cell lines were used. HL60 cells are p53-null cells and therefore are a determinant of non-specific cytotoxicity, SJSA-1 cells have overexpressed HDM2 and therefore show whether or not the cytotoxicity is specific to the p53/MDM2

protein-protein interaction. Finally, A375 cells were used, as these have overexpressed MDMX, which works alongside HDM2 to silence p53 but through inhibition of p53 transcription instead of through E3 ubiquitin ligase activity.

2.6.3 Cytotoxicity data for the isoquinolin-1-ones found active by fluorescence polarisation

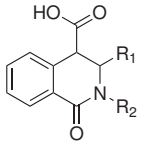

FIGURE 2.14: General structure of the isoquinolinone scaffold in the generated analogues

No.	**R1**	**R2**	**SJSA-1 IC_{50} in μM**	**HL-60 IC_{50} in μM**	**A375 IC_{50} in μM**
A34	4-ClPh	4-FBn	NA	NA	NA
A36	4-BrPh	4-FBn	NA	NA	NA
A42	4-IPh	4-FBn	286.9	10	440.3
A47	4-ClPh	4-ClBn	NA	NA	NA
A51	4-BrPh	4-ClBn	NA	NA	NA
A53	4-ClPh	4-BrBn	more than 500	7.5	242.1
A54	4-BrPh	4-BrBn	478.9	8.1	NA
Nutlin-3a	-	-	5.778	NE	NE

TABLE 2.6: Table of all compounds tested in the MTS assay (NA = No Activity up to 500 μM, NE = Not Examined)

Table **2.6** shows all of the compounds tested in the MTS assay. In order for a compound to be selective for the p53/MDM2 protein-protein interaction, the IC_{50} should be low in SJSA-1 cells (MDM2 overexpressed) and high in the other two cell lines (p53-null and MDMX overexpressed respectively). Although the compounds displayed activity in SJSA-1 cells, it appeared that there was activity (in some cases, greater activity) in the other two cell lines, suggesting that these compounds may also work by an alternative mechanism independent of p53-induced apoptosis.

2.7 Synthesis of Isoquinolin-1-one Esters

As the cellular penetration of the isoquinolin-1-ones was thought to be low (due to their insolubility and their negative charge present on the carboxylate at physiological pH), it was decided that the carboxylic acid would be esterified, as the loss of the carboxylate present at physiological pH on the isoquinolin-1-one would aid permeability into cells. The decision to use a methyl ester was to minimise the steric bulk as the carboxylic acid itself has been shown to be important for binding. This may appear contradictory, as the paper published by Rothweiler *et al.* in 2008 showed that ester formation could increase activity,[124] however all of these esters were highly oxygenated (as opposed to a long hydrocarbon chain) and therefore still capable of performing hydrogen bonding in aqueous environments.

It was decided that the top binder (**A53**) would be esterified first to determine if there was a drop in activity. Esterification was carried out with catalytic sulfuric acid in methanol and went to completion within 1 hour. The product was concentrated *in vacuo* and produced a quantitative yield of the desired methyl ester in position 4. This compound was tested via FP but failed to show activity: we postulated this to be due to the reduced capacity to hydrogen bond with His^{96} within the hydrophobic pocket. Testing in cells has yet to be undertaken.

2.8 Characterisation of Binding Modality Using Saturated Transfer Difference Nuclear Magnetic Resonance Spectroscopy

2.8.1 Basics of Nuclear Magnetic Resonance Spectroscopy

Nuclear magnetic resonance (NMR) was first realised in the 1940s, during which the first spectra of solids and liquids were published.[143] Ten years later, chemical shifts and spin-spin coupling was examined as a structural elucidation tool.Twenty years after the conception of NMR, the Nuclear Overhauser effect would be determined. Thirty years after NMRs conception came the determination of two-dimensional NMR experiments and automated spectroscopy. The 1990s led to the development of coupled activities such as liquid chromatography (LC)-NMR, alongside the production of pulsed field gradients. In the 2000s, high-sensitivity cryogenic probes and shielded magnets became widely available and microscale NMR experiments became possible. Since 2010, it has been possible to produce fast, parallel data acquisitions.

2.8.2 Saturation Transfer Difference (STD) NMR Spectroscopy

Saturation Transfer Difference (STD) NMR is a recently explored form of NMR analysis in which a difference in signal is observed and subtracted between the bound and non-bound ligand and its binding partner.[144] If there is an interaction, a signal is observed on the difference spectra, as the two signals do not completely cancel out. This technique was first published in 1999 by Mayer *et al.*[145] Their initial experiments involved mixtures of ligands for rapid screening and ligand mapping of potential binding compounds. The initial paper focussed on the binding of oligosaccharides and they were even able to characterise GlcNAc as a binder through the proton and STD spectra for this compound. The benefits of this technique include the decreased concentration of target required (compared to techniques such as ^{15}N-HSQC), the relative ease of use of the technique as well as the ability to examine large molecular weight targets.

In 2005, Krishnan *et al.* produced a comprehensive review stating the details of how NMR can be used to determine protein-ligand interactions. Using the notion that receptors and ligands display NMR-type characteristics at equilibrium, it is possible to analyse their binding modality at this point.[144] It is the free resonating receptor and ligand that is NMR-active, whilst the complex itself is NMR-silent. In order to produce a difference in resonance state, a magnetic frequency is applied to the receptor-ligand mixture, which is equal to the resonance frequency of the receptor. This causes the receptor to resonate with greater intensity and resonance travels across the receptor through spin diffusion. It is key to note that there must be no resonance from the ligand, else this would interfere with the resultant difference spectra.

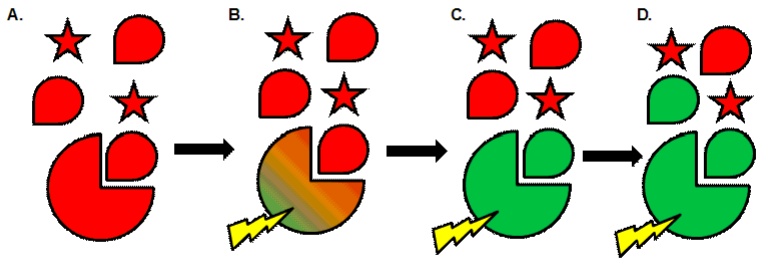

FIGURE 2.15: Diagrammatic representation of spin diffusion and resonance throughout the target, ligand and a non-binder (star). A. No resonance. B. Application of magnetic field and spin diffusion across the target. C. Spin transfer from the target to the ligand D. Exchange of resonating ligand with another ligand in solution

Once the resonance has spread throughout the receptor it is then transferred to the ligand through dipole-dipole interaction of neighbouring protons. This resonance causes the ligand to dissociate from the receptor and causes fresh free ligand to associate with the target, after which the process is repeated.

A reference "off"-resonance signal is then deduced, which is recorded at a frequency in which neither the receptor nor the ligand resonates (this is usually between 25 and 50 ppm from the on-resonance frequency).

In order to maintain consistency, the temperature of the environment is controlled (in the case of our experiments, each run was carried out at 5°C, as this not only preserved the life of the protein but also reduced the speed of which the macromolecule tumbled, hence improving the signal intensities and reducing background noise.

Once the "on" and "off" signals are subtracted, the difference signals left are the result of the saturated receptor and ligand and, as both the receptor and ligand are present in solution at their minimum working concentration, the receptor signal is rarely seen. This technique can also be used to determine K_D values as multiple experiments can be setup in parallel with varying concentrations of ligand, whilst the protein is kept constant.

In order to maximise the signal produced, experiments were carried out on an 800 MHz NMR machine (for the greatest possible resolution of the peaks in **A34**) and in a 300 μL NMR tube to reduce the volume necessary for the experiment. Due to high surface tension, it was vital that components were added to the tube slowly and the tube was later centrifuged in order to force components to the bottom of the tube and the air to the top.

Factors that affect the STD-NMR spectra include the biochemistry of the receptor-ligand interaction, as well as the type of molecules, for example, protons in carbohydrates and in DNA are less capable of spin diffusion as protons are further apart and therefore the transfer of spin is less efficient, hence why proteins are more commonly used, as they rapidly and readily transfer spin between neighbouring protons to saturate the entire macromolecule.[146] Larger proteins also tend to work better, as they tend to tumble more slowly in solution and therefore create a greater difference spectrum.[147] The working concentrations of protein required are between 10 μM and 20 μM when in the sample, whilst the quantity of ligand is approximately 500 μg. For the purpose of this study, the protein concentration was estimated to be approximately 10 μM and the quantity of ligand to be 500 μg.

Additional factors to consider when using this technique includes the K_D of the ligand, which should ideally be in the μM range: if the binding is too stong or weak, the NMR

pulses will not detect a difference between the free and bound states, as any changes in signal would not be detected at the pulse rate of the machine. For this reason, **A34** was chosen, as it was a moderate strength binder (K_i = 7.125 μM) and would not bind too strongly or weakly to the protein.

Another factor to consider includes the buffer system, as the presence of DMSO in the buffer can interfere with the NMR (although interestingly, the presence of DMSO in this case appeared to improve magnetic distribution across the protein). It is also important to note that all components require freeze drying multiple times with deuterium oxide to remove any water present on the molecules that could swamp the NMR signal. Also, it is important to determine the optimum temperature for the experiments, as lower temperatures decrease the tumbling in solution but may improve the stability of the protein for analysis. The buffer used in the analysis was 10% DMSO-d_6 (to solubilise the ligand) in PBS (10 mM $PO_4{}^3$, 137 mM NaCl, and 2.7 mM KCl) at pH 7.4 to stabilise the protein.

2.8.3 Parameters of Components Used in STD-NMR

In order to display an STD-NMR signal, it is vital that the pulse rate and power are optimal. As STD-NMR is a two-dimensional experiment, only resonance in the x-y plane is detectable. As a result, it is necessary to ensure that the angle of resonance is optimised for the x-y plane and that involves producing the optimal strength of pulse, which is known as the free induction decay (FID). The FID is the point at which data acquisition takes place.

2.8.4 Protocol of STD-NMR Processing

The first step with processing is to integrate each peak on each spectrum (figure **2.16** indicates an example difference spectra of **A34**, whilst figure **2.17** and figure **??F11** show examples of the weak and strong binding spectra respectively): for the purposes of the experiment fifteen different pulse rates were used, which produced different levels of "on" binding. The reference spectrum was overlayed and scaled until it perfectly overlapped with each peak, which produces a value for each peak known as the scale factor (that is, the number of times larger or smaller the reference spectra is scaled to perfectly overlap with the difference spectra). This was done for each peak in each spectrum, producing a graph for each peak. The extinction coefficient of each graph was calculated and converted into a ratio against the largest extinction coefficient, as illustrated in the equation below:[147]

$$A_{STD} = \frac{I_0 - I_{SAT}}{I_0} \times \frac{[L]_\Gamma}{[P]} = \frac{I_{STD}}{I_0} \times \frac{[L]_\Gamma}{[P]} \tag{2.7}$$

Where A_{STD} is the STD amplification factor, I_0 is the intensity of the signal in the reference spectrum, I_{STD} is the intensity of the signal in the "bound" spectrum, [L] is the ligand concentration and [P] is the protein concentration. γ is a coefficient of motion in solution.

This allowed the quantitative importance of each proton or proton environment to be determined. Once this was determined, similar molecules were searched for in the literature and molecular modelling adjusted according to the enhanced parameters. It is important to note, however, the weaker the binding becomes (due to a lower pulse rate) the more difficult the scale determination is, as the signal-to-noise ratio greatly increases.

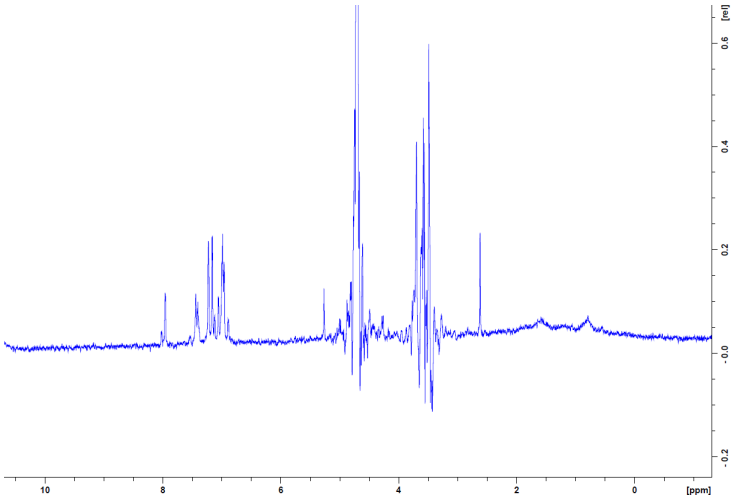

FIGURE 2.16: Difference spectra of **A34**

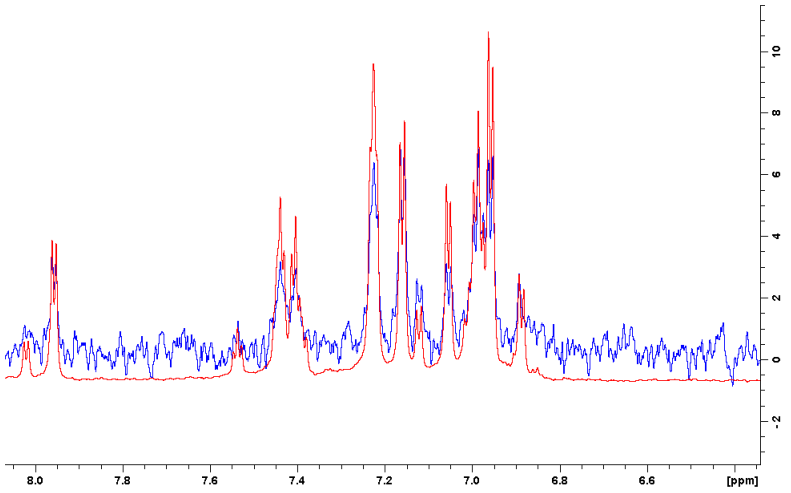

FIGURE 2.17: **A34** weak binding spectrum overlayed with proton spectrum for **A34**. Due to the lack of interaction there is a low signal-to-noise ratio

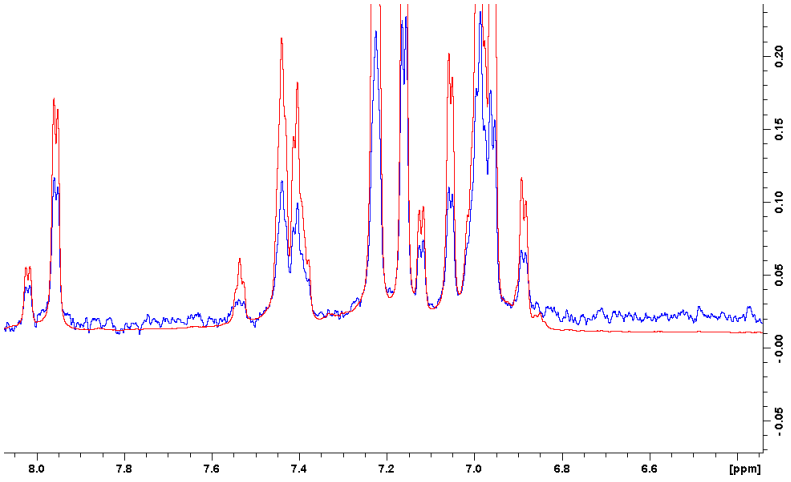

FIGURE 2.18: **A34** strong binding spectrum overlayed with proton spectrum for **A34**. The high degree of interaction results in a high signal-to-noise ratio

Due to the complexity of the isoquinolin-1-one spectra, it was necessary to use the 800 MHz NMR to resolve each proton environment: using proton, COSY, HSQC, HMBC and NOESY, it was possible to assign the different proton environments (see Appendices A to D) for the spectra gathered for **A34**).

Although NOESY was inconclusive, it was possible to determine the proton environments within the spectrum using the other modes of NMR analysis. As the fluorine causes splitting in NMR spectra, it was possible to determine which of the aromatic protons were closest to the fluorine on the lower ring and those that neighboured through HSQC and HMBC. Due to the symmetry in the side chain rings, only one set of signals

was evident for each ring. The aromatic ring on the isoquinolone core was easily determined, as it was shifted furthest downstream compared to the two side chain aromatic rings.

Interestingly, it was also determined that the two doublets in the aliphatic spectrum referred to the methylene group (see 'Appendix A'), which must be due to its three-dimensional conformation in space. The two singlets in the aliphatic region was correctly identified as the two trans protons (the proton adjacent to the carboxylic acid was shifted further downstream).

Although peaks for the cis conformation were also seen, these were much weaker and therefore were not considered within the STD-NMR studies undertaken within this thesis. The STD data was then taken forward and inputted into the *in silico* screening to calculate the most accurate binding motif of the isoquinolinones.

2.9 *In Silico* Studies of Isoquinolin-1-one Binding

In silico screening and molecular modelling are used to predict how a compound may interact within a binding pocket. Macromolecules are obtained either through solution-based NMR studies or through X-ray crystallography and made publically available via the protein databank.[148] Once the protein has been obtained, it is necessary to process gasteiger charges, hydrogen bonds and any associated water molecules to ensure that the hydrophobicity/hydrophilicity of the macromolecule is maintained for the most accurate simulation.

The ligand too requires further processing: once produced (in either ChemDraw or MarvinSketch) all hydrogens are added and the lowest energy 3D conformation is determined and fixed, as the docking programs do not store data on double-bonds and therefore all explicit hydrogens must be visible.[149]

A gridbox is placed on the protein that states the area in which docking is to be simulated: the bigger the gridbox, the more likely a hit will be discovered however the less likely that the compound will bind in the desired pocket. The data is saved as a config.txt file, which enables the script to use the parameters during docking (this and the Python script used for docking is detailed in the 'Experimental' section).

The compound was then processed in Autodock vina and the top screens can then be imported back into Autodock Tools for visualisation of the binding epitope, as shown in Figure **2.19** and Figure **2.20**.

Using STD-NMR, it is possible to input this data (relating to charges and quantitative importance of each proton on binding) experimentally and therefore the binding epitope generated is more accurate than a purely *in silico* approach.

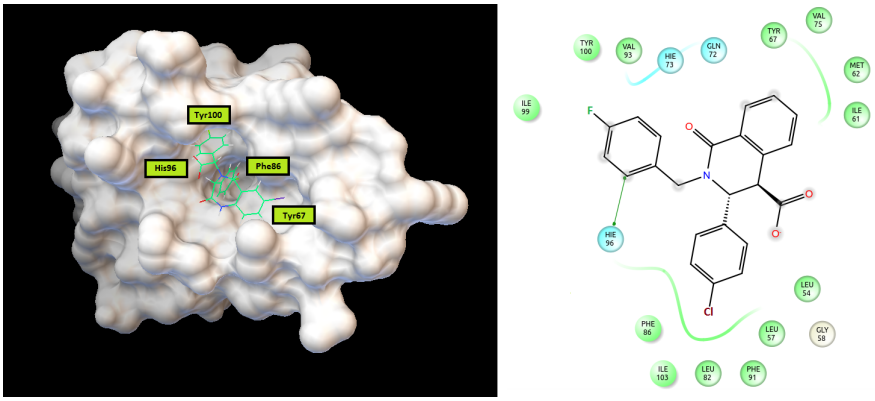

FIGURE 2.19: Docking model of **A34** bound to HDM2

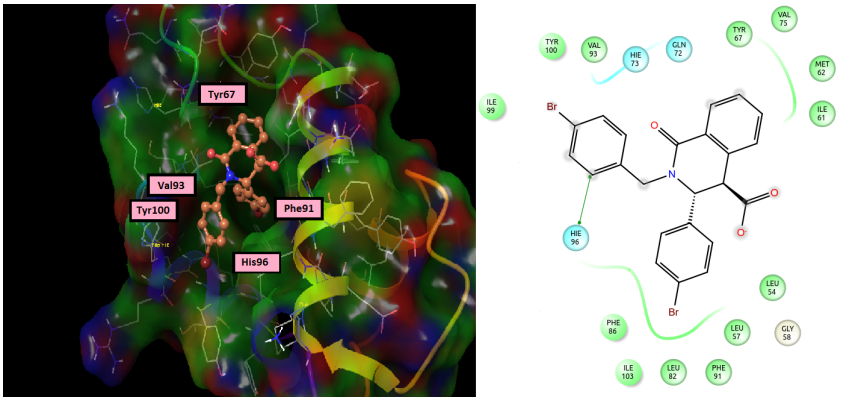

FIGURE 2.20: Docking model of **A54** bound to HDM2

Figure **2.19** and figure **2.20** illustrate the binding models of **A34** and **A54**. In both cases, the bicyclic isoquinolinone core resides in the tryptophan pocket, whilst the fluorine and chlorine of **A34** reside in the phenylalanine and leucine pockets respectively. Interestingly, both **A34** and **A54** adopt the same conformation within the pocket and in both cases, the methylene group had no importance within binding. This binding was compared to that of other inhibitors in the literature and interestingly, the binding of these compounds bears similarity to the binding of the benzodiazepinediones, as indicated in figure **2.21**.

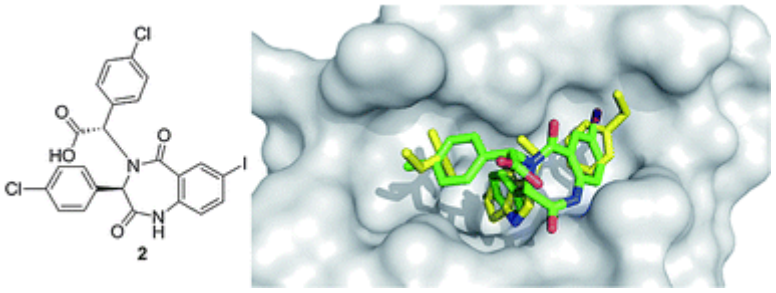

FIGURE 2.21: Docking model of a benzodiazepinedione bound to HDM2, as published in Khoury *et al.*[150] (reproduced with permissions)

2.10 Stereoselective Synthesis of Isoquinolin-1-one Analogues and Subsequenct Optical Rotation Studies

It was proposed that following the results of FP screening that one compound would be analysed in both the cis and the trans forms to determine if one diastereomer displayed better binding.

As a result, the cis and trans diastereomers of model compound **A34** were synthesised, as **A34** inhibited in the FP assay and was produced in moderate to good yields (circa 43%), hence it was theorised that the two diastereomers could also be synthesised and activity determined. Both were analysed by ^{1}H-NMR, with the key difference being the presence of doublets or singlets at 3.98 ppm and 5.14 ppm. If they are doublets, this indicates the diastereotopic protons exist in the same plane, hence the splitting, whereas the singlets illustrate that the two diastereotopic protons are in the opposite directions and therefore the furthest possible points from one another, which can be explained by the Karplus equation mentioned earlier (where the cosine of the J-coupling value indicates whether or not diastereotopic protons will be split on a ^{1}H-NMR).

2.10.1 Synthesis of A34a

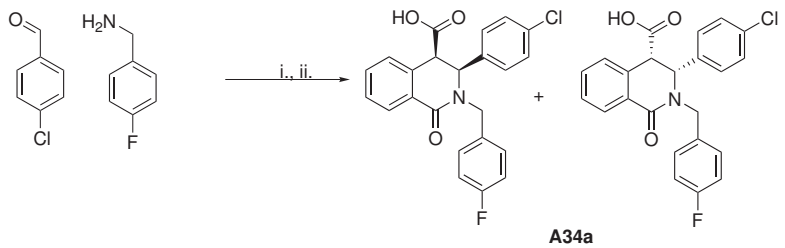

SCHEME 2.7: Formation of cis-**A34** (**A34a**) i. $Si(HClO_4)$, $MgSO_4$, CH_3CN ii. Homophthalic anhydride rt, overnight (29% yield)

A34a was synthesised through the reaction of the amine, aldehyde and homophthalic anhydride in the presence of a perchloric acid silica support, which aides positioning of the isoquinolin-1-one in the cis conformation.

The yield was moderate but purification proved challenging, as the resultant isoquinolin-1-one was only soluble in DMF and it was therefore necessary to dissolve in DMF and precipitate out in the presence of water.

2.10.2 Synthesis of A34b

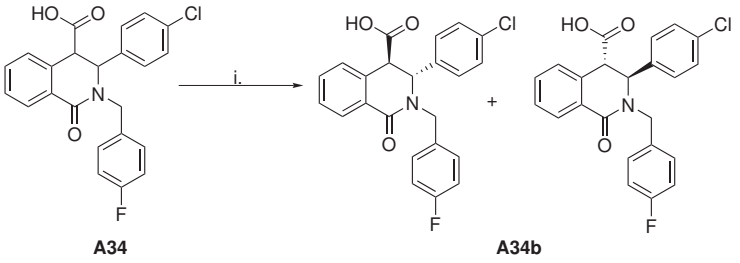

SCHEME 2.8: Formation of **A34b** i. Ac_2O, reflux, 2 h (7% yield)

A34b was synthesised by refluxing **A34** in the presence of acetic anhydride for 2 h. The hypothesis is that this process causes rearrangement of the cis form to produce all-trans arrangement.

The compound only required minimal purification by triturating with diethyl ether.

As well as **A34a** and **A34b**, the remaining top hit compounds from the initial FP screen were then dissolved in DMF and the optical rotation measured. It was initially expected that, as these compounds had been synthesised non-stereoselectively and there should have in theory been equal quantities of both cis and both trans enantiomers, the expected rotation was zero.

DMF was used due to the insolubility of the compounds. The optical rotation was then run in triplicate to determine an average and the results are tabulated below:

No.	**R1**	**R2**	**Optical Rotation**	**Concentration in mg/mL**
A34	ClPh	FBn	+80.00°	10
A34a	ClPh	FBn	+283.33°	10
A34b	ClPh	FBn	+176.73°	10
A36	BrPh	FBn	+27.0°	10
A42	IPh	FBn	-5.67°	10
A47	ClPh	ClBn	-6.79°	10.2
A51	BrPh	ClBn	-6.33°	10
A53	ClPh	BrBn	+25.00°	10.4
A54	BrPh	BrBn	-63.33°	10

TABLE 2.7: Optical rotation data for the top hit compounds (T = 22.0°C). As a control, S-binol was also run through the polarimeter and produced a value of -36.4° (c = 1.066 x 10^{-2} g/ml in THF and T = 23.0°C), which lies within the error margins of the reported value (-35.5°)

This data is very interesting and initially rather surprising as there are very few references in the literature to optical rotation studies of these compounds, as most papers only go as far as to say that these compounds are racemic or only undertake optical rotation studies following purification through chiral HPLC. Cushman made reference to this phenomenon by stating that these compounds display A strain, which is where the central core aromatic substituents occupy the axial conformation due to the central amide linkage.[151] Due to the lack of literature information on this topic it is neccesary to do further study on these compounds.

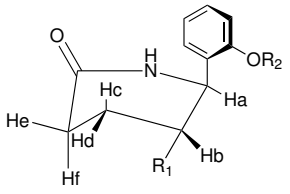

FIGURE 2.22: Illustration of A strain as hypothesised by Cushman and Castagnoli

2.11 Synthesis of Modified Isoquinolin-1-ones with Improved Aqueous Solubility

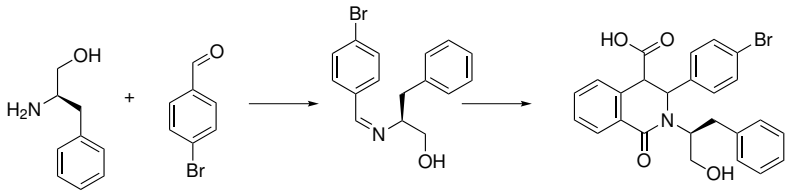

SCHEME 2.9: Synthesis of **A64**. i. L-phenylalaninol, 4-chlorobenzaldehyde, dry THF, $MgSO_4$, rt, 1 h. ii. Homophthalic anhydride, rt, overnight (3% yield)

The STD-NMR data suggested that the methylene group had little to no importance in the binding and would therefore serve as a potential position for improved aqueous solubility, making the compound more drug-like. It was thought that a carboxylic acid or an alcohol could be introduced using an amino acid or an amino alcohol in place of an amine. Attempts to form the imine with an amino acid (in this case, Phenylalanine to preserve the π-π stacking interactions and the carboxylic acid to increase solubility) showed that no reaction was occurring, most likely due to the electron-withdrawing effects of the carboxylic acid, reducing the amine's ability to act as a nucleophile. Additionally, the solvent was changed from dichloromethane to tetrahydrofuran, as the amino alcohols/amino acids were only soluble in THF or methanol.

The successful method involved the use of L-phenylalaninol, which contains a more electronegative amine than phenylalanine. L-phenylalaninol was combined with a suitable solvent to ensure the reactants were all dissolved (in this case, THF). Due to the polarity of the phenylalaninol, it was necessary to column the product twice, as the first normal-phase column isolated the baseline product, after which a second reverse-phase column was used to purify the baseline product. The yield was 3%, but it was possible to characterise this compound by ^{1}H-NMR, with two key peaks integrating to two at 1.23 ppm and 1.26 ppm, corresponding to the methylene adjacent to the aromatic ring and the second methylene adjacent to the alcohol respectively. In theory, both peaks should have been doublets, however the ^{1}H-NMR displayed overlap and therefore it is not possible to distinguish the split peaks.

A64 was screened in the FP assay (figure **2.23**) and was determined to be active (although less so than **A53**), however the MTS assay screen failed to show activity up to 500 μM. It may be that the compound was unable to permeate into cells, or the substitution of the chlorobenzyl substituent present in **A34** with an aryl group may have been responsible for reducing activity. In either case, further work needs to be undertaken to

determine whether or not phenylalaninol-type analogues are a viable route to retaining activity and improving aqueous solubility.

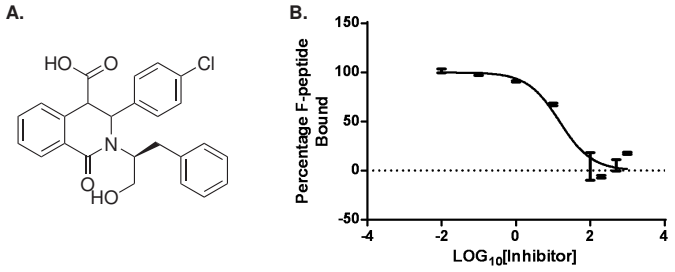

FIGURE 2.23: Inhibition curve of phenylalaninol analogue **A64**, IC_{50} = 15.01 μM (95% CI 8.212 μM to 27.43 μM) K_i = 1.889 μM (95% CI 1.034 μM to 3.453 μM), mean +/- SEM, n = 3, 10 nM HDM2 (17-125), 10 nM F-LTFEHAQWYLTS-$CONH_2$

2.12 Conclusions and Future Work

In conclusion, we were able to successfully synthesise a combinatorial library of isoquinolin-1-ones. 80 compounds were synthesised and of those compounds, 7 showed activity in the FP assay. These compounds were then screened in the MTS assay, with 3 compounds displaying antiproliferative activity, however none of these compounds displayed selectivity for the SJSA-1 (MDM2 overexpressed) cell line.

As well as the biochemical screening a number of physicochemical studies were undertaken, which determined the conformations of the compounds generated and the enantiomeric purity. Interestingly, these compounds appeared to be enantiomerically selective, possibly due to A-strain present within the molecule, however further studies need to be performed as there is a lack of data within the literature. It was also possible to characterise the modality of binding of a model isoquinolin-1-one, which appeared to be analogous to the benzodiazepinedione binding model.

It would be useful to further examine whether or not the binding modality changes for the more potent inhibitors and therefore it would be useful to undertake further STD-NMR studies of the top binding compounds, however there is no guarantee that these models will show by STD-NMR, as compounds may bind to MDM2 too tightly and therefore the NMR machine detector would not detect the change in the "off" and "on" signals.

Another area of interest would be to determine whether or not it is possible to generate specific enantiomers, as our findings showed that the top inhibitors were enantioselective. As certain compounds appeared to be cis diastereomers further studies could be

undertaken to determine whether or not their trans counterparts were active against the p53/MDM2 protein-protein interaction.

In addition, it would be interesting to use the STD-NMR to determine IC_{50} values to act as a comparison to the FP assay and examine any differences in data. This could be especially useful for coloured compounds for which the FP assay was inconclusive.

Finally, further studies to improve aqueous solubility are required, as **A64** proved to be interesting from the FP assay although did not have activity in the MTS assay, possibly due to insolubility within the media or a lack of permeability through cells. Further study could be undertaken to generate additional aqueous-soluble analogues of **A64** that may have increased cell permeability but still retain their aqueous solubility. It maybe possible to esterify with different polyethylene-based carboxylic acids which could esterify with **A64**, as these are the side chains used by Rothweiler *et al.* in 2008 which were present in their inhibitors of the p53-MDM2 protein-protein interaction as explored through ^{1}H-NMR and ^{15}N-HSQC studies.[124]

Chapter 3

Synthesis of Novel Chlorofusin Analogues

The previous chapter examined the isoquinolin-1-one combinatorial library, which bore similarity to the azaphilone potion of chlorofusin. Using this route, it was possible to generate a wide variety of analogues that were shown by FP to inhibit the p53/MDM2 protein-protein interaction. STD-NMR spectroscopy was also used alongside molecular modelling to determine the binding modality of a model isoquinolin-1-one within the pocket and the chirality of different analogues were examined.

Although the peptide on its own bears no inhibitory activity against the p53/MDM2 protein-protein interaction (as shown by Woon *et al* and a separate study by Boger*et al.*, in which the chlorofusin peptide was screened by FP assay and ELISA assay respectively),[77,152] the notion that it plays a role in holding the azaphilone in place to optimise binding suggests that azaphilone replacement with simplified inhibitors utilising the same hydrophobic interactions within the pocket may also produce potent inhibitors.

It was decided that this chapter would shift the focus back to examining analogues focusing on the peptide with replacement of the azaphilone with simple aromatic acids which could condense with the free amine of ornithine 9 to form a variety of vinylogous amides, as well as click-based analogues with a variety of different alkyne.

Following synthesis and characterisation, the synthesised analogues would be tested *in vitro* using an FP assay and inhibitory compounds would then be screened using the MTS assay to determine antiproliferative activity, as described in Chapter 2.

3.1 Synthesis of Novel Chlorofusin Analogues by Simplification of the Chromophore

Although simple monocyclic substitution of the azaphilone chromophore had previously been shown as inactive by ELISA in the paper published by Woon in 2007[77] it was hypothesised that a bicyclic moiety could pose a better fit within the hydrophobic pocket as they bore greater similarity to the azaphilones than their monocyclic counterparts. As a result, it was postulated that bicyclics would provide a better substitute for the azaphilone and would be synthesised. In order to achieve this, the chlorofusin peptide was synthesised using Fmoc-solid phase peptide synthesis, deprotected and reacted with a bicyclic aromatic acid to generate a library of analogues.

3.1.1 Synthesis of the Cyclic Chlorofusin Peptide

Chapter 2 describes in detail the methodology of Fmoc-solid phase peptide synthesis, whilst scheme **3.1** illustrates the solid phase synthesis undertaken in order to produce the chlorofusin peptide.

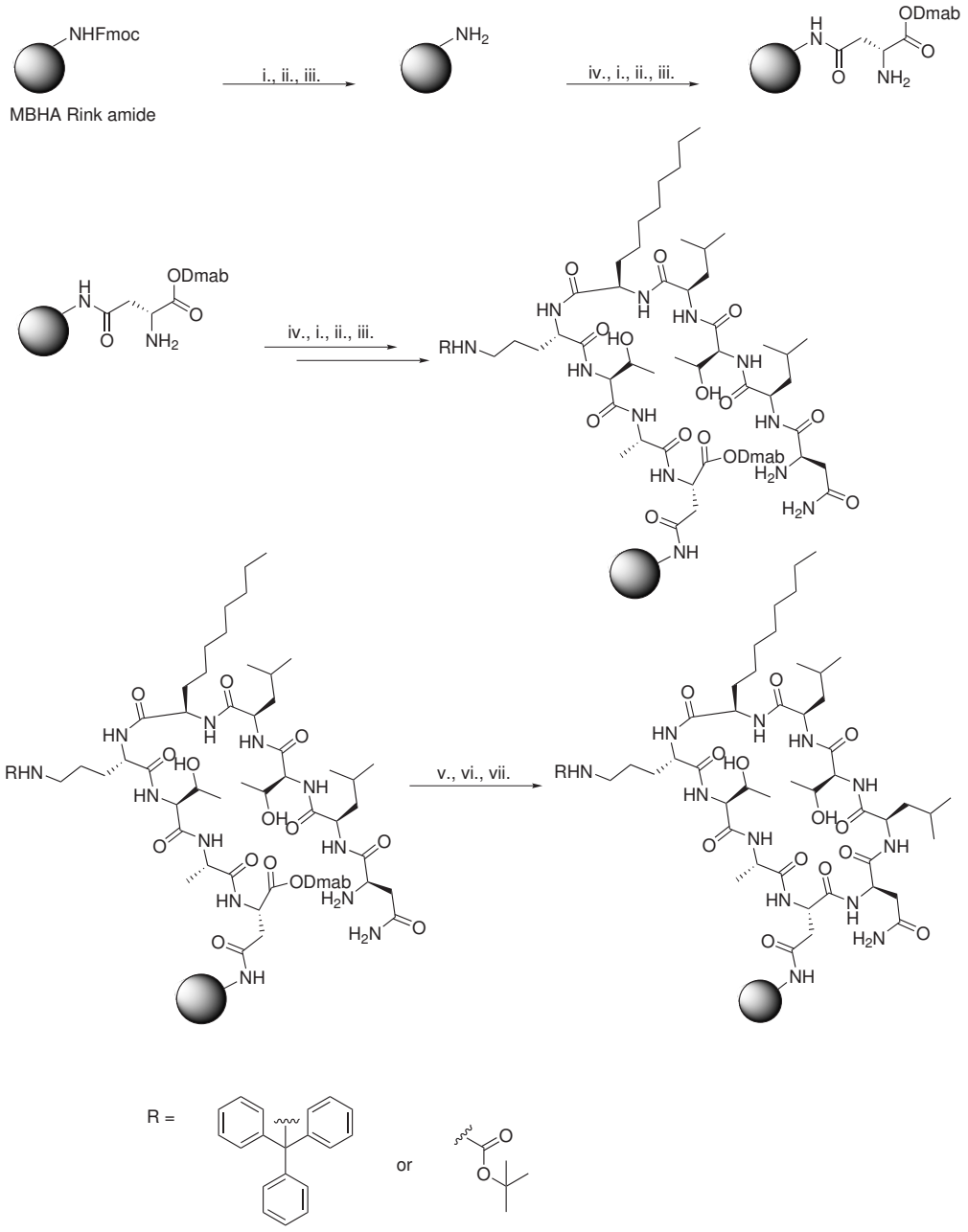

SCHEME 3.1: Fmoc solid phase synthesis of the chlorofusin peptide i. 40% Piperidine in DMF, rt, 5 min ii. 20% Piperidine in DMF, rt, 5 min iii. 20% Piperidine in DMF, rt, 5 min iv. Fmoc-AA-OH, HOBt, HBTU, DIPEA, Et_3N, DMF v. 2% N_2H_2 in DMF vi. 5% DIPEA in DMF vii. DIC, HOBt, DIPEA, DMF, rt, 2 d

The synthesis of the chlorofusin peptide was undertaken as head-to-tail as described previously by Woon *et al.*[77] The peptide was synthesised on Rink Amide MBHA resin to produce a primary amide, as this is what is present in the cyclic backbone of the natural peptide. Dmab-protected Fmoc-aspartic acid was attached first, which was followed by Fmoc-L-Ala-OH, Fmoc-L-Thr(^{t}Bu)-OH, Fmoc-L-Orn(Boc)-OH, Fmoc-D-Ade-OH,

Fmoc-D-Leu-OH, Fmoc-Thr(tBu)-OH, Fmoc-D-Leu-OH and Fmoc-D-Asn(Trt)-OH. Aminodecanoic acid (Ade) was the only peptide that was not comercially available, hence it was synthesised racemically using 1-bromooctane and dimethylaminomalonate.[77] The D-enantiomer was then selected through enzymatic processing using *acylase I* (from *Aspergillus melleus*), which led to the destruction of the L-enantiomer. The Fmoc protecting group was then attached following selective silyl protection and subsequent deprotection of the free carboxy group.

The rationale for the use of Dmab-protected aspartic acid was the facile removal of the Dmab group in the presence of hydrazine (which did not react with any other protected side chains on the molecule nor did it react with the solid support linker), following which the free carboxylic acid can be coupled to the terminal amine using DIC and HOBt. This methodology was undertaken until a negative Kaiser test was observed.

Cyclisation of the chlorofusin peptide reached completion after 2 days, which was determined by a negative Kaiser test. This is aided by the fact that the chlorofusin peptide is made of a mixture of D- and L-amino acids, which naturally produces turns in the peptide.[153] Conversely, peptides consisting solely of L-amino acids have been shown to cyclise less readily, as they generally do not naturally contain a turn within the chain. Methods undertaken to form turns within L-only chains includes the formation of disulfide bridges to "lock" the conformation of the peptide and forces the chain to bend,[154] as does the introduction of a proline, which causes the chain to "kink".

Once all reactions have been completed, the resin was dried using methylene chloride, 1:1 methylene chloride:methanol, then compressed air. This process ensures that no DMF is left, as this would not only affect the weight but could become troublesome to remove later: it could also prevent precipitation of the peptide in the presence of diethyl ether, which is a common way of removing organic impurities from the peptide following synthesis (as the peptide is insoluble in the ether). Cleavage of the chlorofusin peptide was undertaken using 95:2.5:2.5 TFA:H_2O:TIPS, with the latter two reagents preventing side reactions during cleavage through the scavenging of free radicals produced during cleavage. The scheme for this is shown in scheme **3.2**

In order to ascertain whether or not the peptide had been synthesised, a small portion of the peptide was cleaved and the cleaved peptide was analysed by HPLC against a standard chlorofusin peptide sample (synthesised by Woon and coworkers[77]) and was shown to have a consistent retention time of 11.55 min (in a methanol:water system, starting at 5:95 methanol:water with 0.05% TFA in each solvent to prevent band broadening, increasing to 95:5 methanol:water over 15 minutes and re-equilibrating to 5:95 methanol:water over 5 minutes). The crude sample was also run on MALDI mass spectrometry, which displayed the $M+H^+$ (1011.34 m/z), $M+Na^+$ (1033.31 m/z) and $M+K^+$

(1049.30 m/z) adducts of the peptide. The crude peptide was then purified using semi-preparative HPLC and fractions were analysed by analytical HPLC and MALDI to determine that the correct product was isolated.

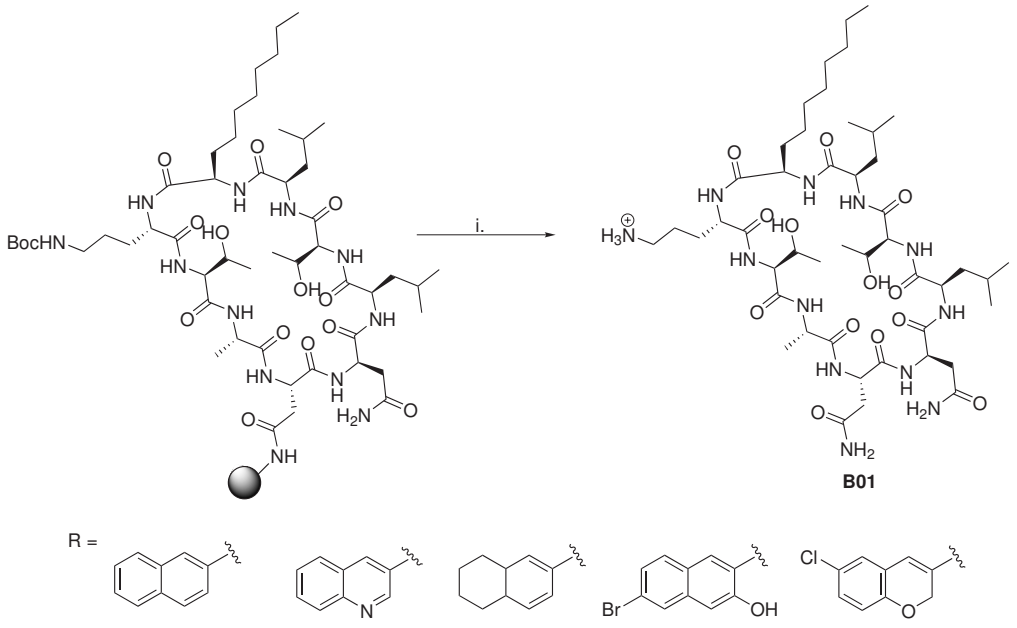

Scheme 3.2: Deprotection of the cyclic chlorofusin peptide from the resin i. 95:2.5:2.5 TFA:H_2O:TIPS, rt, 3 h

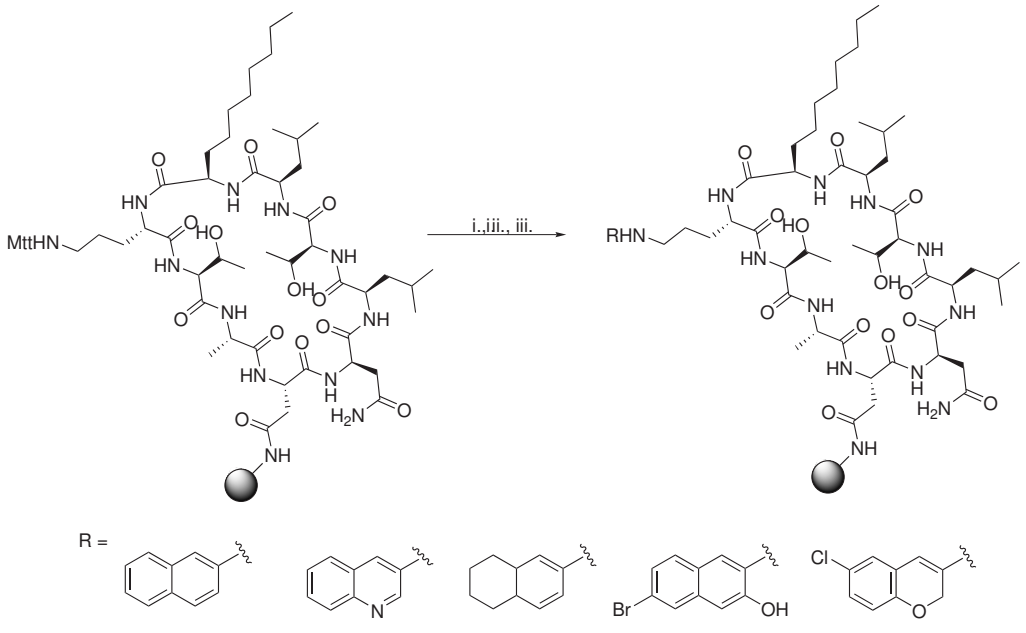

Scheme 3.3: Solid phase synthesis of the bicyclic analogues i. 1% TFA, ii. DMF rinse x 3, iii. aromatic acid, HOBt, HBTU, DIPEA, DMF, rt, overnight

In order to synthesise analogues on solid phase, it was necessary to use a form of amine protection that could be selectively removed without deprotecting any of the other side groups or from the resin. For this reason, 4-methyltrityl (MTT) was used, as it can be selectively removed from the peptide in the presence of 1% TFA, which is insufficient to deprotect other side chains on the peptide or cleavage of the peptide from the resin (this is shown in scheme **3.3**). The resultant trityl cation is also very unreactive due to its low electrophilicity.[155] The subsequent coupling was then undertaken using 5 equivalents of HOBt, HBTU and the acid. Although small quantities of the coupled peptide were witnessed by MALDI, the crude peptide did not bear a major peak and purification by semi-preparative HPLC failed to generate sufficient quantities for testing.

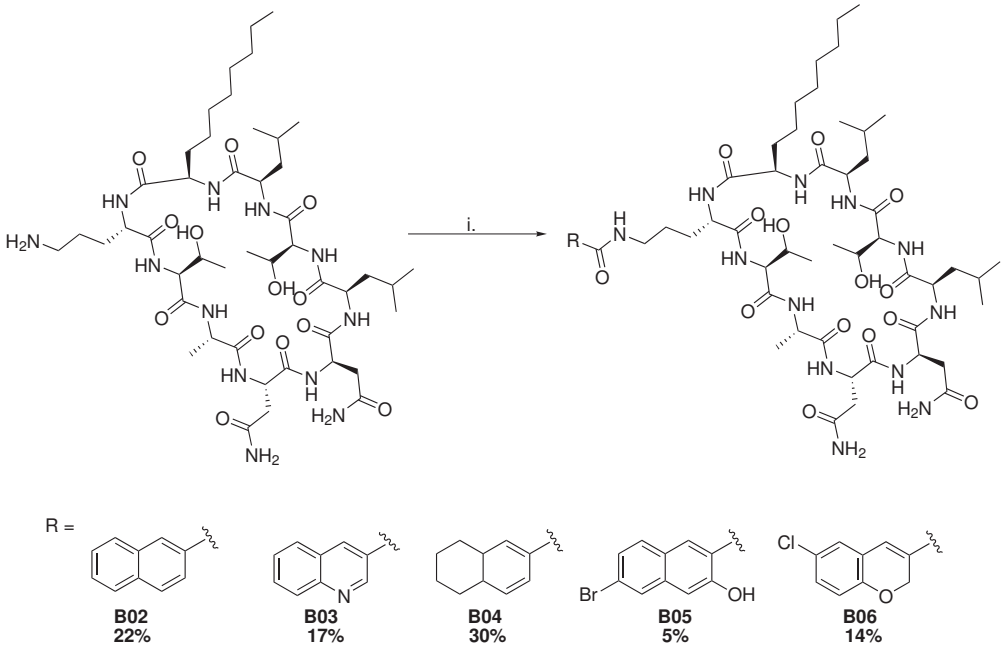

Scheme 3.4: Solution phase synthesis of analogues i. EDCI, HOBt, DMF, DIPEA, rt, overnight

Following difficulties in the solid-phase synthesis of this library, it was postulated that the free amine was too sterically hindered to be able to condense with the free carboxylic acid. To try and increase the number of collisions between the amine and the carboxylic acid the peptide was cleaved from the resin and the reaction was repeated in solution using one equivalent of HOBt, EDCI, peptide and carboxylic acid in DMF, as shown in scheme **3.4**. Using this methodology it was possible to synthesise 5 different analogues, which would then be tested by fluorescence polarisation for activity.

The rationale for choosing said analogues was to produce wide variety: the unsubstituted naphthyl was chosen as the comparator compound as well as containing the rigidity of the azaphilone. The halogenated compounds were chosen to explore the directing effects

of the halogens chosen. The heterocycles were chosen to modify the electron density of the aromatic rings and the tetrahydro compound was chosen to examine how flexibility in one of the rings would affect binding.

3.2 *In vitro* Screening of Compounds Using Fluorescence Polarisation

Compounds were screened at a well concentration of 100 μM and IC_{50} values were calculated for compounds showing activity at less than 100 μM. The FP assay showed that none of the compounds displayed any inhibitory activity: this could be due to the fact that the bicyclics were still oversimplified to mimic the proposed binding of the azaphilone into the hydrophobic pocket. As there are no crystal structures of chlorofusin bound to MDM2, it is not possible to ascertain the exact binding modality of the azaphilone component. It may also be plausable that the ketone functionalities present on the azaphilone are able to provide hydrogen-bonding interactions, as there is a hydrogen bond donor (histidine 96) within the hydrophobic pocket, however this has yet to be shown experimentally.

As this methodology had not produced any novel inhibitors, it was decided that one attempt to produce analogues maintaining the peptide chain would be produced. It was decided that novel analogues based on click chemistry would be explored, as these analogues could be synthesised and purified quickly and efficiently and the triazole ring serves as a bioisostere to an amide bond and is far less susceptible to cleavage.

3.3 Synthesis of Novel Chlorofusin Analogues Based on Click Chemistry

3.3.1 Principles of Click Chemistry

Click chemistry is a well-documented technique originally conceived by Barry Sharpless in 2001.[156] It concerns reactions that are high yielding, have a wide range of applications, require minimal or no purification, are simple to perform, use volatile solvents or "green" solvents (hence are non-toxic) and finally, are insensitive to oxygen or water.

Reactions that fall into the click chemistry category include the following

- Nucleophilic ring opening of strained ring systems (such as epoxides)[157]

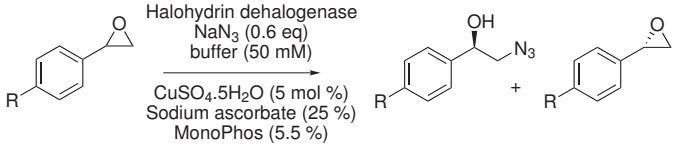

Scheme 3.5: Example of tandem epoxide-ring opening followed by azide substitution

- Non-aldol-type reactions involving carbonyls[158,159]

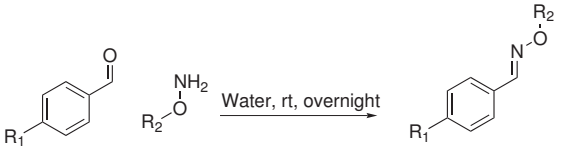

[160]

Scheme 3.6: Click oxime ligation used to form hydrogels

- Addition to alkenes[161]

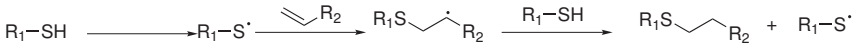

Scheme 3.7: Synthesis of thiolenes through free-radical initiation and propagation

- Cycloaddition reactions[162,163]

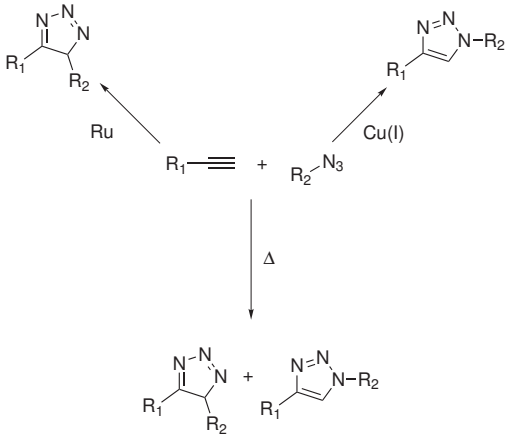

Scheme 3.8: General scheme for azide-alkyne cycloaddition reactions

Another example of a click reaction is a Huisgen 1,3-dipolar cycloaddition, in which an azide and an alkyne react to produce a triazole ring. Using copper(II) sulfate (which is reduced to Cu(I) sulfate in the reaction), 1,4-disubstituted-1,2,3-triazoles are produced.

This approach is amenable for combinatorial chemistry. It is this reaction that is utilised in this chapter. This approach is commonly used for clicking on fluorophores for imaging: this can be done with live cells, DNA and proteins.[164,165,166] It is also commonly used to staple peptides, which "locks" the peptide in a set conformation as determined by the position of the staple.[167] Usually, a "double-click" approach is used, meaning that both ends of the staple are attached to the peptide via a triazole linkage.[168] As an aside, it is possible to reverse the regiochemistry using a ruthenium catalyst to produce 1,5-disubstituted products, but this was not explored in the scope of this thesis.[169]

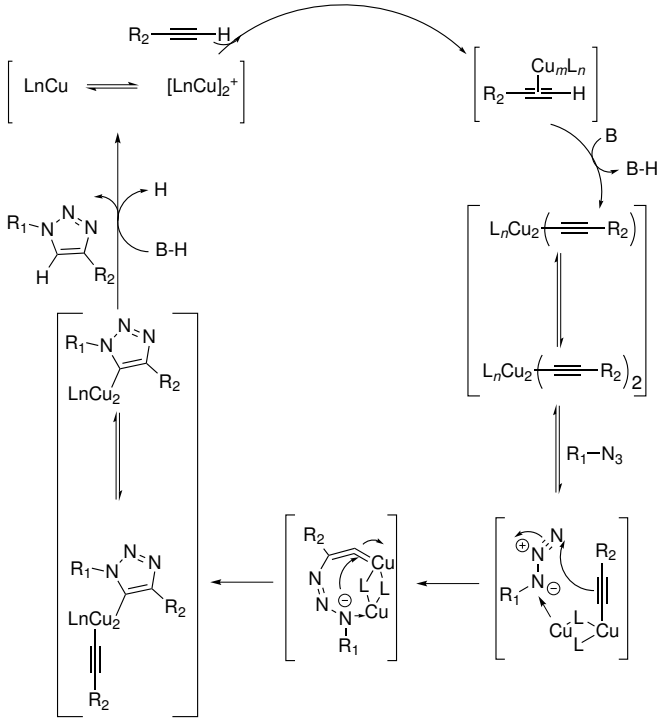

SCHEME 3.9: Mechanism of the Huisgen 1,3-dipolar cycloaddition[170]

Scheme **3.9** illustrates the proposed mechanism for the click reaction. Copper inserts itself within the alkyne and deprotonates in the presence of base to form a copper-alkyne complex. This complex then coordinates with the azide and electrons from the alkyne feed into the azide. This coordinated structure displaces the copper-ligand complex to release the triazole moiety.

Standard conditions for a 1,3-dipolar cycloaddition include Cu(II) salts (co-ordinating metal to produce the correct regioisomer) and sodium ascorbate (ligand). For bioconjugation, TBTA (tris[(1-benzyl-1H-1,2,3-triazol-4-yl)methyl]amine) can be used.[171]

3.3.2 Click Chemistry in Peptide Synthesis

Over recent years the interest in producing peptides containing azides either for direct screening or for clicking onto an organic molecule has increased.[168] The triazole ring is very stable and can be substituted in place of amides to reduce the risk of cleavage. This methodology also permits the addition of functional groups. The triazole ring can act as a hydrogen bond acceptor and perform dipole interactions.

3.3.3 Synthesis of Click Chlorofusin Analogues

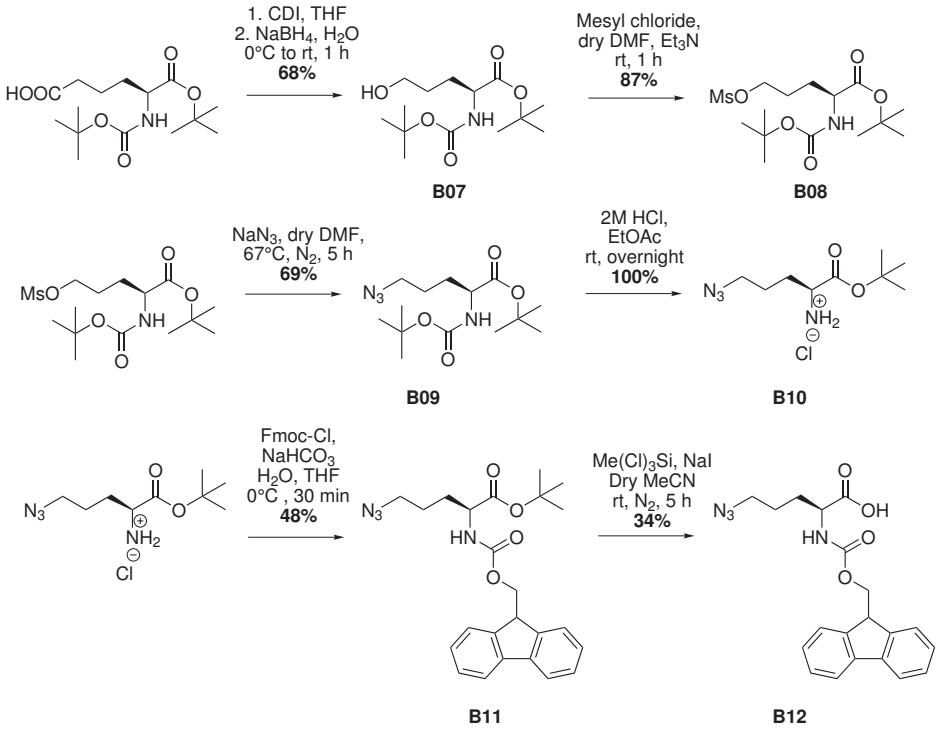

SCHEME 3.10: Synthesis of Fmoc-azidonorvaline-OH

Initially, Fmoc-δ-Nva(N_3)-OH was to be made using a diazotransfer using a sodium azide-triflic anhydride, which produces a highly reactive organic azide species.[172] Although this method has been well-documented in the literature,[173] the risk of explosion of the triflic azide made this route less attractive. It was also discovered that, because of the highly reactive nature of the triflic anhydride, it was difficult to monitor and control, therefore it was decided that the methodology would be amended to use less hazardous reagents.

An alternative method of azide synthesis requires the reaction of a mesyl group with an alcohol, which can then undergo nucleophilic substitution via the azide, as shown in

scheme **3.10**. The greatest difficultly arose from deciding firstly, which forms of protecting group could survive each stage of the synthesis and also, how to form an alcohol in the correct position. As the reaction required basic conditions, acidic side chain protection was required at both the amino terminus and the carboxylic acid terminus. Reduction of an acid-based side chain was most appealing, however selective reduction of the side chain carboxylic acid without reducing the terminal acid proved a challenge.

3.4 Selective Reduction of Boc-Glu-OBu through a CDI Intermediate

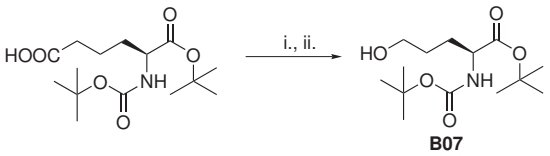

SCHEME 3.11: Selective reduction of Boc-Glu-OBu through a CDI intermediate i. CDI, THF, 0°C, 10 min ii. $NaBH_4$, H_2O, 0°C to rt, 1 h (68% yield)

The synthesis undertaken (scheme **3.11**) utilised ester protection at the terminal carboxylic azide, which could permit selective reduction of the free carboxylic acid side chain by producing a reactive amide intermediate using CDI, which could then be reduced with sodium borohydride to produce the novel amino alcohol. The methodology was adapted from syntheses proposed by Hwang and coworkers.[174] The rationale for using sodium borohydride was that sodium borohydride is unable to reduce esters, but is capable of reducing a ketone or an activated amide. Previously, it was thought that lithium aluminium hydride monitored closely and subsequently quenched could carry out the same reaction, but the reduction of the terminal ester happened readily, forming an alcohol-type species that could not be converted back into the starting carboxylic acid.

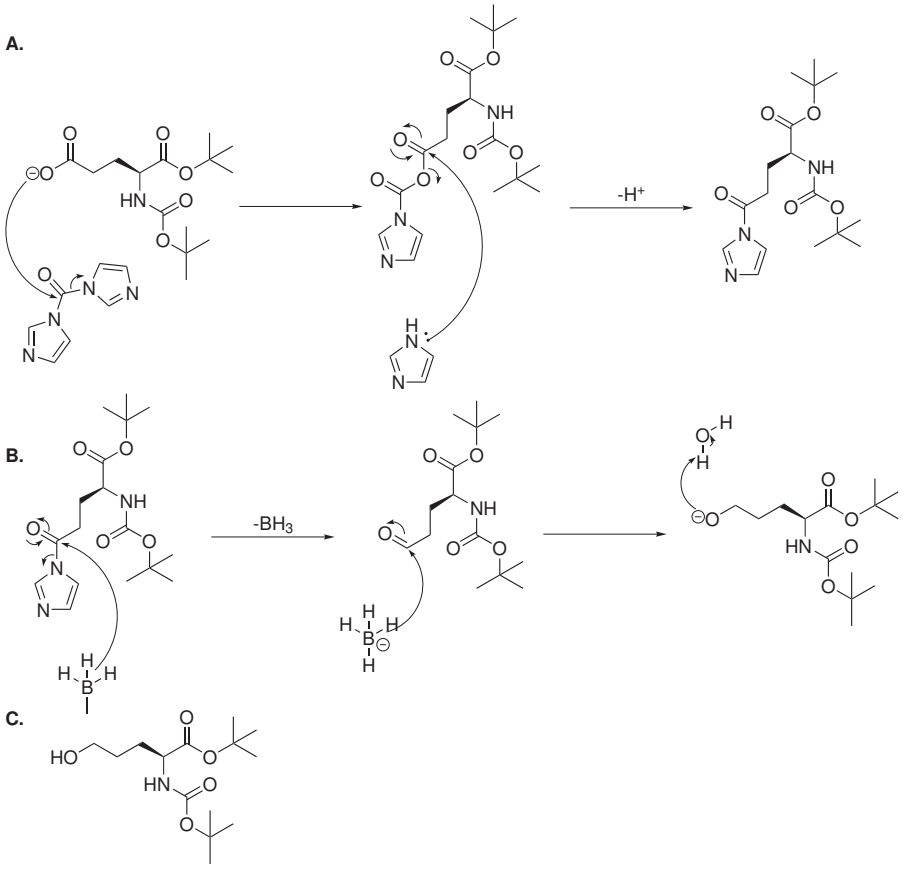

SCHEME 3.12: Mechanism for the selective reduction of Boc-Glu-OtBu. A. Nucleophilic attack on CDI to afford the intermediate. B. Reduction by sodium borohydride. C. Final amino alcohol

The mechanism of this reaction is displayed in scheme **3.12**: the boron-hydrogen bond electrons attack the ketone, eliminating imidazole and producing an aldehyde. This aldehyde could then be further reduced to the alcohol. Following quenching of any additional sodium borohydride and borohydride complexes using aqueous hydrochloric acid, aqueous-organic workup was undertaken, followed by column chromatography to remove any remaining organic impurities such as unconverted intermediate. This method was successful and produced modest yields of 68% on average. The free alcohol was visible by IR as a broad peak at 3363.77 cm^{-1} and this method did not racemise, as shown by the optical rotation of +20.3° in chloroform (c= 1.012 g/100 mL). The ^{1}H-NMR showed two singlets at 1.42 ppm and 1.45 ppm integrating to nine, which represented the Boc and tert-butyl groups. The other characteristic peak was a triplet from 3.64 ppm to 3.67 ppm integrating to two, which represented the protons adjacent to the alcohol. The ^{13}C-NMR also showed these carbons at 28.01 ppm and 28.08 ppm. The mass was consistent with the expected product.

3.5 Mesylation of the Amino Alcohol

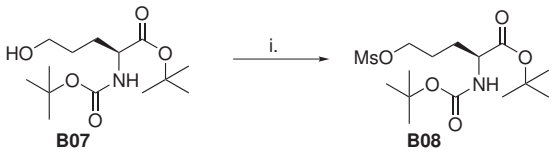

SCHEME 3.13: Mesylation of the alcohol i. MsCl, dry DMF, Et_3N (87% yield)

The alcohol was substituted for an azide through conversion to a mesyl group. The mesyl is a far better leaving group than the alcohol and formation of the mesyl has been well documented in the literature in excellent yields.[175] The triethylamine serves the purpose of neutralising the HCl formed during the reaction, which in theory could deprotect the Boc or the tert-butyl ester if the concentration became too great.

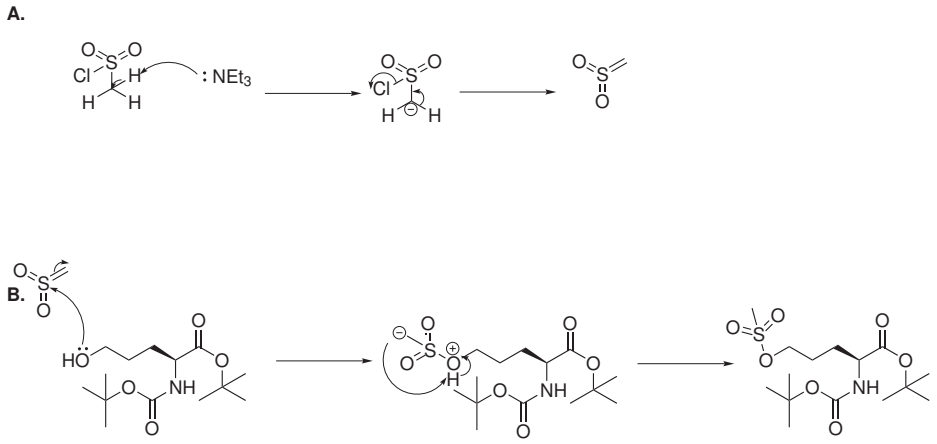

SCHEME 3.14: Mechanism for the mesylation of the side-chain alcohol. A. Formation of the sulfene. B. nucleophilic attack of the sulfene by the alcohol

Scheme **3.14** illustrates the mechanism for the substitution of the alcohol with the mesyl group. The triethylamine undergoes nucleophilic attack on mesyl chloride and further rearrangement produces the sulfene, which is the reactive species that undergoes electrophilic attack on the alcohol via the central sulphur. Proton transfer produces the final mesylated compound.

The reaction completed within 1 hour and produced the mesylate **B08** in excellent yields (87%). The greatest challenge with this reaction and subsequent reactions was the removal of DMF through extraction into ether and ten washes with distilled water, as well as concentrating *in vacuo* for a prolonged period to ensure that the product was

completely dry. In contrast, the removal of the need to purify made this route very efficient at generating large amounts of product quickly.

The ^{1}H-NMR displayed a new singlet integrating to three at 2.97 ppm, representing the methyl functionality of the mesyl group. This was shown in the ^{13}C-NMR at 37.37 ppm. The alcohol peak disappeared from the IR spectra and the mass was consistent with the expected product. and the optical rotation ensured that the chirality was maintained.

3.6 Formation of the Azide through the Displacement of the Mesyl Group

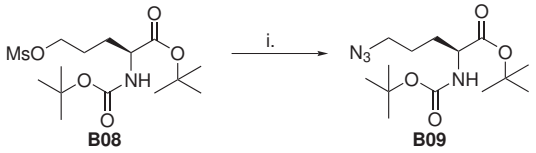

SCHEME 3.15: Substitution of the mesyl for an azide functionality i. NaN_3, dry DMF, 67°C, N_2, 5 h (69% yield)

The mesyl was readily displaced in the presence of sodium azide through an S_N2 mechanism. The reaction was carried out under anhydrous conditions to prevent moisture hydrolysing the mesyl group, as shown in scheme **3.16**. The product was extracted into ether, washed ten times with distilled water and concentrated *in vacuo* to ensure that all the the DMF was removed. Again, the product did not require purification and the product was generated in good yields (69%).

SCHEME 3.16: Mechanism of Fmoc-azidonorvaline-OH synthesis

The mesyl was lost from the ^{1}H-NMR, however the azide peak was distinct by IR, displaying a sharp peak at 2094.81 cm^{-1}. The mass was also consistent with the expected product and the optical rotation ensured that the chirality was maintained through maintenance of the direction of rotation.

3.7 Boc Deprotection of the Azide Species

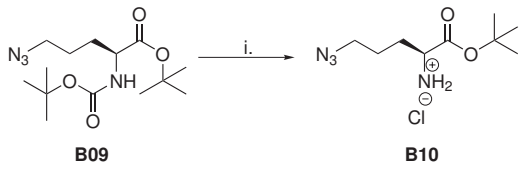

SCHEME 3.17: Boc deprotection to afford the free amine as the hydrochloride salt i. 2M HCl in EtOAc, rt, overnight (100%)

Deprotection of the acid-labile protection could be done one of two ways: it was possible to selectively deprotect the Boc group by treating the amino acid overnight in 2M HCl in ethyl acetate. Alternatively, both protecting groups could be removed in the presence of 6M HCl in water. Although both routes were explored, it was discovered that premature deprotection of the terminal carboxylic acid prohibited the attachment of the Fmoc group to the free amine, as it was postulated that the competing reaction between the free acid and Fmoc chloride halted the progression of the Fmoc amino acid formation.

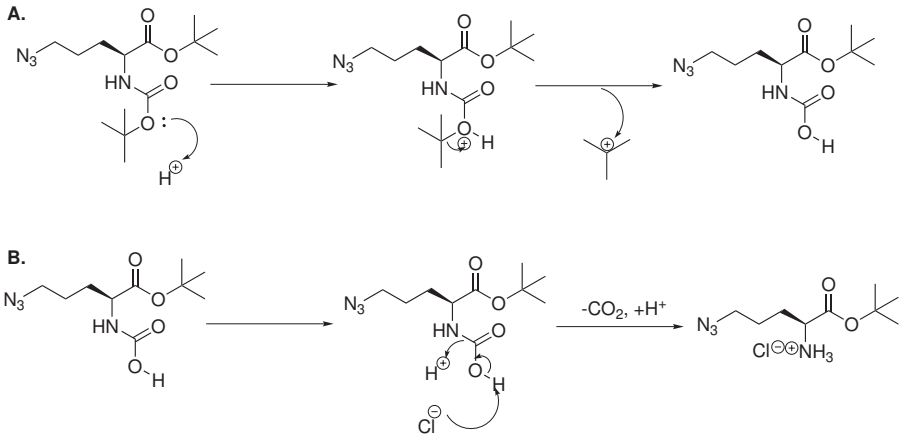

SCHEME 3.18: Boc deprotection to afford the free amine as the hydrochloride salt A. Removal of the tert-butyl cation B. decarboxylation to afford the free amine as a salt

Protonation of the butyloxy functionality causes the breakdown of the tert-butyl component and the release of butene. The chloride anion deprotonates the newly formed carboxylic acid moiety, causing the release of carbon dioxide, as shown in scheme **3.18**.

The subtle difference in lability between the Boc and tert-butyl served as a useful tool, as Fmoc protection of the ester occured readily and purification was facile due to the higly non-polar nature of the product.

3.8 Formation of the Fmoc Amino Acid for Solid Phase Peptide Synthesis

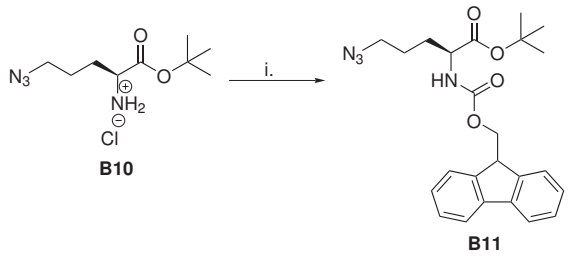

SCHEME 3.19: Synthesis of Fmoc-azidonorvaline-OH as the tert-butyl ester i. FmocCl, $NaHCO_3$, THF, H_2O, 0°C, 30 min (48% yield)

Fmoc protection proved troublesome, as it was not possible to Fmoc-protect with the free terminal acid, however Fmoc-protection with the tert-butyl-ester-protected acid was reasonably successful (48%). Characterisation by ^{1}H-NMR displayed characteristic Fmoc peaks in the aromatic region from 7.27 ppm to 7.29 ppm, 7.35 ppm to 7.39 ppm, 7.64 ppm to 7.67 ppm and 7.76 ppm to 7.78 ppm. Each group integrated to two as the molecule is symmetrical, and the splitting indicated two sets of triplets, a triplet of doublets and a doublet due to neighbouring aromatic protons in each environment. The corresponding aromatic carbons were also displayed in the ^{13}C-NMR spectra, as well as the four quarternary carbons at 145.31, 145.12, 142.58 and 126.21 ppm. Fmoc also produces two further characteristic protons, a triplet integrating to one between 4.18 ppm and 4.21 ppm and a multiplet integrating to two between 4.32 to 4.40 ppm to indicate the two aliphatic environments of Fmoc (in theory, the latter should be a doublet, but appears as a multiplet due to the complexity of the aliphatic region of the molecule). The methylene also appeared in the ^{13}C-NMR DEPT-135 at 67.83 ppm.

3.9 Silyl Deprotection of the Terminal Ester

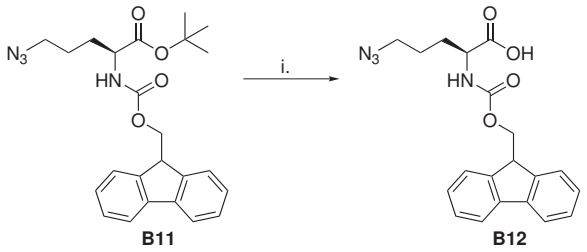

B11 **B12**

SCHEME 3.20: Synthesis of Fmoc-azidonorvaline-OH through silyl deprotection i. Trichloromethylsilane, sodium iodide, dry MeCN, rt, 4 h (34%)

The deprotection of the transesterified product was possible by the *in-situ* formation of triiodomethylsilane, which participated in a nucleophilic substitution at the ^{t}-butyl ester as first described by Olah and coworkers in 1979.[176] Using water, it was then possible to hydrolyse the silyl-oxygen bond to liberate the free acid. Although the carboxylic acid peak was not present in the ^{1}H-NMR in chloroform, the tert-butyl peak integrating to nine had been lost. This was also evident from the carbon NMR. IR also revealed that the azide peak was conserved at 2094.81 cm^{-1}, as it was thought to be possible to reduce the azide with the silyl group.

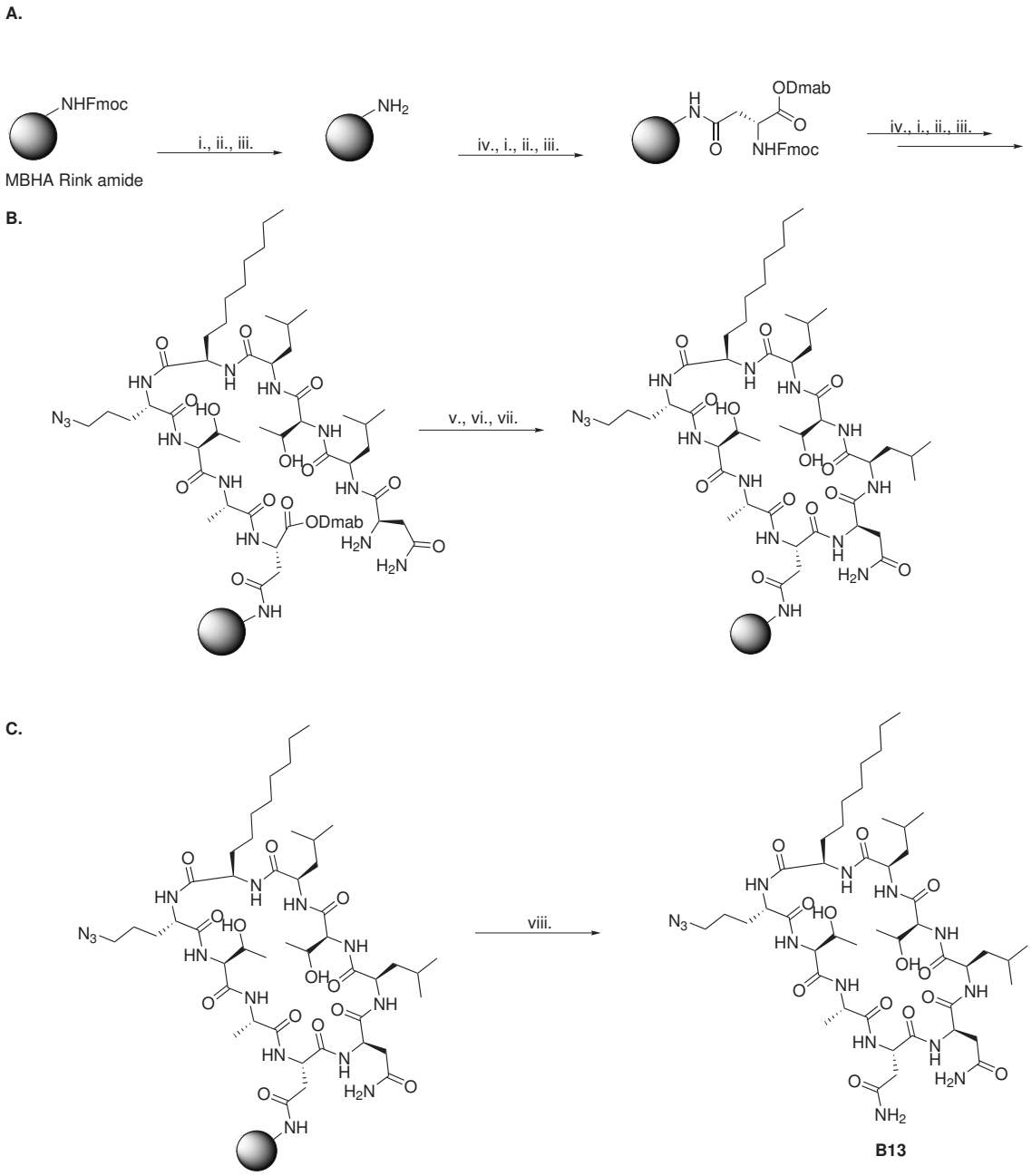

FIGURE 3.1: Synthesis of the cyclic peptide incorporating the azido-amino acid. A. Synthesis of the linear chain. B. Cyclisation of the peptide. C. Cleavage of the peptide from the resin. i. 40% Piperidine in DMF, rt, 5 min ii. 20% Piperidine in DMF, rt, 5 min iii. 20% Piperidine in DMF, rt, 5 min iv. Fmoc-AA-OH, HOBt, HBTU, DIPEA, Et_3N, DMF v. 2% N_2H_2 in DMF vi. 5% DIPEA in DMF vii. DIC, HOBt, DIPEA, DMF, rt, 2 d. viii. TFA:H_2O:TIPS 95:2.5:2.5 rt, 3 h

Subsequent synthesis of azidochlorofusin and cyclisation were carried out as per the original solid phase synthesis of chlorofusin,[77] however the cyclisation required an extra two days to reach completion. Upon completion, a small amount of resin/peptide complex was cleaved to confirm the correct mass by MALDI. Once mass was confirmed, a

test reaction on 58 mg of resin/peptide complex was carried out in the presence of one equivalent of 3-chloro-1-ethynylbenzene, copper sulfate pentahydrate and sodium ascorbate overnight on the solid phase. Following mass confirmation on the first analogue, subsequent analogues were generated in the same manner.

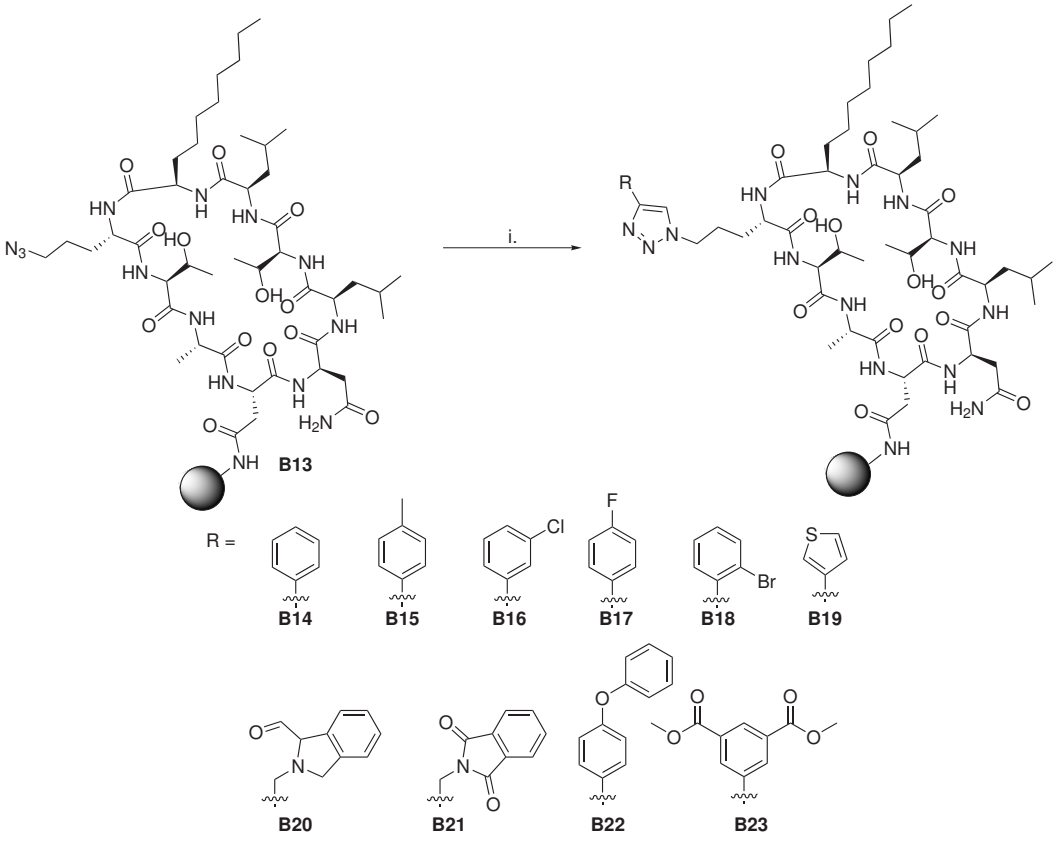

FIGURE 3.2: Synthesis of the cyclic peptide-based analogues i. 10 eq R-alkyne, 10 eq $CuSO_4.5H_2O$, 10 eq Na ascorbate

Table **3.1** indicates the different analogues synthesised, their respective yields (assuming 100% yield in the generation of the click chlorofusin peptide) and characterisation by MALDI and HPLC. The yields for these compounds were poor due to losses of resin during transfer to the vials as well as losses incurred during purification by HPLC, as compounds required filtration both from the reaction vessel and again prior to entry into the HPLC. It was also not until this thesis was completed that the conditions were optimised to improve yields.

No.	Percentage Yield	MALDI MS	HPLC retention time
B13	8%	1060.74 m/z and 1076.75 m/z	17.58 min
B14	2%	1161.64 m/z and 1177.66 m/z	18.07 min
B15	3%	1176.46 m/z	18.365 min
B16	2%	1196.19 m/z and 1212.19 m/z	18.41 min
B17	1%	1176.60 m/z and 1192.59 m/z	18.85 min
B18	1%	1242.70 m/z and 1258.11 m/z	18.28 min
B19	4%	1167.33 m/z and 1183.28 m/z	17.96 min
B20	5%	1258.62 m/z	17.80 min
B21	5%	1244.87 m/z	17.70 min
B22	8%	1253.92 m/z	17.80 min
B23	4%	1277.75 m/z	18.122 min

TABLE 3.1: Characterisation of the Click Chlorofusin Analogues (HPLC was undertaken in a methanol:water system, starting at 5:95 methanol:water with 0.05% TFA in each solvent to prevent band broadening, increasing to 95:5 methanol:water over 15 minutes and re-equilibrating to 5:95 methanol:water over 5 minutes)

No.	**IC_{50} (95% Confidence Interval) /μM**	**K_i (95% Confidence Interval) /μM**	**R^2**
B14	NA	NA	NA
B15	66.01 (40.35 to 108.0)	8.309 (5.079 to 13.59)	0.9443
B16	NA	NA	NA
B17	NA	NA	NA
B18	NA	NA	NA
B19	NA	NA	NA
B20	NA	NA	NA
B21	NA	NA	NA
B22	NA	NA	NA
B23	NA	NA	NA

TABLE 3.2: Biological data for compounds tested in the FP assay (NA = no activity up to 500 μM), where R^2 indicates the correlation coefficient (a value of 0 indicates no correlation whilst a value of 1 indicates 100% correlation)

3.10 *In vitro* screening of Click Chlorofusin Analogues by Fluorescence Polarisation Assay

Table **3.2** illustrates the results of the *in vitro* screening through the FP assay. This data was a breakthrough as this was the first since the first reported isolation of chlorofusin in 2001 that a chlorofusin-based analogue was shown to inhibit the p53/MDM2 interaction. The assay showed that the 4-methylphenyl substituent was active against the p53/MDM2 protein-protein interaction *in vitro*, however as only a small library was synthesised further investigation is required to further examine SAR.

Following this, the importance of the peptide was investigated through replacement of the peptide with the Fmoc-protected amino acid in its place. The side chains displaying activity in the FP assay were used to react with the Fmoc amino acid to produce the click library, as well as a variety of other side chains, which are discussed in more detail in the next section.

3.11 Synthesis of Click Amino Acid Analogues

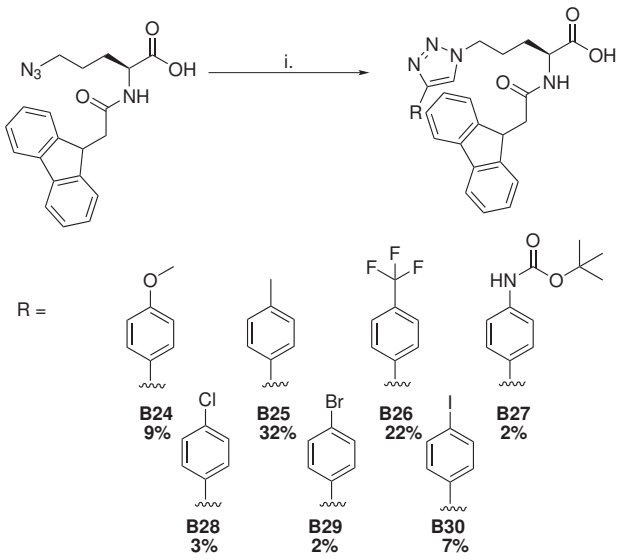

SCHEME 3.21: Synthesis of the click amino acid analogues and their respective yields (i. L-ascorbate,$CuSO_4$, R-alkyne with R-groups and their respective yields listed above, 1:1 ^{t}-BuOH:H_2O, rt, overnight

As a result of the intial FP data, control Fmoc click amino acids were synthesised to determine the importance of the peptide. Interestingly, the IC_{50} drastically decreased when the peptide chain was replaced with the Fmoc group (see table **3.3**). This led to

the synthesis of a larger group of Fmoc click amino acids, with R-groups chosen due to their para-position, lipophilicity and bioisosterism to the active toluene analogue **B15**.

3.12 Removal of the Fmoc Group to Determine Importance in Binding

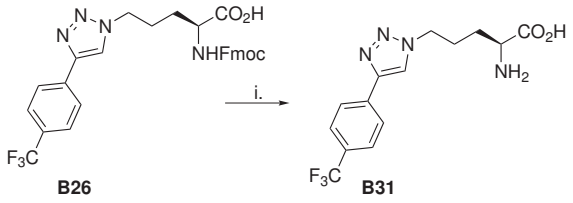

SCHEME 3.22: Deprotection of the Fmoc group. i. 1% DBU in CH_2Cl_2, 1% Piperidine in DMF, MeCN, rt, 10 min (82% yield)

In order to determine whether or not the Fmoc group was participating in binding, it was necessary to selectively remove the Fmoc group. Although the triazole ring is considered very stable, different deprotection conditions appeared to cause the molecule to degrade. It appeared that the compound was not stable to 20% piperidine, DIPEA or triethylamine. Eventually, a methodology utilising 1% piperidine and 1% DBU for 5 minutes was trialled, which proved to be sufficient to deprotect the Fmoc but insufficient to degrade the molecule. This was shown in the ^{1}H-NMR, as the triazole peak at 8.50 ppm remained whilst the Fmoc peaks disappeared. The mass was also confirmed by LCMS, however the compound was unstable and therefore it was not possible to get a high-resolution mass.

3.13 *In vitro* screening of click compounds by Fluorescence Polarisation Assay

Table **3.3** illustrates the click-based compounds that were determined to be active through FP assay. Interestingly and as noted in previous chapters, the presence of a halogen improved activity, with more electronegative halogens demonstrating increased potency. The only click chlorofusin analogue that demonstrated activity was the toluene analogue **B15** and the fact that the click amino acid bearing the methyl group was even more potent suggests that the peptide is not needed for activity.

No.	R-group	IC_{50} (95% Confidence Interval) /μM	K_i (95% Confidence Interval) /μM	R^2
B24	4-OMePh	5.655 (3.391 to 9.431)	0.7118 (0.4268 to 1.187)	0.9659
B25	4-MePh	24.26 (15.13 to 38.90)	3.054 (1.904 to 4.896)	0.9562
B26	4-CF_3Ph	60.31 (25.94 to 140.0)	7.592 (3.266 to 17.65)	0.8953
B27	4-NHBocPh	57.36 (34.28 to 95.97)	7.220 (4.315 to 12.08)	0.9813
B28	4-ClPh	6.065 (5.342 to 6.885)	0.7703 (0.6785 to 0.8746)	0.9976
B29	4-IPh	2.899 (2.035 to 4.131)	0.3649 (0.2561 to 0.52)	0.9829
B30	4-BrPh	5.513 (3.503 to 8.676)	0.6939 (0.4409 to 1.092)	0.9702
Nutlin-3a	-	0.6067 (0.494 to 0.745)	0.0771 (0.0627 to 0.0946)	0.9935

TABLE 3.3: Biological data for compounds shown to inhibit in the FP assay, including Nutlin-3a as a positive control

3.14 MTS Cytotoxicity Assays

No.	SJSA-1 IC_{50} /μM	HL-60 IC_{50} /μM	A375 IC_{50} /μM
B15	NA	NA	NA
B24	33.1	NA	NA
B25	31.2	5.0	49.3
B26	NA	NA	NA
B27	NA	NA	NA
B28	NA	NA	NA
B29	NA	NA	NA
B30	NA	NA	NA
Nutlin-3a	5.778	NE	NE

TABLE 3.4: Biological data for compounds shown to inhibit in the MTS assay in overexpressed MDM2 (SJSA-1), p53-null (HL-60) and MDMX-overexpressed (A375) cell lines (NA = no activity up to 500 μM, NE = not examined)

The MTS data in table **3.4** suggests that B25, although active against p53 and MDM2, may also work via a p53-null mechanism. B24 showed greatest activity in cells over-expressing MDM2, with lower levels of activity in the other two cell lines. Although this indicates promise that B24 may be selective against the p53-MDM2 protein-protein interaction, further work needs to be undertaken to further support this theory, as cell

lines are insufficient to model a full anatomical system and variation in the cells can increase with increasing passage number of the cells (that is, during the cell division and replication process). As for the lack of activity of the other compounds tested in the MTS assay, it is possible that cell permeability could be an issue and therefore future would be to synthesise the compounds as terminal esters on the amino acid.

3.15 Conclusions and Future Work

This chapter explored the synthesis of novel chlorofusin analogues whilst maintaining the structure of the chlorofusin peptide. Despite simple bicyclic acids displaying no activity, the use of novel click products reinstated activity, displaying activity in one analogue, at an IC_{50} value of 66.01 μM. Simplification of click analogues through truncation of the peptide permitted novel analogues with good inhibition of the p53/MDM2 Protein-Protein Interaction as displayed through FP assay, with six compounds displaying activity at concentrations less than 100 μM. Further studies by MTS, however, illustrate the need to improve lipophility in order to improve cellular uptake, if indeed cell permeability is the issue and not that the compounds are inactive. The balance of lipophilicity is extremely delicate, as the terminal carboxylic acid may participate in hydrogen-bonding with His96 within the hydrophobic pocket of MDM2. Also, attempts to form the esters prior to the click reaction were unsuccessful, suggesting that this reaction would require optimisation.

Future work surrounding these novel analogues concerns improving our understanding on the binding modality: it is postulated that STD-NMR would be a useful tool in helping to determine how these novel analogues bind within the hydrophobic pocket. Combining STD-NMR and molecular modelling would give us a great deal more information and aid the generation of further analogues.

The next chapter will explore the azaphilone moiety in more detail, with the intention of creating an azaphilone-based library that can be explored to generate further SAR with respect to the p53/MDM2 protein-protein interaction.

Chapter 4

Synthesis of Analogues Based on the Azaphilone Chromophore of Chlorofusin

4.1 Introduction

The previous chapter involved the synthesis and biological testing of a variety of different analogues based on the chlorofusin peptide. Interestingly, a novel library that was explored involving an ornithine in which the side chain amine was replaced with an azide produced one compound that selectively inhibited the p53/MDM2 protein-protein interaction. Following the success of the click amino acid library, compounded with the fact that the peptide's involvement in binding was not necessary to generate inhibitors in this instance it was decided to shift focus back to the azaphilone component of chlorofusin, which also beared some resemblance to the isoquinolin-1-ones, as it too was a bicyclic chromophore.

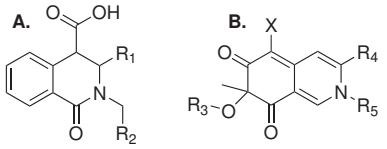

FIGURE 4.1: A. Structure of an isoquinolin-1-one and B. Structure of an azaphilone core unit

This chapter focusses on the generation of novel azaphilone analogues and the molecular modelling used to determine analogue generation.

4.2 Introduction to Azaphilones

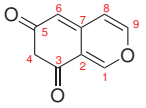

FIGURE 4.2: Core unit of the azaphilone chromophore and subsequent numbering

Azaphilones are bicyclic natural products that are so-called due to their high solubility in ammonia and subsequent ability to condense to form vinylogous amides (see scheme **4.1**).[177]

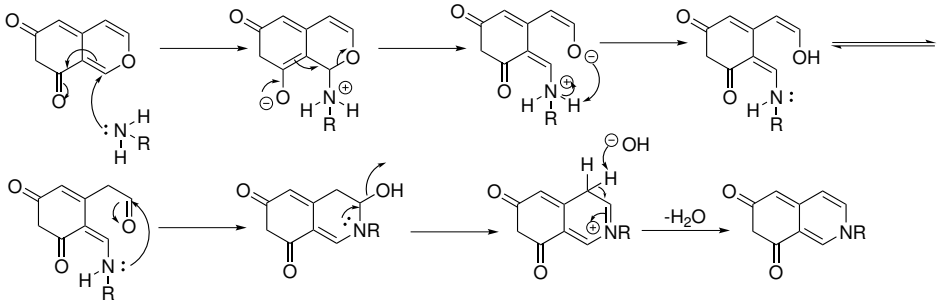

SCHEME 4.1: Mechanism of the condensation of azaphilones to form vinylogous amides

Azaphilones are highly abundant in nature, with chlorofusin containing a condensed azaphilone functionality.

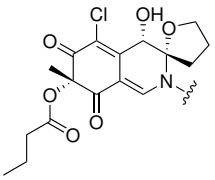

FIGURE 4.3: The azaphilone present in chlorofusin

The chlorofusin azaphilone shown in figure **4.3** consists of a butyric ester and a methyl group at position 4, a chlorine in position 6, a hydroxyl group in position 8 and a tetrahydrofuran ring extending from position 9. In chlorofusin, it has been suggested that the azaphilone moiety is responsible for binding in the hydrophobic pocket of p53, following a conformational change in the MDM2 protein induced by the binding of the peptide around the outer surface of MDM2[119] however no crystal structures have been published to date. The evidence for this unusual type of binding is further supported by the ELISA-based assays undertaken by Woon *et al.*[77] Woon demonstrated that,

by omitting either the peptide or the azaphilone, or by coupling the peptide to simple aromatics, then there was no binding to MDM2 as demonstrated by the ELISA assay.

Boger expanded the ELISA screen in two ways: by firstly examining the conformation of the asparagines (as Yao *et al.* had shown that they were opposite conformations but were unsure of which was which)[122] and by testing stereoisomers of the azaphilone portion of chlorofusin against the natural product.[152] Interestingly, stereochemistry of the azaphilones did not appear to have an appreciable effect on the IC_{50}.

Research carried out by Hardcastle *et al.* surrounding the potency of p53-MDM2 inhibitors illustrated the importance of the halogen group (which is present in the main classes of inhibitors including the nutlins, isoindolinones, spiro-oxindoles and benzodiazepinediones), suggesting that the halogen is important for directing the molecule into the hydrophobic pocket in which the Phe^{19}, Trp^{23}, Leu^{26} of p53 perform key binding interactions. Studies by Hardcastle *et al.* demonstrated that substitution of the halogens with methoxy- and ethoxy- functional groups obliterated the potency of an isoindolinone library.[178]

It was decided that, following from the previous studies on chlorofusin and analogues derived from it, that analogues of the full azaphilone moiety would be synthesised in the hope of attaching it to the natural peptide. By forming azaphilone analogues and keeping the peptide constant, it was hoped that the interactions in the hydrophobic pocket could be maximised whilst ensuring that the azaphilone was held in the correct orientation for binding by the peptide.

4.3 Reported Syntheses of the Azaphilone Chromophore

There are a variety of different methods to achieve the desired Sonogashira precursor and subsequent azaphilone core required in the synthesis of azaphilone analogues. The various methods are listed below, as well as the advantages of each method as well as challenges encountered when trialled in the lab. The methods attempted in the lab were Methods A and E, with Method E being the chosen route for routine synthesis.

4.3.1 Proton Extraction, Lithiation and Demethylation to form the Sonogashira Precursor (Method A)

One route to the azaphilone can be achieved through proton extraction in the presence of *n*-butyllithium, electrophilic aromatic substitution with iodine produced from diiodoethane and deprotection of the methyl ethers in the presence of boron tribromide to

produce **C01**, as demonstrated in scheme **4.2**. This method is rapid and produces a more effective Sonogashira precursor than that used in the final synthesis as iodide is a better leaving group than bromide and hence more effective in the reaction. This method also requires a single column to reach the Sonogashira precursor, as opposed to four in the final adopted route, as demonstrated in scheme **4.3**.

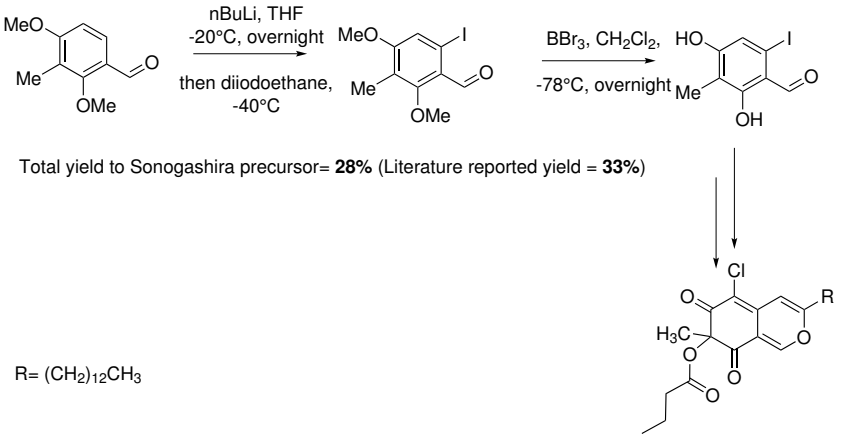

SCHEME 4.2: One route to form the azaphilone moiety as published by Porco *et al*[179]
i. ET_3N, 1.6M *n*-BuLi in THF, diiodoethane, THF, -20°C to rt, overnight then BBr_3, CH_2Cl_2, -70°C to rt, overnight

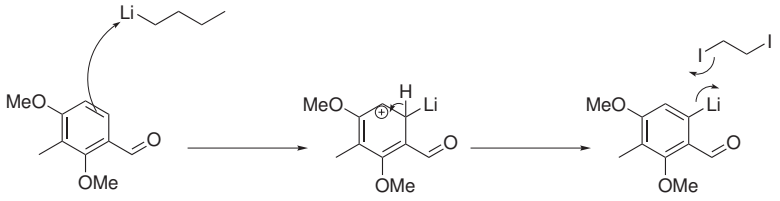

SCHEME 4.3: Mechanism of proton exchange followed by electron transfer

The disadvantage of method A was the difficulty in monitoring and the strict temperature control required to produce the desired product (see scheme **4.2**). Also, the high reactivity of *n*-butyllithium resulted in various side reactions and the n-butyllithium needed discarding frequently due to degradation on storage. Finally, the crude intermediate was difficult to handle and subsequent reactions were carried out assuming 100% yield until the Sonogashira precursor was purified.

4.3.2 Synthesis of the Natural Azaphilone Using Organolithiation and Bromination to form the Sonogashira Precursor (Method B)

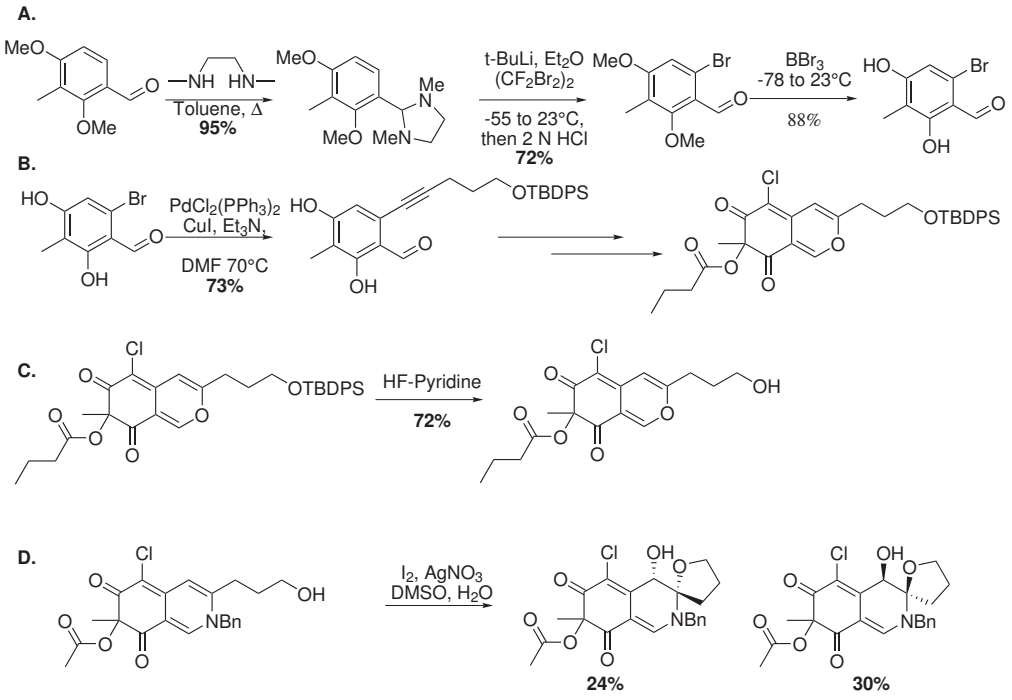

SCHEME 4.4: A. Method B synthesis of the Sonogashira precursor B. Sonogashira cross-coupling of TBDPS-protected pentyn-1-ol C. Deprotection of TBDPS to afford the free alcohol D. Cyclisation of the furan ring of a model chlorofusin azaphilone

Scheme **4.4** illustrates the scheme used by Boger *et al.* to synthesise the natural chlorofusin azaphilone.[122] Boger *et al.* synthesised the natural azaphilone by protection of the aldehyde of 3,5-dimethoxybenzaldehyde then bromination in the presence of *t*-butyllithium to afford the Sonogashira precursor. The precursor was reacted with TBDPS-protected pentyn-1-ol, as this protection was required for the 2-step cyclisation and IBX oxidation. The TBDPS protection was removed following chlorination using HF-pyridine. The furan ring of a model chlorofusin azaphilone was formed through oxidative spirocyclisation using silver(III) nitrate and iodine in DMSO and water. Although this method was successful, it was lengthy and required the use of *t*-butyllithium, which is spontaneously pyrogenic and therefore an alternative route was sought with less hazardous chemicals.

The natural azaphilone is chiral at position 4. Previous attempts to synthesise the azaphilone have been carried out racemically and purification has been carried out using chiral HPLC.

4.3.3 Copper-Catalysed Oxidative Dearomatisation to form the Azaphilone Chromophore (Method C)

Scheme **4.5** illustrates the use of the ligand in the synthesis of the azaphilone core whilst scheme **4.6** illustrates the ligand analogues generated to synthesise the azaphilone. Method C confers the advantage of an enantiomerically-pure product in good yields, however the extraction, purification and synthesis of the sparteine surrogates, as well as the production of the copper catalyst (for which synthesis requires expensive reagents), makes this route longer and more expensive than the final methodology used in our lab (Method E).

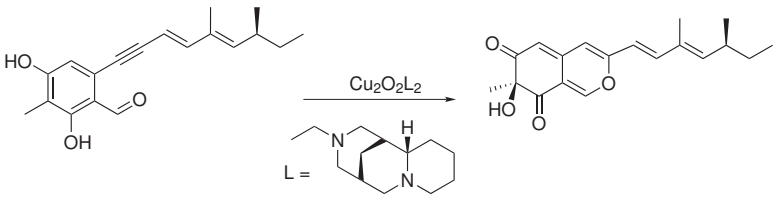

Scheme 4.5: Scheme for the synthesis of Sparteine analogues using a copper-based ligand with *N,N*-diisopropylethylamine, CH_2Cl_2 and DMAP, varying from -10°C to rt overnight[179]

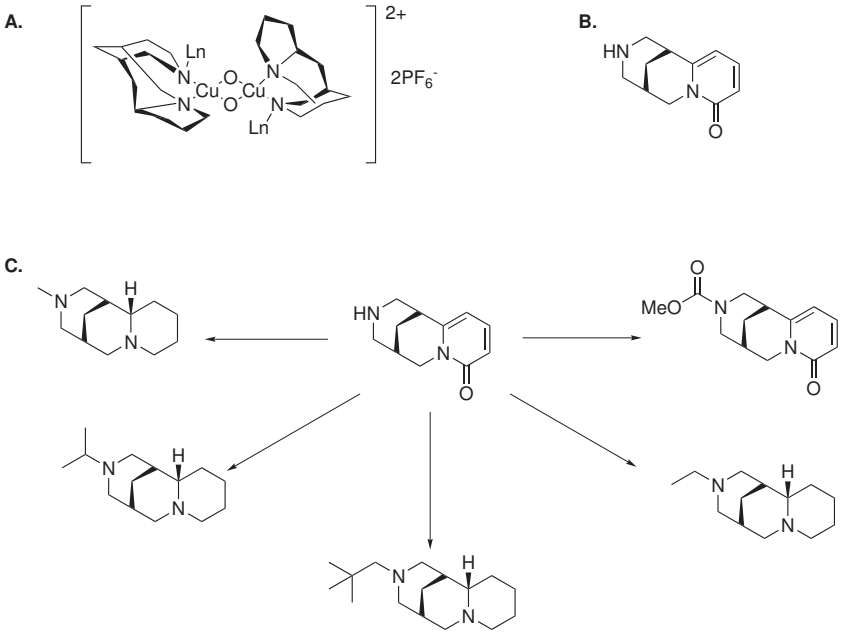

Scheme 4.6: A. Structure of the copper catalyst synthesised for the oxidative dearomatisation of Sonogashira products to form azaphilones B. Chemical structure of (-)-sparteine[179] C. (+)-sparteine surrogates synthesised as ligands for the copper catalyst[180]

4.3.4 Biosynthetic Route to form Azaphilones (Method D)

It is also possible to synthesise azaphilones semi-synthetically using *Aspergillus nidulans*, as displayed in scheme **4.7**.[181] Enzymes within the fungi can be genetically engineered to form the azaphilone precursor, after which water is eliminated and the central bicyclic chromophore is formed. Due to reagents available and complexity of the bioengineering required to use this route, this methodology was not explored in our lab.

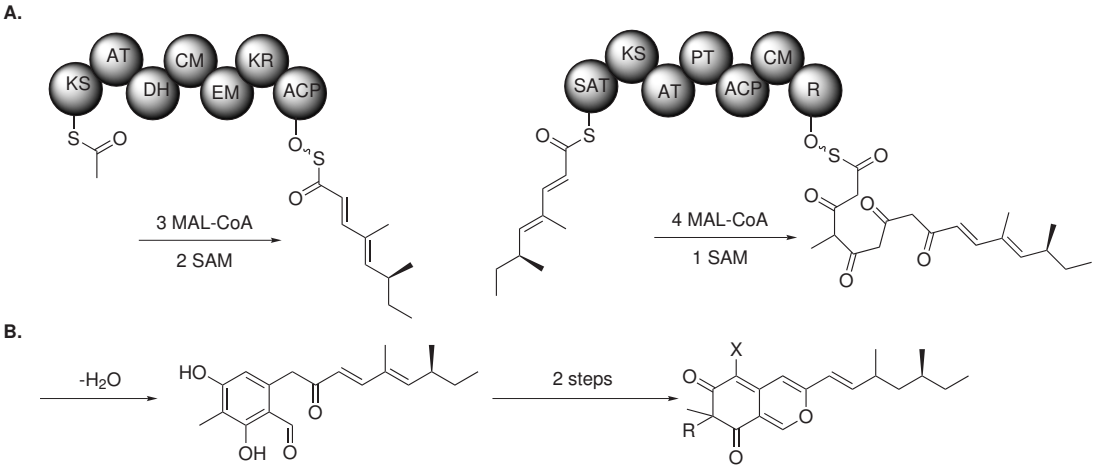

SCHEME 4.7: A. Reengineered pathway to azaphilone synthesis B. Conversion of the Sonogashira product to the azaphilone[181]

4.4 Synthesis Undertaken to Achieve the Azaphilone Moiety (Method E)

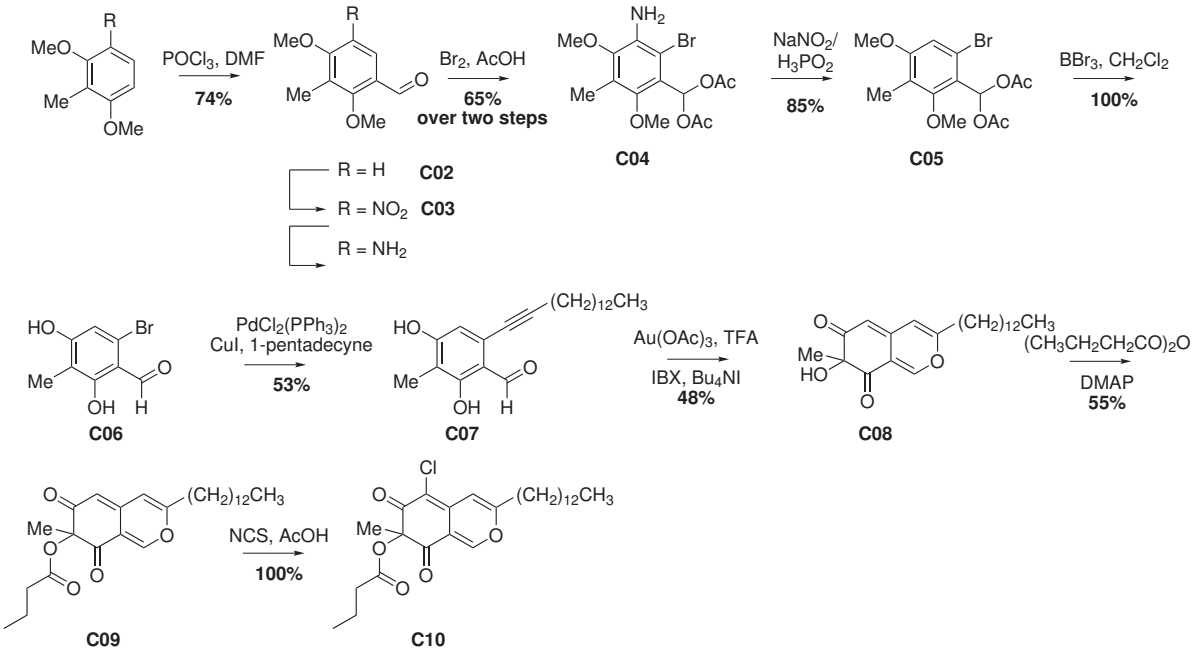

SCHEME 4.8: Initial synthesis to the model azaphilone adopted within this thesis

The initial synthetic route was first realised by Porco *et al*,[182] in which a Sonogashira precursor **C07** is generated, permitting the generation of a variety of analogues, as shown in scheme 4.8. **C07** is then cyclised and oxidised to afford the azaphilone. Finally, to produce the same functionalisation as the chlorofusin azaphilone, the free alcohol is esterified and the azaphilone is halogenated in position 6.

Variants of this procedure had been previously documented in the literature.[179] Instead of using IBX and TFA to produce the azaphilone, the same process can be carried out using a copper catalyst.[179] The ligand was a sparteine surrogate, isolated from Cytisus seeds through dissolution in a dichloromethane, methanol and aqueous ammonium chloride mixture, followed by dichloromethane extraction.[180]

The starting material used was 2,6-dimethoxytoluene, as this was much cheaper than 3,5-dimethoxybenzaldehyde and can be readily converted into the aldehyde through the formation of a Vilsmeier complex and subsequent formylation.

4.4.1 Vilsmeier Formylation of 2,6-dimethoxytoluene

SCHEME 4.9: Addition of an aldehyde group through the *in situ* formation of a Vilsmeier complex i. $POCl_3$, DMF, N_2, 0°C then 100°C, 6 h, (74% yield)

Functionalisation of 2,6-dimethoxytoluene with an aldehyde was required for later cyclisation to form the azaphilone. The Vilsmeier reaction was chosen as the preferred method of aldehyde formation, due to its high literature yields (circa 71%).[183] It is an effective method of formylation of electron-rich arenes. The 2,6-dimethoxyltoluene bears three electron-donating groups, which direct electrophilic attack in the ortho- or para- positions. Due to the structure of the molecule and its symmetry, the ortho- and para- positions of the methoxy groups are equivalent due to positive mesomeric effects outweighing the negative inductive effects, hence electrophilic attack is more likely in these positions due to increased stabilisation.

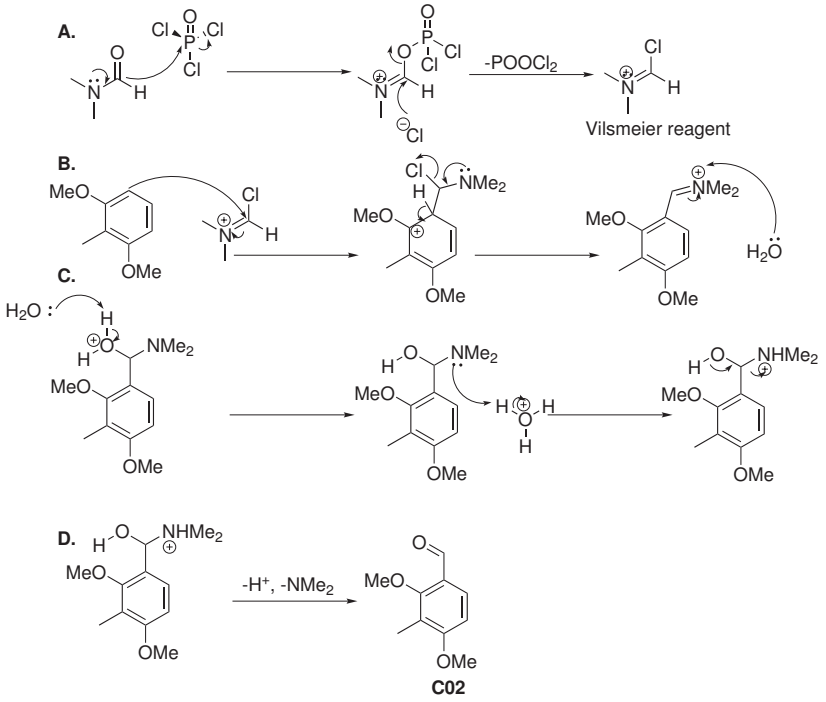

SCHEME 4.10: Mechanism for the Vilsmeier reaction A. formation of the Vilsmeier reagent B. electrophilic aromatic substitution with 2,6-dimethoxytoluene C. proton transfer with water D. Final compound

This method requires the *in situ* formation of the complex, which is formed through nucleophilic attack by the formyl group of DMF, resulting in chloride displacement. The newly formed ether bond is severed and resonance stabilisation produces the Vilsmeier product. The product is moisture sensitive and is hence carried out under strict anhydrous conditions. The reaction is also exothermic hence DMF is added dropwise at 0°C.

The Vilsmeier product was then transferred into a solution of 2,6-dimethoxytoluene in anhydrous DMF, resulting in subsequent electrophilic aromatic substitution. Finally, to quench the reaction of any unreacted Vilsmeier product and form the aldehyde, ice water was added.

Yields were moderate to good, with a representative yield being 74% following column chromatography. Although recrystallisation and purification through the addition and filtration of activated charcoal produced higher yields, the products were less pure. Most likely losses of product were due to diformylation of the starting material with excess Vilsmeier reagent.

Key characterisation was determined through the presence of the aldehyde, which was prominent by ^{1}H-NMR at 10.23 ppm as a singlet and at 189.20 ppm in the ^{13}C-NMR. The presence of only 1 peak in both of these spectra confirmed that there was only one formyl group, and the mass was confirmed by LCMS. ^{1}H-NMR also confirmed that the aldehyde was present in the desired position, as the methoxy groups appeared as 2 peaks (at 3.91 ppm and 3.86 ppm), indicating that these protons were not equivalent, as would be the case if the aldehyde had been introduced at the meta position to the methoxy groups.

4.4.2 Menke Nitration

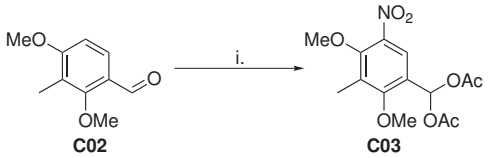

Scheme 4.11: Electrophilic aromatic substitution of a nitro group using the Menke nitration i. $CuNO_4.2.5H_2O$, Ac_2O, 0°C to rt, 6 h (73% yield)

The strategy towards formation of the azaphilone requires bromination in the less activated position: as explained in the Vilsmeier step, electrophilic aromatic substitution is more likely at the position ortho to the methoxy group. To prevent bromination in the

incorrect position, a nitration is undertaken to "block" the more active position. It also prevents dibromination in later steps.

Nitration is generally carried out using a nitrating mixture produced by sulphuric acid and fuming nitric acid. Although this mixture is effective, the conditions are harsh and it can become explosive if handled incorrectly. An alternative form of nitration, coined the Menke nitration, permits the use of less corrosive conditions and is much safer to handle. The additional benefit of this route as the acetic anhydride also reacts with the aldehyde to form a geminal diacetate, which prevents the unintentional reduction of the aldehyde in the next step.

The Menke nitration was first realised in 1925 and utilised cupric nitrate and acetic anhydride (although other nitrate salts have also been shown to be effective).[184] The advantage of using a cupric nitrate salt is that it is very stable upon storage and the change in oxidation state of the copper allows for a visible indicator for the progression of the reaction. The free nitro group is afforded following the formation of a complex with acetic anhydride. The reaction predominantly affords the ortho-substituted product, providing that there is an electron-donating group present.

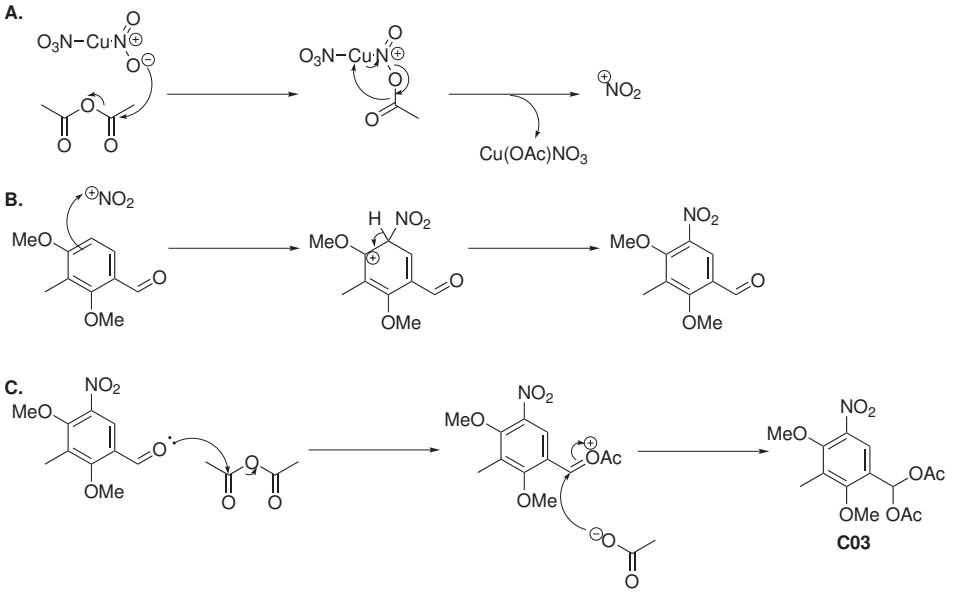

Scheme 4.12: Mechanism for the Menke nitration. A. formation of the free nitronium ion through nucleophilic attack on acetic anhydride. B. Electrophilic aromatic substitution with the nitronium ion. C. Formation of the geminal diacetate using acetic anhydride

The nitration requires quenching with ice water to prevent dinitration. Following an aqueous/organic workup and column chromatography, the reaction produced moderate to good yields (best yield was 73%). There were three key changes in the ^{1}H-NMR: firstly,

the aldehyde peak disappeared and a new peak integrating to six protons appeared at 2.13 ppm and a new singlet proton at 7.92 ppm, which lies inbetween the diacetate and nitro groups. Secondly, the proton at 6.73 ppm disappeared following substitution with the nitro group. LCMS was used to confirm that the product did not dinitrate.

4.4.3 Two-Step Reduction and Bromination

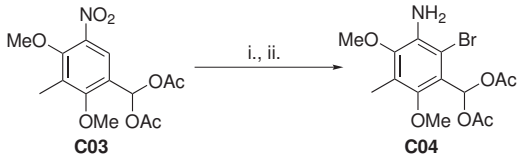

SCHEME 4.13: Two-step reduction and bromination i. Al, $HgCl_2$, 22:7:1 Et_2O:EtOH:H_2O ii. Br_2, AcOH (65% over two steps)

Nitro groups are heavily electron-withdrawing, which would further deactivate the final position available for bromination. In order to improve reactivity, the nitro group must be reduced to an amine to increase the electron density of the ring and to direct to the less favoured position meta to the methoxy groups. The method of reduction of choice for this compound was the mercury-amalgam reduction, as this produces hydrogen in situ and is therefore less explosive than using hydrogen and palladium on carbon.

The first step involves the formation of mercury amalgam by submerging aluminium in 2% aqueous mercury(II) chloride and drying with diethyl ether prior to introduction to the reaction mixture (scheme **4.13**). The solvent consisted of 22:7:1 diethyl ether:ethanol:water. The mixture was determined to ensure that the solvent was monophasic. It was also determined that the water was essential for the production of hydrogen, as ethanol was insufficient. The mechanism is shown in scheme **4.14**

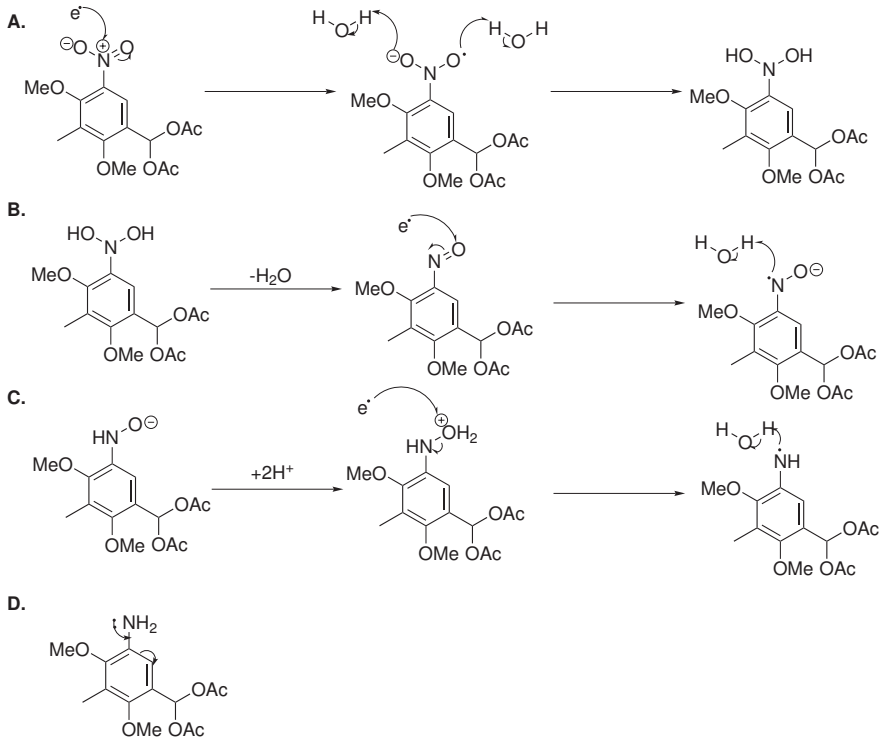

SCHEME 4.14: Mechanism for the reduction of the nitro group A. electrons from the amalgam attack the nitro group, which is followed by nucleophilic attack on water B. The $N(OH)_2$ species forms a hydroxonium ion which is eliminated, after which another electron attacks the nitrous ion, following a second radical attack on water C. the remaining negatively-charged oxygen forms a hydroxonium ion and is eliminated, after which another hydrogen is taken by the nitrogen D. Final product of the reduction[185]

Following successful reduction (as determined by TLC) the amalgam was filtered out using celite and the crude product concentrated *in vacuo*. As the intermediate was unstable and the product required filtration this may have had an impact on the final yield of **C03** in the synthesis.

Once the crude product was dried, it was redissolved in acetic acid and bromine was added (the mechanism of which is shown in scheme **4.15**). Once the reaction had reached completion (as determined by TLC), the bromine was quenched with saturated sodium thiosulfate to prevent side reactions occurring.

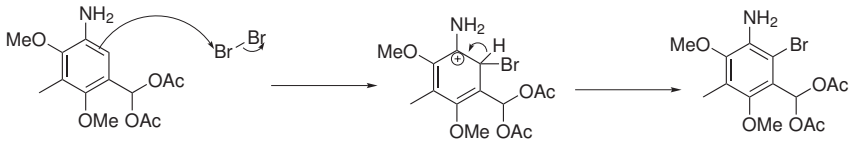

SCHEME 4.15: Mechanism for bromination

The yield for this two-step reaction following column chromatography was moderate (65%). ^{1}H-NMR reveals loss of all aromatic protons and a shift of the remaining singlet proton from 7.93 ppm to 8.14 ppm due to the increased electronegativity introduced by the amine and the bromine. The amine is also present in the IR spectra as characteristic N-H stretches at 3476.95 cm^{-1} and 3378.37 cm^{-1}.

4.4.4 Removal of the Amine Group through Diazotisation and Elimination of the Salt

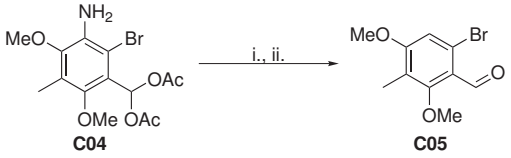

SCHEME 4.16: Removal of the amine through conversion to a diazonium salt i. THF, H_2O, concentrated HCl, $NaNO_2$, 20 min -5°C, ii. urea, 50% w/v hypophosphorus acid, 0°C overnight then 40°C, 4 h (85% yield)

As the amine was no longer required, it was removed through the formation of a diazonium salt. The diazonium salt forms a better leaving group than the primary amine, as the diazonium salt is more energetically favourable to lose from the molecule. In order to produce the diazo, a nitrous ion was produced using HCl in water and THF (to ensure a monohasic system). Urea is then used to quench unreacted nitrite to prevent side reactions. In order to reintroduce a hydrogen, the diazo was displaced through a free-radical reaction using hypophosphorus acid.

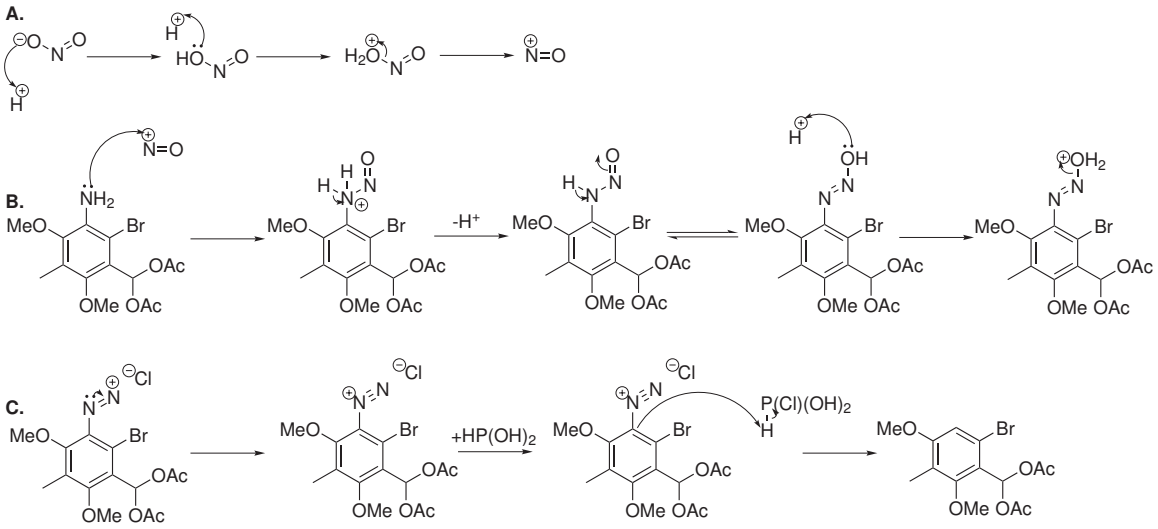

SCHEME 4.17: Mechanism of diazotisation. A. Formation of the nitrous ion. B. nucleophilic attack of the amine on the nitrous ion and rearrangement to form the diazo. C. Elimination of the diazonium salt

As there is no further need for the geminal diacetate, that is also removed and converted back into the aldehyde through acid-catalysed hydrolysis of the acetate groups. The reintroduction of the aldehyde is prominent at 10.27 ppm as well as an aromatic proton singlet at 6.93 ppm in the ^{1}H-NMR spectra. Stretches previously present for the N-H groups are now absent from the IR spectrum.

4.4.5 Demethylation to Afford the Free Alcohol Functionalities

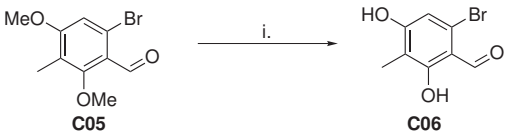

SCHEME 4.18: Alcohol deprotection mediated by boron tribromide i. BBr_3, CH_2Cl_2, -78°C to rt, overnight (100% yield)

Initially, to prevent side reactions, the hydroxyl groups by acetic anhydride the alcohols were protected as methyl ethers. Once the protection is no longer required, demethylation occurs through electrophilic attack of a strong Lewis acid, in this case, boron tribromide, as alkoxides are poor leaving groups. The ether oxygen displaces bromide, which then attacks the methyl group. The reaction is quenched with ice water, which hydrolyses the boron-oxygen complex, producing free alcohols.

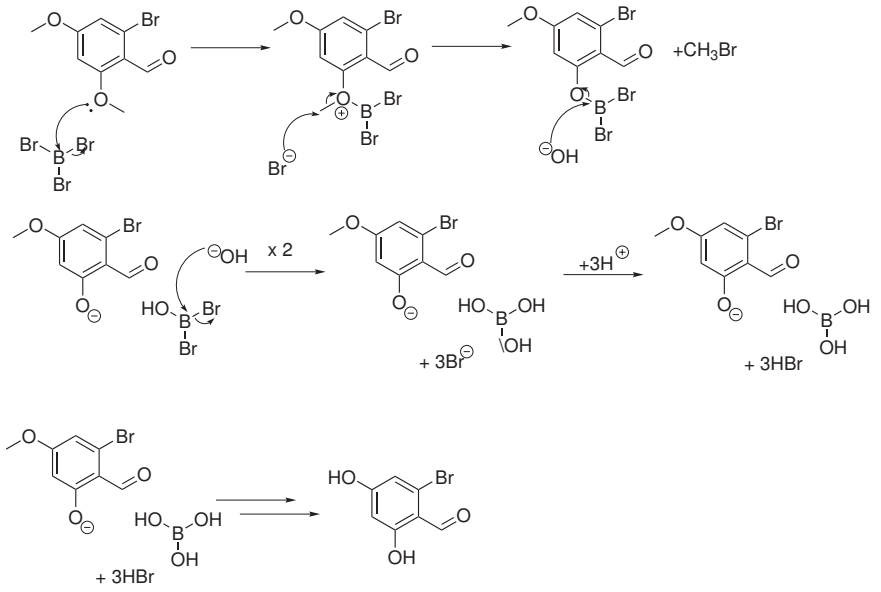

SCHEME 4.19: Alcohol deprotection mechanism through electrophilic attack by boron tribromide

The key indicator that the reaction was successful was the loss of solubility in chloroform due to the increased polarity created from the free alcohols. As the free alcohols are in fast exchange with protic solvents, they were not visible by NMR, however they were clearly visible by IR, with an O-H stretch present at 3334.20 cm^{-1}. LCMS also confirmed the mass to ensure that both ethers were deprotected.

4.4.6 Sonogashira Cross-Coupling with Aliphatic Side Chains

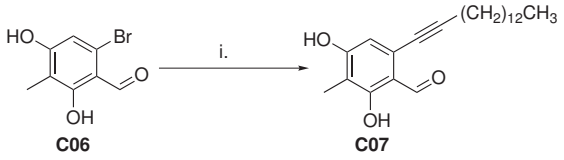

SCHEME 4.20: Sonogashira coupling i. $PdCl_2$(1-pentadecyne, $PPh_3)_2$, CuI, dry DMF, Et_3N, N_2, 60°C, 54% yield

Carbon-carbon bond formation is a particularly useful reaction type in the field of medicinal chemistry. There are many different methodologies that can be employed to carry out this type of reaction: the most commonly used are the Suzuki coupling (following the Miyaura borylation reaction), Hiyama coupling, Kumada coupling, Negishi coupling and the Stille coupling.[186] The method carried out in this synthesis is the Sonogashira cross-coupling reaction.

Sonogashira cross-coupling is one of a plethora of carbon-carbon cross-coupling reactions, which can tolerate a wide variety of substituents. The reagents are comparatively cheap and there is a wide variety of alkynes available and, as this was the previously reported method used to form the azaphilones by Porco and coworkers, this was the methodology undertaken.[182] The Sonogashira cross-coupling requires a halogenated reagent (such as bromine or iodine, chlorine is less electronegative and therefore far less likely to react). The reaction utilises the transmetallation of the reagents with copper(I) iodide and a palladium-ligand complex. As palladium(0) is unstable the palladium complex of choice was bis(triphenylphosphine)palladium(II) dichloride, which converts to palladium(0) *in situ* during the reaction. Due to the sensitivity of the reaction to oxygen, the reaction is performed under anhydrous conditions and solvents were degassed prior through bubbling nitrogen for 30 s to 1 min through the solvents (depending on the volume of solvent).

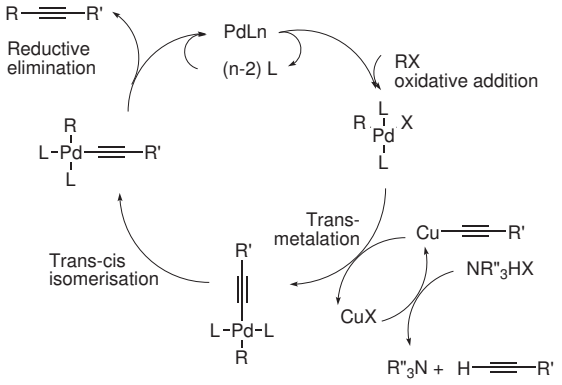

SCHEME 4.21: Mechanism of the Sonogashira Cross-Coupling[187]

Pentadecyne was used as a model alkyne to determine whether or not this method of Sonogashira coupling would be suitable for producing analogues. The yield for this reaction was on average 54%, as excesses of catalysts and alkyne were used and the product had to be purified. Also, any presence of moisture or oxygen reduces the yield and hence the yields worsened when older bottles of anhydrous reagents were used (which were likely to no longer be anhydrous). Characterisation was difficult, as the large overlap of aliphatic protons appeared as a broad peak that was difficult to integrate to the correct number, most likely due to the large number of overlapping aliphatic protons. The mass was confirmed by LCMS, hence the compound was taken forward.

4.5 Formation of the Azaphilone by Oxidative Dearomatisation

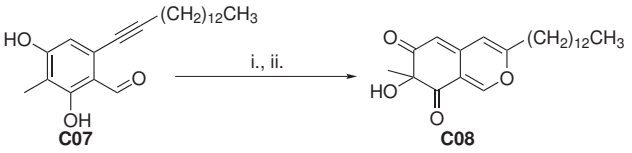

SCHEME 4.22: Two-step synthesis of the azaphilone moiety i. TFA, $Au(OAc)_3$, $CH_3CH_2Cl_2$, rt, 1 min ii. IBX, rt, 1 h, 48% yield over 2 steps

This methodology relies on a two-step process. Firstly, a metal catalyst (in this case, gold(III) acetate) co-ordinates the alkyne to align to the aldehyde. Trifluoroacetic acid (TFA) then removes the metal complex, producing an intermediate. Initial studies on thie methodology explored a variety of different metal salts, but gold(III) acetate was shown to be the best compromise between speed and yield, with the reaction reaching completion within one minute.

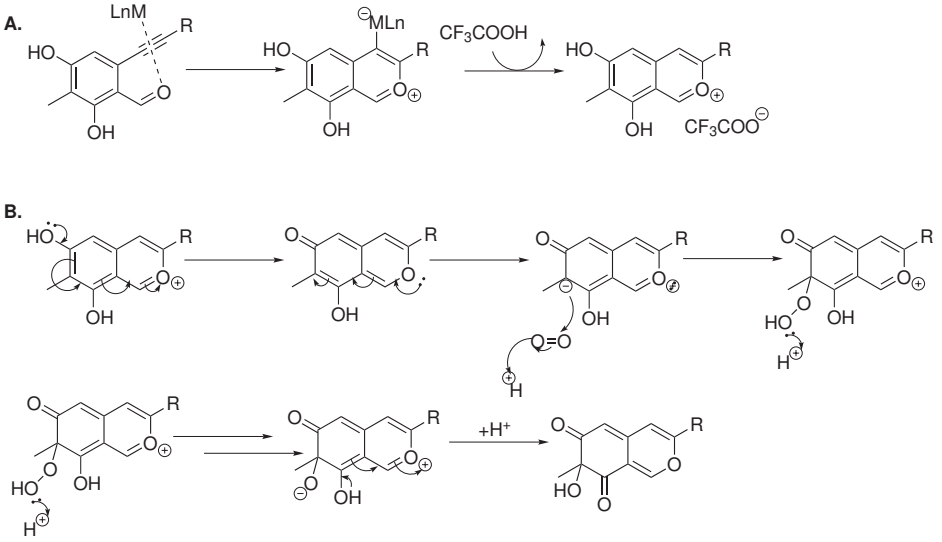

SCHEME 4.23: Mechanism for the 2-step cyclisation and oxidation A. metal-catalysed cyclisation in the presence of trifluoroacetic acid B. oxidation in the presence of IBX

The second step involves o-iodoxybenzoic acid (IBX), a Dess-Martin periodinane which is a powerful oxidising agent, which produces the diketo functionality and introduces an additional hydroxyl group at position 4. Due to the stability of the intermediate, it is necessary to use such a powerful oxidising agent. Due to the high reactivity of IBX, the reaction must be quenched after 1 hour with saturated sodium thiosulfate, however yields for this reaction were moderate at best, with the highest achieved yield being 48%.

Using new IBX and catalyst managed to improve the purity of the final compound, but the yield decreased to 29%. Further modifications of the length of reaction (at both steps) and changing the catalyst did not improve the yield.

Formation of the azaphilone had an appreciable effect on the ^{1}H-NMR and ^{13}C-NMR, with loss of the aldehyde peak at 10.21 ppm and 195.32 ppm respectively. In the ^{1}H-NMR, there are 3 singlet aromatic peaks at 7.88 ppm, 6.10 ppm and 5.52 ppm integrating to one, which correspond to the three aromatic protons on the chromene core. The singlet peak at 1.55 ppm integrating to three is the methyl present on the molecule, whilst the alkyl side chain appears in two regions: a triplet at 2.41 ppm integrating to two (which is the methylene adjacent to the chromene core that is split by the remainder of the alkyl side chian). The remainder of the alkyl side chain appears as a broad peak at 1.26 ppm integrating to twenty protons. The ^{13}C-NMR spectra indicates the correct number of carbons for the molecule, with fifteen aliphatic carbons (thirteen for the aliphatic side chain, one for the methyl group attached to the chromene core and one for the aliphatic carbon within the chromene core) and eight aromatic carbons. The carbons present at 196.28 and 195.80 most likely refer to the two ketones, due to the electron-withdrawing effects of the oxygens.

The product was a racemate and wa carried through without separation of the enantiomers.

4.5.1 Formation of the Butyric Ester as a Model Azaphilone

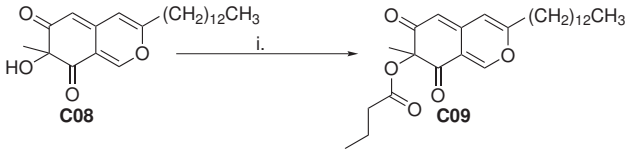

Scheme 4.24: Synthesis of the butyric ester i. Butyric anhydride, DMAP, rt, overnight (53% yield)

As the natural azaphilone bore a butyric ester in position 4, it was decided that the butyric ester would be used for the model compound. Using butyric anhydride and catalytic DMAP, the butyric ester is formed and the unreacted butyric anhydride is quenched with methanol and dessicated overnight (scheme **4.24**). The yield was moderate, most likely due to losses during purification and the incomplete quenching of the butyric anhydride.

The ester shows up as two multiplets at 1.68 ppm and 2.42 ppm by ^{1}H-NMR, integrating to 4 and 3 hydrogens respectively.

4.5.2 Chlorination of the Model Azaphilone

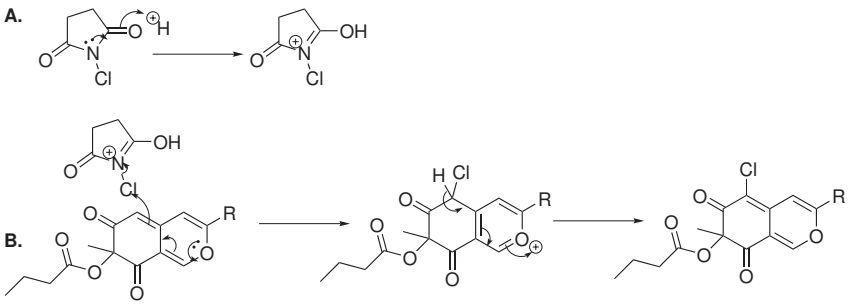

SCHEME 4.25: Chlorination of the azaphilone moiety i. NCS, AcOH, rt, overnight (100% yield)

The final component of the natural azaphilone that was to be generated with the analogues was the chloride in position 6, as it is believed that this helps to direct the azaphilone into the hydrophobic pocket of MDM2, as data published by Hardcastle and coworkers showed that replacement of halogens with methoxy or ethoxy groups abolished activity in their compounds.[100]

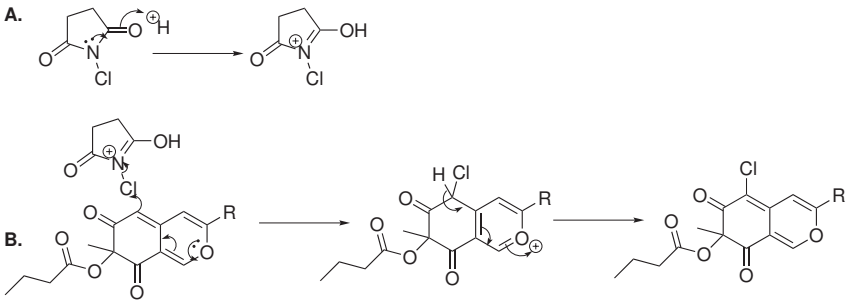

SCHEME 4.26: Mechanism for electrophilic attack of NCS on the azaphilone A. Formation of the active succimidyl species B. Chlorination of the azaphilone

In order to introduce a chloro group on the final azaphilone, a succimidyl ester was used (scheme **4.25**). Succinimides incur the advantage of producing electrophilic halogens, which can then undergo electrophilic aromatic substitution in the presence of aromatic systems. Acetic acid serves as the catalyst as well as the solvent in this reaction. This reaction was also quantitative.

^{1}H-NMR indicated a loss of the proton at 5.52 ppm and mass confirmed that the compound had the correct number of atoms. The LCMS trace also indicated isotope patterns which correspond to the presence of chloride in the sample (a 3:1 ratio of ^{35}Cl and ^{37}Cl respectively).

4.6 Condensation of Azaphilones

Following successful generation of the azaphilone moiety attempts to condense with amines was undertaken. Solid- and solution-phase approaches were carried out to attempt to condense the azaphilone with the natural chlorofusin peptide, but MALDI and HPLC analysis showed that only the uncoupled peptide was visible, as shown in figure **4.4**.

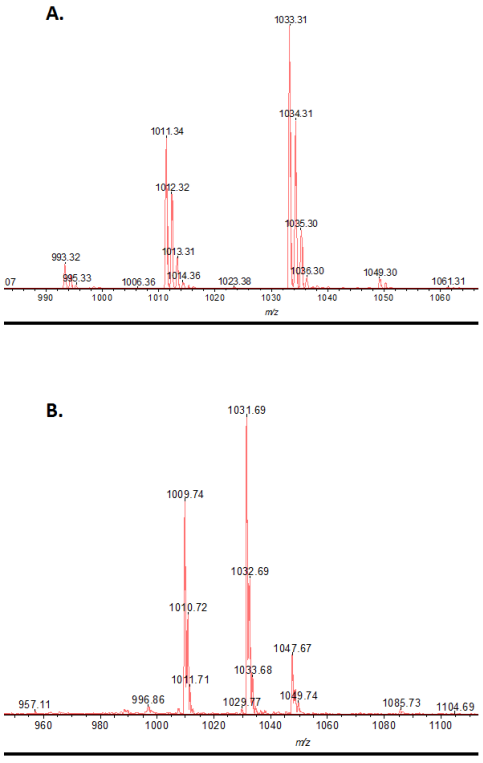

)

FIGURE 4.4: MALDI traces. A. Before coupling (uncoupled peptide seen at 1011.34 $(M+H)^+$ and 1033.31 $(M+Na)^+$) B. After overnight coupling (uncoupled peptide seen at 1009.74 $(M+H)^+$, 1031.69 $(M+Na)^+$ and 1047.67 $(M+K)^+$

It was then postulated that the reason that the azaphilone was unable to couple was due to the flexibility of the cyclic peptide, causing it to sterically hinder the exposed amine on the ornithine. This led to attempts to couple the azaphilone to a dipeptide in solution, however monitoring of the reaction by TLC and ^{1}H-NMR showed that the reaction was not proceeding.

Further literature searching revealed that certain azaphilones can become "locked" in an open state (see figure **4.27**, as it is less energetically favourable to rearomatise following dearomatisation to condense with a free amine. Despite limited success by our lab to

condense the azaphilone with benzylamine previously, it was not possible to condense the azaphilones with the peptide or amino acids.[104]

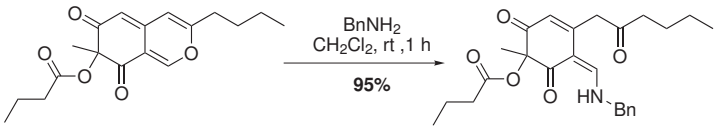

SCHEME 4.27: Scheme for the production and isolation of an azaphilone in the open state

4.7 Computational Studies Towards Azaphilone-Based Inhibitors of the p53-MDM2 Protein-Protein Interaction

Computational analysis using AutoDock Vina was carried out to examine how the azaphilone was likely to bind in the hydrophobic pocket. Although previous studies have shown that the azaphilone moiety alone is insufficient to bind into the pocket, it was postulated that the addition of an additional aromatic group or the natural peptide would be sufficient to promote binding.[77]

Molecular modelling requires peptide bonds to become non-rotatable so that there are reduced degrees of freedom and the software is able to limit the possibilities of binding. As chlorofusin has a large cyclic peptide moeity, which had previously been hypothesised as not being important for binding, it was suggested that replacement of the peptide with ornithine would limit the degrees of freedom for modelling calculations and still not participate in binding (as the pocket is very hydrophobic so in theory it should be the azaphilone chromophore that binds in preference).

Following attempts to condense the azaphilone with the full cyclic peptide it was decided that novel vinylogous amides needed to be synthesised, as these should be easier to synthesise and, if the peptide itself is not binding within the pocket, it was suggested that simpler amine substitutes could still maintain activity. Previous work in our lab had resulted in the synthesis of a benzylamine-based vinylogous amide (data not published), therefore novel analogues were generated using a benzyl group in place of the peptide for an *in silico* screen to determine if it was possible to produce azaphilone analogues condensed with benzylamine that would inhibit the p53-MDM2 interaction. Other variants designed for the *in silico* screen included varying length of alkyl side chain/substitution with an aromatic side chaine, variation of the halogen with either chlorine, bromine, iodine or unsubstituted and variation of the ester up to butyric acid as well as the free alcohol.

As previously explained in Chapter 2 section 2.9, p53 was used as the comparator and compounds were docked into the hydrophobic pocket.

Screening revealed 3 novel compounds with comparable binding affinity to wildtype p53. These compounds contained aromatic side chains, chlorines in position 6 and acetyl esters. The top 3 binding compounds are shown in figure **4.5**, figure **4.6** and figure **4.7**.

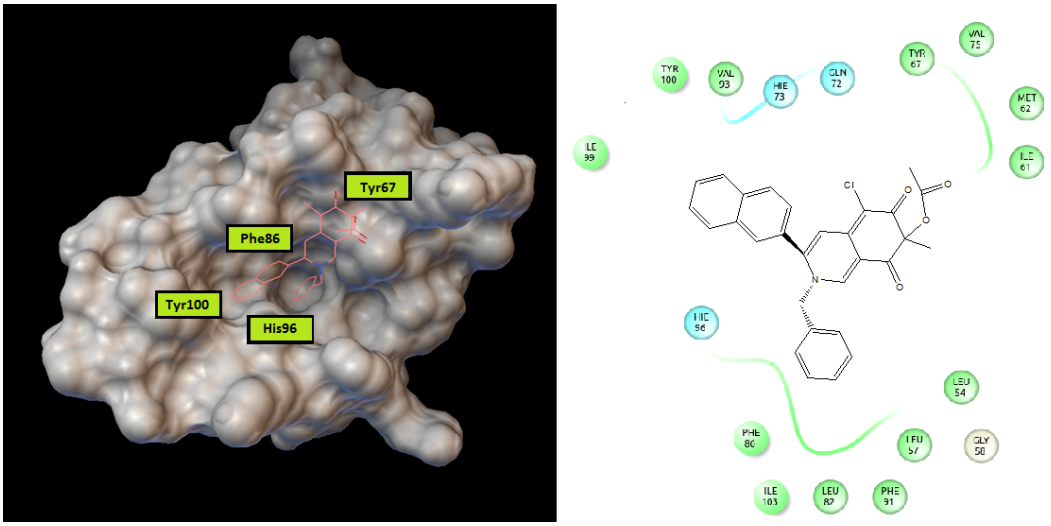

FIGURE 4.5: Top binding compound as determined by Autodock Vina. Naphthyl had a binding energy of -8.8 kcal/mol, whilst wildtype- p53 had a binding energy of -8.5 kcal/mol

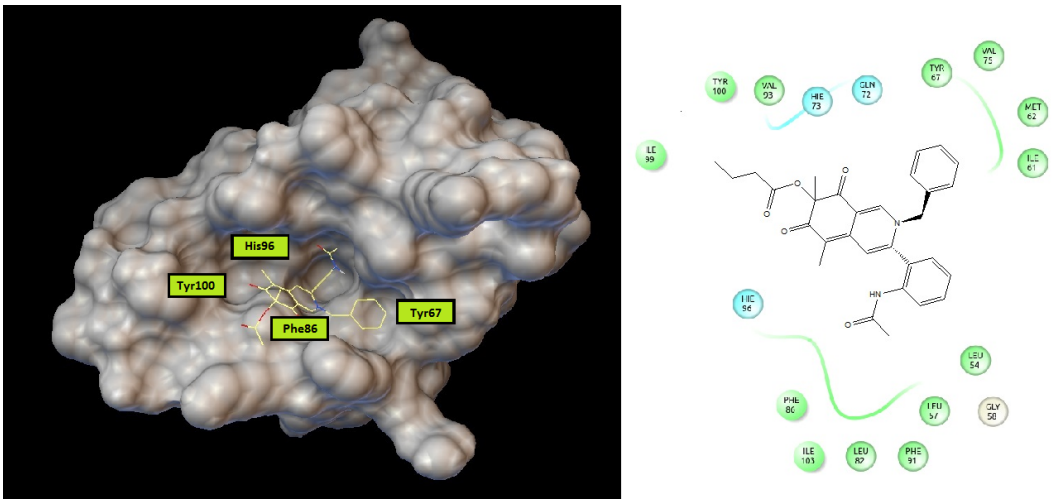

FIGURE 4.6: 2nd best binding compound as determined by Autodock Vina. Acetanilide had a binding energy of -8.4 kcal/mol, whilst wildtype- p53 had a binding energy of -8.5 kcal/mol

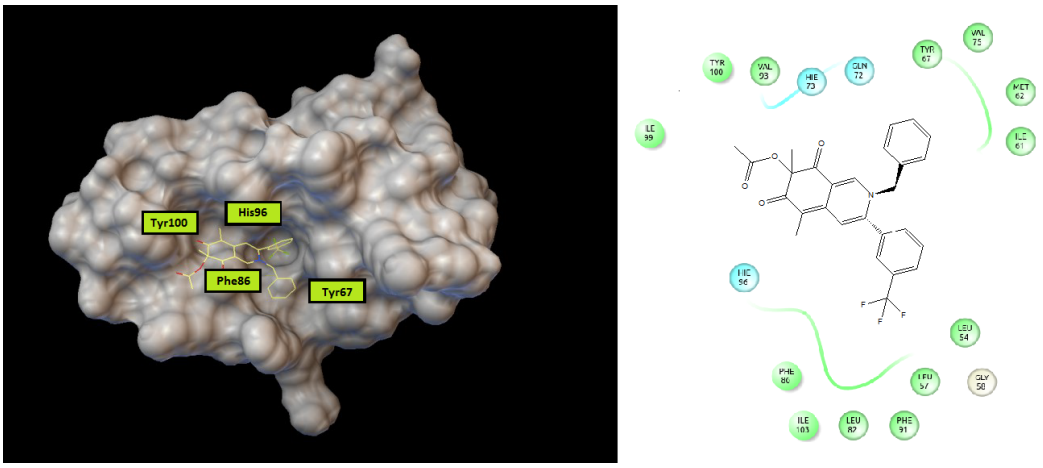

FIGURE 4.7: 3rd best binding compound as determined by Autodock Vina. Trifluoromethyl had a binding energy of -8.3 kcal/mol, whilst wildtype- p53 had a binding energy of -8.5 kcal/mol

4.8 Synthesis of Azaphilone Analogues Bearing an Aromatic Side Chain

Attempts to synthesise the novel aromatic azaphilones using the original Sonogashira methodology did not produce aromatic compounds and, despite variants of ligands and palladium, bases and fresh anhydrous solvents, it was not possible to directly attach an aromatic alkyne onto the Sonogashira precursor. Variants in the temperature were also attempted, but the reaction did not progress (see scheme **4.28**).

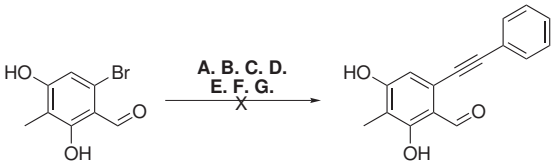

SCHEME 4.28: Scheme for the attempts of different reagents for the Sonogashira coupling A. $PdCl_2(PPh_3)_2$, CuI, Et_3N, dry DMF, 60°C, overnight B. $PdCl_2(PPh_3)_2$, CuI, DIPEA, Dry DMF, 60°C, overnight C. $Pd(PPh_3)_4$, CuCl, Dry DMF, 80°C, overnight D. Dry DMF, $PdCl_2(PPh_3)_2$, $ZnBr_2$, 60°C, overnight E. $PdCl_2(MeCN)_2$, CuI, Et_3N, rt, overnight F. $PdCl_2(MeCN)_2$, CuI, DIPEA, rt , overnight G. $PdCl_2(MeCN)_2$, CuI, diisopropylamine, rt , 2 days

It was then postulated that functionalisation of the Sonogashira with an alkyne could solve this problem, provided that the problem was through coordination of the palladium catalyst and ligand with the bromine. The starting material was then reacted with tri-*t*-butylphosphonium tetrafluoroborate (a more stable salt form of tri-*t*-butylphosphine)

and bis(acetonitrile)palladium(II) dichloride and TMS-acetylene. The TMS group was necesary to ensure that the compounds did not dimerise.

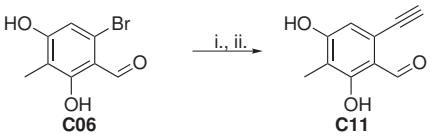

SCHEME 4.29: Scheme for alkyne functionalisation i. TMS-acetylene, $PdCl_2(MeCN)_2$, $(^tBu)_3P.HBF_4$, CuI, DIPA, dry DMF, N_2, 60°C, 3 h then ii. 1M TBAF in THF, rt, 3 h (63% yield over 2 steps)

The trimethylsilyl (TMS) group is a moderately labile protecting group. Silyl protection is usually removed by a fluoride, as the Si-F bond is particularly strong. In this case, *t*-butylammonium fluoride (TBAF) 1M in THF was used and the product was concentrated *in vacuo* without further purification.

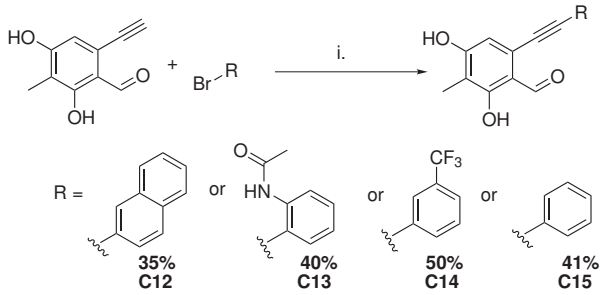

SCHEME 4.30: Synthesis of aromatic Sonogashira products i. $Pd(PPh_3)_4$, CuI, Et_3N, dry DMF, 60°C, overnight

The newly formed alkyne compound was then reacted with brominated aromatic compounds. Starting with bromobenzene as a model compound, the Sonogashira coupling was undertaken using tetrakispalladium(0) and triphenylphosphine. As previously mentioned, palladium(0) is the active species for the Sonogashira coupling and in this case, generation of this species *in situ* was insufficient to drive the reaction. The triphenylphosphine provided the ligand to co-ordinate the alkyne and the halogenated partner.

Following the successful generation of the Sonogashira analogues, the azaphilone synthesis was attempted.

The bromobenzene azaphilone was synthesised first, producing the azaphilone in poor yields. The reaction produced a variety of side products, despite close monitoring. It was also found that, when the top binding aromatics were attempted, the starting material decomposed, indicating that the Sonogashira analogues were not particularly stable.

It was possible to form the ester of the bromobenzene analogue using glacial acetic acid in excellent yields, however the chlorinated product has yet to be synthesised.

The main difficulty with these compounds is the low yields towards the end of the synthesis, resulting in copious amounts of starting materials required for generation. In addition, the stability of the aromatic compounds prohibited the synthesis being taken further.

4.9 Conclusions and Future Work

In conclusion, although it was possible to synthesise an azaphilone analogue, it was not possible to carry out further condensation reactions to produce analogues for biological testing. In order to progress the azaphilones forward it would be necessary to scale up the syntheses to multigram quantities in order to produce sufficient quantities to purify and produce biological testing. Due to the instability of the aromatic analogues it is likely that alternative heterocycles could be trialled as the stability may improve (such as pyridinyl and furyl analogues). There may also be the option of using cyclohexyl groups in place of the aromatic side chains, although these side chains were not screened *in silico* and therefore it is not possible to gauge at present whether or not these would still fit well in the hydrophobic pocket (as the π-π stacking interactions would be lost, but there would still be a high degree of hydrophobic interactions present).

Alternatively it maybe possible to trial one of the alternative methods listed earlier in the chapter, such as Method B for the oxidative dearomatisation, which may offer a greater deal of control in the azaphilone core synthesis. As this method appears to be milder than the use of IBX in the oxidative dearomatisation, it maybe possible that the products maybe less likely to degrade.

Chapter 5

Conclusions and Future Work

Within this thesis we have explored novel inhibitors of the p53-MDM2 protein-protein interaction based on the natural product, chlorofusin.

The first compounds tested within this thesis were the isoquinolin-1-ones, which were synthesised using a modified Castagnoli reaction in which homophthalic anhydride was reacted with the imine Schiff base formed between a chosen primary amine and aldehyde. 80 compounds were generated using this methodology and were originally characterised using ^{1}H-NMR, ^{13}C-NMR, IR and LCMS. The ^{1}H-NMR experiments also revealed the predominant diastereomers, which in the majority of cases were trans (which is also the more stable diastereomer as it is more thermodynamically stable than the cis form).

The 80 compounds synthesised were then tested at 100 μM well concentration in an FP assay and of the 80 compounds tested, 7 were found to have an IC_{50} of less than 100 μM, with the best inhibitor having an IC_{50} of 6.555 μM. These 7 compounds were all halogenated and bore either a fluorine, chlorine or bromine in the amine precursor or a chlorine or bromine in the aldehyde precursor. In both instances, the substituents were para substituted in relation to the central isoquinolinone core. The 7 hit compounds were then tested by MTS and, although 3 of these compounds were active in MDM2-overexpressed cell lines, none of them were selective, suggesting that these compounds also work by an alternative mechanism of action.

In order to determine which diastereomers were active, model compound **A34** were synthesised as both the cis and the trans forms selectively. These compounds were also tested and the cis form was found to be inactive, whilst the trans selective form was comparable to the racemate originally synthesised.

Additional optical rotation studies were undertaken to determine whether or not there was a predominant stereoisomer, which revealed that the compounds that were shown

to be active against the p53/MDM2 protein-protein interaction were predominantly one enantiomer, however there is little data in the literature examining this and the only evidence that could be found related to A-strain in the central isoquinolinone core that could force a particular diastereomer.

These compounds were also studied using a combination of STD-NMR alongside molecular modelling to determine how the compounds were binding into the pocket. **A34** was used as a model compound (as the most potent hits may have bound too tightly to HDM2 and therefore not be able to display "on/off" signals required for STD-NMR). The results of the STD-NMR were that all of the substituents except for the methylene were required for binding. STD-NMR is a very powerful technique and future work could be to further explore the hit compounds (such as the top hit) to see whether or not a signal could be generated. STD-NMR could also be used to determine IC_{50} values, which could be used as a comparator against FP data, especially for compounds for which FP was inconclusive (such as highly fluorescent compounds).

In order to improve aqueous solubility, an alcohol substituent was introduced into the final compound, using phenylalaninol as the starting amine. This compound was successful in the FP assay, however failed to have activity in the MTS assay. Although this compound was not successful, it would be interesting to explore this further with additional analogues potentially bearing polyoxygenated esters at the methylene position, which would have improved aqueous solubility and potentially improve cellular uptake.

The second chapter focussed on the peptide portion of chlorofusin as a starting point and the first compounds synthesised were simple fused bicyclic aromatic acid analogues of the azaphilones (the chromophore portion of chlorofusin), which were condensed with the cyclic chlorofusin peptide. These compounds were synthesised on solid phase and in solution, with solution phase synthesis producing higher yields, which could then be tested in the FP assay. Of this first library of aromatic acid analogues, none of the compounds displayed activity.

Following the investigation of the simple fused bicyclic analogues the decision was made to explore click chemistry, which could be used as a handle to generate novel analogues and for which the azide serves as a bioisostere. Azidonorvaline was synthesised through the reduction of Boc-Glu-OtBu, which was mesylated, azide substituted, deprotected and Fmoc-protected to form the amino acid for incorporation into solid phase synthesis. This was substituted in place of Orn9 in the chlorofusin synthesis and a small portion of the azidochlorofusin was tested for characterisation and for biological testing. A series of analogues were generated through a solid-phase click reaction with the exposed azide and of these 10 analogues, only **B15** displayed activity in the FP assay, with an IC_{50} of 8.309 μM.

In order to determine the importance of the peptide the Fmoc-azidonorvaline-OH was reacted with a series of alkynes to form a second generation library. Of the 7 compounds synthesised, 6 displayed activity. Interestingly, when one of these compounds was Fmoc-deprotected, activity was lost, hence suggesting the importance of the Fmoc group in binding within the pocket.

The 7 active click compounds were then placed into the MTS assay, of which 2 were active and 1 of which was selective against the p53/MDM2 protein-protein interaction. This compound contained a trifluoromethyl substituent in the para position to the triazole ring and further exploration of different positions on the alkyne would be needed to give greater SAR data.

It would also be interesting to use the click analogues in the STD-NMR studies to determine how they bind, as there are no similar compounds in the literature that have been studied prior to the publication of these compounds. It would also be useful to increase the size of the library and to increase the analogues explored to determine if there are any more active analogues.

With the successes of the first two synthetic chapters the last chapter explored the azaphilone chromophore, with the intention of generation of novel azaphilone analogues that could be condensed with the chlorofusin peptide. These analogues would bear greatest similarity to the lead compound and therefore demonstrate how much chlorofusin itself could be substituted but activity could be maintained or improved.

Multiple routes to the Sonogashira precursor were explored and, depending on whether or not the Sonogashira was aliphatic or aromatic, the synthetic route had to be optimised. The aliphatic side chains could be synthesised under standard Sonogashira conditions, however aromatic attachment required a novel double-Sonogashira approach. A variety of different azaphilone precursors were generated with both aromatic and aliphatic side chains, however the oxidative dearomatisation required for the azaphilone chromophone synthesised proved to be difficult, as the only aromatic side chain that could tolerate the reaction conditions was benzylamine, and regardless of the side chain the yields of successful reactions were poor (circa 37% at best).

It was possible to form the complete azaphilone bearing a pentadecyne side chain, however it was not possible to condense this with either the chlorofusin peptide nor a dipeptide for incorporation onto solid phase. In the case of the benzyl side chain analogue, it was not possible to complete the synthesis, although it was possible to get as far as the penultimate stage (the acetylation of the free alcohol).

If the azaphilone work is to be taken further forward it would be necessary to invest time in generating vast quantities of material for the reactions, as the reaction pathway

is lengthy and the yields in the penultimate steps are generally poor. It may also be useful to further explore alternative oxidative dearomatisation methods, which could be less harsh and therefore less likely to degrade the Sonogashira product.

In conclusion, we have considered, synthesised and tested a wide variety of different analogues based on chlorofusin, however much work is still to be done to establish greater SAR data, as well as potential applications in similar protein-protein interactions such as p53/MDMX and the Bcl-2 binding partners.

Chapter 6

Experimental Section

6.1 General Procedures

6.1.1 Reagents and Solvents

All chemicals were reagent grade and were purchased from Sigma Aldrich and Fisher Scientific. NMR solvents were purchased from VWR. Fmoc-amino acids and coupling reagents were purchased from Novabiocchem or AGTC Bioproducts. Anhydrous solvents were bought in and used as supplied. All water used was distilled.

6.1.2 Physical Characterisation and Spectroscopic Techniques

^{1}H and ^{13}C NMR spectra were recorded in Fourier Transform mode on a Bruker 400 or Bruker 800 spectrometer operating at a ^{1}H-NMR frequency of 400 MHz or 800 MHz respectively using the specified deuterated solvent. Subsequent spectra were processed using Topspin 3.0 software. The chemical shifts for both ^{1}H and ^{13}C were recorded in ppm and were referenced to the residual solvent peak. Multiplicities in the NMR spectra are described as s = singlet, d = doublet, t = triplet, q = quartet, m = multiplet, br = broad; coupling constants are reported in Hz. Low resolution mass spectra were recorded using a Shimadzu LCMS 2010EV operated under electrospray ionisation in positive (ES+) mode. Accurate mass spectra were recorded at the EPSRC National Mass Spectroscopy Service Centre, Swansea. Melting points were recorded using open capillary tubes on a Mel-Temp electrothermal melting point apparatus. Infared spectra were recorded as neat samples using a Perkin Elmer Spectrum BX FT-IR and manipulated using Spectrum software. UV spectra was obtained using a Perkin-Elmer Lambda 25 UV/Vis spectrometer at the wavelengths specified.

6.1.2.1 Chromatographic Techniques

Thin layer chromatography was performed on aluminium plates coated with 0.2 mm silica gel-60 F_{254}, which were purchased from VWR. Following elution, the plates were viewed under long and short wave UV light and then developed upon staining and heating with nihydrin or vanillin. Column chromatography took place using 60 μm particle-size silica gel.

Reverse-phase purification was either undertaken using an Isolera 4 automated purification system using 12 g C18 cartridges or an Agilent technologies 1200 series chrromatograph using an Agilent technologies ZORBAX Eclipse XDB-C18 (5 m, 9.4x250 mm) column. HPLC analysis was undertaken using a Agilent technologies ZORBAX Eclipse XDB-C18 (5μ, 4.6x150 mm) column at 40°C and a gradient of 95:5 water:methanol with 0.05% TFA additive to 5:95 water:methanol over 15 min returning to 95:5 water:methanol over 5 min at a flow rate of 1 mL/min.

6.1.2.2 Biochemicals

All biological reagents were purchased from Novabiochem, Fisher Scientific, VWR and Sigma-Aldrich. All reagents were specified as biological grade and assumed to conform to the manufacturer's standards. All water was autoclaved on site before use.

6.2 Protein Expression and Purification

6.2.1 Expression of HDM2 and HDMX

6.2.1.1 General Procedures

Plasmids for expression of His-tagged HDM2 was pET14b, a generous gift from Dr. Gary Parkinson (School of Pharmacy, University College London, UK).

Reagents, antibiotics and media were purchased from Sigma Aldrich, VWR, Novabiochem, Applichem or Fisher and were all molecular biology grade. ddH_2O was used to make buffers, antibiotic stocks and media. Buffers were vaccuum filtered using a 0.2 μm filter (purchased from GE healthcare). DNase was purchased from Invitrogen. All media and glycerol for use in bacterial stocks were autoclaved prior to use. Isolation of DNA was undertaken using a QIAprep mini-prep kit (manufactured by QIAGEN, buffer constituents not disclosed). DNA was analysed by nanodrop (Thermo Fisher Scientific) and

sequenced at Cambridge Biochemistry Sequencing Department and analysed by Bioedit 7.1.11 software. BL21(DE3)PLysS cells were purchased from Novagen.

Nickel-affinity (PrepEase High Yield) resin was purchased from USB and glutathione hi-cap resin was purchased from Qiagen. HiTrap SP HP ion-affinity columns and PD-10 desalting columns were purchased from GE Healthcare. VacuCap vacuum filters were purchased from Pall Corporation. Centrifugal filters were purchased from Merck.

6.2.2 Heat Shock Transformation of JM109 Cells

JM109 cells (2 x 25 μL) were thawed for 15 min. To one batch of cells, plasmid (1 μL) was added and the cells were incubated at 0°C for 30 min. The cells were incubated at 42∘C for 90 s and LB media (250 μL) was added to each batch. The batches were incubated at 37 °C for 1 h. The culture was then plated at various dilutions (10 μL, 100 μL and 140 μL) onto 1.5% LB:agar plates containing ampicillin (100 μg/mL). The cultures were incubated at 37°C overnight, then 4°C overnight, then three colonies were isolated from the plates, grown overnight in 15 mL of LB containing ampicillin (100 μg/mL).

6.2.3 Production of Glycerol Stocks

Overnight culture (750 μL) and 80% glycerol in ddH_2O (250 μL) were mixed together and stored at -80°C until required.

6.2.4 Isolation of Plasmids

JM109 cloning cells containing the desired plasmid were grown overnight in 5 mL of LB medium containing ampicillin (100 μg/mL) at 37°C. DNA was isolated using a QIAprep mini-prep kit (full manufacturer's protocol can be located via www.qiagen.com/gb/resources and is cited in the bibliography[188]). The culture was centrifuged (13,000 rpm, 16°C) for 3 min and supernatant discarded. The pellet was resuspended in 250 μL of buffer P1, followed by the addition of 250 μL of buffer P2 and the suspension was inverted 6 times. 350 μL of buffer N3 was added and the suspension inverted 6 times. The suspension was transferred to spin columns and centrifuged (13,000 rpm, 16 °C) for 30 s and the flow-through was discarded. 500 μL of buffer PB was added, the suspension was centrifuged (13,000 rpm, 16 °C) for 30 s and the flow-through was discarded. 750 μL of buffer PE was added, the suspension was centrifuged (13,000 rpm, 16 °C) for 90 s and the flow-through was discarded. The DNA was eluted for 1 min in ddH_2O, then centrifuged (13,000 rpm, rt) for 1 min. DNA was then analysed by nanodrop.

6.2.4.1 pET14b concentration and purity following isolation

The nanodrop was initially calibrated with ddH_2O and then calibrated with the final buffer solution. The nanodrop gave a reading for the absorbance (calculated against a pathlength of 1 dm, which could then be placed into the Beer-Lambert equation to calculate the final concentration).[189] The machine also gave two further readings: the 260/280 indicates the ratio of DNA to RNA in the sample (a value of approximately 1.8 indicates "pure" DNA whereas a value of 2.0 indicates "pure RNA). The 260/230 value indicates purity of nucleic acids in the sample, with a "pure" sample producing a value between 2.0 and 2.2.

Concentration in solution of pET14b = 197.5 mg/mL, 260/280 = 1.89 and 260/230 = 2.18.

6.2.5 Heat shock transformation of BL21(DE3)PLysS cells

BL21(DE3)PLysS cells (2 x 25 μL) was thawed for 15 min. To one batch of cells, plasmid (1 μL) was added and the cells were incubated at 0°C for 30 min. The cells were incubated at 42°C for 90 s and LB media (250 μL) was added to each batch. The batches were incubated at 37°C for 1 h. The culture was then plated at various dilutions (10 μL, 100 $_m u$L and 140 μL) onto 1.5% LB:agar plates containing ampicillin (100 μg/mL) and chloramphenicol (51 μg/mL). The cultures were incubated at 37°C overnight, then 4°C overnight, then three colonies were isolated from the plates, grown overnight in 15 mL of LB containing ampicillin (100 μg/mL) and chloramphenicol (51 μg/mL).

6.2.6 Expression trial

3 batches of both pET14b- and pRP261-containing BL21(DE3)PLysS cells (10 μL) were grown overnight in LB (10 mL) containing ampicillin (100 μg/mL) and chloramphenicol (51 μg/mL) at 37∘C. The overnight culture (200 μL) was then added to LB (10 mL) containing ampicillin (100 μg/mL) and chloramphenicol (51 μg/mL). The OD_{600} was measured until 0.6 was reached, after which one batch was grown with 0.4 mM IPTG for 5 h at 37°C, the second batch was grown with 0.4 mM IPTG overnight at 25°C and the third batch was grown with no IPTG for 5 h at 37°C. The batches were centrifuged and resuspension buffer (1 mL) containing 20 mM Tris-Cl, 300 mM NaCl, 2 mg/mL $MgCl_2$ and 2 μL of DNase1 20,000 U/μL. Proteins were analysed by 12% SDS-page.

6.2.7 Expression of histidine-tagged HDM2

6.2.7.1 Overnight culture and scale-up culture

Esherichia coli strain BL21(DE3)PLysS containing the plasmid pET14b were grown in 2 x LB medium containing ampicillin (100 μg/mL) and chloramphenicol (51 μg/mL) at 37°C until the OD_{600} = 0.6. IPTG was added to produce a final concentration of 0.4 mM, the temperature was adjusted to 16°C and the culture was incubated for 16 h. The cells were harvested by centrifugation and resuspended using 20 mM Tris-Cl, 300 mM NaCl and 20 mM imidazole. The suspension was then sonicated in 7 x 30 s pulses and the suspension centrifuged again for 30 min at 10,000 rpm. The supernatant was analysed by 12% SDS-PAGE.

6.2.7.2 Purification of HDM2

Protein was purified using resuspension buffer consisting of 20 mM Tris-Cl, 300 mM NaCl and 20 mM imidazole and eluted into 20 mM Tris-Cl, 300 mM NaCl and 300 mM imidazole using 500 mg of dry nickel-affinity resin (that was resuspended in 5 mL of resuspension buffer prior to use). A second purification using an ion-affinity resin was undertaken using a 0-1 M gradient of NaCl in buffer containing 1 mM DTT, 1 mM EDTA, 10 mM phosphate buffer at pH 7.4. Fractions containing protein were desalted using a desalting column and were eluted into 10% glycerol, 10 mM β-mercaptoethanol, 10 mM phosphate buffer (pH 7.4) and ddH_2O. The protein was concentrated by spin filtration and analysed by nanodrop. Final protein concentration = 44.1 μM.

6.2.7.3 Cell Culture

SJSA-1 is derived from fibroblastic osteosarcoma cells from a 19-year-old male and purchased from the American Type Culture Collection (ATCC, Virginia, USA). HL-60 is derived from peripheral blood leukocytes from a 36-year-old female with acute promyelocytic leukaemia and was purchased from the European Collection of Cell Cultures (ECACC, Porton Down UK). Both cells were cultured in RPMI-1640 media containing 2 mM L-glutamine and 10% FCS. Cell were maintained at 37°C and 5% CO_2. Both cell lines were maintained between 1 x 10^5 and 9 x 10^5 cell/mL in 75 cm^3 flasks, split with fresh media every 3.5 days and used until passage 10 for experimentation. For cell number and viability, both cell lines were diluted 1 in 5 in trypan blue and counted using Fisher haemocytometer grid with light microscopy.

6.2.7.4 Fluorescence Polarisation Assay

All solutions were made using doubly-distilled water. Tween-20 and PBS was purchased from Sigma-Aldrich. Fluorescence polarisation assays were carried out in black Costar low binding 96 well microplates on a BMG Labtech Optima microplate reader. The fluorescence polarisation optic measured at 490/520 nm. Data was averaged over 10 readings.

Inhibition curves were generated using 10 nM HDM2, 10 nM fluorescently-tagged peptide in PBS-0.05% Tween-20 at pH 7.4 with 10 μM of varying concentrations of inhibitor (1 mM to 100 pM well concentration). The plate was incubated for 30 min in darkness before readings were taken.

IC_{50} and K_i values were taken and processed using the Cheung-Prusoff equation, shown in **equation 6.1**

$$K_i = \frac{IC_{50}}{1 + \frac{[ligand]}{K_d}} \tag{6.1}$$

6.2.7.5 MTS Cytotoxicity Assay

The antiproliferative activity of compounds was tested by MTS assay using the CellTiter 96 Aqueous One Solution Cell Proliferation Assay and following the manufacturer's instructions. The outer wells of the plate were filled with 200 μL water to prevent evaporation of the cells seeded onto the plate. The remaining plate was seeded with HL-60, A375 or SJSA-1 cells (5 x 10^4 / 100 μL) and left untreated (media control), with DMSO (vehicle control), nutlin-3a (positive control, 100 μM to 1.5625 μM) in triplicate for 72 h at 37°C with 5% CO_2.

The MTS reagent was then added to each well and the plates incubated for 3 h at 37°C with 5% CO_2. The absorbance was measured at 492 nm using the BMG Labtech POLARstar Optima microplate reader. It was assumed that the cells incubated with DMSO alone were taken as 100% cellular proliferation and IC_{50} values were calculated using GraphPad Prism Version 6.0 software.

6.2.7.6 Saturation Transfer Difference NMR

All solvents used were deuterated and freeze dried with deuterium oxide. All solvents and reagents were purchased from Sigma-Aldrich.

Readings were taken using a Bruker 800 MHz NMR spectrometer at 5°C over a period of 15 h. The sample was prepared in a 300 μL NMR tube and centrifuged to ensure homogenicity and removal of bubbles.

95.6 nM HDM2 (100 μL) and 500 μM **A34** (50 μL) in 10% DMSO in PBS (50 μL). One sample was run thirteen times and each run cycle took 30 min and was run at varying pulse rates (1 μs for a definite "on" signal to 1 s for a definite "off" signal).

Data was then processed on Topspin 4.0 software. STD-NMR was processed and analysed as follows:

1. Select run set from corresponding folder
2. Type 'efp 1 2' to subtract the "off" signal from the "on" signal
3. Type '.md' to display multiple spectra
4. Overlay the difference and "off" spectra and adjust the "off" spectra so it overlays as close as possible with each peak in the difference spectra (if no peak is present, the scale factor becomes zero)

6.2.7.7 Computational Screening

PDB entry 1YCR was used for all computational experiments. Ligands and macromolecules were processed in AutoDock Tools and Deepview to add gasteiger chargeses and insert explicit hydrogens.

The code below was used to generate the gridbox

HDM2.pdbqt

center_x = 20
center_y = 20
center_z = -20
size_x = 25
size_y = 25
size_z = 25
num_modes = 9

Once all of the parameters have been set it is then possible to run the simulation (in this case, using autodock vina). The bash shell code is shown below:

```
for f in ligand_*.pdbqt; do
b=‘basename $f .pdbqt‘
echo Processing ligand $b
mkdir -p $b
vina –config conf.txt –ligand $f
–out $b/out.pdbqt –log $b/log.txt
done
```

Following processing, it is possible to use Python script to ascertain the top 10 hits using the code,

```
vina_screen_get_top.py 10
```

The python script used to sort out top hits is as follows:

```
#! /bin/bash
# search all files ending in .pdbqt
for f in *.pdbqt # create a variable $b which is equal to everything before the first _ in the filename
do b=“$f%%_*”
# find all files which contain $b at the beginning with anything following
# then use word count to return how many times $b has been found
o=$(find . -name “$b*” — wc -l)
# first for every file containing $b extract characters 14-17 from the filename
# in this case the PDB I.D. for the receptor
# then extract the second line from the file and print the fourth word
# in this case the energy of docking
e=$(for f in $b*.pdbqt
do n=$(echo $f — cut -c 14-17)
echo $n ,
sed -n 2p $f — awk ‘print $4 “,”’
done)
# put all of the pieces collected so far into a file called Sort_top.txt
echo $b, $o, $e ¿¿ Sort_top.txt
done
# sort through the file Sort_top.txt and delete any duplicate lines and save
# to Sort_top_uniq.txt
uniq Sort_top.txt >Sort_top_uniq.txt
```

6.3 Experimental for Chapter 2

6.3.1 General Procedure for the Formation of the First Generation Isoquinolinones

Aldehyde (2.52 mmol) and amine (2.52 mmol) were shaken with $MgSO_4$ (500 mg) in CH_2Cl_2 (5 mL) and left to stand for 4 h. The mixture was filtered and added to homophthalic anhydride (409 mg, 2.52 mmol) and left to stand overnight at rt. The formed precipitate was then washed with hot ethyl acetate or, if the product did not precipitate, the compound was purified through column chromatography (CH_2Cl_2:MeOH or reverse-phase using H_2O:MeOH with 0.05% TFA).

3-(2,5-dimethoxyphenyl)-2-[phenylmethyl]-1-oxo-1,2,3,4-tetrahydroisoquinoline-4-carboxylic acid (A01)

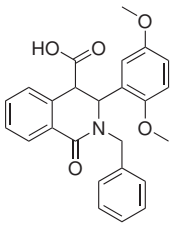

Purification on silica. White solid, 333 mg, 30% yield. mp 199.5°C-201.8°C IR ν_{max} (neat) cm^{-1} 2913.85 (O-H), 1732.39 (C=O), ^{1}H-NMR (400 MHz, DMSO-d_6) δ_H ppm: 3.43 (3*H*, s), 3.60 (3*H*, s), 3.72 (1*H*, d, J = 15.23 Hz), 4.53 (1*H*, d, J = 6.09 Hz), 5.31 (1*H*, d, J = 15.23 Hz), 5.39 (1*H*, d, J = 6.09 Hz), 6.26 (1*H*, d, J = 3.40 Hz), 6.77 (1*H*, dd, J = 3.05 Hz and 8.95 Hz), 6.87 (1*H*, d, J = 9.01 Hz), 7.23 to 7.36 (6H, m), 7.45 to 7.49 (1*H*, m), 7.53 to 7.57 (1*H*, m), 12.72 (1*H*, brs) ^{13}C-NMR (100 MHz, DMSO-d_6) δ_C ppm: 170.79 (C=O), 163.90 (C=O), 151.93 (Ar*C*), 137.87 (Ar*C*), 134.69 (Ar*C*), 132.63 (Ar*C*H), 129.13 (Ar*C*), 128.97 (Ar*C*), 128.02 (Ar*C*H), 127.93 (Ar*C*H), 127.90 (Ar*C*H), 127.67 (Ar*C*H), 126.16 (Ar*C*H), 114.47 (Ar*C*H), 113.71 (Ar*C*H), 112.58 (Ar*C*H), 56.38 (*C*H_3), 55.34 (*C*H_3), 53.20 (*C*H), 48.53 (*C*H), 48.34 (*C*H_2) LRMS (ES+) calculated for $C_{25}H_{24}NO_5$ and $C_{25}H_{23}NO_5Na$ found 418.1 m/z $(M+H)^+$ and 440.1 m/z $(M+Na)^+$

3-(2,4-dimethylphenyl)-2-[phenylmethyl]-1-oxo-1,2,3,4-tetrahydroisoquinoline-4-carboxylic acid (A02)

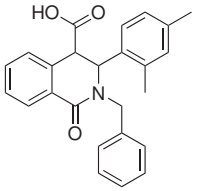

Purification on silica. White solid, 39 mg, 4% yield mp 187.6°C-194.5°C IR ν_{max} (neat) cm^{-1} 3033.51 (O-H), 1740.52 (C=O) ^{1}H-NMR (400 MHz, DMSO-d_6) δ_H ppm: 2.03 (3*H*, s), 2.18 (3*H*, s), 3.59 (1*H*, d, J = 15.54 Hz), 4.53 (1*H*, d, J = 6.25 Hz), 5.11 (1*H*, d, J = 6.42 Hz), 5.40 (1*H*, d, J = 15.30 Hz), 6.78 (2*H*, s), 6.91 (1*H*, s), 7.18 (2*H*, d, J = 7.59 Hz), 7.26 to 7.33 (3*H*, m), 7.42 to 7.44 (1*H*, m), 7.47 to 7.50 (1*H*, m), 7.54 to 7.57 (1*H*, m), 8.10 (1*H*, d , J = 7.64 Hz)) ^{13}C-NMR (100 MHz, DMSO-d_6) δ_C ppm: 170.79 (C=O), 164.22 (C=O, 163.87 (Ar*C*), 137.69 (Ar*C*), 137.63 (Ar*C*), 137.51 (Ar*C*), 136.65 (Ar*C*), 135.52 (Ar*C*H), 132.71 (Ar*C*), 132.27 (Ar*C*H), 131.52 (Ar*C*H), 130.27 (Ar*C*H), 129.34 (Ar*C*), 129.11 (Ar*C*), 129.04 ((Ar*C*H)), 128.71 ((Ar*C*H)), 128.36 ((Ar*C*H)), 128.29 ((Ar*C*H)), 128.06 ((Ar*C*H)), 128.00 (Ar*C*H), 127.91 (Ar*C*H), 127.73 (Ar*C*H), 127.56 (Ar*C*H), 127.39 (Ar*C*H), 127.27 (Ar*C*H), 127.17 (Ar*C*H), 126.89 (Ar*C*H), 125.09 (*C*H), 55.32 (*C*H), 48.47 (*C*H), 47.76 (*C*H_2), 20.97 (*C*H_3), 19.25 (*C*H_3) LRMS (ES+) calculated for $C_{25}H_{24}NO_3$ and $C_{25}H_{23}NO_3Na$ found 386.1 m/z $(M+H)^+$ and 408.1 m/z $(M+Na)^+$ m/z

3-(4-ethoxyphenyl)-2-[phenylmethyl]-1-oxo-1,2,3,4-tetrahydroisoquinoline-4-carboxylic acid (A03)

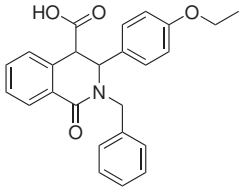

Purification on silica. White solid, 20% yield mp IR ^{1}H-NMR (400 MHz, DMSO-d_6) δ_H ppm: 1.25 to 1.29 (3*H*, t, J = 13.50 Hz), 3.74 (1*H*, d, J = 15.00 Hz), 3.94 (2*H*, q, J = 6.00 Hz and 21.00 Hz), 4.65 (1*H*, d, J = 6.00 Hz), 4.91 (1*H*, d, J = 6.00 Hz), 5.33 (1*H*, d, J = 16.50 Hz), 6.75 (2*H*, d, J = 12.00 Hz), 6.87 (2*H*, d, J = 9.00 Hz) 7.28 to 7.36 (4*H*, m), 7.45 to 7.49 (1*H*, m), 7.53 to 7.57 (2*H*, m), 8.08 (1*H*, d, J = 7.40 Hz), 12.92 (1*H*, s) ^{13}C-NMR (100 MHz, DMSO-d_6) δ_C ppm: 170.75 (C=O), 163.48 (C=O), 158.89 (Ar*C*), 137.87 (Ar*C*), 134.22 (Ar*C*), 132.48 (Ar*C*H), 129.43 (Ar*C*H), 129.16 (Ar*C*), 129.01 (Ar*C*H), 128.71 (Ar*C*), 128.57 (Ar*C*H), 127.99 (Ar*C*H), 127.93 (Ar*C*), 127.88

(Ar*C*H), 127.66 (Ar*C*H), 114.56 (*C*H), 63.39 (*C*H_2), 60.57 (*C*H), 48.54 (*C*H_2), 48.34 (*C*H), 15.07 (*C*H_3) LRMS (ES+) calculated for $C_{26}H_{26}NO_4$ found 416.5 m/z $(M+H)^+$

3-(4-ethylphenyl)-2-[phenylmethyl]-1-oxo-1,2,3,4-tetrahydroisoquinoline-4-carboxylic acid (A04)

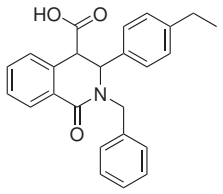

Purification on silica. White solid, 168 mg, 16% yield mp 199.3°C to 200.2°C IR ν_{max} (neat) cm^{-1} 2953.92 (O-H), 1699.35 (C=O), 1641.45 (C=O) ^{1}H-NMR (400 MHz, DMSO-d_6) δ_H ppm: 1.09 (3*H*, t, J = 15.05 Hz), 3.81 (1*H*, d, J = 15.15 Hz), 4.07 (1*H*, s), 5.22 (1*H*, s), 5.29 (1*H*, d, J = 15.12 Hz), 6.95 (2*H*, d, J = 8.20 Hz), 7.07 (2*H*, d, J = 8.25 Hz), 7.26 (6H, brm), 7.42 (2*H*, m), 7.98 to 7.99 (1*H*, m) ^{13}C-NMR (100 MHz, DMSO-d_6) δ_C ppm: 172.56 (C=O), 163.92 (C=O), 143.49 (Ar*C*), 137.73 (Ar*C*), 136.87 (Ar*C*), 134.19 (Ar*C*), 132.39 (Ar*C*H), 130.04 (Ar*C*H), 129.40 (Ar*C*), 128.63 (Ar*C*H), 128.53 (Ar*C*H), 128.31 (Ar*C*H), 127.47 (Ar*C*H), 127.38 (Ar*C*H), 126.46 (*C*H), 61.47 (*C*H), 51.31 (*C*H), 49.66 (*C*H_2), 28.07 (*C*H_2), 15.77 (*C*H_3)LRMS (ES+) calculated for $C_{25}H_{23}FNO_3$ and $C_{25}H_{22}FNO_3Na$ found 385.9 $(M+H)^+$ m/z and 407.9 $(M+Na)^+$ m/z

3-(2-hydroxy-5-nitrophenyl)-2-[phenylmethyl]-1-oxo-1,2,3,4-tetrahydroisoquinoline-4-carboxylic acid (A05)

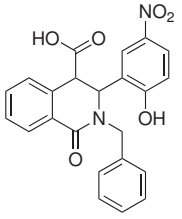

Purification on silica. Yellow solid, 306 mg, 29% yield mp 269.7°C to 274.2°C IR ν_{max} (neat) cm^{-1} 3077.77 (O-H), 1712.76 (C=O) ^{1}H-NMR (400 MHz, DMSO-d_6) δ_H ppm: 3.86 (1*H*, s), 4.26 (1*H*, d, J = 14.67 Hz), 4.99 (1*H*, d, J = 15.03 Hz), 5.54 (1*H*, s), 6.95 (1*H*, dd, J = 9.07 Hz and 1.57 Hz), 7.17 to 7.27 (6H, m, overlap), 7.42 (2*H*, m), 7.89 to 7.91 (1*H*, m), 8.04 (1*H*, m) ^{13}C-NMR (100 MHz, DMSO-d_6) δ_C ppm: 172.46 (C=O), 164.16 (C=O), 162.09 (Ar*C*), 139.20 (Ar*C*), 137.39 (Ar*C*), 134.36 (Ar*C*), 132.62 (Ar*C*H), 130.23 (Ar*C*H), 128.96 (Ar*C*), 128.63 (Ar*C*H), 128.56 (Ar*C*H), 128.47 (Ar*C*H), 127.57

(Ar*C*H), 127.54 (Ar*C*H), 126.34 (Ar*C*), 125.54 (Ar*C*H), 122.70 (Ar*C*H), 116.28 (*C*H), 56.80 (*C*H), 50.06 (*C*H), 48.20 (*C*H) LRMS (ES+) calculated for $C_{23}H_{19}N_2O_6$ found 419.1 $(M+H)^+$ m/z

3-(4-chlorophenyl)-2-[phenylmethyl]-1-oxo-1,2,3,4-tetrahydroisoquinoline-4-carboxylic acid (A06)

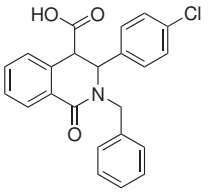

Purification by precipitation. White solid, 89 mg, 9% yield mp 178.9°C to 181.2°C ^{1}H-NMR (400 MHz, DMSO-d_6) δ_H ppm (1:1 ratio of cis to trans): 3.85 (1*H*, d, J = 12.00 Hz), 3.92 (1*H*, s, trans), 3.96 (1*H*, s, trans), 4.71 (1*H*, d, J = 8.07 Hz, cis), 5.01 (1*H*, d, J = 8.07 Hz, cis), 5.17 (1*H*, d, J = 12.00 Hz), 5.24 to 5.29 (1*H*, m), 6.94 to 6.97 (1*H*, m), 7.02 to 7.04 (1*H*, m), 7.19 to 7.45 (17*H*, m), 7.47 to 7.53 (7*H*, m), 7.54 to 7.56 (4*H*, m), 7.87 to 7.92 (2*H*, m), 7.97 to 7.99 (1*H*, m), 8.07 to 8.09 (2*H*, m), 12.88 (2*H*, brs) ^{13}C-NMR (100 MHz, DMSO-d_6) δ_C ppm: 172.94 (C=O), 170.70 (C=O), 163.45 (Ar*C*), 138.69 (Ar*C*), 137.67 (Ar*C*), 137.54 (Ar*C*), 136.75 (Ar*C*), 136.24 (Ar*C*), 133.88 (Ar*C*), 133.39 (Ar*C*), 132.65 (Ar*C*H), 132.59 (Ar*C*H), 132.02 (Ar*C*H), 131.20 (Ar*C*H), 130.83 (Ar*C*H), 130.08 (Ar*C*H), 130.04 (Ar*C*H), 129.25 (Ar*C*), 129.02 (Ar*C*H), 128.97 (Ar*C*H), 128.71 (Ar*C*H), 128.62 (Ar*C*H), 128.52 (Ar*C*), 128.47 (Ar*C*H), 128.09 (Ar*C*H), 128.03 (Ar*C*H), 127.86 (Ar*C*H), 127.69 (Ar*C*H), 127.55 (Ar*C*H), 127.48 (Ar*C*H), 127.39 (Ar*C*H), 126.20 (*C*H), 61.10 (*C*H), 60.54 (*C*H), 51.03 (*C*H), 49.92 (CH_2), 48.71 (*C*H), 48.52 (CH_2), 40.74 (CH_2), 40.73 (*C*H), 40.72 (*C*H) LRMS (ES+) $C_{23}H_{18}ClNO_3$ found 392.1 $(M+H)^+$ m/z

3-(4-bromophenyl)-2-[phenylmethyl]-1-oxo-1,2,3,4-tetrahydroisoquinoline-4-carboxylic acid (A07)

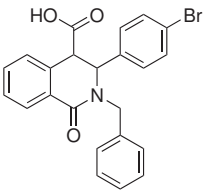

Purification by reverse-phase chromatography. White solid, 23 mg, 2% yield mp 177.5°C to 179.5°C HPLC retention time 16.373 min LRMS (ES+) $C_{23}H_{18}BrNO_3$ found 458.0 $(M+Na)^+$ m/z

3-(2-fluorophenyl)-2-[phenylmethyl]-1-oxo-1,2,3,4-tetrahydroisoquinoline-4-carboxylic acid (A08)

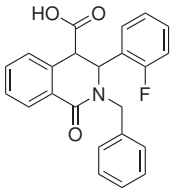

Purification by recrystallisation. White solid, 85 mg, 9% yield mp 212.4°C to 213.7°C IR ν_{max} (neat) cm^{-1} 3025.40 (O-H), 1746.99 (C=O), 1698.86 (C=O) 1:1 mixture of cis and trans ^{1}H-NMR (400 MHz, DMSO-d_6) δ_H ppm: 3.93 (1*H*, d, J = 14.65 Hz), 4.07 (1*H*, d, J = 14.65 Hz), 4.15 (1*H*, s, trans), 4.73 (1*H*, d, J = 7.33 Hz, cis), 5.07 (1*H*, d, J = 5.86 Hz, cis), 5.17 (1*H*, d, J = 14.80 Hz), 5.25 (1*H*, d, J = 15.25 Hz), 5.35 (1*H*, s, trans), 6.73 to 6.86 (3*H*, m), 6.99 to 7.10 (1*H*, m), 7.22 to 7.36 (11*H*, m), 7.41 to 7.54 (3*H*, m), 7.56 to 7.58 (2*H*, m), 8.00 (1*H*, d, J = 7.17 Hz, trans), 8.10 (1*H*, d, J = 7.62 Hz, trans) ^{13}C-NMR (100 MHz, DMSO-d_6) δ_C ppm: 172.26 (C=O), 163.81 (C=O), 137.56 (Ar*C*), 132.54 (Ar*C*H), 131.00 (Ar*C*H), 130.04 (Ar*C*H), 129.21 (Ar*C*), 128.93 (Ar*C*H), 128.58 (Ar*C*H), 128.56 (Ar*C*H), 128.44 (Ar*C*), 128.09 (Ar*C*H), 127.97 (Ar*C*), 127.66 (Ar*C*H), 127.53 (Ar*C*H), 127.43 (Ar*C*), 122.53 (Ar*C*H), 114.73 (Ar*C*H), 113.73 (*C*H), 61.32 (*C*H), 50.97 (*C*H), 50.12 (CH_2, trans) LRMS (ES+) calculated for $C_{23}H_{18}FNO_3$ found 376.1 $(M+H)^+$ m/z and 398.1 $(M+Na)^+$ m/z

3-phenyl-2-[phenylmethyl]-1-oxo-1,2,3,4-tetrahydroisoquinoline-4-carboxylic acid (A09)

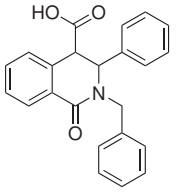

Purification by recrystallisation. White solid, 72 mg, 8% yield mp 203.6°C to 205.8°C IR ν_{max} (neat) cm^{-1} 3000.37 (O-H), 1744.89 (C=O) ^{1}H-NMR (400 MHz, DMSO-d_6) δ_H ppm: 3.77 (1*H*, d, J = 13.52 Hz), 4.70 (1*H*, d, J = 6.76 Hz), 4.98 (1*H*, d, J = 4.51 Hz), 5.32 (1*H*, d, J = 13.77 Hz), 6.97 (2*H*, d, J = 6.88 Hz), 7.26 to 7.33 (9H,

m), 7.47 to 7.56 (3*H*, m), 8.09 (1*H*, d, $J = 7.19$ Hz) ^{13}C-NMR (100 MHz, DMSO-d$_6$) δ_C ppm: 170.71 (C=O), 163.58 (C=O), 137.78 (Ar*C*), 137.09 (Ar*C*), 134.17 (Ar*C*), 132.52 (Ar*C*H), 129.16 (Ar*C*), 129.11 (Ar*C*H), 129.01 (Ar*C*H), 128.74 (Ar*C*H), 128.63 (*C*H) 128.51 (Ar*C*H), 128.39 (Ar*C*H), 128.24 (Ar*C*H), 128.02 (Ar*C*H), 127.94 (Ar*C*H), 127.92 (Ar*C*H), 127.68 (Ar*C*H), 126.50 (*C*H) 61.17 (*C*H), 48.55 (*C*H$_2$), 48.53 (*C*H) LRMS (ES+) calculated for $C_{23}H_{20}NO_3$ found 358.1 $(M+H)^+$ m/z

3-(pyridine-3-yl)-2-[phenylmethyl]-1-oxo-1,2,3,4-tetrahydroisoquinoline-4-car boxylic acid (A10)

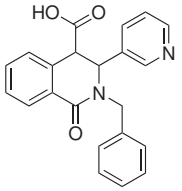

Purification by recrystallisation. White solid, 525 mg, 58% yield mp 226.3°C-227.8°C IR ν_{max} (neat) cm^{-1} 3059.57 (O-H), 1648.34 (C=O) ^{1}H-NMR (400 MHz, DMSO-d$_6$) δ_H ppm: 4.16 to 4.20 (2*H*, d, $J = 14.99$ Hz), 5.06 (1*H*, d, $J = 14.73$ Hz), 5.40 (1*H*, s), 7.18 to 7.34 (8H, m), 7.41 to 7.47 (2*H*, m), 7.99 to 8.01 (1*H*, m) ^{13}C-NMR (100 MHz, DMSO-d$_6$) δ_C ppm: 172.20 (C=O), 163.75 (C=O), 149.11 (Ar*C*H), 148.21 (Ar*C*H), 137.50 (Ar*C*), 135.22 (Ar*C*), 134.23 (Ar*C*H), 133.86 (Ar*C*), 132.62 (Ar*C*H), 130.10 (Ar*C*H), 129.29 (Ar*C*), 128.65 (Ar*C*H), 128.59 (Ar*C*H), 128.53 (Ar*C*H), 127.56 (Ar*C*H), 127.52 (Ar*C*H), 123.85 (*C*H), 59.89 (*C*H), 50.89 (*C*H), 50.14 (*C*H$_2$) LRMS (ES+) calculated for $C_{22}H_{19}N_2O_3$ found 359.1 $(M+H)^+$ m/z

3-(pyridine-4-yl)-2-[phenylmethyl]-1-oxo-1,2,3,4-tetrahydroisoquinoline-4-car boxylic acid (A11)

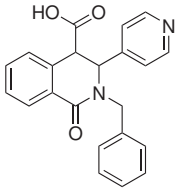

Purification by recrystallisation. White solid, 262 mg, 29% yield mp 252.6°C to 253.6°C IR ν_{max} (neat) cm^{-1} 3062.26 (O-H), 1651.30 (C=O) ^{1}H-NMR (400 MHz, DMSO-d$_6$) δ_H ppm: 4.14 (1*H*, d, $J = 14.95$ Hz), 4.17 (1*H*, s), 5.12 (1*H*, d, $J = 14.95$ Hz), 5.36 (1*H*, s), 7.02 (2*H*, d, $J = 5.77$ Hz), 7.19 to 7.30 (5H, m), 7.40 to 7.43 (2*H*, m), 7.97 (1*H*, m), 8.38 (2*H*, d, $J = 6.10$ Hz) ^{13}C-NMR (100 MHz, DMSO-d$_6$) δ_C ppm: 172.10 (C=O), 163.83

(C=O), 150.17 (Ar*C*H), 148.83 (Ar*C*), 137.44 (Ar*C*), 133.84 (Ar*C*), 132.58 (Ar*C*H), 130.01 (Ar*C*H), 129.15 (Ar*C*H), 128.67 (Ar*C*H), 128.61 (Ar*C*H), 128.50 (Ar*C*H), 127.60 (Ar*C*H), 127.50 (Ar*C*H), 121.83 (*C*H), 61.02 (*C*H), 50.54 (*C*H), 50.29 (*C*H_2) LRMS (ES+) calculated for $C_{22}H_{19}N_2O_3$ found 359.1 $(M+H)^+$ m/z

2-benzyl-1-oxo-3-(thiophen-3-yl),-1,2,3,4-tetrahydroisoquinoline-4-carboxylic acid (A12)

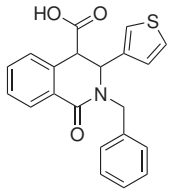

Purified on silica. Yellow solid, 18 mg, 2% yield mp 208.8 °C to 212.4 °C IR ν_{max} (neat) cm^{-1} 3031.68 (O-H), 1730.05 (C=O) ^{1}H-NMR (400 MHz, DMSO-d_6) δ_H ppm: 3.90 (1*H*, d, $J = 16.19$ Hz), 4.63 (1*H*, d, $J = 8.09$ Hz), 5.10 (1*H*, d, $J = 8.09$ Hz), 5.28 (1*H*, d, $J = 16.19$ Hz), 6.49 (1*H*, dd, $J = 1.24$ Hz and 5.19 Hz), 7.18 (1*H*, dd, $J = 1.24$ Hz and 3.05 Hz), 7.27 to 7.34 (6H, m), 7.45 to 7.49 (1*H*, m), 7.55 to 7.59 (1*H*, td, $J = 1.47$ Hz and 15.34 Hz), 7.68 (1*H*, d, $J = 7.78$ Hz), 8.05 (dd, $J = 1.24$ Hz and 7.78 Hz) ^{13}C-NMR (100 MHz, DMSO-d_6) δ_C ppm: 170.75 (C=O), 163.40 (C=O), 138.19 (Ar*C*), 137.96 (Ar*C*), 134.67 (Ar*C*), 132.42 (Ar*C*H), 129.19 (Ar*C*), 128.98 (Ar*C*H), 128.61 (Ar*C*H), 128.43 (Ar*C*H), 128.37 (Ar*C*H), 128.01 (Ar*C*H), 127.96 (Ar*C*H), 127.91 (Ar*C*H), 127.63 (Ar*C*H), 127.46 (Ar*C*H), 127.03 (Ar*C*H), 126.97 (Ar*C*H), 125.08 (*C*H), 57.09 (*C*H), 48.48 (*C*H_2), 48.11 (*C*H) LRMS (ES+) calculated for $C_{21}H_{18}NO_3S$ found 364.1 $(M+H)^+$ m/z

3-(3-phenoxymethyl)-2-[(4-methylphenyl)methyl]-1-oxo-1,2,3,4-tetrahydroiso quinoline-4-carboxylic acid (A13)

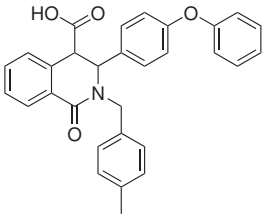

Purification by recrystallisation. Pale yellow solid, 187 mg, 16% yield mp 207.0 °C to 209.5 °C IR ν_{max} (neat) cm^{-1} 3069.94 (O-H) 1640.35 (C=O) 1230.24 (C-O) ^{1}H-NMR (400 MHz, DMSO-d_6) δ_H ppm: 2.25 (3*H*, s), 4.01 (1*H*, d, $J = 14.99$ Hz), 4.04 (1*H*, s), 5.06 (1*H*, d, $J = 15.55$ Hz), 5.25 (1*H*, s), 6.57 (1*H*, m), 6.77 to 6.84 (4*H*, m), 7.05 (2*H*, d, *J*

= 7.87 Hz), 7.11 to 7.15 (3*H*, m), 7.20 to 7.25 (2*H*, m), 7.31 to 7.35 (2*H*, m), 7.41 to 7.47 (2*H*, m), 7.91 (1*H*, dd, J = 7.27 Hz and 1.61 Hz) ^{13}C-NMR (100 MHz, DMSO-d_6) δ_C ppm: 172.46 (C=O), 163.74 (C=O), 157.00 (Ar*C*), 156.49 (Ar*C*), 142.20 (Ar*C*), 136.51 (Ar*C*), 134.46 (Ar*C*), 132.37 (Ar*C*H), 130.74 (Ar*C*H), 130.48 (Ar*C*H), 129.97 (Ar*C*H), 129.33 (Ar*C*), 129.16 (Ar*C*H), 128.62 (Ar*C*H), 128.24 (Ar*C*H), 127.37 (Ar*C*H), 124.00 (Ar*C*H), 121.65 (Ar*C*H), 118.90 (Ar*C*H), 118.76 (Ar*C*H), 117.84 (Ar*C*H), 116.57 (*C*H), 61.47 (*C*H), 49.68 (*C*H_2), 31.16 (*C*H), 21.20 (*C*H_3) LRMS (ES+) calculated for $C_{30}H_{26}NO_4$ found 464.1 $(M+H)^+$ m/z

3-(2,4-dimethylphenylmethyl)-2-[(4-methylphenyl)methyl]-1-oxo-1,2,3,4-tetrahydroisoquinoline-4-carboxylic acid (A14)

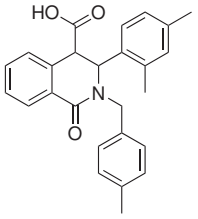

Purification by recrystallisation. White solid, 329 mg, 31% yield mp 197.3 °C to 200.6 °C IR ν_{max} (neat) cm^{-1} 2920.34 (O-H), 1738.30 (C=O) ^{1}H-NMR (400 MHz, DMSO-d_6) δ_H ppm: 2.05 (3*H*, s), 2.19 (3*H*, s), 2.28 (3*H*, s), 3.50 (1*H*, d, J = 14.64 Hz), 4.53 (1*H*, d, J = 6.68 Hz), 5.09 (1*H*, d, J = 6.68 Hz), 5.40 (1*H*, d, J = 15.22 Hz), 6.79 (2*H*, m), 6.93 (1*H*, s), 7.11 (4*H*, dd, J = 7.79 Hz and 24.12 Hz), 7.41 (1*H*, d, J = 7.42 Hz), 7.47 to 7.51 (1*H*, m), 7.54 to 7.56 (1*H*, td, J = 1.48 Hz and 15.22 Hz), 8.11 (1*H*, dd, J = 1.48 Hz and 7.79 Hz) ^{13}C-NMR (100 MHz, DMSO-d_6) δ_C ppm: 171.01 (C=O), 163.73 (C=O), 137.56 (Ar*C*), 136.91 (Ar*C*), 136.61 (Ar*C*), 134.61 (Ar*C*), 132.66 (Ar*C*), 132.52 (Ar*C*H), 131.53 (Ar*C*H), 129.63 Ar*C*H), 129.33 (Ar*C*), 129.12 (Ar*C*), 128.31 (Ar*C*H), 128.07 (Ar*C*H), 128.04 (Ar*C*H), 127.93 (Ar*C*H), 129.35 (Ar*C*H), 127.20 (*C*H), 55.05 (*C*H), 48.36 (*C*H), 47.34 (*C*H_2), 21.15 (*C*H_3), 20.97 (*C*H_3), 19.26 (*C*H_3) LCMS (ES+) calculated for $C_{26}H_{26}NO_3$ and $C_{26}H_{25}NO_3Na$ found 399.9 $(M+H)^+$ and 421.9 $(M+Na)^+$ m/z

3-(4-ethoxyphenyl)-2-[4-(methylphenyl)methyl]-1-oxo-1,2,3,4-tetrahydroisoquinoline-4-carboxylic acid (A15)

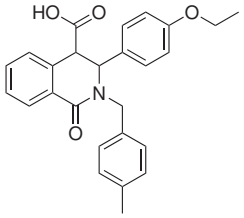

Purification by recrystallisation. White solid, 242 mg, 22% yield mp 180.8 °C to 183.4 °C IR ν_{max} (neat) cm^{-1} 2977.77 (O-H), 1739.49 (C=O), 1622.65 (C=O) ^{1}H-NMR (400 MHz, DMSO-d_6) δ_H ppm: 1.28 (3*H*, t, J = 13.23 Hz), 2.30 (3*H*, s), 3.63 (1*H*, d, J = 16.17 Hz), 3.94 (2*H*, q, J = 7.35 Hz and 22.05 Hz), 4.59 (1*H*, d, J = 7.35 Hz), 4.87 (1*H*, d, J = 5.88 Hz), 5.33 (1*H*, d, J = 16.17 Hz), 6.75 (2*H*, d, J = 8.82 Hz), 6.86 (2*H*, d, J = 8.82 Hz), 7.17 (4*H*, q, J = 5.88 Hz and 22.05 Hz), 7.45 to 7.49 (1*H*, m), 7.52 to 7.59 (2*H*, m), 8.08 (1*H*, d, J = 7.35 Hz) ^{13}C-NMR (100 MHz, DMSO-d_6) δ_C ppm: 170.74 (C=O), 163.40 (C=O), 158.87 (Ar*C*), 136.84 (Ar*C*), 134.75 (Ar*C*), 134.65 (Ar*C*), 132.43 (Ar*C*H), 129.62 (Ar*C*H), 129.42 (Ar*C*H), 129.23 (Ar*C*), 128.70 (Ar*C*), 128.59 (Ar*C*H), 128.06 (Ar*C*H), 127.91 (Ar*C*H), 127.85 (Ar*C*H), 114.55 (*C*H), 63.39 (*C*H_2), 60.28 (*C*H), 48.56 (*C*H), 47.85 (*C*H_2), 21.17 (*C*H_3), 15.07 (*C*H_3) $C_{26}H_{26}NO_4$ and $C_{26}H_{25}NO_4Na$ 415.9 $(M+H)^+$ and 437.9 $(M+Na)^+$ m/z

3-(4-ethylphenyl)-2-[4-(methylphenyl)methyl]-1-oxo-1,2,3,4-tetrahydroisoquinoline-4-carboxylic acid (A16)

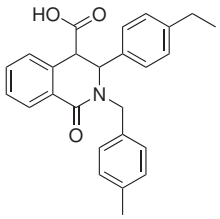

Purification by recrystallisation. White solid, 232 mg, 23% yield mp 163.0°C to 167.8 °C IR ν_{max} (neat) cm^{-1} 2952.44 (O-H), 1700.10 (C=O), 1638.84 (C=O) ^{1}H-NMR (400 MHz, DMSO-d_6) δ_H ppm: 1.09 (3*H*, t, J = 15.65 Hz), 2.26 (3*H*, s), 3.72 (1*H*, d, J = 13.87 Hz), 4.05 (1*H*, s), 5.17 (1*H*, s), 5.28 (1*H*, d, J = 13.87 Hz), 6.94 (2*H*, d, J = 8.51 Hz), 7.08 (4*H*, m) 7.14 (2*H*, d, J = 8.51 Hz) 7.18 to 7.21 (1*H*, m), 7.40 to 7.44 (2*H*, m), 7.98 to 8.00 (1*H*, m) ^{13}C-NMR (100 MHz, DMSO-d_6) δ_C ppm: 172.51 (C=O), 163.89 (C=O), 143.53 (Ar*C*), 136.77 (Ar*C*), 136.55 (Ar*C*), 134.51 (Ar*C*), 134.08 (Ar*C*), 132.41 (Ar*C*H), 129.99 (Ar*C*H), 129.41 (Ar*C*), 129.25 (Ar*C*H), 128.54 (Ar*C*H), 128.38 (Ar*C*H), 128.33 (Ar*C*H), 127.40 (Ar*C*H), 126.43 (*C*H), 61.19 (*C*H), 51.27 (*C*H), 49.22

(CH_2), 28.06 (CH_2), 21.18 (CH_3), 15.76 (CH_3) LRMS (ES+) calculated for $C_{26}H_{26}NO_3$ found 400.1 $(M+H)^+$ m/z

3-(4-chlorophenyl)-2-[4-(methylphenyl)methyl]-1-oxo-1,2,3,4-tetrahydroisoquinoline-4-carboxylic acid (A17)

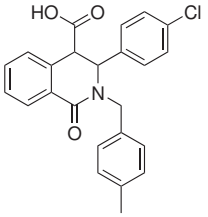

Purification by recrystallisation. White solid, 20 mg, 2% yield mp 220.0°C to 223.4°C IR ν_{max} (neat) cm^{-1} 2951.07 (O-H), 1716.11 (C=O), 1698.69 (C=O) ^{1}H-NMR (400 MHz, DMSO-d_6) δ_H ppm: 2.26 (3*H*, s), 3.87 (1*H*, d, $J = 14.87$ Hz), 4.08 (1*H*, s), 5.18 (1*H*, d, $J = 14.87$ Hz), 5.25 (1*H*, s), 7.05 (4*H*, m), 7.14 (2*H*, m), 7.19 (1*H*, m), 7.29 (2*H*, d, $J = 8.41$ Hz), 7.43 (2*H*, m), 7.98 (1*H*, m), 12.96 (1*H*, brs) ^{13}C-NMR (100 MHz, DMSO-d_6) δ_C ppm: 172.23 (C=O), 163.72 (C=O), 138.69 (Ar*C*), 136.59 (Ar*C*), 134.42 (Ar*C*), 133.85 (Ar*C*), 132.59 (Ar*C*), 132.50 (Ar*C*H), 130.00 (Ar*C*H), 129.30 (Ar*C*), 129.21 (Ar*C*H), 129.04 (Ar*C*H), 128.58 (Ar*C*H), 128.46 (Ar*C*H), 128.44 (CH: hidden underneath 128.46 as shown by HSQC)), 127.47 (*C*H), 60.86 (*C*H), 51.01 (*C*H), 49.46 (CH_2), 21.20 (CH_3) HRMS (ES-) calculated for $C_{24}H_{19}ClNO_3$ found 404.1059 $(M-H)^-$ m/z

3-(3-trifluoromethyl-4-chlorophenyl)-2-[4-(methylphenyl)methyl]-1-oxo-1,2,3,4-tetrahydroisoquinoline-4-carboxylic acid (A18)

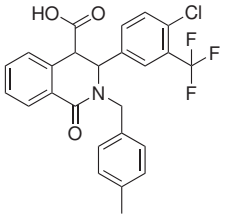

Purification by recrystallisation. White solid, 382 mg, 32% yield mp 249.4°C to 253.0°C IR ν_{max} (neat) cm^{-1} 2918.73 (O-H) 1716.33 (C=O), 1701.61 (C=O) ^{1}H-NMR (400 MHz, DMSO-d_6) δ_H ppm: 2.22 (3*H*, s), 4.17 (1*H*, s), 4.39 (1*H*, d, $J = 14.50$ Hz), 4.84 (1*H*, d, $J = 14.50$ Hz), 7.00 (2*H*, d, $J = 7.91$ Hz), 7.16 (2*H*, d, $J = 7.91$ Hz), 7.25 (2*H*, m), 7.36 (1*H*, m), 7.41 to 7.48 (2*H*, m), 7.52 (1*H*, d, $J = 8.44$ Hz), 7.98 to 8.02 (1*H*, m) ^{13}C-NMR (100 MHz, DMSO-d_6) δ_C ppm: 172.01 (C=O), 163.49 (C=O), 140.04 (Ar*C*), 136.71 (Ar*C*),

134.30 (Ar*C*), 133.63 (Ar*C*), 132.65 (Ar*C*H), 132.10 (Ar*C*H), 132.02 (Ar*C*H), 130.12 (Ar*C*H), 129.99 (Ar*C*), 129.18 (Ar*C*), 129.06 (Ar*C*H), 128.96 (Ar*C*H), 128.59 (Ar*C*H), 127.49 (Ar*C*H), 126.94 (Ar*C*), 126.37 (Ar*C*H), 126.32 (*C*H), 60.82 (*C*H), 50.68 (*C*H), 50.04 (*C*H_2), 21.10 (*C*H_3) LRMS (ES+) calculated for $C_{25}H_{20}ClFNO_3$ found 474.1 $(M+H)^+$ m/z

3-(4-bromophenyl)-2-[4-(methylphenyl)methyl]-1-oxo-1,2,3,4-tetrahydroisoquinoline-4-carboxylic acid (A19)

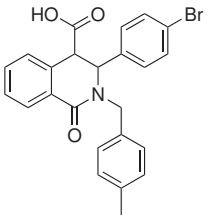

Purification by recrystallisation. White solid, 45 mg, 4% yield mp 197.5°C to 204.0°C IR ν_{max} (neat) cm^{-1} 2951.08 (O-H), 1745.67 (C=O), 1698.33 (C=O) ^{1}H-NMR (400 MHz, DMSO-d_6) δ_H ppm: (1:2 ratio Cis:trans) 2.25 (3*H*, s), 3.87 (1*H*, d, J = 15.01 Hz), 4.07 (1*H*, s), 5.17 (1*H*, d, J = 15.01 Hz), 5.23 (1*H*, s), 6.92 (2*H*, d, J = 8.44 Hz), 7.06 (2*H*, d, J = 8.44 Hz), 7.11 to 7.19 (4*H*, m), 7.39 to 7.43 (3*H*, m), 7.96 to 7.98 (1*H*, m) ^{13}C-NMR (100 MHz, DMSO-d_6) δ_C ppm: 172.23 (C=O), 163.74 (C=O), 139.10 (Ar*C*), 136.61 (Ar*C*), 134.39 (Ar*C*), 133.81 (Ar*C*), 131.96 (Ar*C*H), 130.38 (Ar*C*H), 129.99 (Ar*C*), 129.59 (Ar*C*H), 129.22 (Ar*C*H), 128.80 (Ar*C*H), 128.58 (Ar*C*H), 128.46 (Ar*C*H), 128.16 (Ar*C*H), 127.60 (Ar*C*H), 121.14 (Ar*C*), 60.91 (*C*H), 50.96 (*C*H), 49.45 (*C*H_2), 21.20 (*C*H_3) LRMS (ES+) calculated for $C_{24}H_{21}BrNO_3$ found 450.9 $(M+H)^+$ m/z

3-(2-fluorophenyl)-2-[4-(methylphenyl)methyl]-1-oxo-1,2,3,4-tetrahydroisoquinoline-4-carboxylic acid (A20)

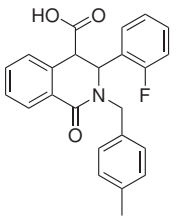

Purification by recrystallisation. White solid, 78 mg, 8% yield mp 270.3°C to 273.2°C IR ν_{max} (neat) cm^{-1} 2956.90 (O-H), 1739.90 (C=O) ^{1}H-NMR (400 MHz, DMSO-d_6) δ_H ppm: 2.26 (3*H*, s), 3.78 (1*H*, d, 14.85 Hz), 4.07 (1*H*, s), 5.25 (2*H*, sd overlap, J =

17.64 Hz), 7.05 (4*H*, m), 7.13 to 7.26 (6H, m), 7.40 to 7.44 (2*H*, m), 7.98 to 8.00 (1*H*, m) ^{13}C-NMR (100 MHz, DMSO-d_6) δ_C ppm: 172.45 (C=O), 163.87 (C=O), 139.65 (Ar*C*), 136.53 (Ar*C*), 134.53 (Ar*C*), 134.10 (Ar*C*), 132.38 (Ar*C*H), 129.98 (Ar*C*H), 129.42 (Ar*C*), 129.22 (Ar*C*H), 129.12 (Ar*C*H), 128.45 (Ar*C*H), 128.32 (Ar*C*H), 127.99 (Ar*C*H), 127.40 (Ar*C*H), 126.48 (*C*H), 61.44 (*C*H), 51.29 (*C*H), 49.36 (*C*H$_2$), 21.20 (*C*H$_3$) LRMS (ES+) calculated for $C_{24}H_{21}FNO_3$ found 389.9 $(M+H)^+$ m/z

2-benzyl-1-oxo-3-(thiophen-3-yl),-1,2,3,4-tetrahydroisoquinoline-4-carboxylic acid (A21)

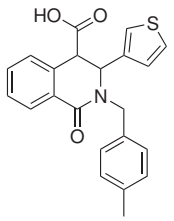

Purification on silica. White solid, 352 mg, 37% yield mp 274.5°C to 275.1°C IR ν_{max} (neat) cm^{-1} 2918.86 (O-H), 1716.18 (C=O), 1698.75 (C=O) ^{1}H-NMR (400 MHz, DMSO-d_6) δ_H ppm: (1:3 ratio of cis: trans) 2.28 (3*H*, s), 3.95 (1*H*, d, J = 15.28 Hz), 4.15 (1*H*, s), 5.21 (1*H*, d, J = 14.55 Hz), 5.28 (1*H*, s), 6.73 (1*H*, d, J = 5.09 Hz), 7.08 to 7.11 (3*H*, m), 7.12 to 7.16 (3*H*, m), 7.18 to 7.21 (1*H*, m), 7.27 (1*H*, d, J = 7.18 Hz), 7.39 to 7.50 (3*H*, m), 7.97 (1*H*, d, J = 7.52 Hz), 13.00 (1*H*, brs) ^{13}C-NMR (100 MHz, DMSO-d_6) δ_C ppm: 172.32 (C=O), 163.41 (C=O), 141.33 (Ar*C*), 136.48 (Ar*C*), 134.76 (Ar*C*), 134.72 (Ar*C*), 132.37 (Ar*C*H), 130.01 (Ar*C*H), 129.60 (Ar*C*H), 129.33 (Ar*C*H), 129.21 (Ar*C*H), 128.47 (Ar*C*H), 128.27 (Ar*C*H), 128.05 (Ar*C*H), 127.63 (Ar*C*H), 127.47 (Ar*C*H), 126.40 (Ar*C*H), 122.86 (*C*H), 58.29 (*C*H), 50.34 (*C*H), 49.45 (*C*H$_2$), 21.21 (*C*H$_3$) LRMS (ES+) calculated for $C_{22}H_{20}NO_3S$ found 377.9 $(M+H)^+$ m/z

3-(2,4-dimethylphenyl)-2-[methoxyphenylmethyl]-1-oxo-1,2,3,4-tetrahydroiso quinoline-4-carboxylic acid (A22)

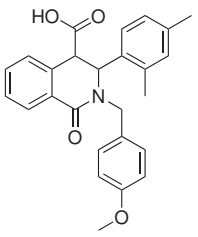

Purification by recrystallisation. White solid, 430 mg, 41% yield mp 198.2°C to 200.9°C IR ν_{max} (neat) cm^{-1} 3003.82 (O-H), 1737.86 (C=O) ^{1}H-NMR (400 MHz, DMSO-d_6) δ_H ppm: 2.07 (3*H*, s), 2.19 (3*H*, s), 3.50 (1*H*, d,$J = 14.38$ Hz), 3.73 (3*H*, s), 4.55 (1*H*, d, $J = 7.19$ Hz), 5.09 (1*H*, d, $J = 6.16$ Hz), 5.37 (1*H*, d, 15.41 Hz), 6.78 (2*H*, m), 6.88 (2*H*, d, $J = 9.24$ Hz), 6.93 (1*H*, s), 7.10 (2*H*, d, $J = 8.22$ Hz), 7.39 (1*H*, d, $J = 7.19$ Hz), 7.49 (1*H*, t, $J = 7.50$ Hz and 14.79 Hz), 7.53 to 7.57 (1*H*, td, $J = 1.19$ Hz and 15.50 Hz), 8.10 (1*H*, dd, $J = 1.19$ Hz and 8.91 Hz), 12.84 (1*H*, brs) ^{13}C-NMR (100 MHz, DMSO-d_6) δ_C ppm: 172.17 (C=O), 171.07 (C=O), 164.03 (Ar*C*), 163.75 (Ar*C*), 159.01 (Ar*C*), 158.91 (Ar*C*), 136.62 (Ar*C*), 132.49 (Ar*C*H), 132.27 (Ar*C*H), 131.54 (Ar*C*H), 129.84 (Ar*C*H), 129.51 (Ar*C*), 129.47 (Ar*C*), 129.44 (Ar*C*), 129.35 (Ar*C*H), 129.19 (Ar*C*), 128.30 (Ar*C*H), 128.07 (Ar*C*H), 128.03 (Ar*C*H), 127.41 (Ar*C*H), 127.32 (Ar*C*H), 127.18 (Ar*C*H), 126.90 (Ar*C*H), 125.13 (Ar*C*H), 114.44 (Ar*C*H), 114.16 (*C*H), 57.87 (*C*H), 55.50 (*C*H_3), 55.45 (*C*H), 54.99 (*C*H), 49.11 (*C*H), 48.48 (*C*H), 48.36 (*C*H_2), 47.04 (*C*H_2), 20.98 (*C*H_3), 20.84 (*C*H_3), 19.30 (*C*H_3), 18.90 (*C*H_3) LRMS (ES+) calculated for $C_{26}H_{26}NO_4$ found 416.1 $(M+H)^+$ m/z

3-(2-hydroxy-5-nitrophenyl)-2-[methoxyphenylmethyl]-1-oxo-1,2,3,4-tetrahydroisoquinoline-4-carboxylic acid (A23)

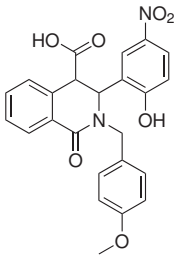

Purification by recrystallisation. Yellow solid, 249 mg, 22% yield mp 263.9°C to 264.0°C IR ν_{max} (neat) cm^{-1} 3077.92 (O-H), 1712.89 (C=O) ^{1}H-NMR (400 MHz, DMSO-d_6) δ_H ppm: 3.68 (3*H*, s), 4.03 (1*H*, s), 4.18 (1*H*, d, $J = 14.50$ Hz), 4.95 (1*H*, d, $J = 14.50$ Hz), 5.50 (1*H*, s), 6.80 (2*H*, d, $J = 8.92$ Hz), 6.95 (1*H*, d, $J = 8.92$ Hz), 7.18 (2*H*, d, $J = 8.92$ Hz), 7.23 (2*H*, m), 7.43 (3*H*, q, $J = 3.30$ Hz and 9.20 Hz), 7.93 (1*H*, dd, $J = 2.70$ Hz and 11.63 Hz), 8.04 (1*H*, q, $J = 3.52$ Hz and 9.20 Hz), 12.42 (1*H*, brs) ^{13}C-NMR (100 MHz, DMSO-d_6) δ_C ppm: 172.29 (C=O), 163.93 (C=O), 158.89 (Ar*C*), 139.41 (Ar*C*), 134.13 (Ar*C*), 132.57 (Ar*C*H), 130.17 (Ar*C*H), 130.12 (Ar*C*H), 129.28 (Ar*C*), 129.09 (Ar*C*), 128.51 (Ar*C*H), 127.54 (Ar*C*H), 126.31 (Ar*C*), 125.46 (Ar*C*H), 125.30 (Ar*C*), 122.76 (Ar*C*H), 116.22 (Ar*C*H), 113.98 (Ar*C*H), 56.31 (*C*H), 55.43 (*C*H_3), 49.23 (*C*H_2), 48.01 (*C*H) LRMS (ES+) calculated for $C_{24}H_{21}N_2O_7$ found 449.3 $(M+H)^+$ m/z

3-(2-nitrophenyl)-2-[methoxyphenylmethyl]-1-oxo-1,2,3,4-tetrahydroisoquinoline-4-carboxylic acid (A24)

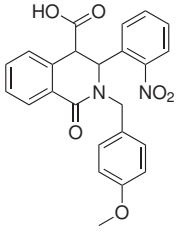

Purification by recrystallisation. White solid, 338 mg, 31% yield mp 215.4°C to 220.2°C IR ν_{max} (neat) cm^{-1} 2357.80 (O-H), 1708.15 (C=O) ^{1}H-NMR (400 MHz, DMSO-d_6) δ_H ppm: 3.68 (3*H*, s), 4.15 (1*H*, s), 4.20 (1*H*, d, $J = 14.05$ Hz), 4.83 (1*H*, d, $J = 14.05$ Hz), 5.88 (1*H*, s), 6.71 (3*H*, m), 6.79 to 6.81 (2*H*, m), 7.11 to 7.13 (3*H*, m), 7.26 to 7.28 (2*H*, m), 7.43 to 7.47 (6H, m), 8.02 to 8.06 (3*H*, m), 12.94 (1*H*, brs) ^{13}C-NMR (100 MHz, DMSO-d_6) δ_C ppm: 171.88 (C=O), 163.81 (C=O), 158.86 (Ar*C*), 148.01 (Ar*C*), 134.57 (Ar*C*), 134.10 (Ar*C*H), 133.43 (Ar*C*), 132.65 (Ar*C*H), 130.47 (Ar*C*H), 130.34

(Ar*C*H), 129.54 (Ar*C*H), 128.98 (Ar*C*), 128.84 (Ar*C*), 128.66 (Ar*C*H), 128.36 (Ar*C*H), 127.51 (Ar*C*H), 125.97 (Ar*C*H), 113.92 (*C*H), 57.06 (*C*H), 55.45 18(*C*H), 49.50 ($C H_2$), 49.22 (*C*H) LRMS (ES+) calculated for $C_{24}H_{20}N_2O_6$ 433.4 $(M+H)^+$ m/z

3-(2-fluorophenyl)-2-[methoxyphenylmethyl]-1-oxo-1,2,3,4-tetrahydroisoquinoline-4-carboxylic acid (A25)

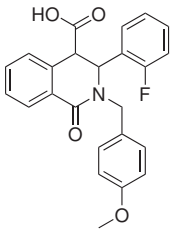

Purification by recrystallisation. White solid, 460 mg, 45% yield mp 190.0°C to 191.3°C IR ν_{max} (neat) cm^{-1} 2957.25 (O-H), 1738.82 (C=O) ^{1}H-NMR (400 MHz, DMSO-d_6) δ_H ppm: 3.72 (3*H*, s), 3.96 (1*H*, d, $J = 13.67$ Hz), 4.13 (1*H*, s), 5.13 (1*H*, d, $J = 14.80$ Hz), 5.30 (1*H*, s), 6.08 to 6.83 (4*H*, m), 6.99 to 7.04 (1*H*, td, $J = 19.16$ Hz and 2.13 Hz), 7.19 to 7.22 (3*H*, m), 7.26 to 7.28 (1*H*, m), 7.43 (2*H*, m), 7.97 to 8.00 (1*H*, m) ^{13}C-NMR (100 MHz, DMSO-d_6) δ_C ppm: 172.16 (C=O), 163.65 (C=O), 158.89 (Ar*C*), 144.84 (Ar*C*), 142.78 (Ar*C*) 133.89 (Ar*C*), 132.49 (Ar*C*H), 131.08 (Ar*C*H, split peak), 131.00 (Ar*C*H, split peak), 130.12 (Ar*C*H), 129.99 (Ar*C*H), 129.39 (Ar*C*), 129.33 (Ar*C*), 128.45 (Ar*C*H), 127.45 (Ar*C*H), 122.55 (Ar*C*H), 122.52 (Ar*C*H), 114.02 (Ar*C*H), 113.70 (*C*H), 60.84 (*C*H), 55.46 (CH_3), 50.90 (*C*H), 49.29 (CH_2) LRMS (ES+) calculated for $C_{24}H_{21}FNO_4$ found 406.6 $(M+H)^+$ m/z

3-[(4-methoxyphenyl)methyl]- 1-oxo-3-(pyridine-3-yl)-1,2,3,4-tetrahydroisoquinoline-4-carboxylic acid (A26)

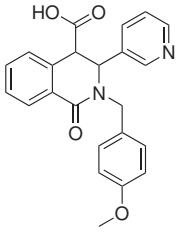

Purification by recrystallisation. White solid, 645 mg, 66% yield mp 246.0 °C to 242.1 °C IR ν_{max} (neat) cm^{-1} 2913.05 (O-H), 1682.65 (C=O) ^{1}H-NMR (400 MHz, DMSO-d_6) δ_H ppm: 3.71 (3*H*, s) 4.06 (1*H*, d, $J = 14.60$ Hz, 4.17 (1*H*, s), 5.09 (1*H*, d, $J = 14.60$ Hz), 5.33 (1*H*, s), 6.79 to 6.82 (2*H*, m), 7.02 to 7.03 (2*H*, d, $J = 6.05$ Hz), 7.18 to 7.23

(3*H*, m), 7.39 to 7.46 (2*H*, m), 7.97 to 8.00 (1*H*, m), 8.38 to 8.40 (2*H*, m), 13.00 (1*H*, brs) ^{13}C-NMR (100 MHz, DMSO-d_6) δ_C ppm: 171.99 (C=O), 163.64 (C=O), 158.94 (Ar*C*), 150.16 (Ar*C*H), 148.80 (Ar*C*), 133.69 (Ar*C*), 132.51 (Ar*C*H), 130.25 (Ar*C*H), 129.95 (Ar*C*H), 129.29 (Ar*C*), 128.51 (Ar*C*H), 127.51 (Ar*C*H), 121.82 (Ar*C*H), 114.03 (*C*H), 60.53 (*C*H), 55.47 (*C*H_3), 50.41 (*C*H), 49.47 (*C*H_2) LRMS (ES+) calculated for $C_{23}H_{21}FN_2O_4$ found 388.9 $(M+H)^+$ m/z

3-[(4-phenoxyphenyl)methyl]-1-oxo-3-(-(fluorophenyl)methyl)-1,2,3,4-tetrahydroisoquinoline-4-carboxylic acid (A27)

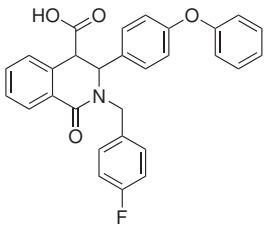

Purification by recrystallisation. White solid, 330 mg, 28% yield mp 233.2°C to 235.6°C IR ν_{max} (neat) cm^{-1} 2900.00 (O-H), 1698.93 (C=O) ^{1}H-NMR (400 MHz, DMSO-d_6) δ_H ppm: 4.06 to 4.10 (2*H*, sd, overlap), 5.05 (1*H*, d, J = 14.80 Hz), 5.29 (1*H*, s), 6.57 (1*H*, t, J = 2.03 Hz), 6.76 to 6.84 (4*H*, m), 7.03 to 7.07 (2*H*, m), 7.12 to 7.15 (1*H*, m), 7.21 to 7.25 (2*H*, m), 7.29 to 7.35 (4*H*, m), 7.41 to 7.46 (2*H*, m), 7.89 (1*H*, dd, J = 7.52 Hz and 1.45 Hz) ^{13}C-NMR (100 MHz, DMSO-d_6) δ_C ppm: 172.29 (C=O), 163.72 (C=O), 157.02 (Ar*C*), 156.47 (Ar*C*), 141.98 (Ar*C*), 133.97 (Ar*C*), 132.50 (Ar*C*H), 130.84 (Ar*C*H), 130.76 (Ar*C*H), 130.74 (Ar*C*H), 130.48 (Ar*C*H), 130.01 (Ar*C*H), 129.25 (Ar*C*), 128.40 (Ar*C*H), 127.42 (Ar*C*H), 124.02 (Ar*C*H), 121.68 (Ar*C*), 118.92 (Ar*C*H), 117.86 (Ar*C*H), 117.07 (Ar*C*H), 116.60 (Ar*C*H), 115.39 (Ar*C*H, split peak), 115.18 (Ar*C*H, split peak), 61.41 (*C*H), 51.10 (*C*H), 49.27 (*C*H_2) LRMS (ES+) calculated for $C_{29}H_{23}FNO_4$ found 468.2 $(M+H)^+$ m/z

3-(2,5-dimethoxyphenyl)-2-[4-(fluorophenyl)methyl]-1-oxo-1,2,3,4-tetrahydroisoquinoline-4-carboxylic acid (A28)

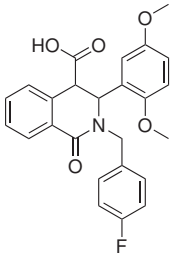

Purification by recrystallisation. White solid, 650 mg, 53% yield mp 227.1°C to 232.0°C IR ν_{max} (neat) cm^{-1} 3003.69 (O-H), 1747.47 (C=O) ^{1}H-NMR (400 MHz, DMSO-d_6) δ_H ppm: (Pure cis form) 3.44 (3*H*, s), 3.63 (3*H*, s), 3.82 (1*H*, d, J = 15.57 Hz), 4.56 (1*H*, d, J = 5.84 Hz), 5.20 to 5.23 (1*H*, d, J = 15.57 Hz), 5.40 (1*H*, d, J = 5.84 Hz), 6.24 (1*H*, d, J = 2.89 Hz), 6.76 to 6.78 (1*H*, dd, J = 2.89 Hz and 12.54 Hz), 6.86 to 6.88 (1*H*, d, J = 9.16 Hz), 7.11 to 7.15 (2*H*, m), 7.27 to 2.30 (2*H*, m), 7.35 to 7.37 (1*H*, m), 7.46 to 7.50 (1*H*, m), 7.54 to 7.58 (1*H*, td, J = 1.45 Hz and 16.87 Hz) ^{13}C-NMR (100 MHz, DMSO-d_6) δ_C ppm: 170.82 (C=O), 163.91 (C=O), 152.93 (Ar*C*), 151.86 (Ar*C*), 150.71 (Ar*C*), 134.75 (Ar*C*), 134.03 (Ar*C*), 132.65 (Ar*C*H), 130.09 (Ar*C*H), 130.01 (Ar*C*H), 129.12 (Ar*C*), 128.01 (Ar*C*H), 127.89 (Ar*C*H), 126.17 (Ar*C*), 115.75 (Ar*C*H, split peak), 115.53 (Ar*C*H, split peak), 114.50 (Ar*C*H), 113.72 (Ar*C*H), 112.53 (Ar*C*H), 56.36 (*C*H_3), 55.33 (*C*H_3), 53.26 (*C*H), 48.52 (*C*H), 47.80 (*C*H_2) LRMS (ES+) calculated for $C_{25}H_{23}FNO_5$ and $C_{25}H_{22}FNO_5Na$ found 465.9 $(M+H)^+$ m/z and 487.9 $(M+Na)^+$ m/z

3-(2,4-dimethylphenyl)-2-[4-(fluorophenyl)methyl]-1-oxo-1,2,3,4-tetrahydroisoquinoline-4-carboxylic acid (A29)

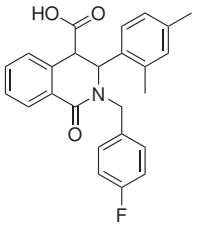

Purification by recrystallisation. White solid, 118 mg, 11% yield mp 216.9°C to 218.1°C IR ν_{max} (neat) cm^{-1} 3029.17 (O-H), 1741.94 (C=O) ^{1}H-NMR (400 MHz, DMSO-d_6) δ_H ppm: (Pure cis form) 2.07 (1*H*, s), 2.18 (1*H*, s), 3.69 (1*H*, d, J = 14.95 Hz), 4.57 (1*H*, d, J = 6.65 Hz), 5.12 (1*H*, d, J = 6.65 Hz), 5.29 (1*H*, d, J = 14.95 Hz), 6.76 to 6.79 (2*H*, m), 6.92 (1*H*, s), 7.10 to 7.14 (2*H*, m), 7.19 to 7.23 (2*H*, m), 7.40 (2*H*, d, J = 7.50 Hz), 7.49 (1*H*, t, J = 7.50 Hz and 14.67 Hz), 7.54 to 7.58 (1*H*, td, J = 1.63 Hz and 16.63 Hz), 8.09 (1*H*, dd, J = 1.63 Hz and 9.13 Hz), 12.82 (1*H*, brs) ^{13}C-NMR (100 MHz, DMSO-d_6) δ_C ppm: 171.03 (C=O), 163.87 (C=O), 160.64 (Ar*C*), 137.57 (Ar*C*), 136.56 (Ar*C*), 134.71 (Ar*C*), 133.89 (Ar*C*), 133.86 (Ar*C*), 132.59 (Ar*C*H), 131.55 (Ar*C*H), 130.02 (Ar*C*H), 129.94 (Ar*C*H), 129.07 (Ar*C*), 128.28 (Ar*C*H), 128.10 (Ar*C*H), 128.08 (*C*H) 127.40 (Ar*C*H), 127.17 (Ar*C*H), 115.83 (Ar*C*H, split peak), 115.62 (Ar*C*H, split peak), 55.43 (*C*H), 48.39 (*C*H), 47.25 (*C*H_2), 20.97 (*C*H_3), 19.28 (*C*H_3) LRMS (ES+) calculated for $C_{25}H_{23}FNO_3$ and $C_{25}H_{22}FNO_3Na$ found 403.9 $(M+H)^+$ m/z and 425.9 $(M+Na)^+$ m/z

3-(4-ethoxyphenyl)-2-[4-(fluorophenyl)methyl]-1-oxo-1,2,3,4-tetrahydroisoquinoline-4-carboxylic acid (A30)

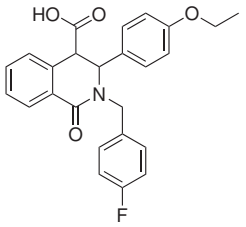

Purification by recrystallisation. White solid, 368 mg, 33% yield mp 238.6°C to 240.8°C IR ν_{max} (neat) cm^{-1} 2977.21 (O-H), 1698.45 (C=O) ^{1}H-NMR (400 MHz, DMSO-d_6) δ_H ppm: 1.25 (3*H*, t, $J = 7.39$ Hz and 14.78 Hz), 3.85 (1*H*, d, $J = 14.80$ Hz), 3.92 (2*H*,q, $J =$ 6.96 Hz and 20.87 Hz), 4.03 (1*H*, d, $J = 1.19$ Hz), 5.18 to 5.23 (2*H*, d and s overlap), 6.76 to 6.78 (2*H*, m), 6.91 to 6.93 (2*H*, m), 7.05 to 7.09 (2*H*, m), 7.19 to 7.21 (1*H*, m), 7.29 to 7.33 (2*H*, m), 7.40 to 7.44 (2*H*, m), 7.96 to 7.99 (1*H*, m), 12.88 (1*H*, brs) ^{13}C-NMR (100 MHz, DMSO-d_6) δ_C ppm: 172.51 (C=O), 163.77 (C=O), 158.36 (Ar*C*), 134.22 (Ar*C*), 134.03 (Ar*C*), 134.00 (Ar*C*), 132.43 (Ar*C*H), 131.16 (Ar*C*), 130.63 (Ar*C*H, split peak), 130.55 (Ar*C*H, split peak), 130.04 (Ar*C*H), 128.32 (Ar*C*H), 127.70 (Ar*C*H), 127.41 (Ar*C*), 115.43 (Ar*C*H, split peak), 115.22 (Ar*C*H, split peak), 114.92 (*C*H), 63.41 (*C*H_2), 61.02 (*C*H), 51.36 (*C*H), 48.65 (*C*H_2), 15.06 (*C*H_3) LRMS (ES+) calculated for $C_{25}H_{23}FNO_4$ and $C_{25}H_{22}FNO_4Na$ found 420.1 $(M+H)^+$ m/z and 443.3 $(M+Na)^+$ m/z

3-(4-ethylphenyl)-2-[(4-fluorophenyl)methyl]-1-oxo-1,2,3,4-tetrahydroisoquinoline-4-carboxylic acid (A31)

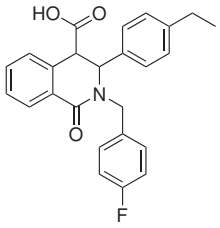

Purification by recrystallisation. White solid, 203 mg, 19% yield mp 271.5°C-275.7°C IR ν_{max} (neat) cm^{-1} 2956.44 (O-H), 1697.88 (C=O), 1640.69 (C=O) ^{1}H-NMR (400 MHz, DMSO-d_6) δ_H ppm: 1.09 (3*H*, t, $J = 14.77$ Hz), 3.84 (1*H*, d, $J = 16.52$ Hz), 4.07 (1*H*, s), 5.24 (2*H*, d, overlap, $J = 16.52$ Hz), 6.94 (2*H*, d, $J = 7.91$ Hz) 7.07 (4*H*, m), 7.20 (1*H*, m), 7.31 (2*H*, m), 7.42 (2*H*, m), 7.98 (1*H*, m) ^{13}C-NMR (100 MHz, DMSO-d_6) δ_C ppm: 172.72 (C=O) 163.91 (C=O), 163.00 (Ar*C*), 160.59 (Ar*C*), 143.43 (Ar*C*), 136.99 (Ar*C*), 134.51 (Ar*C*), 134.02 (Ar*C*), 133.99 (Ar*C*H), 132.36 (Ar*C*H), 130.58 (Ar*C*H),

130.50 (Ar*C*H), 130.08 (Ar*C*H), 129.32 (Ar*C*H), 128.47 (Ar*C*H), 128.18 (Ar*C*H), 127.33 (Ar*C*H), 126.45 (Ar*C*H), 115.40 (Ar*C*H), 115.18 (*C*H), 61.54 (*C*H), 51.64 (*C*H), 49.05 (*C*H_2), 28.07 (*C*H_2), 15.80 (*C*H_3) LRMS (ES+) calculated for $C_{25}H_{23}FNO_3$ and $C_{25}H_{22}FNO_3Na$ found 404.1 $(M+H)^+$ m/z and 425.1 $(M+Na)^+$ m/z

3-(2-hydroxy-5-nitrophenyl)-2-[(4-fluorophenyl)methyl]-1-oxo-1,2,3,4-tetrahydroisoquinoline-4-carboxylic acid (A32)

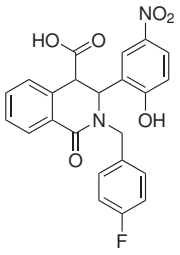

Purification by recrystallisation. White solid, 288 mg, 25% yield mp 269.8°C to 271.3°C IR ν_{max} (neat) cm^{-1} 2969.84 (O-H), 1716.86 (C=O) ^{1}H-NMR (400 MHz, DMSO-d_6) δ_H ppm: 4.06 (1*H*, s), 4.19 (1*H*, d, $J = 14.43$ Hz), 5.02 (1*H*, d, $J = 14.43$ Hz), 5.50 (1*H*, s), 6.93 to 6.95 (1*H*, m), 7.00 to 7.05 (2*H*, m), 7.22 to 7.26 (2*H*, m), 7.29 to 7.32 (2*H*, m), 7.42 to 7.44 (2*H*, m), 7.94 (1*H*, dd, $J = 2.31$ Hz and 11.55 Hz), 8.01 to 8.04 (1*H*, m) ^{13}C-NMR (100 MHz, DMSO-d_6) δ_C ppm: 172.33 (C=O), 164.08 (C=O), 163.06 (Ar*C*), 160.64 (Ar*C*), 139.28 (Ar*C*), 134.24 (Ar*C*), 133.75 (Ar*C*), 132.66 (Ar*C*H), 130.87 (Ar*C*H, split peak), 130.78 (Ar*C*H, split peak), 130.24 (Ar*C*H), 128.52 (Ar*C*H), 127.53 (Ar*C*H), 126.28 (Ar*C*), 125.61 (Ar*C*H), 122.65 (Ar*C*H), 116.33 (Ar*C*H), 115.39 (Ar*C*H, split peak), 115.18 (Ar*C*H, split peak), 56.63 (*C*H), 49.15 (*C*H_2), 48.04 (*C*H) LRMS (ES+) calculated for $C_{23}H_{18}FN_2O_6$ and $C_{23}H_{17}FN_2O_6Na$ found 436.9 $(M+H)^+$ m/z and 458.9 $(M+Na)^+$ m/z

3-(2-nitrophenyl)-2-[(4-fluorophenyl)methyl]-1-oxo-1,2,3,4-tetrahydroisoquinoline-4-carboxylic acid (A33)

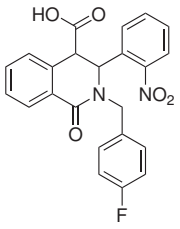

Purification by recrystallisation. White solid, 568 mg, 51% yield mp 240.9°C to 244.6°C IR ν_{max} (neat) cm^{-1} 2873.87 (O-H), 1698.75 (C=O) ^{1}H-NMR (400 MHz, DMSO-d_6)

δ_H ppm: 4.17 (1*H*, s), 4.25 (1*H*, d, $J = 13.89$ Hz), 4.87 (1*H*, d, $J = 14.81$ Hz), 5.92 (1*H*, s), 6.79 to 6.81 (1*H*, m), 6.97 to 7.02 (2*H*, m), 7.26 to 7.30 (3*H*, m), 7.44 to 7.46 (4*H*, m), 8.01 to 8.08 (2*H*, m), 12.97 (1*H*, brs) ^{13}C-NMR (100 MHz, DMSO-d_6) δ_C ppm: 171.94 (C=O), 163.97 (C=O), 163.00 (Ar*C*), 160.59 (Ar*C*), 148.02 (Ar*C*), 134.59 (Ar*C*), 134.18 (Ar*C*H), 133.49 (Ar*C*), 132.75 (Ar*C*H), 131.01 (Ar*C*H, split peak), 130.93 (Ar*C*H, split peak), 130.55 (Ar*C*H), 129.62 (Ar*C*H), 128.77 (Ar*C*), 128.68 (Ar*C*H), 128.34 (Ar*C*H), 127.52 (Ar*C*H), 126.10 (Ar*C*H), 115.30 (Ar*C*H, split peak), 115.09 (Ar*C*H, split peak), 57.52 (*C*H), 49.45 (*C*H_2), 49.21 (*C*H) LRMS (ES+) calculated for $C_{23}H_{18}FN_2O_5$ and $C_{23}H_{17}FN_2O_5Na$ found 420.9 $(M+H)^+$ m/z and 442.9 $(M+Na)^+$ m/z

3-(4-chlorophenyl)-2-[(4-fluorophenyl)methyl]-1-oxo-1,2,3,4-tetrahydroisoquinoline-4-carboxylic acid (A34)

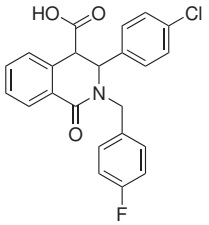

Purification by recrystallisation. White solid, 444 mg, 43% yield $\alpha_D{}^{22.0}$ +80.00° (c = 10 mg/mL in DMF) mp 254.0°C-255.6°C IR ν_{max} (neat) cm^{-1} 3074.53 (O-H), 1697.87 (C=O), 1643.70 (C=O) ^{1}H-NMR (400 MHz, DMSO-d_6) δ_H ppm: 4.00 (1*H*, d, $J =$ 14.27 Hz), 4.08 (1*H*, s), 5.14 (1*H*, d, $J = 14.81$ Hz), 5.31 (1*H*, s), 6.97 to 7.03 (2*H*, m), 7.04 to 7.11 (2*H*, m), 7.19 to 7.21 (2*H*, m), 7.21 to 7.24 (1*H*, m), 7.26 to 7.30 (2*H*, m), 7.31 to 7.33 (2(2*H*, m), 8.00 (1*H*, d, $J = 4.55$ Hz) ^{13}C-NMR (100 MHz, DMSO-d_6) δ_C ppm: 170.65 (C=O), 169.08 (C=O), 137.43 (Ar*C*), 136.27 (Ar*C*), 133.94 (Ar*C*), 133.42 (Ar*C*), 132.42 (Ar*C*H), 132.00 (Ar*C*H), 131.63 (Ar*C*), 130.66 (Ar*C*H), 130.08 (Ar*C*H), 129.57 (Ar*C*H), 129.48 (Ar*C*H), 128.66 (Ar*C*H), 128.03 (Ar*C*H), 127.13 (Ar*C*H), 115.73 (Ar*C*H), 115.46 (Ar*C*H), 115.25 (*C*H), 60.67 (*C*H), 48.59 (*C*H), 42.00 (*C*H_2) LRMS (ES+) calculated for $C_{23}H_{18}ClFNO_3$ found 410.1 m/z $(M+H)^+$ m/z

3-[4-chloro-3-(trifluoromethyl)phenyl]-2-[(4-fluorophenyl)methyl]-1-oxo-1,2,3,4-tetrahydroisoquinoline-4-carboxylic acid (A35)

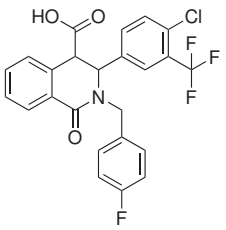

Purification by recrystallisation. White solid, 602 mg, 50% yield mp 267.5°C to 268.5°C IR ν_{max} (neat) cm^{-1} 2937.04 (O-H), 1698.23 (C=O), 1644.23 (C=O) ^{1}H-NMR (400 MHz, DMSO-d_6) δ_H ppm: 4.13 (1*H*, s), 4.38 (1*H*, d, J = 15.11 Hz), 4.90 (1*H*, d, J = 15.11), 5.49 (1*H*, s), 7.20 to 7.30 (4*H*, m), 7.30 to 7.36 (2*H*, m), 7.40 to 7.49 (3*H*, m), 7.97 to 7.99 (1*H*, m) ^{13}C-NMR (100 MHz, DMSO-d_6) δ_C ppm: 171.98 (C=O), 133.78 (Ar*C*), 133.64 (C=O), 132.73 (Ar*C*), 132.08 (Ar*C*), 131.12 (Ar*C*H), 131.04 (Ar*C*H), 130.16 (Ar*C*H), 130.07 (Ar*C*), 129.07 (Ar*C*), 128.63 (Ar*C*H), 127.49 (Ar*C*H), 126.44 (Ar*C*H), 126.40 (Ar*C*H), 115.31 (Ar*C*H), 115.10 (*C*H), 60.81 (*C*H), 50.60 (*C*H), 49.52 (*C*H_2) LRMS (ES+) calculated for $C_{24}H_{17}O_2NF_3Cl$ found 478.2 m.Z $(M+H)^+$ m/z

3-(4-bromophenyl)-2-[(4-fluorophenyl)methyl]-1-oxo-1,2,3,4-tetrahydroisoquinoline-4-carboxylic acid (A36)

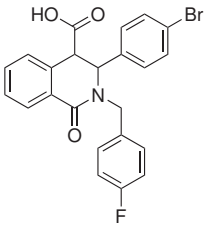

Purification by recrystallisation. White solid, 343 mg, 30% yield $\alpha_D{}^{22.0}$ +27.00° (c = 10 mg/mL in DMF) mp 260.3°C to 263.3°C IR ν_{max} (neat) cm^{-1} 2959.78 (O-H), 1698.29 (C=O), 1643.81 (C=O) ^{1}H-NMR (400 MHz, DMSO-d_6) δ_H ppm: 3.96 (1*H*, d, 15.61 Hz), 4.04 (1*H*, s), 5.12 (1*H*, d, J = 15.61 Hz), 5.26 (1*H*, s), 6.85 to 7.17 (5H, m), 7.30 to 7.52 (6H, m), 7.94 to 8.06 (1*H*, m) ^{13}C-NMR (100 MHz, DMSO-d_6) δ_C ppm: 172.30 (C=O), 163.78 (C=O), 160.66 (Ar*C*), 139.14 (Ar*C*), 133.86 (Ar*C*), 133.83 (Ar*C*), 132.55 (Ar*C*H), 131.91 (Ar*C*H), 131.56 (Ar*C*H), 130.79 (Ar*C*H), 130.70 (Ar*C*H), 130.42 (Ar*C*H), 130.04 (Ar*C*H), 129.20 (Ar*C*), 128.81 (Ar*C*H), 128.41 (Ar*C*H), 127.47 (Ar*C*H), 121.12 (Ar*C*), 115.43 (Ar*C*H), 115.22 (Ar*C*H), 61.10 (*C*H), 51.12 (*C*H), 49.16 (*C*H_2) HRMS (ES+) calculated for $C_{23}H_{18}BrFNO_3$ found 454.0449 m/z

3-(2-fluorophenyl)-2-[(4-fluorophenyl)methyl]-1-oxo-1,2,3,4-tetrahydroisoquinoline-4-carboxylic acid (A37)

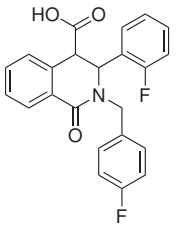

Purification by recrystallisation. White solid, 566 mg, 47% yield mp 247.3°C to 250.8°C IR ν_{max} (neat) cm^{-1} 2964.80 (O-H), 1697.86 (C=O) ^{1}H-NMR (400 MHz, DMSO-d_6) δ_H ppm: 4.05 (1*H*, s), 4.10 (1*H*, d, J = 13.50 Hz), 5.12 (1*H*, d, J = 13.50 Hz), 5.35 (1*H*, s), 6.83 to 6.5 (2*H*, m), 7.03 to 7.08 (2*H*, m), 7.20 to 7.22 (1*H*, m), 7.24 to 7.28 (2*H*, m), 7.32 to 7.36 (3*H*, m), 7.40 to 7.44 (2*H*, td, J = 1.66 Hz to 15.13 Hz), 7.96 to 7.99 (1*H*, m) ^{13}C-NMR (100 MHz, DMSO-d_6) δ_C ppm: 172.22 (C=O), 163.78 (C=O), 161.31 (Ar*C*), 142.98 (Ar*C*), 134.27 (Ar*C*), 133.92 (Ar*C*), 133.89 (Ar*C*), 132.52 (Ar*C*H), 131.05 (Ar*C*H, split peak), 130.97 (Ar*C*H, split peak), 130.83 (Ar*C*H, split peak), 130.74 (Ar*C*H, split peak), 130.05 (Ar*C*H), 129.15 (Ar*C*), 128.34 (Ar*C*H), 127.40 (Ar*C*H), 122.54 (Ar*C*H, split peak), 122.52 (Ar*C*H, split peak), 115.37 (Ar*C*H, split peak), 115.15 (Ar*C*H, split peak), 114.88 (Ar*C*H, split peak), 114.67 (Ar*C*H, split peak), 113.73 (Ar*C*H, split peak), 113.51 (Ar*C*H, split peak), 61.32 (*C*H), 51.17 (*C*H), 49.38 (*C*H_2) LRMS (ES+) calculated for $C_{24}H_{17}ClF_4NO_3$ found 478.2 $(M+H)^+$ m/z

3-phenyl-2-[(4-fluorophenyl)methyl]-1-oxo-1,2,3,4-tetrahydroisoquinoline-4-carboxylic acid (A38)

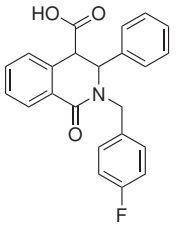

Purification by recrystallisation. White solid, 587 mg, 62% yield mp 259.8°C to 261.9°C IR ν_{max} (neat) cm^{-1} 2919.25 (O-H), 1696.35 (C=O) ^{1}H-NMR (400 MHz, DMSO-d_6) δ_H ppm: 3.93 (1*H*, d, J = 15.13 Hz), 4.04 (1*H*,s), 5.19 (1*H*, d, J = 14.47 Hz), 5.20 (1*H*, s), 7.02 to 7.08 (3*H*, m), 7.17 to 7.24 (4*H*, m), 7.31 7.35 (2*H*, m), 7.39 to 7.42 (2*H*, m), 7.46 to 7.51 (1*H*, m), 7.97 to 8.00 (1*H*, m) ^{13}C-NMR (100 MHz, DMSO-d_6) δ_C ppm: 170.44 (C=O), 161.82 (C=O), 137.79 (Ar*C*), 132.54 (Ar*C*), 131.90 (Ar*C*), 131.87 (Ar*C*), 130.21 (Ar*C*H), 128.50 (Ar*C*H, split peak), 128.42 (Ar*C*H, split peak), 127.91 (Ar*C*H), 127.20 (Ar*C*), 126.92 (Ar*C*H), 126.00 (Ar*C*H), 125.76 (Ar*C*H), 125.21 (Ar*C*H), 124.36 (Ar*C*H), 113.26 (Ar*C*H, split peak), 113.05 (Ar*C*H, split peak), 59.74 (*C*H), 49.66 (*C*H), 47.07 (*C*H_2) LRMS (ES+) calculated for $C_{23}H_{19}FNO_3$ found 376.1 $(M+H)^+$ m/z

3-[(4-fluorophenyl)methyl]- 1-oxo-3-(pyridine-3-yl)-1,2,3,4-tetrahydroisoquinoline-4-arboxylic acid (A39)

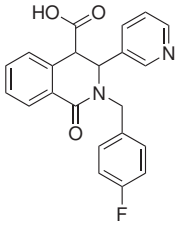

Purification by recrystallisation. White solid, 464 mg, 49% yield mp 265.1°C to 266.2°C IR ν_{max} (neat) cm^{-1} 2919.25 (O-H), 1715.95 (C=O), 1651.37 (C=O) ^{1}H-NMR (400 MHz, DMSO-d_6) δ_H ppm: 4.17 (2*H*, ds overlap, $J = 14.26$ Hz), 5.04 (1*H*, d, $J = 14.81$ Hz), 5.41 (1*H*, s), 7.02 to 7.06 (2*H*, m), 7.18 to 7.22 (2*H*, m), 7.30 to 7.35 (3*H*, m), 7.42 to 7.45 (2*H*, m), 7.97 to 8.00 (1*H*, m), 8.27 (1*H*, d, $J = 2.19$ Hz), 8.36 (1*H*, dd, $J = 1.10$ Hz and 6.03 Hz), 13.01 (1*H*, brs) ^{13}C-NMR (100 MHz, DMSO-d_6) δ_C ppm: 172.15 (C=O), 163.68 (C=O), 149.10 (Ar*C*H), 148.23 (Ar*C*H), 135.16 (Ar*C*), 134.24 (Ar*C*H), 133.96 (Ar*C*), 133.83 (Ar*C*), 133.81 (Ar*C*), 132.65 (Ar*C*H), 130.95 (Ar*C*H, split peak), 130.87 (Ar*C*H, split peak), 130.12 (Ar*C*H), 129.25 (Ar*C*), 128.56 (Ar*C*H), 127.54 (Ar*C*H), 123.84 (Ar*C*H), 115.40 (Ar*C*H, split peak), 115.19 (Ar*C*H, split peak), 59.71 (*C*H), 50.80 (Ar*C*), 49.32 (*C*H_2) LRMS (ES+) calculated for $C_{22}H_{18}FN_2O_3$ found 376.9 $(M+H)^+$ m/z

3-[(4-fluorophenyl)methyl]- 1-oxo-3-(pyridine-4-yl)-1,2,3,4-tetrahydroisoquinoline-4-carboxylic acid (A40)

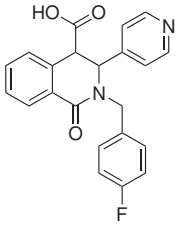

Purification by recrystallisation. White solid, 493 mg, 52% yield mp 253.2°C to 256.3°C IR ν_{max} (neat) cm^{-1} 2906.83 (O-H), 1716.59 (C=O), 1651.54 (C=O) ^{1}H-NMR (400 MHz, DMSO-d_6) δ_H ppm: 4.12 (1*H*, d, $J = 14.45$ Hz), 4.18 (1*H*, s), 5.09 (1*H*, d, $J = 14.45$ Hz), 5.35 (1*H*, s), 7.1 to 7.03 (2*H*, m), 7.04 to 7.07 (2*H*, m), 7.18 to 7.20 (1*H*, m), 7.32 to 7.36 (2*H*, m), 7.40 to 7.43 (2*H*, m), 7.95 to 7.98 (1*H*, m), 8.37 to 8.39 (2*H*, m), 13.01 (1*H*, brs) ^{13}C-NMR (100 MHz, DMSO-d_6) δ_C ppm: 172.04 (C=O), 163.76 (C=O), 150.17 (Ar*C*), 148.77 (Ar*C*), 133.80 (Ar*C*), 133.76 (Ar*C*), 132.62 (Ar*C*H), 130.97 (Ar*C*H), 130.89 (Ar*C*H), 130.01 (Ar*C*H), 129.12 (Ar*C*), 128.54 (Ar*C*H), 127.52 (Ar*C*H), 121.84 (Ar*C*H), 115.42 (Ar*C*H, split peak), 115.21 (Ar*C*H, split peak), 60.81

(*C*H), 50.40 (*C*H), 49.43 (*C*H_2) LRMS (ES+) calculated for $C_{22}H_{18}FN_2O_3$ found 376.9 $(M+H)^+$ m/z

3-[(4-fluorophenyl)methyl]- 1-oxo-3-(furan-3-yl)-1,2,3,4-tetrahydroisoquinoline-4-carboxylic acid (A41)

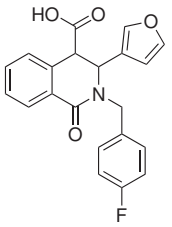

Purification by recrystallisation. White solid, 332 mg, 36% yield mp 263.3°C to 265.8°C IR ν_{max} (neat) cm^{-1} 2964.80 (O-H), 1698.65 (C=O) ^{1}H-NMR (400 MHz, DMSO-d_6) δ_H ppm: 4.09 (2*H*, sd overlap, $J = 14.95$ Hz), 5.12 (1*H*, d, $J = 14.95$ Hz), 5.16 (1*H*, s), 5,98 (1*H*, m), 7.07 to 7.12 (2*H*, m), 7.32 (1*H*, d, $J = 7.16$ Hz), 7,34 to 7.37 (2*H*, m), 7.40 to 7.41 (1*H*, m), 7.43 (1*H*, d, $J = 1.29$ Hz), 7.45 (1*H*, d, $J = 1.39$ Hz), 7.46 (1*H*, t, $J = 3.47$ Hz), 7.48 to 7.50 (1*H*, td, $J = 1.52$ Hz and 16.38 Hz), 7.93 (1*H*, dd, $J = 1.27$ Hz and 8.90 Hz), 12.90 (1*H*, brs) ^{13}C-NMR (100 MHz, DMSO-d_6) δ_C ppm: 172.26 (C=O), 163.27 (C=O), 144.26 (Ar*C*H), 140.67 (Ar*C*H), 134.99 (Ar*C*), 134.25 (Ar*C*), 134.22 (Ar*C*), 132.44 (Ar*C*H), 130.71 (Ar*C*H), 130.63 (Ar*C*H), 130.05 (Ar*C*H), 129.22 (Ar*C*), 128.30 (Ar*C*H), 127.49 (Ar*C*H), 125.05 (Ar*C*), 115.44 (Ar*C*H, split peak), 115.23 (Ar*C*H, split peak), 109.47 (*C*H), 54.64 (*C*H), 49.73 (*C*H), 48.86 (*C*H_2) LRMS (ES+) calculated for $C_{21}H_{17}FNO_4$ found 366.2 $(M+H)^+$ m/z

3-(4-iodophenyl)-2-[(4-fluorophenyl)methyl]-1-oxo-1,2,3,4-tetrahydroisoquinoline-4-carboxylic acid (A42)

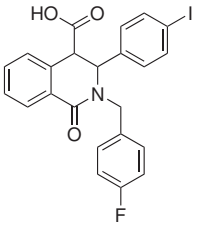

Purification by recrystallisation. White solid, 51 mg, 4% yield $\alpha_D{}^{22.0}$ -5.67° (c = 10 mg/mL in DMF) mp 228.5°C to 231.6°C IR ν_{max} (neat) cm^{-1} 2958.48 (O-H), 1700.09 (C=O), 1695.81 (C=O) ^{1}H-NMR (400 MHz, DMSO-d_6) δ_H ppm: 3.96 (1*H*, d, $J = 12.22$ Hz), 4.09 (1*H*, s), 5.18 (1*H*, d, 14.70 Hz), 5.25 (1*H*, s), 6.84 (1*H*, d, $J = 8.17$ Hz), 7.05 to 7.12 (2*H*, m), 7.19 to 7.21 (1*H*, m), 7.31 to 7.34 (4*H*, m), 7.36 to 7.40 (4*H*, td, $J =$ 1.26 Hz and 16.46 Hz), 7.59 to 7.61 (2*H*, m), 7.90 (2*H*, dd, $J = 0.89$ Hz and 7.65 Hz), 7.97 to 7.99 (1*H*, m), 12.48 (1*H*, brs) ^{13}C-NMR (100 MHz, DMSO-d_6) δ_C ppm: 172.25

(C=O), 163.76 (C=O), 163.06 (Ar*C*), 160.65 (Ar*C*), 139.48 (Ar*C*), 137.77 (Ar*C*H), 133.89 (Ar*C*), 132.55 (Ar*C*H), 130.76 (Ar*C*H, split peak), 130.68 (Ar*C*H, split peak), 130.03 (Ar*C*H), 129.20 (Ar*C*), 128.90 (Ar*C*H), 128.43 (Ar*C*H), 127.45 (Ar*C*H), 115.43 (Ar*C*H, split peak), 115.22 (Ar*C*H, split peak), 94.12 (Ar*C*), 61.12 (*C*H), 50.99 (*C*H), 49.08 (*C*H_2) HRMS (ES+) calculated for $C_{23}H_{18}FINO_3$ found 502.0312 m/z

3-(3-bromophenyl)-2-[(4-fluorophenyl)methyl]-1-oxo-1,2,3,4-tetrahydroiso quinoline-4-carboxylic acid (A43)

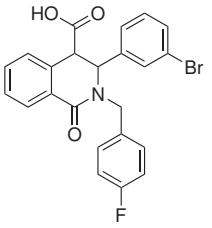

Purification by recrystallisation. White solid, 552 mg, 48% yield mp 291.6°C to 295.5°C IR ν_{max} (neat) cm^{-1} 2954.73 (O-H), 1698.29 (C=O) ^{1}H-NMR (400 MHz, DMSO-d_6) δ_H ppm: 4.10 (1*H*, d, J = 14.89 Hz), 4.13 (1*H*, s), 5.08 (1*H*, d, J = 14.89 Hz), 5.35 (1*H*, s), 6.99 (1*H*, d, J = 7.70 Hz), 7.05 (2*H*, t, J = 8.83 Hz and 17.67 Hz), 7.17 to 7.22 (3*H*, m), 7.32 to 7.37 (3*H*, m), 7.41 to 7.44 (2*H*, m), 7.97 to 7.99 (1*H*, m), 12.92 (1*H*, brs) ^{13}C-NMR (100 MHz, DMSO-d_6) δ_C ppm: 172.24 (C=O), 163.74 (C=O), 163.06 (Ar*C*), 160.64 (Ar*C*), 142.65 (Ar*C*), 133.90 (Ar*C*, split peak), 133.87 (Ar*C*, split peak), 132.58 (Ar*C*H), 131.11 (Ar*C*H), 130.87 (Ar*C*H), 130.79 (Ar*C*H), 130.08 (Ar*C*H), 129.55 (Ar*C*H), 129.16 (Ar*C*), 128.44 (Ar*C*H), 127.42 (Ar*C*H), 125.54 (Ar*C*H), 122.25 (Ar*C*), 115.37 (Ar*C*H, split peak), 115.16 (Ar*C*H, split peak), 61.18 (*C*H), 51.13 (*C*H), 49.39 (*C*H_2) LRMS (ES+) calculated for $C_{23}H_{18}FBrNO_3$ found 456.1 m/z $(M+H)^+$

3-(3,4-dibromophenyl)-2-[4-(fluorophenyl)methyl]-1-oxo-1,2,3,4-tetrahydroiso quinoline-4-carboxylic acid (A44)

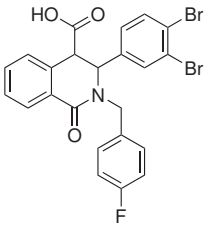

Purification by recrystallisation. White solid, 740 mg, 55% yield mp 276.6°C to 278.6°C IR ν_{max} (neat) cm^{-1} 2948.24 (O-H), 1698.53 (C=O) ^{1}H-NMR (400 MHz, DMSO-d_6) δ_H

(ppm) = 4.14 (2*H*, d, overlap, $J = 14.11$ Hz), 5.04 (1*H*, d, $J = 14.11$ Hz), 5.34 (1*H*, s), 6.87 (1*H*, dd, $J = 1.90$ Hz and 6.33 Hz), 7.04 to 7.08 (2*H*, m), 7.21 to 7.23 (1*H*, m), 7.33 to 7.36 (2*H*, m), 7.39 to 7.46 (3*H*, m), 7.58 (1*H*, d, $J = 8.23$ Hz), 7.97 to 7.98 (1*H*, m) ^{13}C-NMR (100 MHz, DMSO-d_6) δ_C (ppm) = 172.00 (C=O), 163.60 (C=O), 141.49 (Ar*C*), 141.40 (Ar*C*), 134.18 (Ar*C*H), 133.85 (Ar*C*), 133.80 (Ar*C*), 133.75 (Ar*C*), 132.69 (Ar*C*H), 132.16 (Ar*C*H), 130.96 (Ar*C*H), 130.88 (Ar*C*H), 130.11 (Ar*C*H), 129.06 (Ar*C*), 128.58 (Ar*C*H), 127.48 (Ar*C*H), 127.40 (Ar*C*H), 124.46 (Ar*C*), 123.29 (Ar*C*), 122.39 (Ar*C*H), 115.39 (Ar*C*H, split peak), 115.17 (Ar*C*H, split peak), 60.58 (*C*H), 50.62 (*C*H), 49.33 (*C*H_2) LRMS (ES+) calculated for $C_{23}H_{17}FBr_2NO_3$ found 534.0 m/z $(M+H)^+$

3-(2-chlorophenyl)-2-[(4-fluorophenyl)methyl]-1-oxo-1,2,3,4-tetrahydroisoquinoline-4-carboxylic acid (A45)

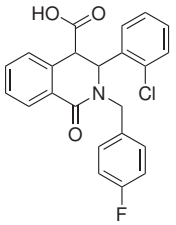

Purification by recrystallisation. White solid, 250 mg, 23% yield mp 239.8°C to 240.1°C IR ν_{max} (neat) cm^{-1} 3069.09 (O-H), 1709.76 (C=O) ^{1}H-NMR (400 MHz, DMSO-d_6) δ_H ppm: 3.95 (1*H*, d, $J = 14.60$ Hz), 4.03 (1*H*, s), 5.12 (1*H*, d, $J = 14.60$ Hz), 5.57 (1*H*, s), 6.66 (1*H*, d, $J = 7.86$ Hz), 7.03 to 7.10 (3*H*, m), 7.23 to 7.31 (4*H*, m), 7.43 to 7.47 (3*H*, m), 8.03 (1*H*, m), 13.00 (1*H*, brs) ^{13}C-NMR (100 MHz, DMSO-d_6) δ_C ppm: 172.09 (C=O), 164.04 (C=O), 160.76 (Ar*C*), 135.99 (Ar*C*), 133.58 (Ar*C*), 133.53 (Ar*C*, split peak), 133.50 (Ar*C*, split peak), 132.63 (Ar*C*H), 132.28 (Ar*C*), 130.81 (Ar*C*H), 130.73 (Ar*C*H), 130.62 (Ar*C*H), 130.33 (Ar*C*H), 129.97 (Ar*C*H), 129.04 (Ar*C*), 128.57 (Ar*C*H), 127.71 (Ar*C*H), 127.50 (Ar*C*H), 115.52 (Ar*C*H, split peak), 115.31 (Ar*C*H, split peak), 58.78 (*C*H), 49.82 (*C*H_2), 48.62 (*C*H) LRMS (ES+) calculated for $C_{23}H_{17}FClNO_3Na$ found 432.1 m/z $(M+Na)^+$

3-(3-phenoxymethyl)-2-[(4-chlorophenyl)methyl]-1-oxo-1,2,3,4-tetrahydroisoquinoline-4-carboxylic acid (A46)

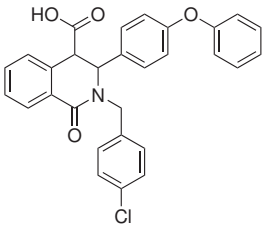

Purification by recrystallisation. White solid, 634 mg, 52% yield mp 247.1°C to 249.8°C IR ν_{max} (neat) cm^{-1} 3339.19 (O-H), 1698.20 (C=O) ^{1}H-NMR (400 MHz, DMSO-d_6) δ_H ppm: 3.98 (1*H*, s), 4.15 (1*H*, d, $J = 14.27$ Hz), 4.99 (1*H*, d, $J = 14.27$ Hz), 5.32 (1*H*, s), 6.56 (1*H*, s), 6.76 to 6.83 (3*H*, m), 7.11 to 7.14 (1*H*, m), 7.20 to 7.24 (1*H*, m), 7.26 to 7.33 (5H, m), 7.37 to 7.44 (2*H*, m), 7.44 to 7.36 (2*H*, m), 7.89 (1*H*, d, $J = 7.43$ Hz) ^{13}C-NMR (100 MHz, DMSO-d_6) δ_C ppm: 172.88 (C=O), 163.89 (C=O), 156.98 (Ar*C*), 156.49 (Ar*C*), 142.35 (Ar*C*), 136.78 (Ar*C*), 134.73 (Ar*C*), 132.40 (Ar*C*H), 132.08 (Ar*C*), 130.68 (Ar*C*H), 130.61 (Ar*C*H), 130.47 (Ar*C*H), 130.08 (Ar*C*H), 129.14 (Ar*C*), 128.47 (Ar*C*H), 128.11 (Ar*C*H), 127.33 (Ar*C*H), 124.00 (Ar*C*H), 121.66 (Ar*C*H), 118.89 (Ar*C*H), 117.77 (Ar*C*H), 116.60 (Ar*C*H), 62.00 (*C*H), 51.84 (*C*H), 49.59 (*C*H_2) LRMS (ES+) calculated for $C_{29}H_{23}ClNO_4$ found 484.3 $(M+H)^+$ m/z

3-(4-chlorophenyl)-2-[(4-chlorophenyl)methyl]-1-oxo-1,2,3,4-tetrahydroisoquinoline-4-carboxylic acid (A47)

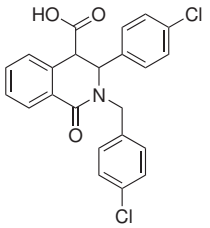

Purification by recrystallisation. White solid, 762 mg, 71% yield ${\alpha_D}^{22.0}$ -6.79° (c = 10.2 mg/mL in DMF) mp 173.0°C to 175.0°C IR ν_{max} (neat) cm^{-1} 2959.59 (O-H), 1701.17 (C=O), 1697.60 (C=O) ^{1}H-NMR (400 MHz, DMSO-d_6) δ_H ppm: 3.96 (1*H*, d, $J = 14.80$ Hz), 4.11 (1*H*, s), 5.18 (1*H*, d, $J = 14.73$ Hz), 5.30 (1*H*, s), 7.05 (1*H*, d, $J = 8.47$ Hz), 7.22 to 7.56 (9H, m), 7.97 to 7.99 (1*H*, m), 13.00 (1*H*, brs) ^{13}C-NMR (100 MHz, DMSO-d_6) δ_C ppm: 172.30 (C=O), 163.86 (C=O), 138.53 (Ar*C*), 136.71 (Ar*C*), 133.88 (Ar*C*), 132.77 (Ar*C*), 132.62 (Ar*C*H), 132.31 (Ar*C*H), 130.58 (Ar*C*H), 130.12 (Ar*C*H), 130.04 (Ar*C*H), 129.19 (Ar*C*), 129.05 (Ar*C*H), 128.99 (Ar*C*), 128.85 (Ar*C*H), 128.70 (Ar*C*H), 128.58 (Ar*C*H), 128.47 (Ar*C*H), 127.57 (*C*H), 61.12 (*C*H), 51.09 (*C*H), 49.25 (*C*H_2) HRMS calculated for $C_{23}H_{18}Cl_2NO_3$ found 426.0658 m/z

3-[4-chloro-3-(trifluoromethyl)phenyl]-2-[(4-chlorophenyl)methyl]-1-oxo-1,2,3,4-tetrahydroisoquinoline-4-carboxylic acid (A48)

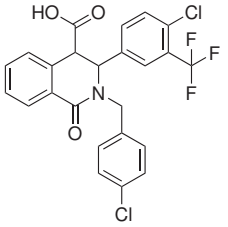

Purification by recrystallisation. White solid, 710 mg, 57% yield mp 269.0°C to 271.0°C IR ν_{max} (neat) cm^{-1} 2935.08 (O-H). 1701.17 (C=O), 1698.13 (C=O) ^{1}H-NMR (400 MHz, DMSO-d_6) δ_H ppm: 4.10 (1*H*, brs), 4.37 (1*H*, d, J = 13.59 Hz), 4.85 (1*H*, d, J = 13.59 Hz), 5.49 (1*H*, s), 6.99 to 7.02 (2*H*, m), 7.18 to 7.22 (2*H*, m), 7.30 to 7.32 (2*H*, m), 7.36 (1*H*, brs), 7.42 (2*H*, t, J = 12.63 Hz), 7.51 (1*H*, d, J = 8.42 Hz), 7.96 to 7.97 (1*H*, m) ^{13}C-NMR (100 MHz, DMSO-d_6) δ_C (ppm) = 172.15 (C=O), 163.67 (C=O), 140.12 (Ar*C*), 139.21 (Ar*C*), 136.66 (Ar*C*), 134.06 (Ar*C*), 132.69 (Ar*C*H), 132.26 (Ar*C*), 132.10 (Ar*C*H), 130.83 (Ar*C*H), 130.18 (Ar*C*H), 130.09 (Ar*C*), 128.98 (Ar*C*), 128.58 (Ar*C*H), 128.43 (Ar*C*H), 127.44 (*C*H) 127.03 (Ar*C*H), 126.42 (*C*H), 61.14 (*C*H), 50.93 (*C*H), 49.64 (*C*H_2) LRMS (ES+) calculated for $C_{24}H_{17}Cl_2F_3NO_3$ found 494.0 m/z $(M+H)^+$

3-(4-bromophenyl)-2-[(4-chlorophenyl)methyl]-1-oxo-1,2,3,4-tetrahydroisoquinoline-4-carboxylic acid (A49)

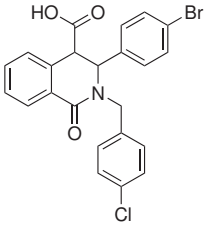

Purification by recrystallisation. White solid, 343 mg, 29% yield mp 270.0°C to 271.1°C IR ν_{max} (neat) cm^{-1} 2959.58 (O-H), 1701.50 (C=O), 1697.92 (C=O) ^{1}H-NMR (400 MHz, DMSO-d_6) δ_H ppm: 3.95 (1*H*d, J = 14.95 Hz), 4.09 (1*H*, s), 5.18 (1*H*, d, J = 14.98 Hz), 5.28 (1*H*, s), 6.99 (2*H*, d, J = 7.40 Hz), 7.20 (1*H*, d, J = 6.51 Hz), 7.31 (5H, brm), 7.42 to 7.43 (3*H*, m), 7.97 (1*H*, d, J = 7.12 Hz) ^{13}C-NMR (100 MHz, DMSO-d_6) δ_C ppm: 172.25 (C=O), 163.82 (C=O), 139.05 (Ar*C*), 136.74 (Ar*C*), 133.95 (Ar*C*), 132.61 (Ar*C*H), 132.18 (Ar*C*), 131.95 (Ar*C*H), 130.57 (Ar*C*H), 130.42 (Ar*C*H), 130.05 (Ar*C*H), 129.11 (Ar*C*), 128.82 (Ar*C*H), 128.54 (Ar*C*H), 128.46 (Ar*C*H), 128.02 (Ar*C*H), 127.46 (Ar*C*H), 121.17 (Ar*C*), 61.18 (*C*H), 50.99 (*C*H), 49.22 (*C*H_2) HRMS calculated for $C_{23}H_{18}ClBrNO_3$ found 470.0153 m/z $(M+H)^+$

3-phenyl-2-[(4-chlorophenyl)methyl]-1-oxo-1,2,3,4-tetrahydroisoquinoline-4-carboxylic acid (A50)

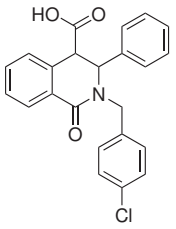

Purification by recrystallisation. White solid, 366 mg, 37% yield mp 288.0°C to 293.0°C IR ν_{max} (neat) cm^{-1} 2960.44 (O-H), 1698.51 (C=O) ^{1}H-NMR (400 MHz, DMSO-d_6) δ_H ppm: 3.90 (1*H*, d, J = 14.95 Hz), 4.11 (1*H*, s), 5.22 to 5.26 (1*H*, s, J = 15.01 Hz), 5.28 (1*H*, s), 7.04 to 7.06 (2*H*, m), 7.21 to 7.26 (4*H*, m), 7.27 (4*H*, s), 7.42 to 7.44 (2*H*, m), 7.98 to 8.00 (1*H*, m) ^{13}C-NMR (100 MHz, DMSO-d_6) δ_C ppm: 172.46 (C=O), 163.94 (C=O), 139.53 (Ar*C*), 136.85 (Ar*C*), 134.11 (Ar*C*), 132.50 (Ar*C*H), 132.14 (Ar*C*), 130.49 (Ar*C*H), 130.05 (Ar*C*H), 129.26 (Ar*C*), 129.11 (Ar*C*H), 128.54 (Ar*C*H), 128.38 (Ar*C*H), 128.01 (Ar*C*H), 127.41 (Ar*C*H), 126.51 (*C*H), 61.69 (*C*H), 51.23 (*C*H), 49.20 (*C*H_2) LRMS calculated for $C_{23}H_{19}ClNO_3$ found 392.1 $(M+H)^+$

3-(3-bromophenyl)-2-[(4-chlorophenyl)methyl]-1-oxo-1,2,3,4-tetrahydroisoquinoline-4-carboxylic acid (A51)

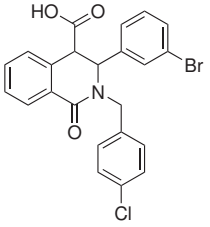

Purification by recrystallisation. White solid, 555 mg, 47% yield $\alpha_D{}^{22.0}$ -6.33° (c = 10 mg/mL in DMF) mp 299.3°C to 300.1°C IR ν_{max} (neat) cm^{-1} 2964.80, 1698.83 ^{1}H-NMR (400 MHz, DMSO-d_6) δ_H ppm: 4.06 (1*H*, d, J = 14.76 Hz), 4.16 (1*H*, s), 5.11 (1*H*, d, J = 14.76 Hz), 5.34 (1*H*, s), 7.00 (1*H*, d, J = 7.85 Hz), 7.16 to 7.24 (3*H*, m), 7.28 to 7.34 (4*H*, m), 7.38 (1*H*, dd, J = 0.93 Hz and 8.22 Hz), 7.42 to 7.45 (2*H*, m), 7.97 to 7.99 (1*H*, m), 12.97 (1*H*, s) ^{13}C-NMR (100 MHz, DMSO-d_6) δ_C (ppm): 172.17 (C=O), 163.77 (C=O), 142.45 (Ar*C*), 136.75 (Ar*C*), 133.89 (Ar*C*), 132.66 (Ar*C*H), 132.21 (Ar*C*), 131.16 (Ar*C*H), 130.89 (Ar*C*H), 130.66 (Ar*C*H), 130.11 (Ar*C*H), 129.59 (Ar*C*H), 129.08 (Ar*C*), 128.50 (Ar*C*H), 127.45 (Ar*C*H), 125.53 (Ar*C*H), 122.30 (Ar*C*),

61.19 (*C*H), 50.86 (*C*H), 49.42 (*C*H_2) LRMS calculated for $C_{23}H_{18}ClBrNO_3$ found 469.9 $(M+H)^+$ m/z

3-(4-nitrophenyl)-2-[4-(chlorophenyl)methyl]-1-oxo-1,2,3,4-tetrahydroisoquinoline-4-carboxylic acid (A52)

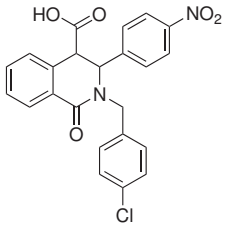

Purification by recrystallisation. White solid, 319 mg, 29% yield mp 239.2°C to 241.4°C IR ν_{max} (neat) cm^{-1} 2955.45 (O-H), 1698.84 (C=O) ^{1}H-NMR (400 MHz, DMSO-d_6) δ_H ppm: 4.07 (1*H*, d, J = 14.54 Hz), 4.19 (1*H*, s), 5.15 (1*H*, d, J = 15.65 Hz), 5.49 (1*H*, s), 7.19 to 7.21 (1*H*, m), 7.28 to 7.34 (6H, m), 7.41 to 7.44 (2*H*, m), 7.97 to 8.00 (1*H*, m), 8.08 (2*H*, d, J = 8.75 Hz) ^{13}C-NMR (100 MHz, DMSO-d_6) δ_C (ppm): 172.00 (C=O), 163.77 (C=O), 147.34 (Ar*C*), 147.31 (Ar*C*), 136.61 (Ar*C*), 133.65 (Ar*C*), 132.73 (Ar*C*H), 132.27 (Ar*C*), 130.72 (Ar*C*H), 130.06 (Ar*C*H), 128.98 (Ar*C*), 128.61 (Ar*C*H), 128.55 (Ar*C*H), 128.09 (Ar*C*H), 127.57 (Ar*C*H), 124.13 (*C*H), 61.32 (*C*H), 50.66 (*C*H), 49.44 (*C*H_2) LRMS calculated for $C_{23}H_{18}ClN_2O_4$ found 437.1 $(M+H)^+$ m/z

3-(4-chlorophenyl)-2-[4-(bromophenyl)methyl]-1-oxo-1,2,3,4-tetrahydroisoquinoline-4-carboxylic acid (A53)

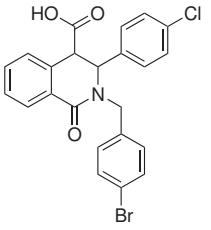

Purification by recrystallisation. White solid, 166 mg, 14% yield $\alpha_D{}^{22.0}$ +25.00° (c = 10.4 mg/mL in DMF) mp 250.5°C to 251.5°C IR ν_{max} (neat) cm^{-1} 2958.05 (O-H), 1701.60 (C=O), 1698.35 (C=O) ^{1}H-NMR (400 MHz, DMSO-d_6) δ_H (ppm) = 3.95 (1*H*, d, J = 14.64 Hz), 4.10 (1*H*, s), 5.16 (1*H*, d, J = 14.64 Hz), 5.31 (1*H*, s), 7.05 (2*H*, d, J = 8.36 Hz), 7.21 (1*H*, d, J = 7.05 Hz), 7.26 (2*H*, d, J = 8.22 Hz),7.31 (2*H*d, J = 8.81 Hz), 7.42 to 7.46 (4*H*, m), 7.98 (1*H*, d, J = 7.64 Hz) ^{13}C-NMR (100 MHz, DMSO-d_6) δ_C (ppm) = 172.25 (C=O), 163.82 (C=O), 138.64 (Ar*C*), 137.18 (Ar*C*), 133.98 (Ar*C*),

132.63 (Ar*C*), 132.60 (Ar*C*H), 131.95 (Ar*C*H), 131.45 (Ar*C*H), 130.92 (Ar*C*H), 130.07 (Ar*C*H), 129.10 (Ar*C*), 129.03 (Ar*C*H), 128.49 (Ar*C*H), 127.45 (Ar*C*H), 120.27 (Ar*C*), 61.15 (*C*H), 51.03 (*C*H), 49.30 (*C*H_2) HRMS (ES+) calculated for $C_{23}H_{18}BrClNO_3$ found 470.0153 $(M+H)^+$ m/z

3-(4-bromophenyl)-2-[(4-bromophenyl)methyl]-1-oxo-1,2,3,4-tetrahydroisoquinoline-4-carboxylic acid (A54)

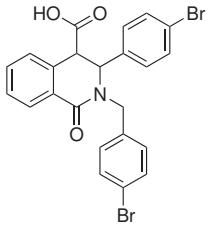

Purification by recrystallisation. White solid, 271 mg, 21% yield ${\alpha_D}^{22.0}$ -63.33° (c = 10 mg/mL in DMF) mp 225.3°C to 232.5°C IR ν_{max} (neat) cm^{-1} 2958.44 (O-H), 1697.95 (C=O) ^{1}H-NMR (400 MHz, DMSO-d_6) δ_H ppm: 3.91 to 3.95 (1*H*, d, $J = 14.48$ Hz), 4.06 (1*H*, s), 5.14 (1*H*, d, $J = 15.17$ Hz), 5.28 (1*H*, s), 6.98 (2*H*, d, $J = 8.28$ Hz), 7.18 to 7.26 (3*H*, m), 7.41 to 7.44 (6H, m), 7.96 (1*H*, d, $J = 6.90$ Hz) ^{13}C-NMR (100 MHz, DMSO-d_6) δ_C ppm: 172.27 (C=O), 163.82 (C=O), 139.65 (Ar*C*), 139.07 (Ar*C*), 137.17 (Ar*C*), 132.60 (Ar*C*H), 131.95 (Ar*C*H), 131.45 (Ar*C*H), 130.91 (Ar*C*H), 129.82 (Ar*C*H), 128.82 (Ar*C*H), 128.43 (Ar*C*H), 127.45 (Ar*C*H), 121.16 (Ar*C*), 120.72 (Ar*C*), 120.07 (Ar*C*), 61.21 (*C*H), 51.02 (*C*H), 49.29 (*C*H_2) HRMS (ES+) calculated for $C_{23}H_{18}Br_2NO_3$ found 513.9648 $(M+H)^+$ m/z

3-phenyl-2-[4-(bromophenyl)methyl]-1-oxo-1,2,3,4-tetrahydroisoquinoline-4-carboxylic acid (A55)

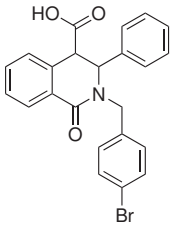

Purification by recrystallisation. White solid, 155 mg, 14% yield mp 255.3°C to 257.4°C IR ν_{max} (neat) cm^{-1} 2956.52 (O-H), 1701.73 (C=O), 1698.37 (C=O) ^{1}H-NMR (400 MHz, DMSO-d_6) δ_H (ppm) = 3.85 (1*H*, d, $J = 14.37$ Hz), 4.09 (1*H*, s), 5.20 (1*H*, d, $J =$ 17.23 Hz), 5.26 (1*H*, s), 7.02 (2*H*, d, $J = 7.02$ Hz), 7.19 (3*H*, t, $J = 7.55$ Hz and 14.01 Hz),

7.23 (3*H*, d, $J = 7.55$ Hz), 7.40 to 7.44 (4*H*, m), 7.97 (1*H*, d, $J = 6.47$ Hz), 12.94 (1*H*, brs) ^{13}C-NMR (100 MHz, DMSO-d_6) δ_C (ppm) = 172.45 (C=O), 163.93 (C=O), 139.52 (Ar*C*), 137.29 (Ar*C*), 134.09 (Ar*C*), 132.50 (Ar*C*H), 131.45 (Ar*C*H), 130.84 (Ar*C*H), 130.05 (Ar*C*H), 129.25 (Ar*C*), 129.11 (Ar*C*H), 128.37 (Ar*C*H), 128.01 (Ar*C*H), 127.40 (Ar*C*H), 126.51 (Ar*C*H), 120.67 (Ar*C*), 61.69 (*C*H), 51.19 (*C*H), 49.25 (*C*H_2) LRMS (ES+) calculated for $C_{23}H_{19}BrNO_3$ found 438.1 $(M+H)^+$ m/z

3-(4-iodophenyl)-2-[4-(bromophenyl)methyl]-1-oxo-1,2,3,4-tetrahydroisoquinoline-4-carboxylic acid (A56)

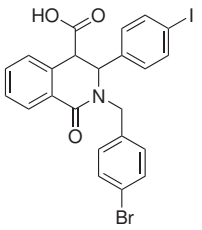

Purification by recrystallisation. White solid, 266 mg, 19% yield mp 204.3°C to 205.5°C IR ν_{max} (neat) cm^{-1} 2358.91 (O-H), 1698.61 (C=O) ^{1}H-NMR (400 MHz, DMSO-d_6) δ_H (ppm) = 3.90 (1*H*, d, $J = 14.58$ Hz), 4.10 (1*H*, s), 5.18 (1*H*, d, $J = 14.90$ Hz), 5.25 (1*H*, s), 6.84 to 6.86 (2*H*, m), 7.19 to 7.22 (1*H*, m), 7.24 to 7.26 (2*H*, m), 7.41 to 7.48 (5H, m), 7.58 to 7.61 (2*H*, m), 7.96 to 7.98 (1*H*, m), 12.93 (1*H*, s) ^{13}C-NMR (100 MHz, DMSO-d_6) δ_C (ppm) = 172.25 (C=O), 163.82 (C=O), 139.39 (Ar*C*), 137.80 (Ar*C*H), 137.18 (Ar*C*), 133.84 (Ar*C*), 132.61 (Ar*C*H), 131.46 (Ar*C*H), 130.90 (Ar*C*H), 130.06 (Ar*C*), 129.10 (Ar*C*H), 128.90 (Ar*C*H), 128.47 (Ar*C*H), 127.45 (Ar*C*H), 120.74 (Ar*C*), 94.19 (Ar*C*), 61.23 (*C*H), 50.88 (*C*H), 49.22 (*C*H_2) LRMS (ES+) calculated for $C_{23}H_{18}BrINO_3$ found 563.9 $(M+H)^+$ m/z

3-(3-bromophenyl)-2-[4-(bromophenyl)methyl]-1-oxo-1,2,3,4-tetrahydroisoquinoline-4-carboxylic acid (A57)

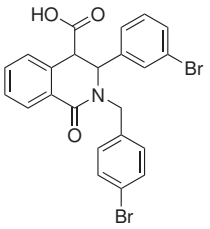

Purification by recrystallisation. White solid, 493 mg, 38% yield mp 294.5°C to 295.1°C IR ν_{max} (neat) cm^{-1} 2952.56 (O-H), 1699.50 (C=O) ^{1}H-NMR (400 MHz, DMSO-d_6)

δ_H (ppm) = 4.05 (1*H*, d, J = 14.87 Hz), 4.16 (1*H*, s), 5.11 (1*H*, d, J = 14.87 Hz), 5.34 (1*H*, s), 7.01 (1*H*, d, J = 7.65 Hz), 7.17 to 7.21 (2*H*, m), 7.22 to 7.28 (3*H*, m), 7.40 to 7.49 (5H, m), 7.99 (1*H*, dd, J = 2.04 Hz and 9.18 Hz), 12.99 (1*H*, brs) ^{13}C-NMR (100 MHz, DMSO-d_6) δ_C (ppm) = 172.17 (C=O), 163.78 (C=O), 142.45 (Ar*C*), 137.17 (Ar*C*), 133.91 (Ar*C*), 132.66 (Ar*C*H), 131.66 (Ar*C*), 131.42 (Ar*C*H), 131.17 (Ar*C*H), 131.00 (Ar*C*H), 130.90 (Ar*C*H), 130.11 (Ar*C*H), 129.59 (Ar*C*H), 129.06 (Ar*C*), 128.52 (Ar*C*H), 127.44 (Ar*C*H), 125.53 (Ar*C*H), 122.30 (Ar*C*), 120.77 (Ar*C*), 61.21 (*C*H), 50.87 (*C*H), 49.47 (*C*H_2) LRMS (ES+) calculated for $C_{23}H_{18}Br_2NO_3$ found 515.9 $(M+H)^+$ m/z **3-(4-iodophenyl)-2-[4-(iodophenyl)methyl]-1-oxo-1,2,3,4-tetrahydroisoquinoline-4-carboxylic acid (A58)**

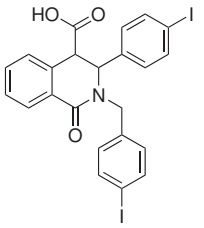

Purification by recrystallisation. White solid, 76 mg, 5% yield mp 225.0°C to 227.6°C ^{1}H-NMR (400 MHz, DMSO-d_6) δ_H (ppm) = 3.94 (1*H*, s), 4.32 to 4.33 (1*H*, s), 5.97 (1*H*, d, J = 3.63 Hz), 7.22 to 7.24 (1*H*, m), 7.33 to 7.35 (3*H*, m), 7.38 to 7.39 (1*H*, m), 7.51 to 7.53 (2*H*, m), 7.57 to 7.60 (1*H*, td, J = 1.15 Hz and 15.38 Hz), 7.70 to 7.76 (2*H* ,m), 7.81 to 7.83 (2*H*, m), 8.05 (1*H*, dd, J = 1.35 Hz and 6.54 Hz) ^{13}C-NMR (100 MHz, DMSO-d_6) δ_C (ppm) = 172.91 (C=O), 170.36 (C=O), 164.40 (Ar*C*), 138.06 (Ar*C*), 137.79 (Ar*C*H), 137.52 (Ar*C*H), 137.39 (Ar*C*), 134.47 (Ar*C*H), 130.84 (Ar*C*), 130.22 (Ar*C*H), 129.28 (Ar*C*H), 128.52 (Ar*C*H), 128.28 (Ar*C*H), 127.45 (Ar*C*H), 125.40 (Ar*C*), 94.90 (Ar*C*), 78.50 (*C*H) , 49.45 (*C*H), 40.50 (*C*H_2) LRMS (ES-) calculated for $C_{23}H_{18}I_2NO_3$ found 607.9 $(M-H)^-$ m/z

3-(4-bromophenyl)-2-[3,4-(dichlorophenyl)methyl]-1-oxo-1,2,3,4-tetrahydroisoquinoline-4-carboxylic acid (A59)

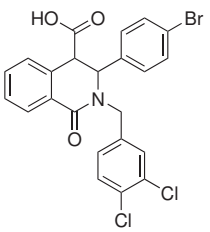

Purification by recrystallisation. White solid, 624 mg, 49% yield mp 278.8°C to 279.2°C IR ν_{max} (neat) cm^{-1} 3074.58 (O-H), 1749.59 (C=O) ^{1}H-NMR (400 MHz, DMSO-d_6) δ_H (ppm) = Cis:trans (5:1) 4.15 (1*H*, d, J = 15.25 Hz), 4.84 (1*H*, d, J = 6.17 Hz), 4.94 (1*H*, d, J = 15.58 Hz), 5.14 (1*H*, d, J = 6.17 Hz), 6.90 (2*H*, d, J = 8.44 Hz), 7.32 (1*H*, dd, J = 1.95 Hz to 10.62 Hz), 7.39 (2*H*, d, J = 8.44 Hz), 7.44 to 7.59 (6H, m), 8.08 (1*H*, d, J = 7.46 Hz), 13.08 (1*H*, brs) ^{13}C-NMR (100 MHz, DMSO-d_6) δ_C (ppm) = 170.72 (C=O), 163.64 (C=O), 139.18 (Ar*C*), 136.81 (Ar*C*), 134.12 (Ar*C*), 132.78 (Ar*C*H), 131.94 (Ar*C*H), 131.54 (Ar*C*H), 131.35 (Ar*C*), 130.89 (Ar*C*H), 130.68 (Ar*C*), 130.42 (Ar*C*H), 130.35 (Ar*C*H), 130.11 (Ar*C*), 128.87 (Ar*C*H), 128.57 (Ar*C*H), 128.48 (Ar*C*H), 128.01 (Ar*C*H), 122.04 (Ar*C*), 61.25 (*C*H), 48.51 (*C*H_2), 48.47 (*C*H) LRMS (ES+) calculated for $C_{23}H_{17}Cl_2BrNO_3$ found 505.9 $(M+H)^+$ m/z

3-phenyl-2-[3,4-(dichlorophenyl)methyl]-1-oxo-1,2,3, -tetrahydroisoquinoline-4-carboxylic acid (A60)

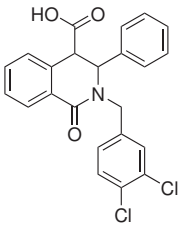

Purification by recrystallisation. White solid, 258 mg, 24% yield mp 228.3°C to 229.0°C IR ν_{max} (neat) cm^{-1} 2930.00 (O-H), 1698.72 (C=O) ^{1}H-NMR (400 MHz, DMSO-d_6) δ_H (ppm) = 3.98 (1*H*, d, J = 14.81 Hz), 4.12 (1*H*, d, J = 1.20 Hz), 5.17 (1*H*, d, J = 14.81 Hz), 5.35 (1*H*, brs), 7.05 to 7.07 (2*H*, m), 7.19 to 7.27 (4*H*, m), 7.30 to 7.32 (1*H*, m), 7.41 to 7.45 (2*H*, m), 7.50 to 7.52 (2*H*, m), 7.59 (1*H*, d, J = 2.12 Hz), 7.97 to 7.99 (1*H*, m) ^{13}C-NMR (100 MHz, DMSO-d_6) δ_C (ppm) = 172.44 (C=O), 163.98 (C=O), 139.56 (Ar*C*), 139.21 (Ar*C*), 132.62 (Ar*C*H), 131.12 (Ar*C*), 130.72 (Ar*C*H), 130.67 (Ar*C*H), 130.16 (Ar*C*H), 130.05 (Ar*C*), 129.08 (Ar*C*H), 129.06 (Ar*C*), 129.02 (Ar*C*H), 128.43 (Ar*C*H), 128.02 (Ar*C*H), 127.40 (Ar*C*H), 126.55 (*C*H), 61.85 (*C*H), 51.11 (*C*H), 49.14 (*C*H_2) LRMS (ES+) calculated for $C_{23}H_{18}Cl_2NO_3$ and $C_{23}H_{17}Cl_2NO_3Na$ found 426.1 $(M+H)^+$ and 448.0 $(M+Na)^+$

***cis*-3-(4-chlorophenyl)-2-[(4-fluorophenyl)methyl]-1-oxo-1,2,3,4-tetrahydrois oquinoline-4-carboxylic acid (A34a)**

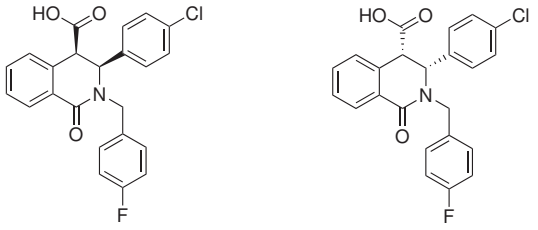

Purification by recrystallisation. Pale orange solid, 300 mg, 29% yield $\alpha_D{}^{22.0}$ +283.33° ^{1}H-NMR (400 MHz, DMSO-d_6) δ_H (ppm) = 3.96 (1*H*, d, J = 14.87 Hz), 4.74 (1*H*, d, J = 6.61 Hz), 5.06 (1*H*, d, J = 6.61 Hz), 5.16 (1*H*, d, J = 14.87 Hz), 6.95 to 6.97 (2*H*, m), 7.10 to 7.14 (2*H*, m), 7.25 to 7.28 (2*H*, m), 7.32 to 7.36 (2*H*, m), 7.46 to 7.50 (1*H*, m), 7.54 to 7.56 (2*H*, m), 8.08 to 8.10 (1*H*, m) ^{13}C-NMR (100 MHz, DMSO-d_6) δ_C (ppm) = 170.70 (C=O), 163.47 (C=O), 163.06 (Ar*C*), 160.65 (Ar*C*), 136.29 (Ar*C*), 133.94 (Ar*C*), 133.91 (Ar*C*), 133.35 (Ar*C*), 132.68 (Ar*C*H), 130.30 (Ar*C*H, split peak), 130.22 (Ar*C*H, split peak), 130.08 (Ar*C*H), 129.00 (Ar*C*H), 128.66 (Ar*C*H), 128.48 (Ar*C*H),

128.02 (Ar*C*H), 115.72 (Ar*C*H, split peak), 115.51 (Ar*C*H, split peak), 60.65 (*C*H), 48.55 (*C*H), 48.23 (*C*H_2). matches data for **A34**

***trans*-3-(4-chlorophenyl)-2-[(4-fluorophenyl)methyl]-1-oxo-1,2,3,4-tetrahydro isoquinoline-4-carboxylic acid (A34b)**

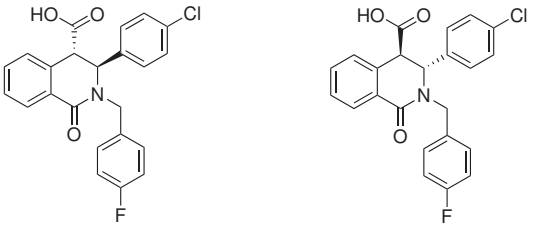

Purification by recrystallisation. Pale yellow solid, 72 mg, 7% yield $\alpha_D{}^{22.0}$ +176.73° ^{1}H-NMR (400 MHz, DMSO-d$_6$) δ_H (ppm) = 3.99 (1*H*, d, *J* = 14.76 Hz), 4.10 (1*H*, d, *J* = 1.36 Hz), 5.15 (1*H*, d, *J* = 13.96 Hz), 5.30 (1*H*, s), 7.05 (4*H*, m), 7.19 to 7.21 (1*H*, m), 7.28 to 7.33 (4*H*, m), 7.41 to 7.45 (2*H*, m), 7.97 to 7.99 (1*H*, m), 12.94 (1*H*, brs) ^{13}C-NMR (100 MHz, DMSO-d$_6$) δ_C (ppm) = 172.23 (C=O), 163.73 (C=O), 160.63 (Ar*C*), 138.63 (Ar*C*), 133.86 (Ar*C*), 132.59 (Ar*C*H), 130.81 (Ar*C*H, split peak), 130.73 (Ar*C*H, split peak), 130.05 (Ar*C*H), 129.87 (Ar*C*), 129.72 (Ar*C*), 129.20 (Ar*C*), 129.00 (Ar*C*H), 128.48 (Ar*C*H), 128.48 (ArC, overlap by HSQC), 127.47 (Ar*C*H), 115.42 (Ar*C*H, split peak), 115.21 (Ar*C*H, split peak), 60.95 (*C*H), 50.96 (*C*H), 49.13 (*C*H_2). matches data for **A34**

5(6)FAM-LTFEHAQWYLTS-CONH$_2$ (A62) MALDI-TOF 1855.48 m/z (M+H), 1877.56 m/z (M+Na) and 1893.45 (M+K) m/z HPLC retention time 15.324 min. matches literature values[182]

3-(4-chlorophenyl)-2-[(phenylalaninol)methyl]-1-oxo-1,2,3,4-tetrahydroisoquinoline-4-carboxylic acid (A64)

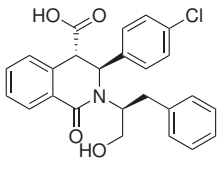

L-phenylalaninol (381 mg, 2.52 mmol), 4-chlorobenzaldehyde (354 mg, 2.52 mmol) and $MgSO_4$ (2 g) was stirred in dry THF (25 mL) at rt for 1 h, after which homophthalic anhydride (408 mg, 2.52 mmol) was added and the mixture was stirred at room temperature overnight. The mixture was concentrated *in vacuo* and purified firstly on silica (to

isolate the baseline spot) and then by reverse-phase preparative HPLC, affording 2.6 mg of a white solid (3% yield) ^{1}H-NMR (400 MHz, $CDCl_3$) δ_H (ppm) = 1.21 (2*H*, t, J = 6.99 Hz and 13.58 Hz), 1.26 (2*H*, s), 3.50 (1*H*, q, J = 3.47 to 3.52), 3.95 (1*H*, s), 4.96 (1*H*, s), 7.05 (2*H*, d, J = 8.45 Hz), 7.14 to 7.20 (3*H*, m), 7.31 to 7.35 (1*H*, td, J = 1.21 Hz and 16.90 Hz), 7.41 to 7.49 (4*H*, m), 7.62 to 7.64 (1*H*, m), 8.01 (1*H*, d, J = 6.64 Hz), 8.36 (1*H*, dd, J =1.02 Hz and 8.90 Hz) ^{13}C-NMR (100 MHz, $CDCl_3$) δ_C (ppm) = 161.59 (C=O), 148.34 (Ar*C*), 137.92 (Ar*C*), 136.24 (Ar*C*), 135.12 (Ar*C*H), 133.50 (Ar*C*), 130.54 (Ar*C*H), 130.40 (Ar*C*H), 130.05 (Ar*C*H), 129.74 (Ar*C*H), 129.25 (Ar*C*H), 129.05 (Ar*C*H), 128.70 (Ar*C*H), 128.22 (Ar*C*H), 128.11 (Ar*C*), 123.25 (Ar*C*H), 122.51 (Ar*C*H), 121.37 (Ar*C*), 109.82 (Ar*C*), 65.87 (*C*H_2), 39.81 (*C*H), 29.71 (*C*H_2), 15.20 (Ar*C*) LRMS (ES+) calculated for $C_{25}H_{23}ClNO_4$ found 436.1 $(M+H)^+$ m/z

6.4 Experimental for Chapter 3

6.5 Synthesis of the chlorofusin Peptide (B01)

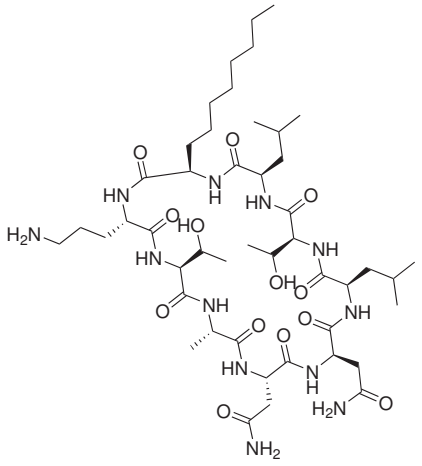

500 mg of MBHA Rink Amide resin (0.35 mmol, 0.7 mmol/g) was suspended in 15 mL of DMF. The resin was then allowed to swell for 30 min. DMF was removed under reduced pressure and Fmoc deprotection was carried out by addition of 3 x 5 mL of 5% piperazine in DMF, which was shaken for 5 minutes each. The resin was then washed with 4 x 20 mL of DMF. The resin was treated with a solution of Fmoc-Asp-ODMab (1.17 g, 1.75 mmol, 5 eq), to which HBTU (663.8 mg, 1.75 mmol, 5 eq) and HOBt (267.8 mg, 1.75 mmol, 5 eq) and DIPEA (608 μLs, 10 eq) in DMF were added. The mixture was then shaken for 30 min.

Fmoc deprotection and washes were repeated for each subsequent coupling. A Kaiser test was carried out at each stage to ensure that the coupling had gone to completion. A single, 30 min coupling with 5 eq of HBTU and HOBT and 10 eq of DIPEA was used at each stage in the order of Fmoc-Ala-OH, Fmoc-Thr(tBu)-OH, Fmoc-Orn(Boc)-OH, Fmoc-D-Ade-OH, Fmoc-D-Leu-OH, Fmoc-Thr(tBu)-OH, Fmoc-D-Leu-OH and Fmoc-D-Asn(Trt)-OH respectively.

Following the attachment of the final amino acid, the DMab group was removed by 3 x 10mLs of 2% hydrazine (581.4 μL in 30 mL) in DMF, shaken for 5 minutes each. The resin was washed with 4 x 20mLs of DMF, and then washed 4 times with 5% DIPEA in DMF (5.39 mL in 80 mL). Resin was then shaken with DIC (271 μL, 1.75 mmol, 5 eq) and HOBt (267.8 mg, 1.75 mmol, 5 eq) for 2 x 24 hours and then 1 x 48 hours.

The resin was washed 3 times with DMF, then 3 times with CH_2Cl_2, then 3 times with 1:1 CH_2Cl_2:MeOH to remove any residual DMF. The resin was then dried *in vacuo* over KOH overnight.

A small amount was cleaved from the resin for characterisation: 100 mg of peptide-resin complex was shaken with 4.706 mLs of 95:2.5:2.5 TFA:H_2O:TIPS for 3 hours. The resin was washed 3 times with TFA and the solution was concentrated in vacuo. The peptide was precipitated out using cold diethyl ether, which was then filtered off, producing 30.9 mg as a white powder. HPLC was carried out over 30 minutes ranging from 5% acetonitrile:H_2O 0.05% TFA to 95% acetonitrile:H_2O 0.05% TFA. Peptide had a retention time of 11.553 min and MALDI-TOF confirmed an M+H^+ at 1011.34, an M+Na^+ at 1033.31 and an M+K^+ at 1049.30 m/z

6.5.1 Synthesis of Aromatic Acid Analogues of Chlorofusin

6.5.1.1 Solid-Phase Method

Chlorofusin peptide on-resin (50 mg) was treated with 1% TFA three times to deprotect Orn9. The resin was washed with DMF three times and aromatic acid (1 eq), HOBt (117 mg, 0.175 mmol), HBTU (117 mg, 0.175 mmol) and DIPEA (60.8 μL) in the minimum volume of DMF was shaken overnight.

6.5.1.2 Solution-Phase Method

chlorofusin peptide (25 mg, 0.025 mmol), benzoic acid (0.025 mmol), EDCI (5 mg, 0.027 mmol), HOBt (4 mg, 0.029 mmol), DIPEA (5 μL, 0.029 mmol) was stirred in DMF overnight. Compounds were precipitated out using water, filtered and redissolved in HPLC-grade methanol and purified by semi-preparative HPLC. HPLC analysis was undertaken over 30 min ranging from 5% acetonitrile:H_2O 0.05% TFA to 95% acetonitrile:H_2O 0.05% TFA.

2-[(2R,5R,8S,11R,14R,17S,20S,23S,26S)-17-3-naphthoic acid)-1*H*-1,2,3-triazol-1-yl]propyl-bis(2-methylpropyl)-14-octyl-3,6,9,12,15,18,21,24,27-nonaoxo-1,4,7,10,13,16,19,22,25- nonaazacycloheptacosan-2-yl]acetamide (B02)

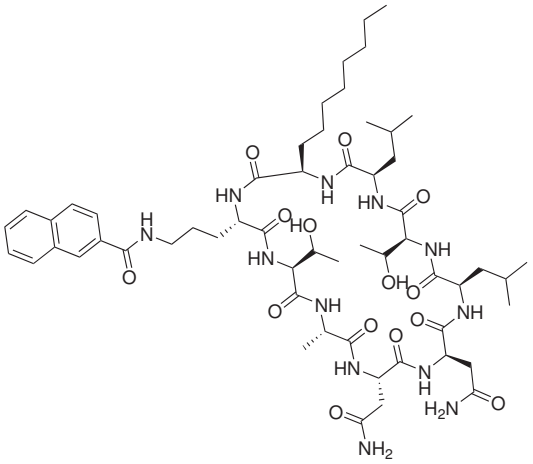

White gel, 6.4 mg, 22% yield HPLC retention time 13.87 min, MALDI mass spectrometry found 1187.18 $(M+Na)^+$ m/z

2-[(2R,5R,8S,11R,14R,17S,20S,23S,26S)-17-3-quinolic acid)-1*H*-1,2,3-triazol-1-yl]propyl-2(2-methylpropyl)-14-octyl-3,6,9,12,15,18,21,24,27-nonaoxo-1,4,7,10,13,16,19,22,25-nonaazacycloheptacosan-2-yl]acetamide (B03)

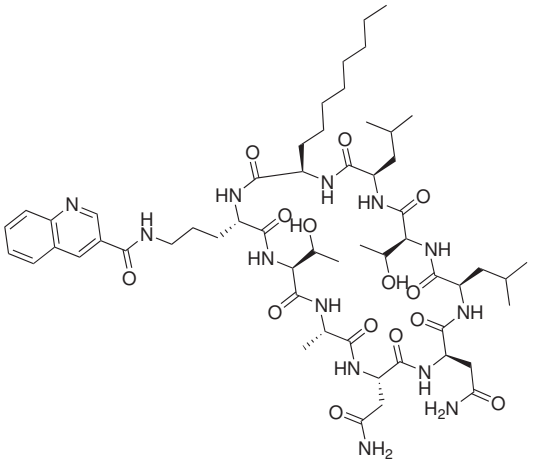

White gel, 1.5 mg, 5% yield HPLC retention time 11.29 min, MALDI mass spectrometry found 1192.25 $(M+Na)^+$ m/z

2-[(2R,5R,8S,11R,14R,17S,20S,23S,26S)-17-3-[1,2,3,4-tetrahydronaphthoic acid])-1*H*-1,2,3-triazol-1-yl]propyl-26-(carbamoylmethyl)-8,20-bis(1-hydroxyethyl)-23-

methyl-5,11-bis(2-methylpropyl)-14-octyl-3,6,9,12,15,18,21,24,27-nonaoxo-1,4,7, 10,13,16,19,22,25-nonaazacycloheptacosan-2-yl]acetamide (B04)

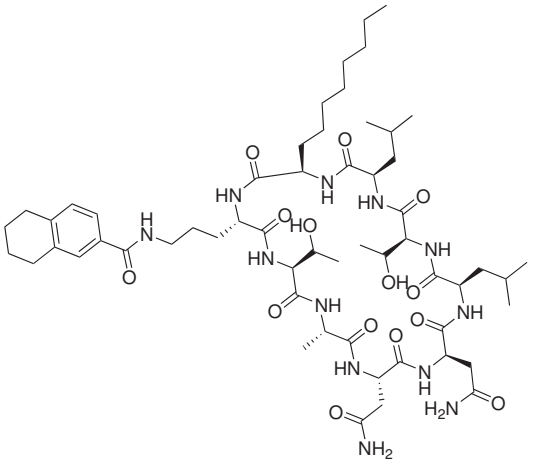

White gel, 8.7 mg, 30% yield HPLC retention time 12.54 min, MALDI mass spectrometry found 1190.56 $(M+Na)^+$ m/z

2-[(2R,5R,8S,11R,14R,17S,20S,23S,26S)-17-3-[2-hydroxy-5-bromonaphthoic acid])-1*H*-1,2,3-triazol-1-yl]propyl-26-(carbamoylmethyl)-8,20-bis(1-hydroxyethyl)-23-methyl-5,11-bis(2-methylpropyl)-14-octyl-3,6,9,12,15,18,21,24,27-nonaoxo-1,4,7, 10,13,16,19,22,25-nonaazacycloheptacosan-2-yl]acetamide (B05)

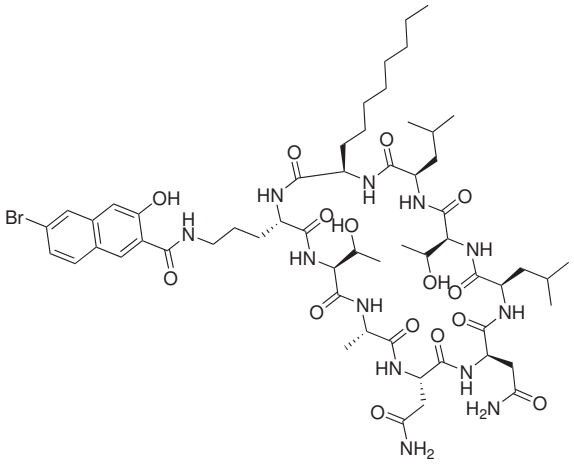

Orange gel, 1.6 mg, 5% yield HPLC retention time 14.76 min, MALDI mass spectrometry found 1282.87 $(M+Na)^+$ m/z

2-[(2R,5R,8S,11R,14R,17S,20S,23S,26S)-17-3-[6-chloroisochloromene carboxylic acid])-1*H*-1,2,3-triazol-1-yl]propyl-26-(carbamoylmethyl)-8,20-bis(1-hydroxyethyl)-

23-methyl-5,11-bis(2-methylpropyl)-14-octyl-3,6,9,12,15,18,21,24,27-nonaoxo-1,4,7,10,13,16,19,22,25-nonaazacycloheptacosan-2-yl]acetamide (B06)

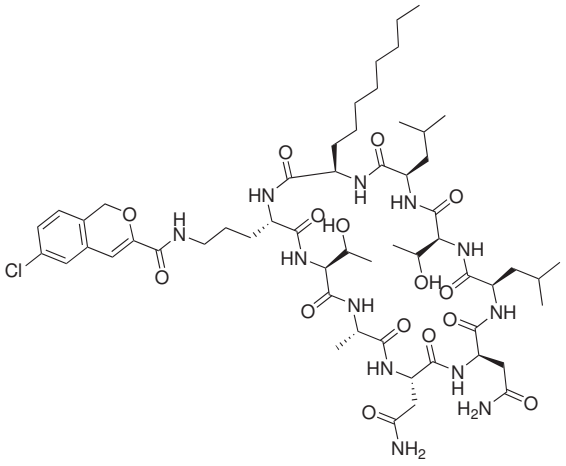

Orange gel, 4.4 mg, 14% yield HPLC retention time 14.76 min MALDI mass spectrometry found 1282.87 $(M+Na)^+$ m/z

6.5.2 Synthesis of Click-Based Analogues of chlorofusin

Boc-L-δ-Nva(OH)-OtBu (B07)

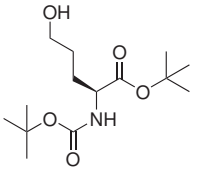

Boc-L-Glu-OtBu (613 mg, 2.12 mmol) and 1,1-carbonyldiimidazole (427 mg, 2.62 mmol) were stirred in THF (4.904 mL) at rt for 10 min. The solution was cooled to 0°C and a solution of $NaBH_4$ (123 mg, 3.24 mmol) in H_2O (2 mL) was added dropwise. The resultant mixture was warmed to rt and stirred for 1 h. The mixture was neutralised with 0.1 M HCl and extracted with ethyl acetate (3 x 10 mL). The extracts were washed with saturated sodium bicarbonate and brine. The organic phase was then dried over $MgSO_4$, filtered, and concentrated in vacuo. Purification on silica (100% Hexane to 1:1 Ethyl Acetate: Hexane) produced 383 mg (68% yield) as a colourless oil. ^{1}H-NMR (400 MHz, $CDCl_3$), δH ppm 1.42 (9H, s), 1.45 (9H, s), 1.60 to 1.71 (3*H*, brm), 1.83 to 1.86 (1*H*, brm), 3.66 (2*H*, t, J = 11.50 Hz), 4.19 (1*H*, brs) ^{13}C-NMR (100 MHz, $CDCl_3$) $CDCl_3$), δC ppm 172.05 (C=O), 155.67 (Ar*C*), 82.00 (*C*H), 79.81 (*C*H), 62.18

(CH_2), 53.72 (CH), 29.75 (CH_2), 28.41 (CH_3)$_3$, 28.35 (CH_2), 28.08 (CH_3)$_3$, 21.12 (CH) $[\alpha D]^{23.1}$ = + 20.1° (CH_2Cl_2) HRMS (ES+) calculated for $C_{14}H_{28}NO_5$ $(M+H)^+$ found 290.1962 m/z

Boc-L-δ-Nva(OMs)-OtBu (B08)

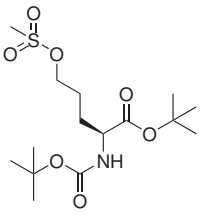

Boc-L-δ-Nva(OH)-OtBu (353 mg, 1.29 mmol) and triethylamine (785 μL, 1.937 mmol) were stirred in dry DMF (3 mL). The mixture was cooled to 0°C and mesyl chloride (313 μL, 1.937 mmol) was added dropwise. The resulting mixture was then stirred for 45 min at 0°C. The mixture was then diluted with water and extracted 5 times with diethyl ether (5 mL). The organic layer was then washed 10 times with water, dried over $MgSO_4$, filtered and concentrated in vacuo. The reaction produced 387 mg (85%) of yellow oil that did not require further purification. ^{1}H-NMR (400 MHz, $CDCl_3$), δH ppm 1.39 (9H, s), 1.42 (9H, s), 1.58 to 1.87 (4*H*, m), 2.97 (3*H*, s), 4.14 (1*H*, brs), 4.20 (2*H*, t, J = 10.78 Hz), 4.99 to 5.10 (1*H*, brs) ^{13}C-NMR (100 MHz, $CDCl_3$), δC ppm 171.39 (C=O), 163.21 (Ar*C*), 155.43 (Ar*C*), 84.37 (*C*H), 82.31 (*C*H), 82.12 (*C*H), 79.85 (CH_2), 69.41 (CH_2), 53.29 (*C*H), 46.28 (CH_2), 39.33 (CH_2), 37.37 (CH_2), 28.33 (CH_3)$_3$, 28.00 (CH_3)$_3$, 25.19 (C3) $[\alpha D]^{26.8}$ = + 8.9 ° (CH_2Cl_2) HRMS (ES+) calculated for $C_{15}H_{30}NO_7S$ $(M+H)^+$ found 368.1737 m/z

Boc-L-δ-Nva(N_3)-OtBu (B09)

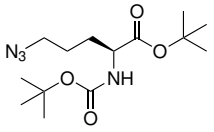

Boc-L-δ-Nva(OMs)-OtBu (285 mg, 0.776 mmol), NaN_3 (123 mg, 1.892 mmol) and dry DMF (2 mL) was stirred at 67°C for 5 h. The resultant mixture was extracted into diethyl ether (5 x 5 mL). The organic layer was washed 10 times with water, dried over $MgSO_4$, filtered and concentrated in vacuo. The reaction produced 169 mg (69% yield) of yellow oil that did not require further purification. ^{1}H-NMR (400 MHz, $CDCl_3$), δH ppm 1.41 (9H, s), 1.44 (9H, s), 1.82 (3*H*, m), 1.84 (1*H*, m), 3.27 to 3.28 (2*H*, m), 4.16 (1*H*, d, J = 5.88 Hz), 5.08 (1*H*, d, J = 7.84 Hz) ^{13}C-NMR (100 MHz, $CDCl_3$), δC ppm

171.62 (C=O), 155.45 (Ar*C*), 82.21 (*C*H), 79.83 (*C*H), 53.48 (*C*H), 51.01 (*C*H_2), 30.30 (*C*H_2), 28.38 (*C*H_3)$_3$, 28.06 (*C*H_3)$_3$, 24.83 (*C*H_2) $[\alpha D]^{23.4}$ = + 4.0° (CH_2Cl_2) HRMS (ES+) calculated for Ar*C*4*H*27N_4O_4 $(M+H)^+$ found 315.2027 m/z

$^+$H$_3$N-L-δ-Nva(N$_3$)-OtBu (B10)

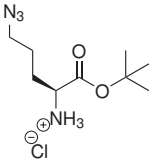

Boc-L-δ-Nva(N_3)-OtBu (117 mg, 0.391 mmol) was stirred in 2 M HCl in ethyl acetate (2 mL) at rt overnight. The mixture was concentrated *in vacuo*. The yield of yellow oil was quantitative (84 mg) and carried forward without further purification. HRMS (ES+) calculated for $C_9H_{19}N_4O_2$ $(M+H)^+$ found 215.1503 m/z

Fmoc- L-δ-Nva(N$_3$)-OtBu (B11)

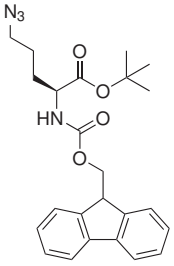

$^+$$H_3$N-L-$\delta$-Nva($N_3$)-OtBu (100 mg, 0.465 mmol), NaHCO3 (158 mg, 1.881 mmol), water (1.602 mL) and tetrahydrofuran (6.409 mL) was cooled to 0°C and a solution of Fmoc-Cl (162 mg, 0.626 mmol) in tetrahydrofuran (1.602 mL) was added dropwise. The resultant solution was stirred at 0°C for 20 min. The mixture was quenched with methanol (15 mL) for 5 min and concentrated in vacuo. The mixture was acidified with aqueous 1M HCl and extracted with ethyl acetate (3 x 20 mL). The organic layers were dried over $MgSO_4$, filtered and concentrated in vacuo. Purification on silica (100% hexane to 1:9 ethyl acetate: hexane) produced 100 mg (49% yield) of yellow semi-solid. ^{1}H-NMR (400 MHz, MeOD) δH ppm 1.45 (9H, s), 1.60 to 1.73 (3*H*, brm), 1.81 to 1.90 (1*H*, brm) 4.20 (1*H*, t, J = 13.46 Hz), 4.32 to 4.40 (2*H*, m) 7.27 to 7.29 (2*H*, td, J= 1.08 Hz and 14.87 Hz), 7.37 (2*H*, t, J = 14.56 Hz), 7.66 (2*H*, t, J = 13.39 Hz), 7.77 (2*H*, d, J = 7.57 Hz) ^{13}C-NMR (100 MHz, MeOD), δC ppm 173.07 (C=O), 158.59 (Ar*C*), 145.31 (Ar*C*), 145.12 (Ar*C*), 142.58 (Ar*C*), 128.76 (Ar*C*), 128.13 (Ar*C*), 126.21 (Ar*C*), 125.91 (Ar*C*),

120.91 (Ar*C*), 82.81 (*C*H), 67.83 (*C*H_2), 55.66 (*C*H_2), 51.88 (*C*H), 29.87 (*C*H_2), 28.24 (*C*H_3)$_3$, 26.37 (*C*H_2) HRMS (ES+) calculated for $C_{24}H_{29}N_4O_4$ found 437.2183 m/z

Fmoc- L-δ-Nva(N_3)-OH (B12)

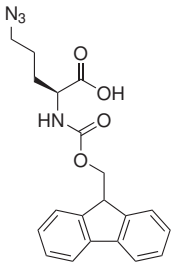

Fmoc- L-δ-Nva(N_3)-OtBu (50 mg, 0.1225 mmol) and methyltrichlorosilane (17 μL, 0.147 mmol) was added successively to NaI (22 mg, 0.147 mmol) in dry acetonitrile (1 mL). The mixture was stirred at rt for 6 h under nitrogen. The mixture was quenched using saturated sodium thiosulfate and extracted into diethyl ether (5 x 5 mL). The organic phases were washed with water and brine, dried over $MgSO_4$, filtered and concentrated in vacuo. Purification on silica (100% hexane to 7:3 ethyl acetate: hexane) afforded 32 mg (69% yield). ^{1}H-NMR (400 MHz, MeOD) δH ppm 1.61 to 1.76 (3*H*, m), 1.90 to 1.94 (1*H*, m), 4.16 to 4.21 (2*H*, m), 4,35 to 4.38 (1*H*, m), 7.30 (2*H*, t, J = 13.75 Hz), 7.37 (2*H*, t, J = 15.13 Hz), 7.66 (2*H*, t, J = 13.75 Hz), 7.77 (2*H*, d, J = 7.26 Hz) ^{13}C- NMR (100 MHz, MeOD) 175.54 (C=O), 158.65 (Ar*C*), 145.33 (Ar*C*), 145.12 (Ar*C*), 142.57 (Ar*C*), 128.75 (Ar*C*)2, 128.13 (Ar*C*)$_2$, 126.23 (Ar*C*)$_2$, 120.89 (Ar*C*)2, 67.88 (*C*H_2), 54.83 (*C*H), 51.92 (*C*H_2), 48.42 (*C*H), 29.91 (*C*H_2), 26.42 (*C*H_2) HRMS (ES+) calculated for $C_{20}H_{21}N_4O_4$ $(M+H)^+$ found 381.1557 m/z

6.5.2.1 Click chlorofusin yields

200 mg of MBHA Rink Amide resin (0.14 mmol, 0.7 mmol/g) was suspended in 10 mL of DMF. The resin was then allowed to swell for 30 min. DMF was removed under reduced pressure and Fmoc deprotection was carried out by addition of 3 x 5 mL of 5% piperazine in DMF, which was shaken for 5 minutes each. Resin was then washed with 4 x 20 mL of DMF. Resin was treated with a solution of Fmoc-Asp-ODMab (94 mg, 0.14 mmol, 1 eq), to which HBTU (53 mg, 0.14 mmol, 1 eq) and HOBt (21 mg, 0.14 mmol, 1 eq) and DIPEA (24 μLs, 2 eq) in DMF were added. The mixture was then shaken for 30 min.

Fmoc deprotection and washes were repeated for each subsequent coupling. A Kaiser test was carried out at each stage to ensure that the coupling had gone to completion.

A single, 30 min coupling with 5 eq of HBTU and HOBT and 10 eq of DIPEA (or 1 eq of HBTU and HOBT and 10 eq of DIPEA for amino acids bearing a *) was used at each stage in the order of Fmoc-Ala-OH and Fmoc-Thr(tBu), Fmoc- L-δ-Nva(N_3)-OH*, Fmoc-D-Ade-OH*, Fmoc-D-Leu-OH, Fmoc-Thr(tBu)-OH, Fmoc-D-Leu-OH and Fmoc-D-Asn(Trt)-OH* respectively.

Following the attachment of the final amino acid, the DMab group was removed by 3 x 10mLs of 2% hydrazine (581.4 μL in 30 mL) in DMF, shaken for 5 minutes each. The resin was washed with 4 x 20mLs of DMF, and then washed 4 times with 5% DIPEA in DMF (5.39 mL in 80 mL). Resin was then shaken with DIC (108 μL, 0.7 mmol, 5 eq) and HOBt (107 mg, 0.7 mmol, 5 eq) for 4 x 24 hours.

Resin was washed 3 times with DMF, then 3 times with CH_2Cl_2, then 3 times with 1:1 CH_2Cl_2:MeOH to remove any residual DMF. The resin was then dried *in vacuo* over KOH overnight.

A small amount was cleaved from the resin for characterisation: 100 mg of peptide-resin complex was shaken with 4.706 mLs of 95:2.5:2.5 TFA:H_2O:TIPS for 3 hours. The resin was washed 3 times with TFA and the solution was concentrated in vacuo. The peptide was precipitated out using cold diethyl ether, which was then filtered off, producing 30.9 mg as a white powder.

Subsequent click reactions took place with peptide-resin complex (50 mg, 0.035 mmol), Alkyne (1 eq), 1 M sodium ascorbate (192 μL), 1 M $CuSO_4.5H_2O$ (19.2 μL) and DMF (6 mL) was shaken overnight.

2-[(2R,5R,8S,11R,14R,17S,20S,23S,26S)-17-3-azidopropyl)-1*H*-1,2,3-triazol-1-yl] propyl-26-(carbamoylmethyl)-8,20-bis(1-hydroxyethyl)-23-methyl-5,11-bis(2-methylpropyl)-14-octyl-3,6,9,12,15,18,21,24,27-nonaoxo-1,4,7,10,13,16,19,22,25-nonaazacycloheptacosan-2-yl]acetamide (B13)

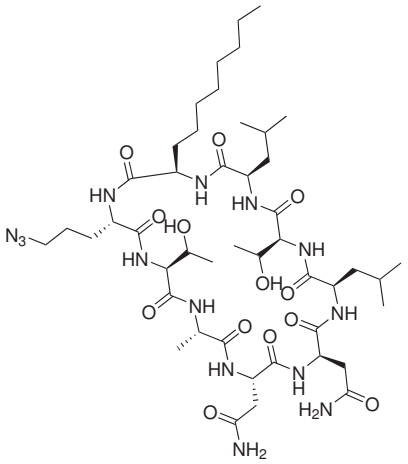

Yellow gel, 2.8 mg, 8% yield MALDI-TOF 1060.74 (M+Na) and 1076.75 (M+K) m/z HPLC retention time 17.58 min

2-[(2R,5R,8S,11R,14R,17S,20S,23S,26S)-17-3-(4-phenyl)-1*H*-1,2,3-triazol-1-yl] propyl-26-(carbamoylmethyl)-8,20-bis(1-hydroxyethyl)-23-methyl-5,11-bis(2-methylpropyl)-14-octyl-3,6,9,12,15,18,21,24,27-nonaoxo-1,4,7,10,13,16,19,22,25-nonaazacycloheptacosan-2-yl]acetamide (B14)

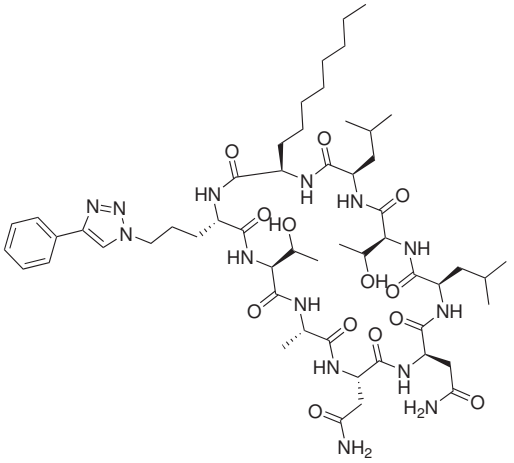

White gel, 0.8 mg, 2% yield MALDI-TOF 1161.64 (M+Na) and 1177.66 (M+K) m/z HPLC retention time 18.066 min

2-[(2R,5R,8S,11R,14R,17S,20S,23S,26S)-17-3-[4-(4-methylphenyl)-1*H*-1,2,3-triazol-1-yl]propyl-26-(carbamoylmethyl)-8,20-bis(1-hydroxyethyl)-23-methyl-5,11-bis(2-methylpropyl)-14-octyl-3,6,9,12,15,18,21,24,27-nonaoxo-1,4,7,10,13,16,19,22,25-nonaazacycloheptacosan-2-yl]acetamide (B15)

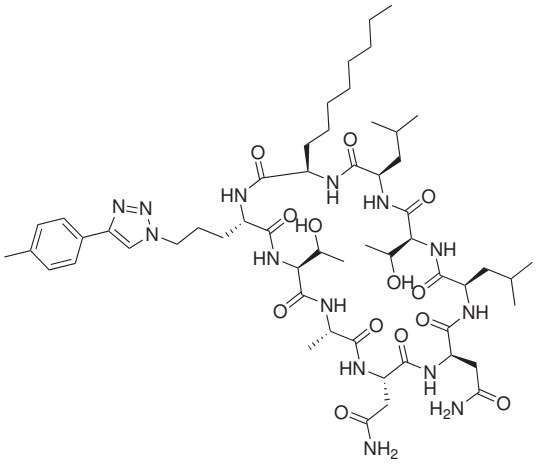

White gel, 1 mg, 3% yield MALDI-TOF 1176.46 (M+Na) m/z HPLC retention time 18.37 min

2-[(2R,5R,8S,11R,14R,17S,20S,23S,26S)-17-3-[4-(3-chlorophenyl)-1*H*-1,2,3-triazol-1-yl]pro bis(2-methylpropyl)-14-octyl-3,6,9,12,15,18,21,24,27-nonaoxo-1,4,7,10,13,16,19,22,25-nonaazacycloheptacosan-2-yl]acetamide (B16)

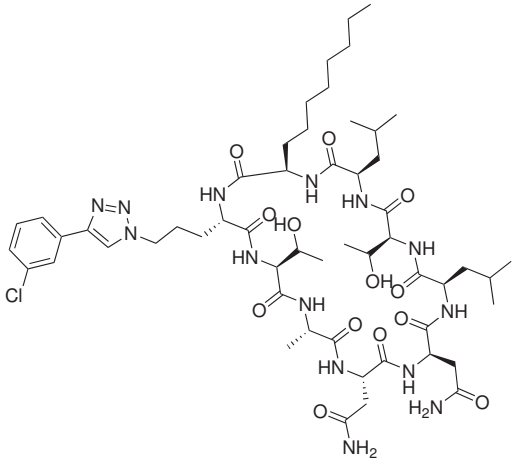

White gel, 0.8 mg, 2% yield MALDI-TOF 1196.19 (M+Na) and 1212.19 (M+K) m/z HPLC retention time 18.41 min

2-[(2R,5R,8S,11R,14R,17S,20S,23S,26S)-17-3-[4-(4-fluorophenyl)-1*H*-1,2,3-triazol-1-yl]pro bis(2-methylpropyl)-14-octyl-3,6,9,12,15,18,21,24,27-nonaoxo-1,4,7,10,13,16,19,22, 25-nonaazacycloheptacosan-2-yl]acetamide (B17)

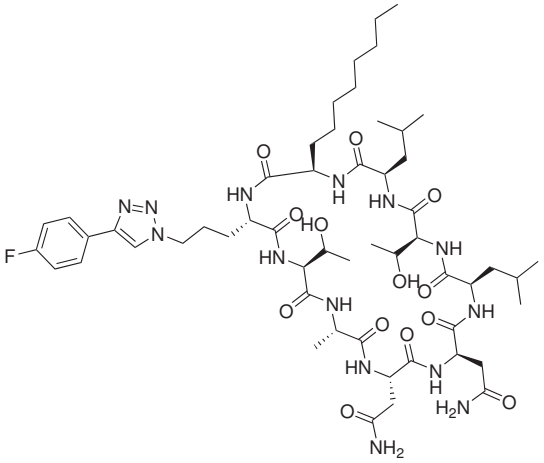

White gel, 0.9 mg, 1% yield MALDI-TOF 1176.60 (M+Na) and 1192.59 (M+K) m/z
HPLC retention time 18.85 min

2-[(2R,5R,8S,11R,14R,17S,20S,23S,26S)-17-3-[4-(2-bromophenyl)-1*H*-1,2,3-triazol-1-yl]pr bis(2-methylpropyl)-14-octyl-3,6,9,12,15,18,21,24,27-nonaoxo-1,4,7,10,13,16,19,22, 25-nonaazacycloheptacosan-2-yl]acetamide (B18)

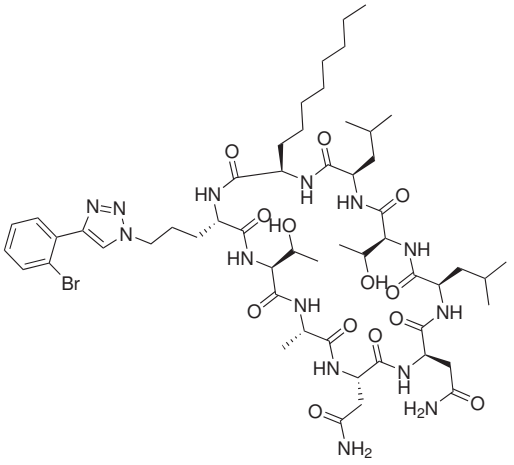

Orange gel, 0.6 mg, 1% yield MALDI-TOF 1242.70 (M+Na) and 1258.11 (M+K) m/z
HPLC retention time 18.28 min

2-[(2R,5R,8S,11R,14R,17S,20S,23S,26S)-17-3-[4-(3-thoiphene)-1*H*-1,2,3-triazol-1-yl]propy bis(2-methylpropyl)-14-octyl-3,6,9,12,15,18,21,24,27-nonaoxo-1,4,7,10,13, 16,19,22,25-nonaazacycloheptacosan-2-yl]acetamide (B19)

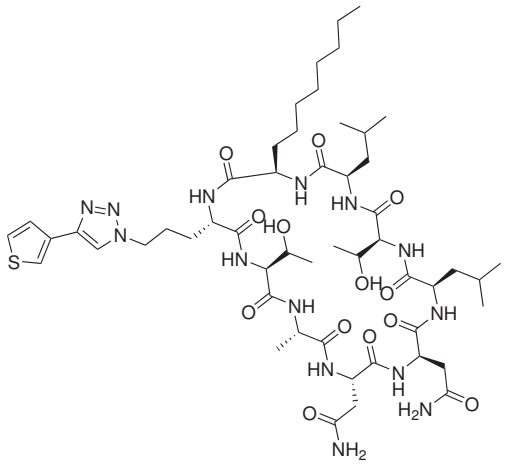

White gel, 1.8 mg, 4% yield MALDI-TOF 1167.33 (M+Na) and 1183.28 (M+K) m/z HPLC retention time 17.96 min

2-[(2R,5R,8S,11R,14R,17S,20S,23S,26S)-17-3-[4-(2-isoindoline-3-acetaldehyde)-1*H*-1,2,3-triazol-1-yl]propyl-26-(carbamoylmethyl)-8,20-bis(1-hydroxyethyl)-23-methyl-5,11-bis(2-methylpropyl)-14-octyl-3,6,9,12,15,18,21,24,27-nonaoxo-1,4,7,10,13,16,19,22,25-nonaazacycloheptacosan-2-yl]acetamide (B20)

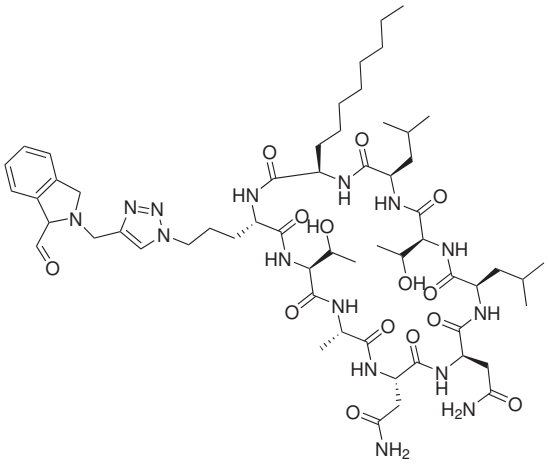

White gel, 2.1 mg, 5% yield MALDI-TOF 1258.62 (M+Na) m/z HPLC retention time 17.80 min

2-[(2R,5R,8S,11R,14R,17S,20S,23S,26S)-17-3-[4-(2-phthalimide)-1*H*-1,2,3-triazol-1-yl]pro
bis(2-methylpropyl)-14-octyl-3,6,9,12,15,18,21,24,27-nonaoxo-1,4,7,10,13,16,19,22,25-nonaazacycloheptacosan-2-yl]acetamide (B21)

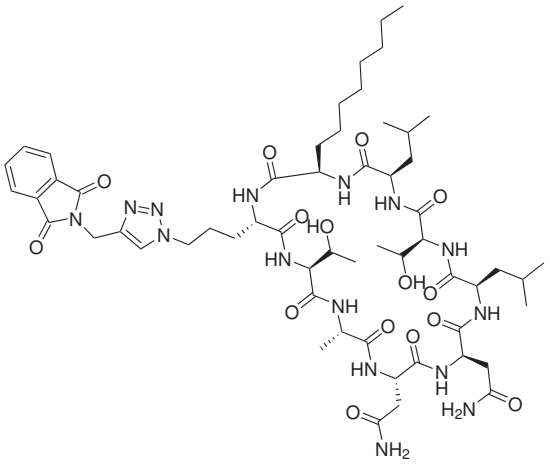

White gel, 2.3 mg, 5% yield MALDI-TOF 1244.87 (M+Na) m/z HPLC retention time 17.70 min

2-[(2R,5R,8S,11R,14R,17S,20S,23S,26S)-17-3-[4-(4-phenoxyphenyl)-1*H*-1,2,3-triazol-1-yl]propyl-26-(carbamoylmethyl)-8,20-bis(1-hydroxyethyl)-23-methyl-5,11-bis(2-methylpropyl)-14-octyl-3,6,9,12,15,18,21,24,27-nonaoxo-1,4,7,10,13,16,19,22,25-nonaazacycloheptacosan-2-yl]acetamide (B22)

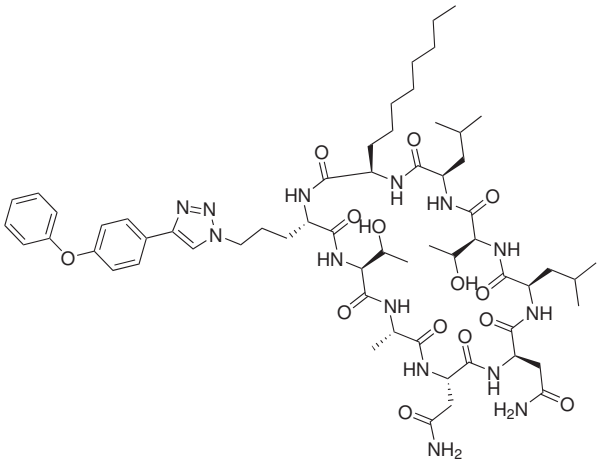

White gel, 3.3 mg, 8% MALDI-TOF 1253.92 (M+Na) m/z HPLC retention time 17.80 min

2-[(2R,5R,8S,11R,14R,17S,20S,23S,26S)-17-3-[4-(3,5-dimethylisophthalate)-1*H*-1,2,3-triazol-1-yl]propyl-26-(carbamoylmethyl)-8,20-bis(1-hydroxyethyl)-23-methyl-5,11-bis(2-methylpropyl)-14-octyl-3,6,9,12,15,18,21,24,27-nonaoxo-1,4,7,10,13,16,19,22,25-nonaazacycloheptacosan-2-yl]acetamide (B23)

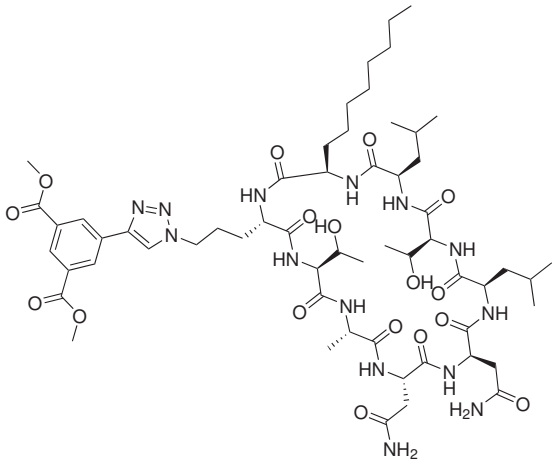

Pale yellow gel, 1.5 mg, 4% yield MALDI-TOF 1277.75 (M+Na) m/z HPLC retention time 18.11 min

6.5.3 Click amino acids

Fmoc- L-δ-Nva(N_3)-OH (50 mg, 0.131 mmol), Alkyne (1 eq), 1 M sodium ascorbate (92 μL), 1 M $CuSO_4.5H_2O$ (9.2 μL) and 1:1 ^{t}Bu:H_2O (1 mL) was stirred overnight. Compounds were then purified through reverse-phase preparative HPLC.

(2S)-2-[(9H-fluoren-9-ylmethoxy)carbonyl]amino-5-[4-(4-methoxyphenyl)-1*H*-1,2,3-triazol-1-yl]pentanoic acid (**B24**)

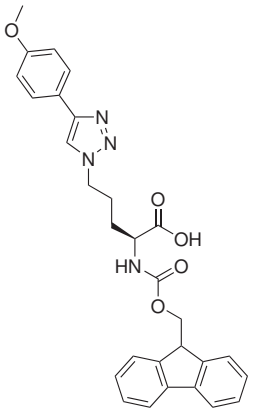

White solid, 9% yield ^{1}H-NMR (400 MHz, MeOD) δ_H ppm 1.71 to 1.73 (1*H*, m), 1.83 to 1.95 (1*H*, m), 2.00 to 2.02 (2H, m), 3.82 (3H, s), 4.21 (2H, t, J = 7.39 Hz and 12.94 Hz), 4.35 to 4.38 (2H, m), 4.46 (2H, t, J = 6.47 Hz and 12.94 Hz), 6.97 (2H, d, J = 8.23 Hz), 7.28 to 7.30 (2H, m), 7.34 to 7.38 (2H, m), 7.65 (2H, m), 7.71 (2H, d, J = 9.24

Hz), 7.77 (2H, d, $J = 7.39$ Hz), 8.28 (1*H*, s) HRMS (ES+) calculated for $C_{29}H_{29}N_4O_5$ $(M+H)^+$ found 513.2132 m/z

(2S)-2-[(9H-fluoren-9-ylmethoxy)carbonyl]amino-5-[4-(4-methylphenyl)-1*H*-1,2,3-triazol-1-yl]pentanoic acid (**B25**)

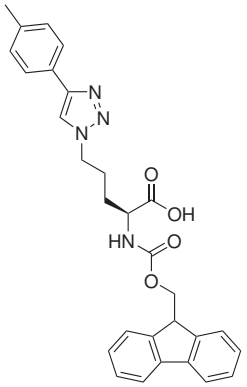

White solid, 5.9 mg, 9% yield ^{1}H-NMR (400 MHz, MeOD) δ_H ppm 1.60 to 1.68 (1*H*, m), 1.80 to 1.85 (1*H*, m), 1.91 to 1.95 (2*H*, m), 2.26 (3*H*, s), 4.11 to 4.13 (2*H*, m), 4.25 to 4.28 (2*H*, m), 4.38 (2*H*, t, $J = 6.96$ Hz and 13.93 Hz), 7.13 to 7.20 (4*H*, m), 7.25 to 7.28 (2*H*, m), 7.54 to 7.59 (4*H*, m), 7.68 (2*H*, d, $J = 7.84$ Hz), 8.14 (1*H*, s) HRMS (ES+) calculated for $C_{29}H_{29}N_4O_4$ $(M+H)^+$ found 497.2183 m/z HPLC retention time 16.567 min

(2S)-2-[(9H-fluoren-9-ylmethoxy)carbonyl]amino-5-[4-(4-(trifluoromethyl)phenyl)-1*H*-1,2,3-triazol-1-yl]pentanoic acid (**B26**)

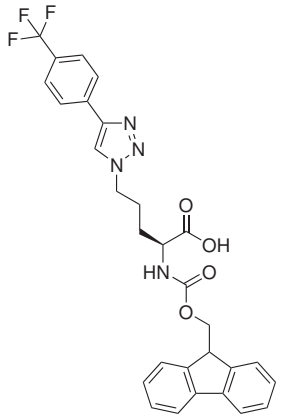

White solid, 15.9 mg, 22% yield ^{1}H-NMR (400 MHz, MeOD) δ_H ppm 1.73 to 1.76 (1*H*, m), 1.90 to 1.92 (1*H*, m), 2.03 to 2.06 (2*H*, m), 4.20 to 4.22 (2*H*, m), 4.35 to 4.38 (2*H*, m), 4.51 (2*H*, t, $J = 6.78$ Hz and 13.55 Hz), 7.28 (2*H*, t, $J = 7.91$ Hz to 14.68 Hz), 7.36

(2*H*, t, $J = 7.91$ Hz and 15.81 Hz), 7.65 (2*H*, t, $J = 6.78$ Hz and 13.55 Hz), 7.71 (2*H*, d, $J = 7.91$ Hz), 7.77 (2*H*, d, $J = 6.78$ Hz), 7.99 (2*H*, d, $J = 9.04$ Hz), 8.43 (1*H*, s) HRMS (ES+) calculated for $C_{29}H_{26}F_3N_4O_4$ $(M+H)^+$ 551.1901 m/z found 551.1890 m/z

(2S)-5-[4-(4-[(tert-butoxy)carbonyl]aminomethylphenyl)-1*H*-1,2,3-triazol-1-yl]-2-[(9H-fluoren-9-ylmethoxy)carbonyl]aminopentanoic acid (**B27**)

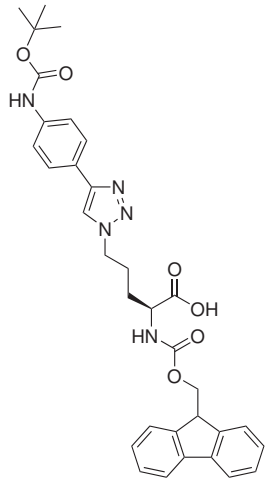

Pale orange solid, 1.6 mg, 2% yield ^{1}H-NMR (400 MHz, MeOD) δ_H ppm 1.50 (9H, s), 1.67 to 1.80 (1*H*, m), 1.83 to 1.95 (1*H*, m), 1.96 to 2.09 (2*H*, m), 4.22 (2*H*, t, $J = 6.28$ Hz and 12.97 Hz), 4.38 (2*H*, t, $J = 7.18$ Hz and 12.17 Hz), 4.47 (2*H*, t, $J = 7.18$ Hz and 13.47 Hz), 7.29 (2*H*, t, $J = 7.08$ Hz and 15.04 Hz), 7.37 (2*H*, t, $J = 7.08$ Hz and 15.04 Hz), 7.64 to 7.66 (2H, m), 7.70 (2*H*, d, $J = 8.43$ Hz), 7.78 (2*H*, d, $J = 6.94$ Hz), 8.22 (1*H*, s) LCMS (ES+) calculated for $C_{33}H_{36}N_5O_6$ found 598.4 m/z

(2S)-5-[4-(4-chlorophenyl)-1*H*-1,2,3-triazol-1-yl]-2-[(9H-fluoren -9-ylmethoxy)carbonyl]a minopentanoic acid (**B28**)

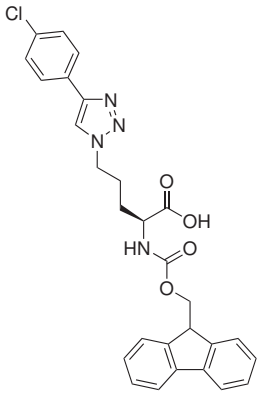

White solid, 2 mg, 3% yield ^{1}H-NMR (400 MHz, MeOD) δ_H ppm 1.72 (1*H*, m), 1.88 (1*H*, m), 2.03 (2*H*, m), 4.20 (1*H*, m), 4.34 to 4.39 (1*H*, m), 4.49 (2*H*, t, J = 7.24 Hz and 13.04 Hz), 7.28 to 7.30 (2*H*, m), 7.35 to 7.39 (2*H*, m), 7.42 (2*H*, d, J = 6.08 Hz), 7.64 to 7.65 (2*H*, m), 7.77 to 7.79 (4*H*, m), 8.32 (1*H*, s) HRMS (ES+) calculated for $C_{28}H_{26}N_4O_4Cl$ $(M+H)^+$ found 517.1637 m/z

(2S)-5-[4-(4-bromophenyl)-1*H*-1,2,3-triazol-1-yl]-2-[(9H-fluoren -9-ylmethoxy)carbonyl]a minopentanoic acid (**B29**)

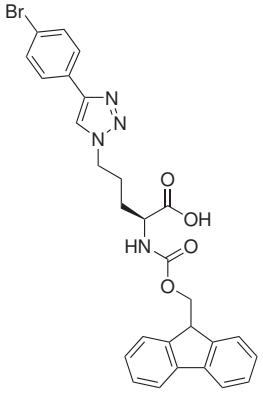

White solid, 1.5 mg, 2% yield ^{1}H-NMR (400 MHz, MeOD) δ_H ppm 1.56 to 1.66 (1*H*, m), 1.67 to 1.81 (1*H*, m), 1.85 to 1.95 (1*H*, m), 1.97 to 2.01 (2*H*, m), 4.18 to 4.23 (1*H*, m), 4.35 to 4.43 (1*H*, m), 4.45 to 4.51 (2*H*, m), 7.29 (2*H*, t, J = 6.52 Hz to 19.59 Hz), 7.37 (2*H*, t, J = 7.25 Hz and 14.86 Hz), 7.567 (2*H*, d, J = 8.33 Hz), 7.63 to 7.67 (2*H*, m), 7.72 (2*H*, d, J = 8.52 Hz), 7.78 (2*H*, d, J = 7.79 Hz), 8.32 (1*H*, s) HRMS (ES+) calculated for $C_{28}H_{26}N_4O_4Br$ $(M+H)^+$ found 561.1132 m/z

(2S)-5-[4-(4-iodophenyl)-1*H*-1,2,3-triazol-1-yl]-2-[(9H-fluoren -9-ylmethoxy)carbonyl]a minopentanoic acid (**B30**)

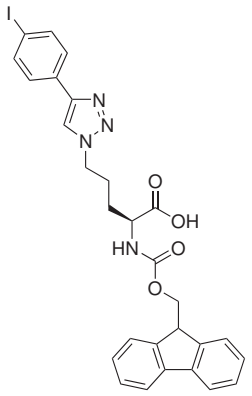

White solid, 5.6 mg, 7% yield ^{1}H-NMR (400 MHz, MeOD) δ_H ppm 1.68 to 1.80 (1*H*, m), 1.84 to 1.96 (1*H*, m), 1.97 to 2.08 (2H, m), 4.20 to 4.22 (2H, t, J = 6.31 Hz and 13.01 Hz), 4.35 to 4.38 (2H, m), 4.49 (2H, t, J = 7.10 Hz and 13.41 Hz), 7.29 (2H, t, J = 7.40 Hz and 14.80 Hz), 7.37 (2H, t, J = 7.40 Hz and 14.80 Hz), 7.58 (2H, d, J = 8.33 Hz), 7.66 (2H, t, J = 6.48 Hz and 12.03 Hz), 7.76 to 7.79 (4H, m), 8.32 (1*H*, s) HRMS (ES+) calculated for $C_{28}H_{26}N_4O_4I$ $(M+H)^+$ 609.0993 m/z found 609.0993 m/z

(2S)-2-amino-5-[4-(4-(trifluoromethyl)phenyl)-1*H*-1,2,3-triazol-1-yl]pentanoic acid (**B31**)

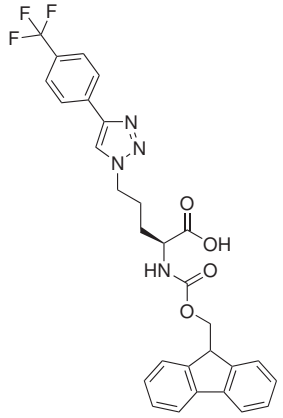

White solid, 2.5 mg, 82% yield ^{1}H-NMR (400 MHz, MeOD) δ_H ppm 1.92 to 2.24 (4*H*, m), 4.05 (1*H*, t, J = 6.08 Hz and 12.77 Hz), 4.60 (2*H*, t, J = 6.69 Hz and 13.37 Hz), 7.77 (2*H*, d, J = 8.51 Hz, 8.04 (2*H*, d, J = 8.51 Hz), 8.50 (1*H*, s) HRMS (ES+) calculated for $C_{29}H_{26}F_3N_4O_4I$ $(M+H)^+$ 551.1894 m/z found 551.1901 m/z

6.6 Experimental for Chapter 4

6.6.1 Initial Synthesis to the Sonogashira Precursor

2,4-dimethoxy-3-methylbenzaldehyde (C01)

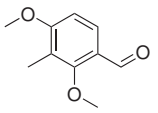

Phosphorus(V) oxychloride (2.8 mL, 30 mmol) was added dropwise to dry DMF (5 mL) at 0°C under nitrogen. The resulting Vilsmeier reagent was then warmed to room temperature and stirred for a further 30 minutes. The Vilsmeier reagent was then added to a solution of 2,6-dimethoxytoluene (3.9 g, 25 mmol) in dry DMF (5 mL) and the mixture was stirred for 4 hours at 100°C under nitrogen. The reaction was then quenched with ice water. The mixture was extracted using ethyl acetate (4 x 20 mL) and the organic phases were combined and washed with brine. The organic phase was then dried over magnesium sulphate, filtered and concentrated in vacuo. Purification on silica (100% Hexane to 1:9 Ethyl Acetate:Hexane) afforded 3.39 g (74% yield) as an off-white solid. mp 53-55°C. IR ν_{max} (neat) /cm^{-1} 2844.78 (C-H), 1767.02 (C=O), 1744.46 (C=O), 1106.68 (C-O); ^{1}H NMR (400 MHz, $CDCl_3$) δ_H ppm: 10.23 (1*H*, s), 7.75 (1*H*, d, $J = 9.99$ Hz), 6.75 (1*H*, d, $J = 9.99$ Hz), 3.91 (3*H*, s), 3.86 (3*H*, s), 2.16 (3*H*, s) ^{13}C NMR (100 MHz, $CDCl_3$) δ_C ppm: 189.20 (*C*OH), 164.01 (Ar*C*), 162.61 (Ar*C*), 127.96 (Ar*C*), 122.84 (Ar*C*), 120.14 (Ar*C*H), 106.55 (*C*H), 62.91 (*C*H$_3$), 55.70 (*C*H$_3$), 8.52 (*C*H$_3$). Data matches literature values.[182]

(Acetyloxy)(2,4-dimethoxy-3-methyl-5-nitrophenyl)methyl acetate (C02)

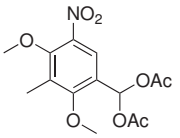

2,4-dimethoxy-3-methylbenzaldehyde (5 g, 27.8 mmol) was dissolved in acetic anhydride (17.3 mL). The solution was added slowly to a mixture of copper(III) nitrite hemipentahydrate (3.86 g, 16.5 mmol) and 17.3 mL of acetic anhydride at 0°C. The mixture was warmed to room temperature and stirred for 6 hours. The product was extracted with ethyl acetate (3 x 20 mL) and the organic phases were washed with distilled water,

dried over magnesium sulphate, filtered and concentrated in vacuo. Purification on silica (1:9 Ethyl Acetate:Hexane) 1:9 Ethyl Acetate:Hexane produced 6.63 g of pale cream solid (73% yield). mp 45-47°C; IR ν_{max} (neat) /cm^{-1} 2844.67 (C-H), 1681.18 (C=O), 1107.83 (C-O); ^{1}H NMR (400 MHz, $CDCl_3$) δ_H ppm: 2.13 (6*H*, s), 2.35 (3*H*, s), 3.87 (3*H*, s), 3.91 (3*H*, s), 7.90 (1*H*, s), 7.92 (1*H*, s); ^{13}C NMR (100 MHz, $CDCl_3$) δ_H ppm: 168.66 (Ar*C*), 162.60 (Ar*C*), 150.21 (Ar*C*), 147.17 (Ar*C*), 129.20 (Ar*C*), 141.02 (Ar*C*), 124.54 (Ar*C*H), 122.20 (Ar*C*), 105.94 (*C*H), 84.86 (*C*H), 62.05 (*C*H$_3$), 61.74 (*C*H$_3$), 20.82 ((*C*H$_3$)$_2$), 10.06 (*C*H$_3$). Data matches literature values.[182]

(Acetyloxy)(3-amino-2-bromo-4,6-dimethoxy-5-methylphenyl) methyl acetate (C03)

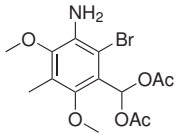

(Acetyloxy)(2,4-dimethoxy-3-methyl-5-nitrophenyl)methyl acetate (5 g, 15.29 mmol) was dissolved in 22:7:1 diethyl ether: ethanol: water (500 mL). Aluminium foil (4.11 g, 152.9 mmol) was cut into strips and rolled into coils before being dipped into 2% aqueous mercury solution. Once amalgamated, the aluminium was dipped again in diethyl ether to dry and added to the reaction mixture. The reaction mixture was stirred for 1 h at room temperature. The product was filtered through celite and concentrated under reduced pressure. The product was redissolved in acetic acid (30 mL), to which a solution of bromine (858 μL, 16.82 mmol, 1.1 eq) in acetic acid (20 mL) was added dropwise and stirred over 30 min. The reaction was quenched with saturated sodium thiosulphate and the product was extracted with ethyl acetate (4 x 30 mL), the organic phases were washed with saturated sodium bicarbonate and water, then dried over magnesium sulphate, filtered and concentrated in vacuo. Purification on silica in a gradient of (1:9 Ethyl Acetate:Hexane to 4:6 Ethyl Acetate:Hexane) afforded 3.74 g (65% yield) of orange solid. mp 126-129°C; IR ν_{max} (neat) /cm^{-1} 3476.95 (N-H), 3378.37 (N-H), 1738.54 (C=O), 1210.73 (C-O); ^{1}H NMR (400 MHz, $CDCl_3$) δH ppm: 2.10 (6H, s), 2.18 (3*H*, s), 3.73 (3*H*, s), 3.76 (3*H*, s), 8.14 (1*H*, s); ^{13}C NMR (100 MHz, $CDCl_3$) δ_C ppm: 168.66 (Ar*C*), 150.21 (Ar*C*), 147.17 (Ar*C*), 124.54 (Ar*C*), 123.33 (Ar*C*), 105.94 (Ar*C*), 87.75 (Ar*C*), 62.20 (*C*H$_3$), 60.37 (*C*H$_3$), 20.89 ((*C*H$_3$)$_2$), 14.19 (*C*H$_3$), 9.71 (*C*H$_3$). Data matches literature values.[182]

2-bromo-4,6-dimethoxy-5-methylbenzaldehyde (C04)

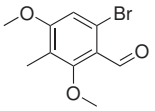

(Acetyloxy)(3-amino-2-bromo-4,6-dimethoxy-5-methylphenyl)methyl acetate (500 mg, 1.33 mmol) was dissolved in THF (5.42 mL) and distilled water (3.61 mL). Concentrated HCl (0.904 mL) was added to the mixture and it was cooled to -5°C. To the mixture, of sodium nitrite (101.2 mg (1.46 mmol) in distilled water (0.361 mL) was added to the mixture, which was subsequently stirred for 20 minutes at -5°C. Urea (36.1 mg) was then added, after which 50% w/v hypophosphorus acid (3.01 mL) was added dropwise over 20 minutes. The resultant mixture was reacted overnight at 0°C and then warmed to 40°C for 4 hours. The mixture was extracted using ethyl acetate (3 x 10 mL) and the organic phases were washed with distilled water. The organic phases were dried over magnesium sulphate, which was filtered and the solution was concentrated in vacuo. Purification on silica (1:9 Ethyl Acetate:Hexane to 4:6 Ethyl Acetate:Hexane) afforded 340 mg (99% yield) of yellow solid. mp 76-78°C; ^{1}H NMR (400 MHz, $CDCl_3$) δH ppm: 2.10 (3*H*, s), 3.81 (3*H*, s), 3.90 (3*H*, s), 6.93 (1*H*, s), 10.27 (1*H*, s); ^{13}C NMR (100 MHz, $CDCl_3$) δ_C ppm: 189.90 (*C*OH), 162.74 (Ar*C*), 161.97 (Ar*C*), 124.19 (Ar*C*H), 120.93 (Ar*C*), 120.90 (Ar*C*), 112.43 (Ar*C*), 62.57 (*C*H_3), 56.12 (*C*H_3), 14.12 (*C*H), 8.42 (*C*H_3). Data matches literature values.[182]

2,4-dihydroxy-3-methyl-6-bromobenzaldehyde (C05)

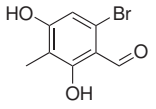

2-bromo-4,6-dimethoxy-5-methylbenzaldehyde (1.4 g, 6.060 mmol) was dissolved in CH_2Cl_2 (17.92 mL) and the solution was cooled down to -78°C. To the solution, of BBr3 (5.38 g, 2.17 mL, 21.48 mmol) was added dropwise. The reaction mixture was stirred for 30 minutes at -78°C, then warmed to room temperature over 30 minutes. The mixture was then stirred at room temperature for 18 hours and quenched with ice water, after which it was stirred for a further hour.

The mixture was extracted with ethyl acetate (3 x 20 mL) and the organic phases were washed with brine. Magnesium sulphate was used to dry the organic layers, after which the magnesium was filtered off and the solution was concentrated in vacuo. Purification on silica in 1:9 Ethyl Acetate:Hexane afforded 1.03 g as a white solid (83%). ^{1}H NMR (400 MHz, MeOD) δ_H ppm: 2.02 (3*H*, s), 6.72 (1*H*, s), 10.08 (1*H*, s); ^{13}C NMR (100 MHz,

MeOD) δ_C ppm: 196.78 (*C*OH), 165.17 (Ar*C*), 164.83 (Ar*C*), 126.73 (Ar*C*H), 113.77 (Ar*C*), 112.67 (Ar*C*), 112.45 (Ar*C*), 7.28 (*C*H_3). Data matches literature values.[182]

Alkynylbenzaldehyde (C06)

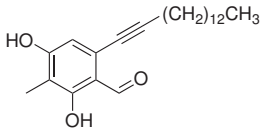

2-iodo-4,6-dihydroxy-5-methylbenzaldehyde (500 mg, 2.16 mmol), $PdCl_2(PPh_3)_2$ (152 mg, 0.216 mmol), CuI (41 mg, 0.22 mmol), of 1-pentadecyne (540.8 mg, 2.6 mmol, 680 μL), dry DMF (16 mL) and triethylamine (1 mL) were stirred under nitrogen at 60°C for 4 hours. The mixture was allowed to cool to room temperature, was diluted with distilled water and then neutralised with 1M aqueous HCl. The mixture was extracted with ethyl acetate (3 x 10 mL) and the organic phases were washed with brine. The organic phase was dried over magnesium sulphate, filtered and concentrated in vacuo. Purification on silica in (5:95 Ethyl Acetate:Hexane to 4:6 Ethyl Acetate:Hexane) afforded 382 mg (52% yield) as a pale yellow solid. ^{1}H-NMR (400 MHz, $CDCl_3$) δ_H ppm: 1.26 (25H, brm, overlap), 2.11 (3*H*, s), 2.44 (2*H*, t, *J*= 14.17 Hz), 6.48 (1*H*, s), 10.21 (1*H*, s), 12.34(1*H*, s); ^{13}C-NMR (100 MHz, $CDCl_3$) δ_H ppm: 195.32 (*C*OH), 162.97 (Ar*C*), 160.28 (Ar*C*), 114.56 (Ar*C*H), 112.15 (Ar*C*), 111.36 (Ar*C*), 97.49 (*C*H), 34.67 (*C*H), 31.93 (*C*H), 31.59 (*C*H_2), 29.66 (*C*H_2), 29.52 (*C*H_2), 29.36 (*C*H_2), 29.12 (*C*H_2), 29.00 (*C*H_2), 28.50 (*C*H_2), 26.92 (*C*H_2), 25.28 (*C*H_2), 22.66 (*C*H_2), 20.69 (*C*H_2), 19.53 (*C*H_2), 14.12 (*C*H_3), 7.09 (*C*H_3). HRMS (APCI+) calculated for $C_{23}H_{35}O_3$ $(M+H)^+$ 359.2572 found 359.2581 m/z

7-methyl-6,8-dimethylidene-3-tridecyl-7,8-dihydro-6H-isochromen-7-ol (C07)

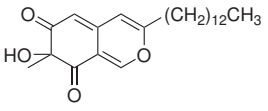

Alkynylbenzaldehyde (373 mg, 1.1396 mmol) was dissolved in dichloroethane (5.647 mL). To the solution, $Au(OAc)_3$ (21.13 mg, 0.0564 mmol) and TFA (564 μL) were added. The mixture was stirred for 1 minute at room temperature. Dry IBX (342.6 mg, 1.243mmol) and TBAI (20.8 mg, 0.0564 mmol) were then added to the reaction mixture, which was stirred for a further hour. After this time the reaction was quenched with saturated sodium thiosulphate. The mixture was extracted with ethyl acetate (3 x 10 mL), then the organic phases were washed with brine. The organic phases were dried

over magnesium sulphate, filtered and concentrated in vacuo. Purification on silica (1:9 EtOAc:Hexane to 2:8 EtOAc:Hexane), afforded 180 mg (48% yield) as an orange solid. ^{1}H-NMR (400 MHz, $CDCl_3$) δ_H ppm: 0.88 (4*H*, brm, overlap), 1.26 (20H, brm, overlap), 1.55 (3*H*, s), 2.41 (2*H*, t, $J = 15.61$ Hz), 5.52 (1*H*, s), 6.10 (1*H*, s), 7.88 (1*H*, s); ^{13}C-NMR (100 MHz, $CDCl_3$) δ_C ppm: 196.28 (C=O), 195.80 (C=O), 163.08 (Ar*C*), 152.95 (Ar*C*), 144.14 (Ar*C*), 115.82 (Ar*C*H), 108.28 (Ar*C*H), 104.95 (Ar*C*H), 83.46 (Ar*C*H), 60.37 (*C*H), 33.20 ($C H_2$), 31.89 ($C H_2$), 29.63 ($C H_2$), 29.61 ($C H_2$), 29.55 ($C H_2$), 29.40 ($C H_2$), 29.32 ($C H_2$), 29.19 ($C H_2$), 28.91 ($C H_2$), 28.51 ($C H_2$), 26.48 ($C H_2$), 22.66 ($C H_3$), 14.10 ($C H_3$). HRMS (ES+) calculated for $C_{23}H_{38}NO_4$ $(M+NH_4)^+$ 392.2799 found 392.2795 m/z

7-methyl-6,8-dimethylidene-3-tridecyl-7,8-dihydro-6H-isochromen-7-yl butanoate (C08)

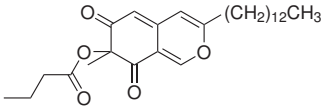

7-methyl-6,8-dimethylidene-3-tridecyl-7,8-dihydro-6H-isochromen-7-ol (140 mg, 0.4032 mmol),CH_2Cl_2 (4.172 mL), butyric anhydride (319.9 mg, 5 eq, 328.16 μL, 2.016 mmol) and DMAP (4.928 mg, 0.1 eq, 0.04032 mmol) were stirred at room temperature for 22 hours. The reaction was then quenched with MeOH (4.172 mL) for 15 minutes, concentrated and left overnight *in vacuo*. Purification on silica (1:9 Ethyl Acetate:Hexane to 2:8 Ethyl Acetate:Hexane) afforded 90.8 mg (55% yield) as an orange oil. ^{1}H-NMR (400 MHz, $CDCl_3$) δ_H ppm: 0.95 (5H, t, $J = 13.90$ Hz), 0.97 (5H, t, $J = 13.90$ Hz), 1.26 (25H, brm, overlap), 1.52 (3*H*, s), 1.66 (2*H*, t, overlap), 1.68 (3*H*, m, overlap), 2.34 (1*H*, t, overlap), 2.42 (4*H*, m, overlap), 5.57 (1*H*, s), 6.08 (1*H*, s), 7.87 (1*H*, s); ^{13}C-NMR (100 MHz, $CDCl_3$) δ_H ppm: 192.80 (C=O), 172.82 (C=O), 162.37 (Ar*C*), 153.90 (Ar*C*), 142.70 (Ar*C*), 115.11 (Ar*C*H), 108.56 (Ar*C*H), 106.72 (Ar*C*H), 84.03 (Ar*C*H), 35.01 ($C H_2$), 33.04 ($C H_2$), 31.86 ($C H_2$), 31.53 ($C H_2$), 29.60 ($C H_2$), 29.58 ($C H_2$), 29.37 ($C H_2$), 29.29 ($C H_2$), 29.17 ($C H_2$), 28.85 ($C H_2$), 26.85 ($C H_2$), 26.48 ($C H_2$), 22.63 ($C H_2$), 22.59 ($C H_2$), 22.12 ($C H_2$), 18.16 ($C H_3$), 14.04 ($C H_3$), 13.42 ($C H_3$). HRMS (ES+) calculated for $C_{27}H_{44}NO_5$ $(M+NH_4)^+$ 462.3212 found 462.3214 m/z

5-chloro-7-methyl-6,8-dimethylidene-3-tridecyl-7,8-dihydro-6H-isochromen-7-yl butanoate (C09)

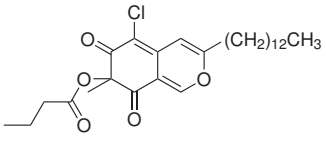

7-methyl-6,8-dimethylidene-3-tridecyl-7,8-dihydro-6H-isochromen-7-yl butanoate (60 mg, 0.147 mmol) and NCS (25.96 mg, 0.192 mmol) were dissolved in 1.716 mLs of glacial acetic acid and stirred for 24 hours. The product was filtered to remove the NCS and the product dried *in vacuo* overnight. The yield of the orange oil produced was quantitative. ^{1}H-NMR (400 MHz, $CDCl_3$) δ_H ppm: 0.95 (4*H*, t, $J = 15.06$ Hz), 0.97 (3*H*, $J = 14.49$ Hz), 1.26 (28H, brm), 1.65 (3*H*, s), 1.67 (5H, m), 2.44 (2*H*, m), 2.48 (2*H*, m), 6.57 (1*H*, s), 7.90 (1*H*, s). HRMS (ES+) calculated for $C_{27}H_{43}NClO_6$ $(M+NH_4)^+$ 496.2820 found 496.2824 m/z

6.6.2 Alternative synthesis to the Sonogashira Precursor

2,4-dihydroxy-3-methyl-6-iodobenzaldehyde (C10)

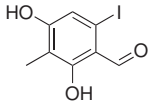

To a solution of triethylamine (3.9 mL, 30.5 mmol) in THF (200 mL), 1.6M nBuLi (22.5 mL, 36.07 mmol) was added and the resultant mixture was stirred for 15 minutes at 0°C. The reaction was then cooled to -20°C and a solution of 2,4-dimethoxy-3-methylbenzaldehyde (5g, 27.7mmoles) in THF (50mLs) was added. The mixture was stirred for a further 30 minutes. A solution of 1.6M nBuLi (46mLs, 73.3mmoles) was then added dropwise and the reaction mixture was stirred overnight.

The reaction mixture was cooled to -40°C and a solution of diiodoethane (23.5 g, 83.2 mmoles) in THF (50 mL) was added dropwise. After 5 minutes the reaction was warmed to room temperature and quenched with 100mLs of saturated ammonium chloride and 40mLs of saturated sodium thiosulphate. The product was extracted using diethyl ether and magnesium sulphate was used to remove any additional water in the organic phase. The magnesium sulphate was removed by filtration and the product was concentrated in vacuo.

The product was then dissolved in 114mLs of CH_2Cl_2 and cooled to -78°C for 30 minutes, then warmed to room temperature over 30 minutes. The solution was then stirred

overnight. Purification on silica (1:9 ethyl acetate:hexane) afforded 2.04g (26% yield) of off-white solid ^{1}H NMR (400 MHz, MeOD) δ_H ppm: 9.72 (1*H*, s), 7.08 (1*H*, s), 1.93 (3*H*, s). ^{13}C NMR (100 MHz, $CDCl_3$) δ_H ppm: 201.23 (*C*OH), 164.67 (Ar*C*), 164.50 (Ar*C*), 121.21 (Ar*C*H), 113.95 (Ar*C*), 113.35 (Ar*C*), 100.76 (Ar*C*), 7.50 (*C*H_3). HRMS (AP+) calculated for $C_8H_8IO_3$ $(M+H)^+$ 278.9505 m/z found 278.9499 m/z

6.6.3 Synthesis for the Generation of Azaphilones with an Aromatic Side Chain

6-ethynyl-2,4-dihydroxy-3-methylbenzaldehyde (C11)

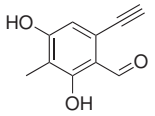

2,4-dihydroxy-3-methyl-6-bromobenzaldehyde (400 mg, 1.728 mmol), $PdCl_2(MeCN)_2$ (27 mg, 0.104 mmol), CuI (14 mg, 0.072 mmol), $(^tBu)_3.HBF_4$ (60 mg, 0.208 mmol), TMS-acetylene (306 mg, 3.12 mmol, 440 μL), dry THF (3.2 mL) and diisopropylamine (388 μL) were stirred under nitrogen at 50°C for 3 h. The mixture was allowed to cool to room temperature, was diluted with ethyl acetate and then neutralised with 1M aqueous HCl. The mixture was extracted with ethyl acetate (3 x 10 mL) and the organic phases were washed with brine. The organic phase was dried over magnesium sulphate, filtered and concentrated in vacuo. Purification on silica in (5:95 Ethyl Acetate:Hexane to 4:6 Ethyl Acetate:Hexane) afforded a pale yellow solid, which was then deprotected using 1 M TBAF in THF (2.032 mL, 2.032 mmol) and THF (61.15 mL) at room temperature for 3 hours. The mixture was diluted with ethyl acetate and then neutralised with 1M aqueous HCl. The mixture was extracted with ethyl acetate (3 x 10 mL) and the organic phases were washed with brine. The organic phase was dried over magnesium sulphate, filtered and concentrated in vacuo. Purification on silica in (5:95 Ethyl Acetate:Hexane to 4:6 Ethyl Acetate:Hexane) afforded 195 mg (64% yield) as a pale yellow solid mp 172-174°C. ^{1}H NMR (400 MHz, MeOD) δ_H ppm: 2.00 (3*H*, s) 3.84 (1*H*, s), 6.55 (1*H*, s), 10.13 (1*H*, s); ^{13}C NMR (100 MHz, MeOD) δ_H ppm: 195.53 (*C*OH), 164.11 (Ar*C*), 126.35 (Ar*C*H), 113.96 (Ar*C*), 84.83 (Ar*C*), 79.73 (Ar*C*), 32.56 (*C*H), 23.71 (*C*H), 14.44 (*C*H), 7.42 (*C*H_3). HRMS (ES-) calculated for $C_{10}H_7O_3$ $(M-H)^-$ found 175.0401 m/z

2,4-dihydroxy-3-methyl-6(2-phenylethynyl)-benzaldehyde (C12)

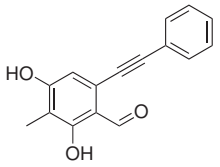

6-ethynyl-2,4-dihydroxy-3-methylbenzaldehyde (102 mg, 0.567 mmol), $Pd(PPh_3)_4$ (34 mg, 0.03 mmol), CuI (5 mg, 0.03 mmol), bromobenzene (179 mg, 1.159 mmol, 121 μL) anhydrous THF (1.05 mL) and triethylamine (161 μL) was stirred at 50°C under nitrogen for 2 h. The resulting mixture was diluted with ethyl acetate, and neutralised using 1M aqueous HCl. The mixture was then extracted using ethyl acetate and the organic phases were washed with brine. The organic phases were dried over magnesium sulphate, filtered and concentrated *in vacuo*. Purification on silica (5:95 EtOAc:Hexane 4:6 EtOAc:Hexane) afforded 60 mg (41% yield) as an orange solid mp 198-200°C ; IR max (neat) /cm-1 3015.11 (O-H), 2206.63 (C≡C), 1737.16 (C=O) ^{1}H NMR (400 MHz, $CDCl_3$) δ_H ppm: 2.15 (3*H*, s), 6.64 (1*H*, s), 7.39 (3*H*, m), 7.52 (2*H*, m), 10.35 (1*H*, s), 12.38 (1*H*, s); ^{13}C NMR (400 MHz, MeOD) δ_H ppm: 199.86 (Ar*C*), 195.52 (*C*OH), 164.22 (Ar*C*), 164.16 (Ar*C*), 132.65 (Ar*C*), 130.19 (Ar*C*H), 129.73 (Ar*C*), 127.30 (Ar*C*H), 123.64 (Ar*C*H), 123.84 (Ar*C*H), 113.20 (Ar*C*), 95.88 (Ar*C*H), 85.41 (Ar*C*H), 12.44 (*C*H), 7.46 (*C*H_3) HRMS (ES-) calculated for $C_{16}H_{11}O_3$ $(M-H)^-$ 251.0709 found 251.0714 m/z

7-hydroxy-3,7-dimethyl-7,8-dihydro-6H-isochromene-6,8-dione (C13)

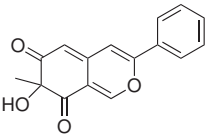

2,4-dihydroxy-3-methyl-6(2-phenylethynyl)-benzaldehyde (60 mg, 0.238 mmol), $Au(OAc)_3$ (4.11 mg, 0.011 mmol), TFA (118 μL) and dichloroethane (1.18 mL). The mixture was stirred for 1 minute at room temperature. Dry IBX (71.23 mg, 0.259 mmol) and TBAI (4.11 mg, 0.011 mmol) were added to the reaction mixture, and stirred for a further hour. The reaction was quenched with saturated sodium thiosulphate and mixture was extracted with ethyl acetate (3 x 10 mL), then the organic phases were washed with brine. The organic phases were dried over magnesium sulphate, filtered and concentrated *in vacuo* and reacted further as crude.

To the crude mixture, acetic anhydride (123 mg, 113 μL, 1.195 mmol 5 eq), DMAP (3 mg, 0.0239 mmol, 0.1 eq) and CH_2Cl_2 (2.08 mL) was stirred at rt for 22 h. Methanol (1 mL) was then added and the mixture was stirred for a further 15 min. The methanol was

removed under reduced pressure and the product was dried *in vacuo*. Purification on silica (1:9 Ethyl Acetate:Hexane to 100% Ethyl Acetate), afforded 23 mg (36% yield) as an orange glassy solid. ^{1}H NMR (400 MHz, $CDCl_3$) δ_H ppm: 1.60 (3*H*, s), 5.70 (1*H*, s), 6.77 (1*H*, s), 7.52 (3*H*, m), 7.74 (2*H*, d, $J = 4.00$ Hz), 8.04 (1*H*, s); ^{13}C-NMR (100 MHz, $CDCl_3$) δ_H ppm: 171.24 (Ar*C*) 132.35 (Ar*C*H), 132.13 (Ar*C*H), 132.03 (Ar*C*H), 128.77 (Ar*C*H), 128.65 (Ar*C*H), 76.70 (*C*H), 60.43 (*C*H_3) 31.59 (*C*H), 22.66 (*C*H), 22.62 (*C*H), 14.20 (*C*H), 14.12 (*C*H_3) HRMS (EI+) calculated for $C_{16}H_{12}O_4$ $(M)^+$ found 268.06951 m/z

7-methyl-6,8-dioxo-3-phenyl-7,8-dihydro-6H-isochromen-7-yl acetate (C14)

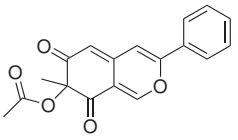

7-hydroxy-3,7-dimethyl-7,8-dihydro-6H-isochromene-6,8-dione (23 mg, 0.0857 mmol), acetic anhydride (45.57 mg, 40.52 μL, 0.4287 mmol, 5 eq), DMAP (1 mg, 0.00857, 0.1 eq) and CH_2Cl_2 (888 μL) was stirred at rt for 22 h. The resulting mixture was stirred with methanol (5 mL) for 15 min, the solvent was removed under reduced pressure and dried *in vacuo* overnight. Purification on silica (100% Hexane to 3:7 Ethyl Acetate: Hexane) afforded 13 mgs of orange solid. ^{1}H NMR (400 MHz, $CDCl_3$) δ_H ppm: 1.58 (3*H*, s), 2.18 (3*H*, s), 2.19 (3*H*, s), 5.70 (1*H*, s), 6.76 (1*H*, s), 7.51 (4*H*, m), 7.73 (3*H*, m), 8.04 (1*H*, s); HRMS (AP+) calculated for $C_{18}H_5O_5$ $(M+H)^+$ found 311.0914 m/z

2,4-dihydroxy-3-methyl-6-[2-(naphthalen-2-yl)ethynyl]benzaldehyde (C15)

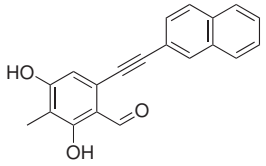

6-ethynyl-2,4-dihydroxy-3-methylbenzaldehyde (200 mg, 1.112 mmol), $Pd(PPh_3)_4$ (66 mg, 0.06 mmol), CuI (10 mg, 0.06 mmol), bromonaphthalene (470 mg, 2.272 mmol) anhydrous THF (2.06 mL) and triethylamine (316 μL) was stirred at 50°C under nitrogen for 4 h. The resulting mixture was diluted with ethyl acetate, and neutralised using 1M aqueous HCl. The mixture was then extracted using ethyl acetate and the organic phases were washed with brine. The organic phases were dried over magnesium sulphate, filtered and concentrated in vacuo. Purification on silica (1:9 Ethyl Acetate:Hexane to 4:6 Ethyl Acetate:Hexane) afforded 120 mg (35%) as a yellow solid Mp 100.9-102.5°C IR ν_{max} (neat) /cm^{-1} ^{1}H-NMR (400 MHz, MeOD) δ_H ppm: 2.17 (3*H*, s) 7.30 (6H, m), 7.38 (14*H*, m), 7.48-7.47 (15H, m, overlap), 7.69-7.67 (8H, m, overlap), 9.68 (1*H*, s), 10.33 (1*H*, s); ^{13}C-NMR (100 MHz, MeOD) δ_C ppm: 196.18 (Ar*C*), 195.37 (Ar*C*), 164.94 (Ar*C*), 163.24 (Ar*C*), 134.30 (Ar*C*), 133.04 (Ar*C*), 132.77 (Ar*C*), 131.30 (Ar*C*H), 130.89 (Ar*C*H), 130.14 (Ar*C*H), 129.42 (Ar*C*), 128.92 (CHH), 127.94 (Ar*C*H), 127.50 (Ar*C*H), 120.64 (Ar*C*H), 115.73 (Ar*C*), 113.28 (Ar*C*), 108.93 (Ar*C*), 54.81 (Ar*C*), 7.31 (*C*H$_3$) HRMS (AP+) calculated for $C_{20}H_5O_3$ $(M+H)^+$ found 303.1016 m/z

N-2-(bromophenyl)acetamide (C16)

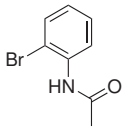

2-bromoaniline (2 g, 131.6 μL, 11.70 mmol) and acetic anhydride (2.62 g, 2.44 mLs, 25.74 mmol) were added together at 0°C and underwent an instantaneous reaction. The solid was dissolved in ethyl acetate, washed with saturated sodium hydrogen carbonate, dried over magnesium sulphate, filtered and concentrated *in vacuo*. The yield of pale orange solid was quantitative (2.50 g). ^{1}H-NMR (400 MHz, $CDCl_3$) δ_H ppm: 2.24 (3*H*, s), 6.97 (1*H*, m), 7.31 (1*H*, t, $J = 14.87$ Hz), 7.53 (1*H*, d, $J = 6.99$ Hz), 7.62 (1*H*, s), 8.31 (1*H*, s); ^{13}C-NMR (100 MHz, $CDCl_3$) δ_H ppm: 168.39 (C=O), 135.65 (Ar*C*), 132.22 (Ar*C*), 128.40 (Ar*C*H), 125.24 (Ar*C*H), 122.02 (Ar*C*H), 113.27 (*C*H), 24.84 (*C*H), 20.64 (*C*H_3).

N-2-[2-(2-formyl-3,5-dihydroxy-4-methylphenyl)ethynyl]phenylacetamide (C17)

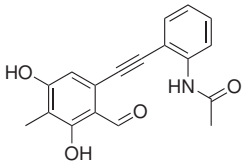

6-ethynyl-2,4-dihydroxy-3-methylbenzaldehyde (95 mg, 0.528 mmol), $Pd(PPh_3)_4$ (31 mg, 0.03 mmol), CuI (5 mg, 0.03 mmol), 2-bromoacetamide (231 mg, 1.079 mmol) anhydrous THF (978 μL) and triethylamine (150 μL) was stirred at 50°C under nitrogen for 3 h. The resulting mixture was diluted with ethyl acetate, and neutralised using 1M aqueous HCl. The mixture was then extracted using ethyl acetate and the organic phases were washed with brine. The organic phases were dried over magnesium sulphate, filtered and concentrated in vacuo. Purification on silica (1:9 Ethyl Acetate:Hexane to 4:6 Ethyl Acetate:Hexane) afforded 66 mg (40%) as a yellow solid ^{1}H-NMR (400 MHz, $CDCl_3$) δ_H ppm: 2.14 (3*H*, s), 6.74 (1*H*, s), 7.47 (6H, m, overlap), 7.54 (2*H*, m), 7.66 (5H, m, overlap), 10.28 (1*H*, s), 12.28 (1*H*, s); ^{13}C-NMR (100 MHz, $CDCl_3$) δ_H ppm: 171.24 (*C*OH), 132.35 (Ar*C*), 132.13 (Ar*C*H), 132.03 (Ar*C*H), 130.41 (Ar*C*H), 128.77 (Ar*C*H), 128.65 (Ar*C*), 60.43 (*C*H), 31.59 (*C*H), 29.06 (*C*H), 27.67 (*C*H), 25.28 (*C*H), 22.56 (*C*H), 22.62 (*C*H), 14.26 (*C*H_3), 14.12 (*C*H_3).

2,4-dihydroxy-3-methyl-6-2-[3-(trifluoromethyl)phenyl]ethynylbenzaldehyde (C18)

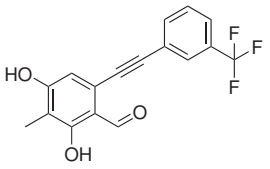

6-ethynyl-2,4-dihydroxy-3-methylbenzaldehyde (200 mg, 1.112 mmol), $Pd(PPh_3)_4$ (66 mg, 0.06 mmol), CuI (10 mg, 0.06 mmol), 3-bromobenzotrifluoride (511 mg, 2.272 mmol, 317 μL) anhydrous THF (2.06 mL) and triethylamine (316 μL) was stirred at 50°C under nitrogen for 2.5 h. The resulting mixture was diluted with ethyl acetate, and neutralised using 1M aqueous HCl. The mixture was then extracted using ethyl acetate and the organic phases were washed with brine. The organic phases were dried over magnesium sulphate, filtered and concentrated in vacuo. Purification on silica (1:9 Ethyl Acetate:Hexane to 4:6 Ethyl Acetate:Hexane) afforded 180 mg (50% yield) as a yellow solid. Mp 179-180°C IR ν_{max} (neat) /cm^{-1} 3083.10 (O-H), ^{1}H-NMR (400 MHz, $CDCl_3$) δ_H ppm: 2.13 (1*H*, s), 7.34 (1*H*, m), 7.48 (4*H*, m), 7.65 (4*H*, m), 7.74 (1*H*,brm), 10.27 (1*H*, s), 12.29 (1*H*, s); ^{13}C-NMR (100 MHz, MeOD) δ_C ppm: 195.42 (*C*OH), 146.17 (Ar*C*), 136.20 (Ar*C*), 131.31 (Ar*C*H), 130.75 (Ar*C*H), 129.94 (Ar*C*H), 129.17 (Ar*C*H), 126.65 (Ar*C*H), 126.43 (Ar*C*), 124.79 (Ar*C*), 114.52 (Ar*C*), 113.54 (Ar*C*), 93.90 (Ar*C*), 87.09 (Ar*C*), 32.76 (*C*H), 7.53 (*C*H$_3$) ppm: HRMS (AP+) calculated for $C_{17}H_{12}O_3F_3$ $(M+H)^+$ found 321.0733 m/z

6.6.4 Formation of the dipeptide

Fmoc-Orn(Boc)-Thr-OBzl (C19)

Fmoc-Orn(Boc)-OH (1.5 g, 3.3 mmol), L-Thr-OBn.Oxalate (1.793 g, 5.78 mmol), HOBt·2.5H$_2$O (1.52 g, 9.89 mmol) and EDCI (1.89 g, 9.89 mmol) were purged with N_2, then dissolved in dry DMF (13.42 mL) and stirred under N2 at room temperature overnight. The mixture was extracted three times using ethyl acetate (3 x 10 mL) and the organic portions were washed with 1M HCl, saturated sodium hydrogen carbonate, water and brine. The organic extracts were dried over magnesium sulphate, filtered and concentrated in vacuo. Purification on silica (10% EtOAc in Hexane 100% EtOAc) afforded 1.38 g (65% yield) of yellow foam. ^{1}H-NMR (400 MHz, $CDCl_3$) δH ppm: 1.09 (3*H*, d, $J = 7.89$ Hz), 1.33 (5H, brs), 1.44 (1*H*, t, $J = 14.20$ Hz), 1.57 (1*H*, s), 1.79 (1*H*, brs), 1.95 (9H, s), 4.04 (1*H*, m), 4.30 (3*H*, m), 4.55 (1*H*, dd, $J = 9.02$ Hz), 4.78 (1*H*, brs), 5.05 (1*H*, q, $J = 38.32$ Hz), 5.89 (1*H*, d, $J = 11.27$ Hz), 7.22 (7H, brm), 7.28 (2*H*, t, $J = 14.22$ Hz), 7.48 (1*H*, brm), 7.64 (2*H*, d, $J = 8.13$ Hz); ^{13}C-NMR (100 MHz, $CDCl_3$) δ_H ppm: 207.08 (Ar*C*), 170.60 (Ar*C*), 156.50 (Ar*C*), 143.71 ((Ar*C*)$_2$), 141.28 ((Ar*C*)$_2$), 135.19

((ArCH)$_2$), 128.61 ((ArCH)$_2$), 128.23 ((ArCH)$_2$), 127.71 (ArCH), 127.08 ((ArCH)$_2$), 119.95 ((ArCH)$_2$), 79.40 (CH), 67.38 (CH), 60.41 (CH), 57.72 (CH$_2$), 47.09 (CH$_2$), 39.56 (CH$_2$), 30.93 (CH$_2$), 28.42 (CH$_2$), 20.08 (CH$_2$), 14.20 (CH$_3$)$_3$. $[\alpha_D]^{18.8}$ = -3.958. HRMS (AP+) calculated for $C_{36}H_{44}N_3O_8$ $(M+H)^+$ 646.3126 found 646.3123 m/z

Fmoc-Orn-Thr-OBzl (C20)

Fmoc-Orn(Boc)-Thr-OBn (56 mg, 0.086 mmol) was stirred in 1M HCl in Ethyl Acetate (30 mL) for 1.5 days. The product was then concentrated in vacuo, affording 30 mg (60% yield) of yellow foam. ^{1}H-NMR (400 MHz, MeOD) δ_H ppm: 1.23 (4H, m), 1.45 (4H, d, J = 4.86 Hz), 1.80 (5H, brm), 3.00 (2H, brs), 3.33 (1H, s), 4.31 (2H, d, J = 28.35 Hz), 4.36 (2H, s), 5.23 (2H, s), 5.56 (1H, s), 7.22 (7H, brm), 7.28 (9H, brm), 7.65 (2H, brm), 7.78 (3H, brm); ^{13}C-NMR (100 MHz, MeOD) δ_H ppm: 175.29 (ArC), 172.20 (ArC), 168.01 (ArC), 158.68 (ArC), 145.27 ((ArC)$_2$), 145.14((ArC)$_2$), 142.60 ((ArCH)$_2$), 129.85 ((ArCH)$_2$), 129.69 ((ArCH)$_2$), 128.90 ((ArCH)$_2$), 128.28 ((ArCH)$_2$), 126.29 ((ArCH)$_2$), 121.05 (ArCH), 69.93 (CH), 68.24 (CH), 61.62 (CH), 57.73 (CH$_2$), 54.91 (CH$_2$), 40.32 (CH$_2$), 29.02 (CH$_2$), 25.12 (CH$_2$), 21.00 (CH$_2$), 17.26 (CH$_2$), 14.60 (CH$_3$). $[\alpha_D]^{23}$ = -13.58. HRMS (ES+) calculated for $C_{31}H_{36}N_3O_6$ $(M+H)^+$ 546.2954 found 546.2599 m/z

Appendix A

Proton NMR of Compound A34 in PBS with 10% DMSO

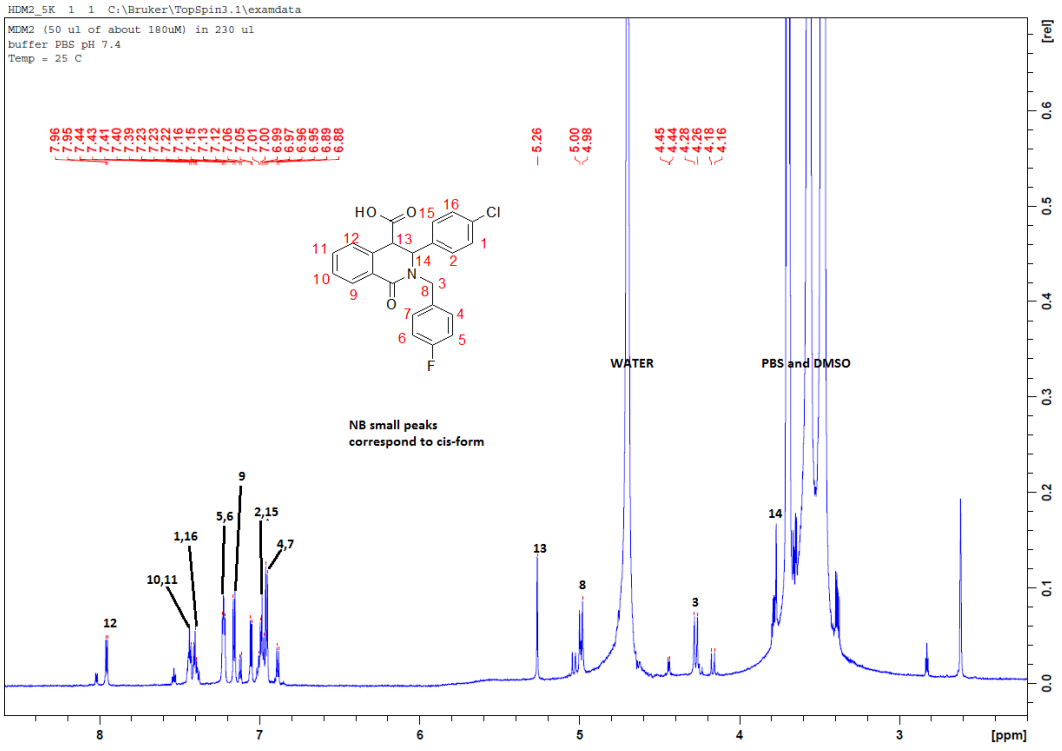

Appendix B

COSY NMR of Compound A34

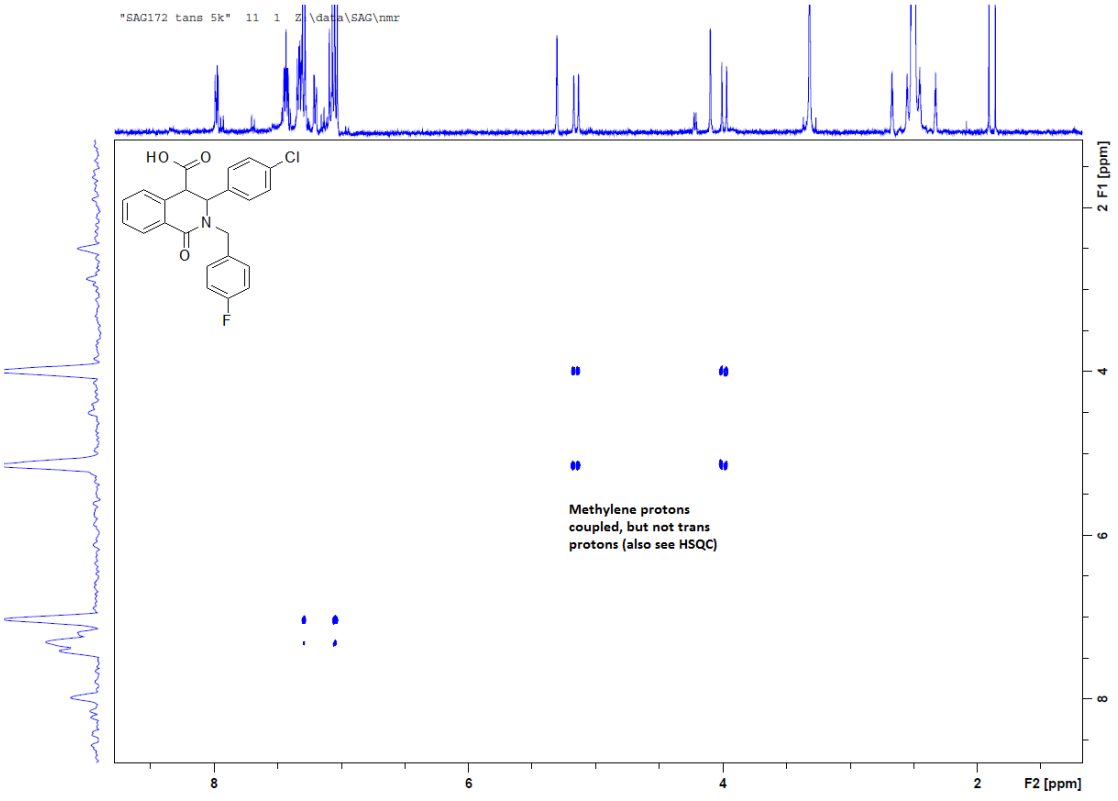

Appendix C

HSQC NMR of Compound A34

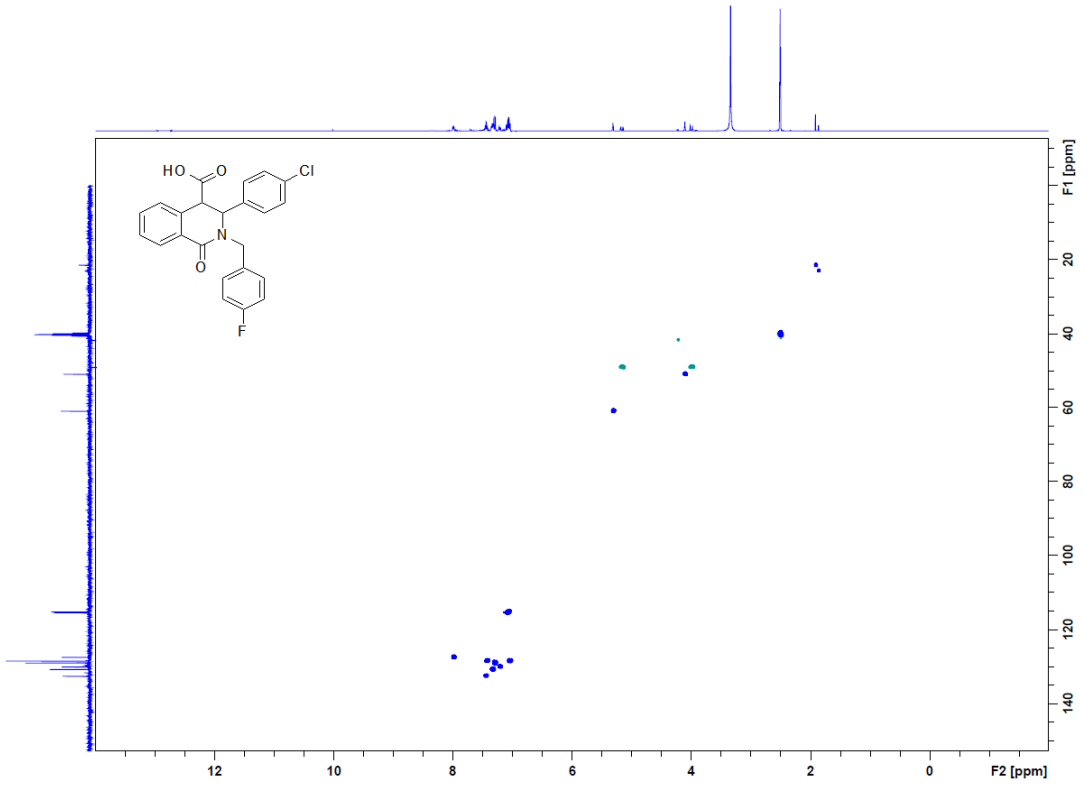

Appendix D

Carbon-13 NMR of Compound A34

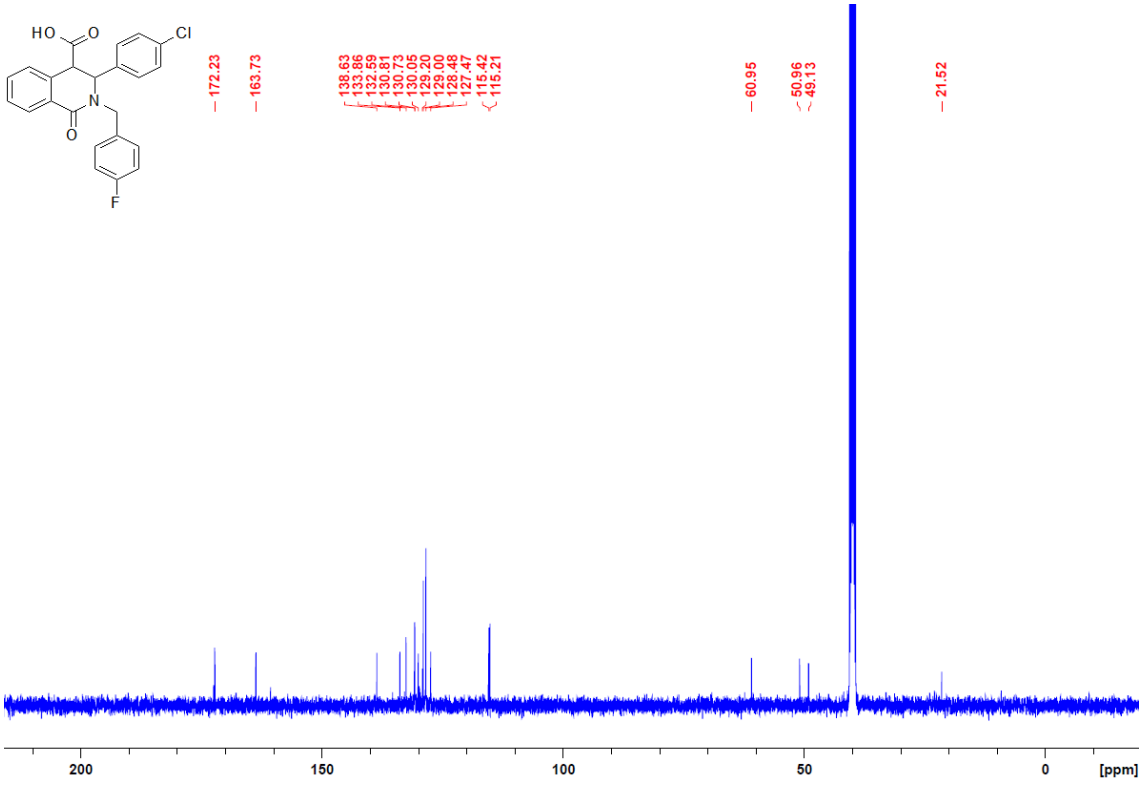

Bibliography

[1] Thanos D Halazonetis, Vassilis G Gorgoulis, and Jiri Bartek. An oncogene-induced dna damage model for cancer development. *science*, 319(5868):1352–1355, 2008.

[2] C. J. Hawthorn, K. P. Weber, and R. E. Scholten. Cancer incidence and mortality worldwide: Iarc cancerbase no. 11. *International Agency for Research on Cancer [Internet]*, page Accessed on 10.09.2014, Accessed on 19.09.2014 2012.

[3] M. P. Coleman, B. Rachet, Y. Alencar, R. Abrahao, J. Ahn, C. Allemani, A. Belot, S. Majano, A. Bonaventure, H. Carreira, L. Ellis, A. Exarchakou, H. Fowler, R. Harewood, J. Jegu, T. Lewis, R. Li, C. Maringe, M. Matz, M. Morris, P. Muller, M. Quaresma U. Nur, R. Schaffar N. Sanz, D. Spika T. Solomon, A. D. Turculet, and L. Woods. Uk cancer survival rates 2011, cancer research uk cancer survival group, london school of hygiene and tropical medicine. *UK Cancer Survival Rates 2011, Cancer Research UK Cancer Survival Group*, March 2014.

[4] J. Rashbass, D. W. Huws, D. Brewster, and A. Gavin. Cancer statistics registration, england (series mb1). *Office of National Statistics*, June 2013.

[5] P. C. Adamson, S. M. Blaney, and M. Devidas. Cancer statistics registration, england (series mb1). *Childhood Cancer Registrations, Great Britain, 2006 to 2008 [Internet]*, page Accessed on 10.09.2014, June 2013.

[6] J. E. Joy, E. E. Penhoet, and D. B. Petitti. Saving women's lives: Strategies for improving breast cancer detection and diagnosis. *Institute of Medicine (US) and National Research Council (US) Committee on New Approaches to Early Detection and Diagnosis of Breast Cancer*, page Accessed on 08.08.15, Accessed on 19.09.2014 2005.

[7] R. Peto, A. D. Lopez, J. Boreham, and M. Thun. Mortality from smoking in developed countries. *Clinical Trials Unit [Internet]*, page Accessed on 18.02.2014, June 2013.

[8] J. Rashbass, D. W. Huws, D. Brewster, and A. Gavin. Do smoking rates vary between more and less advantaged areas? *Office for National Statistics [Internet]*, page Accessed on 01.04.2014, June 2012.

[9] D. M. Parkin. Cancers attributable to consumption of alcohol in the uk in 2010. *British Journal of Cancer*, 105:S14–S18, 2011.

[10] D. M. Parkin, D. Mesher, and P. Sasieni. Cancers attributable to solar (ultraviolet) radiation exposure in the uk in 2010. *British Journal of Cancer*, 105:S66–S69, 2011.

[11] D. M. Parkin and S. C. Darby. Cancers in 2010 attributable to ionising radiation exposure in the uk. *British Journal of Cancer*, 105:S57–S65, 2011.

[12] D. M. Parkin. Cancers attributable to infection in the uk in 2010. *British Journal of Cancer*, 105:S49–S56, 2011.

[13] A. Murray, T. Lourenco, R. De Verteuil, R. Hernandez, C. Fraser, A. McKinley, Z. Krukowski, L. Vale, and A Grant. Clinical effectiveness and cost-effectiveness of laparoscopic surgery for colorectal cancer: Systematic reviews and economic evaluation. *Health Technology Assessments*, 10:1–141, 2006.

[14] G. Delaney, S. Jacob, C. Featherstone, and M. Barton. The role of radiotherapy in cancer treatment. *Cancer*, 104(6):1129–1137, 2005.

[15] R. Peto, C. Davies, J. Godwin, R. Gray, H. C. Pan, M. Clarke, D. Cutter, S. Darby, P. McGale, C. Taylor, Y. C. Wang, J. Bergh, A. Di Leo, K. Albain, S. Swain, M. Piccart, and K. Pritchard. Effects of chemotherapy and hormonal therapy for early breast cancer on recurrence and 15-year survival: an overview of the randomised trials. *The Lancet*, 365(9472):1687–1717, 2005.

[16] Vladimir A Botchkarev, Elena A Komarova, Frank Siebenhaar, Natalia V Botchkareva, Pavel G Komarov, Marcus Maurer, Barbara A Gilchrest, and Andrei V Gudkov. p53 is essential for chemotherapy-induced hair loss. *Cancer Research*, 60(18):5002–5006, 2000.

[17] Shulin Wang and Wafik S El-Deiry. The p53 pathway: Targets for the development of novel cancer therapeutics. In *Molecular Targeting and Signal Transduction*, pages 175–181. Springer, 2004.

[18] C. Main, L. Bojke, S. Griffin, G. Norman, M. Barbieri, L. Mather, D. Stark, S. Palmer, and R. Riemsma. Topotecan, pegylated liposomal doxorubicin hydrochloride and paclitaxel for second-line or subsequent treatment of advanced ovarian cancer: a systematic review and economic evaluation. *Health Technology Assessments*, 10(9):1–132, 2006.

[19] Brian J Druker. Sti571 (gleevec) as a paradigm for cancer therapy. *Trends in molecular medicine*, 8(4):S14–S18, 2002.

[20] P. W. Manley, S. W. Cowan-Jacob, E. Buchdunger, D. Fabbro, G. Fendrich, P. Furet, T. Meyer, and J. Zimmermann. Imatinib: a selective tyrosine kinase inhibitor. *European Journal of Cancer*, 38:S19–S27, 2002.

[21] L. Jin, W. Wang, and G. Fang. Targeting protein-protein interaction by small molecules. *Annual Review of Pharmacology and Toxicology*, 54:435–456, 2014.

[22] E. Kansanen, S. M. Kuosmanen, H. Leinonen, and A.-L. Levonen. The keap1-nrf2 pathway: Mechanisms of activation and dysregulation in cancer. *Redox Biology*, 1(1):45 – 49, 2013.

[23] Michelle Aarts, Yitao Liu, Lidong Liu, Shintaro Besshoh, Mark Arundine, James W Gurd, Yu-Tian Wang, Michael W Salter, and Michael Tymianski. Treatment of ischemic brain damage by perturbing nmda receptor-psd-95 protein interactions. *Science*, 298(5594):846–850, 2002.

[24] J. A. Wells and C. L. McClendon. Reaching for high-hanging fruit in drug discovery at protein-protein interfaces. *Nature*, 450(7172):1001–1009, 2007.

[25] S. N. Willis, L. Chen, G. Dewson, A. Wei, E. Naik, J. I. Fletcher, J. M. Adams, and D. C. S. Huang. Proapoptotic bak is sequestered by mcl-1 and bcl-xl, but not bcl-2, until displaced by bh3-only proteins. *Genes & Development*, 19(11):1294–1305, 2005.

[26] M. F. van Delft, A. H. Wei, K. D. Mason, C. J. Vandenberg, L. Chen, P. E. Czabotar, S. N. Willis, C. L. Scott, C. L. Day, and S. Cory. The bh3 mimetic abt-737 targets selective bcl-2 proteins and efficiently induces apoptosis via bak/bax if mcl-1 is neutralized. *Cancer cell*, 10(5):389–399, 2006.

[27] A. Strasser. The role of bh3-only proteins in the immune system. *Nature Reviews Immunology*, 5(3):189–200, 2005.

[28] P. Zhou, L. Qian, K. M. Kozopas, and R. W. Craig. Mcl-1, a bcl-2 family member, delays the death of hematopoietic cells under a variety of apoptosis-inducing conditions. *Blood*, 89(2):630–643, 1997.

[29] S. Acoca, Q. Cui, G. C. Shore, and E. O. Purisima. Molecular dynamics study of small molecule inhibitors of the bcl-2 family. *Proteins: Structure, Function, and Bioinformatics*, 79(9):2624–2636, 2011.

[30] WW Westerfeld, Dan A Richert, and Edwin S Higgins. The metabolic reduction of organic nitro groups. *Journal of Biological Chemistry*, 227(1):379–391, 1957.

[31] Urs A Boelsterli, Han K Ho, Shufeng Zhou, and Koon Yeow Leow. Bioactivation and hepatotoxicity of nitroaromatic drugs. *Current drug metabolism*, 7(7):715–727, 2006.

[32] C. Tse, A. R. Shoemaker, J. Adickes, M. G. Anderson, J. Chen, S. Jin, E. F. Johnson, K. C. Marsh, M. J. Mitten, and P. Nimmer. Abt-263: a potent and orally bioavailable bcl-2 family inhibitor. *Cancer Research*, 68(9):3421–3428, 2008.

[33] Matthew S Davids and Anthony Letai. Abt-199: Taking dead aim at bcl-2. *Cancer cell*, 23(2):139–141, 2013.

[34] A. J. Souers, J. D. Leverson, E. R. Boghaert, S. L. Ackler, N. D. Catron, J. Chen, B. D. Dayton, H. Ding, S. H. Enschede, and W. J. Fairbrother. Abt-199, a potent and selective bcl-2 inhibitor, achieves antitumor activity while sparing platelets. *Nature Medicine*, 19(2):202–208, 2013.

[35] Mai Nguyen, Richard C Marcellus, Anne Roulston, Mark Watson, Lucile Serfass, SR Murthy Madiraju, Daniel Goulet, Jean Viallet, Laurent Bélec, Xavier Billot, et al. Small molecule obatoclax (gx15-070) antagonizes mcl-1 and overcomes mcl-1-mediated resistance to apoptosis. *Proceedings of the National Academy of Sciences*, 104(49):19512–19517, 2007.

[36] E. Kansanen, S. M. Kuosmanen, H. Leinonen, and A.-L. Levonen. The keap1-nrf2 pathway: Mechanisms of activation and dysregulation in cancer. *Redox Biology*, 1(1):45–49, 2013.

[37] Anju Singh, Vikas Misra, Rajesh K Thimmulappa, Hannah Lee, Stephen Ames, Mohammad O Hoque, James G Herman, Stephen B Baylin, David Sidransky, Edward Gabrielson, et al. Dysfunctional keap1-nrf2 interaction in non-small-cell lung cancer. *PLoS Med*, 3(10):e420, 2006.

[38] Thomas W Kensler, Nobunao Wakabayashi, and Shyam Biswal. Cell survival responses to environmental stresses via the keap1-nrf2-are pathway. *Annual Reviews of Pharmacology and Toxicology*, 47:89–116, 2007.

[39] Ken Itoh, Nobunao Wakabayashi, Yasutake Katoh, Tetsuro Ishii, Kazuhiko Igarashi, James Douglas Engel, and Masayuki Yamamoto. Keap1 represses nuclear activation of antioxidant responsive elements by nrf2 through binding to the amino-terminal neh2 domain. *Genes & Development*, 13(1):76–86, 1999.

[40] H. Motohashi and M. Yamamoto. Nrf2-keap1 defines a physiologically important stress response mechanism. *Trends in Molecular Medicine*, 10(11):549–557, 2004.

[41] R. J. Steel, J. Cowan, E. Payerne, M. A. O'Connell, and M. Searcey. Anti-inflammatory effect of a cell-penetrating peptide targeting the nrf2/keap1 interaction. *ACS Medicinal Chemistry Letters*, 3(5):407–410, 2012.

[42] L. Hu, S. Magesh, L. Chen, L. Wang, T. A. Lewis, Y. Chen, C. Khodier, D. Inoyama, L. J. Beamer, and T. J. Emge. Discovery of a small-molecule inhibitor and cellular probe of keap1-nrf2 protein-protein interaction. *Bioorganic & Medicinal Chemistry Letters*, 23(10):3039–3043, 2013.

[43] D. Marcotte, W. Zeng, J.-C. Hus, A. McKenzie, C. Hession, P. Jin, C. Bergeron, A. Lugovskoy, I. Enyedy, and H. Cuervo. Small molecules inhibit the interaction of nrf2 and the keap1 kelch domain through a non-covalent mechanism. *Bioorganic & Medicinal Chemistry*, 21(14):4011–4019, 2013.

[44] Z.-Y. Jiang, M.-C. Lu, Li-Li Xu, T.-T. Yang, M.-Y. Xi, X.-L. Xu, X.-K. Guo, X.-J. Zhang, Q.-D. You, and H.-P. Sun. Discovery of potent keap1-nrf2 protein-protein interaction inhibitor based on molecular binding determinants analysis. *Journal of Medicinal Chemistry*, 57(6):2736–2745, 2014.

[45] K. K. Hoe, C. S. Verma, and D. P. Lane. Drugging the p53 pathway: Understanding the route to clinical efficacy. *Nature Reviews Drug Discovery*, 13(3):217–236, 2014.

[46] U. M. Moll and O. Petrenko. The mdm2-p53 interaction. *Molecular Cancer Research*, 1:1001–1008, 2003.

[47] D. P. Lane. p53, guardian of the genome. *Nature*, 358(6381):15–16, 1992.

[48] D. Michael and M. Oren. The p53-mdm2 module and the ubiquitin system. In *Seminars in Cancer Biology*, volume 13, pages 49–58. Elsevier, 2003.

[49] R. K. Geyer, K. Y. Zhong, and C. G. Maki. The mdm2 ring-finger domain is required to promote p53 nuclear export. *Nature Cell Biology*, 2(9):569–573, 2000.

[50] B. Vogelstein, D. Lane, and A. J. Levine. Surfing the p53 network. *Nature*, 408(6810):307–310, 2000.

[51] A. Villunger, E. M. Michalak, L. Coultas, F. Müllauer, G. Böck, M. J. Ausserlechner, J. M. Adams, and A. Strasser. p53- and Drug-Induced Apoptotic Responses Mediated by BH3-Only Proteins Puma and Noxa. *Science*, 302:1036–1038, 2003.

[52] M. F. van Delft, A. H. Wei, K. D. Mason, C. J. Vandenberg, L. Chen, P. E. Czabotar, S. N. Willis, C. L. Scott, C. L. Day, S. Cory, J. M. Adams, A. W. Roberts, and D. C. S. Huang. The BH3 Mimetic ABT-737 Targets Selective Bcl2 Proteins and Efficiently Induces Apoptosis via Bak/Bax if Mcl-1 is Neutralized. *Cancer Cell*, 10:389–399, 2006.

[53] E. Oda, R. Ohki, H. Murasawa, J. Nemoto, T. Shibue, T. Yamashita, T. Tokino, T. Taniguchi, and N. Tanaka. Noxa, a bh3-only member of the bcl-2 family and candidate mediator of p53-induced apoptosis. *Science*, 288(5468):1053–1058, 2000.

[54] A. Lujambio, L. Akkari, J. Simon, D. Grace, D. F. Tschaharganeh, J. E. Bolden, Z. Zhao, V. Thapar, J. A. Joyce, V. Krizhanovsky, and S. W. Lowe. Non-cell-autonomous tumor suppression by p53. *Cell*, 153(2):449 – 460, 2013.

[55] C. Deng, P. Zhang, J. Wade, S. J. Elledge, and P. Leder. Mice lacking p21cip1/waf1 undergo normal development, but are defective in {G1} checkpoint control. *Cell*, 82(4):675 – 684, 1995.

[56] Y. Samuels-Lev, D. J. O'Connor, D. Bergamaschi, G. Trigiante, J.-K. Hsieh, S. Zhong, I. Campargue, L. Naumovski, T. Crook, and X. Lu. {ASPP} proteins specifically stimulate the apoptotic function of p53. *Molecular Cell*, 8(4):781 – 794, 2001.

[57] D. Bergamaschi, Y. Samuels, A. Sullivan, M. Zvelebil, H. Breyssens, A. Bisso, G. Del Sal, N. Syed, P. Smith, M. Gasco, T. Crook, and X. Lu. iASPP Preferentially Binds p53 Proline-Rich Region and Modulates Apoptotic Function of Codon 72Polymorphic p53. *Nature Genetics*, 38:1133–1141, 2006.

[58] Min Lu, Hilde Breyssens, Victoria Salter, Shan Zhong, Ying Hu, Caroline Baer, Indrika Ratnayaka, Alex Sullivan, Nicholas R Brown, Jane Endicott, et al. Restoring p53 function in human melanoma cells by inhibiting mdm2 and cyclin b1/cdk1-phosphorylated nuclear iaspp. *Cancer Cell*, 23(5):618–633, 2013.

[59] W. Tao and A. J. Levine. P19ARF Stabilizes p53 by Blocking Nucleo-Cytoplasmic Shuttling of Mdm2. *Proceedings of The National Academy of Sciences*, 96:6937–6941, 1999.

[60] C. M. Eischen, J. D. Weber, M. F. Roussel, C. J. Sherr, and J. L. Cleveland. Disruption of the ARF-Mdm2-p53 Tumor Suppressor Pathway in Myc-induced lymphomagenesis. *Genes & Development*, 13:2658–2669, 1999.

[61] J. Liu and A. Gregg. USP1 Deubiquitinates ID Proteins to Preserve a Mesenchymal Stem Cell Program in Osteosarcoma. *Cell*, 146:918–930, 2011.

[62] Y. Levav-Cohen, Z. Goldberg, V. Zuckerman, T. Grossman, S. Haupt, and Y. Haupt. C-abl as a modulator of p53. *Biochemical and Biophysical Research Communications*, 331(3):737 – 749, 2005. p53 in Apoptosis Control.

[63] K. Schlereth, J. P. Charles, A. C. Bretz, and T. Stiewe. Life or Death: p53-Induced Apoptosis Requires DNA Binding Cooperativity. *Cell Cycle*, 9:4068–4076, 2010.

[64] C. J. Sherr and J. D. Weber. The ARF/p53 Pathway. *Current Opinion in Genetics & Development*, 10:94–99, 2000.

[65] L. Castéra, A. Sabbagh, C. Dehainault, D. Michaux, A. Mansuet-Lupo, B. Patillon, E. Lamar, I. Aerts, L. Lumbroso-Le Rouic, and J. Couturier. Mdm2 as a modifier gene in retinoblastoma. *Journal of the National Cancer Institute*, 102(23):1805–1808, 2010.

[66] C. Uchida, S. Miwa, K. Kitagawa, T. Hattori, T. Isobe, S. Otani, T. Oda, H. Sugimura, T. Kamijo, and K. Ookawa. Enhanced mdm2 activity inhibits prb function via ubiquitin-dependent degradation. *The EMBO Journal*, 24(1):160–169, 2005.

[67] J. W. Schneider, W. Gu, L. Zhu, V. Mahdavi, and B. Nadal-Ginard. Reversal of terminal differentiation mediated by p107 in rb-/-muscle cells. *Science*, 264(5164):1467–1471, 1994.

[68] H. N. Rajabi, C. Takahashi, and M. E. Ewen. Retinoblastoma protein and myod function together to effect the repression of fra-1 and in turn cyclin d1 during terminal cell cycle arrest associated with myogenesis. *Journal of Biological Chemistry*, 289(34):23417–23427, 2014.

[69] Z. Zhang, H. Wang, M. Li, E. R. Rayburn, S. Agrawal, and R. Zhang. Stabilization of e2f1 protein by mdm2 through the e2f1 ubiquitination pathway. *Oncogene*, 24(48):7238–7247, 2005.

[70] C. Stevens, S. Pettersson, B. Wawrzynow, M. Wallace, K. Ball, A. Zylicz, and T. R. Hupp. Atp stimulates mdm2-mediated inhibition of the dna-binding function of e2f1. *FEBS Journal*, 275(19):4875–4886, 2008.

[71] M. Wunderlich and S. J. Berberich. Mdm2 Inhibition of p53 Induces E2F1 Transactivation via p21. *Oncogene*, 21:4414–4421, 2002.

[72] M. Irwin, M. C. Marin, A. C. Phillips, R. S. Seelan, D. I. Smith, W. Liu, E. R. Flores, K. Y. Tsai, T. Jacks, and K. H. Vousden. Role for the p53 homologue p73 in e2f-1-induced apoptosis. *Nature*, 407(6804):645–648, 2000.

[73] L. T. Vassilev, B. T. Vu, B. Graves, D. Carvajal, F. Podlaski, Z. Filipovic, N. Kong, U. Kammlott, C. Lukacs, and C. Klein. In vivo activation of the p53 pathway by small-molecule antagonists of mdm2. *Science*, 303(5659):844–848, 2004.

[74] D. Sun, Z. Li, Y. Rew, M. Gribble, M. D. Bartberger, H. P. Beck, J. Canon, A. Chen, X. Chen, and D. Chow. Discovery of amg 232, a potent, selective, and orally bioavailable mdm2-p53 inhibitor in clinical development. *Journal of Medicinal Chemistry*, 57(4):1454–1472, 2014.

[75] Priyabrata Pattnaik. Surface plasmon resonance. *Applied Biochemistry and Biotechnology*, 126(2):79–92, 2005.

[76] W. A. Lea and A. Simeonov. Fluorescence polarization assays in small molecule screening. *Expert Opinion on Drug Discovery*, 6(1):17–32, 2011.

[77] E. C. Y. Woon, M. Arcieri, A. F. Wilderspin, J. P. Malkinson, and M. Searcey. Solid-phase synthesis of chlorofusin analogues. *The Journal of Organic Chemistry*, 72(14):5146–5151, 2007.

[78] M. Pazgier, M. Liu, G. Zou, W. Yuan, C. Li, C. Li, J. Li, J. Monbo, D. Zella, S. G. Tarasov, and W. Lu. Structural Basis for High-Affinity Peptide Inhibition of p53 Interactions with MDM2 and MDMX. *Proceedings of The National Academy of Sciences*, 106:4665–4670, 2009.

[79] Marzena Pazgier, Min Liu, Guozhang Zou, Weirong Yuan, Changqing Li, Chong Li, Jing Li, Juahdi Monbo, Davide Zella, Sergey G Tarasov, et al. Structural basis for high-affinity peptide inhibition of p53 interactions with mdm2 and mdmx. *Proceedings of the National Academy of Sciences*, 106(12):4665–4670, 2009.

[80] B. J. Stähelin, U. Marti, M. Solioz, H. Zimmermann, and J. Reichen. False positive staining in the tunel assay to detect apoptosis in liver and intestine is caused by endogenous nucleases and inhibited by diethyl pyrocarbonate. *Molecular Pathology*, 51(4):204, 1998.

[81] Burcu Anil, Christiane Riedinger, Jane A Endicott, and Martin EM Noble. The structure of an mdm2-nutlin-3a complex solved by the use of a validated mdm2 surface-entropy reduction mutant. *Acta Crystallographica Section D: Biological Crystallography*, 69(8):1358–1366, 2013.

[82] H. Wang, X. Ma, S. Ren, J. K. Buolamwini, and C. Yan. A small-molecule inhibitor of mdmx activates p53 and induces apoptosis. *Molecular Cancer Therapeutics*, 10(1):69–79, 2011.

[83] C. Tovar, B. Graves, K. Packman, Z. Filipovic, B. Xia, M. Higgins, C. Tardell, R. Garrido, E. Lee, K. Kolinsky, and K.-H. To. Mdm2 small-molecule antagonist rg7112 activates p53 signalling and regresses human tumors in preclinical cancer models. *Cancer Research*, 73(8):2587–2597, 2013.

[84] B. Vu, P. Wovkulich, G. Pizzolato, A. Lovey, Q. Ding, N. Jiang, J.-J. Liu, C. Zhao, K. Glenn, and Y. Wen. Discovery of rg7112: a small-molecule mdm2 inhibitor in clinical development. *ACS Medicinal Chemistry Letters*, 4(5):466–469, 2013.

[85] S. J. Wei, T. Joseph, A. Y. L. Sim, L. Yurlova, K. Zolghadr, D. Lane, C. Verma, and F. Ghadessy. In vitro selection of mutant hdm2 resistant to nutlin inhibition. *PloS One*, 8(4):e62564, 2013.

[86] J.-S. Shin, J.-H. Ha, F. He, Y. Muto, K.-S. Ryu, H. S. Yoon, S. Kang, S. G. Park, B. C. Park, and S.-U. Choi. Structural insights into the dual-targeting mechanism of nutlin-3. *Biochemical and Biophysical Research Communications*, 420(1):48–53, 2012.

[87] K. Ding, Y. Lu, Z. Nikolovska-Coleska, G. Wang, S. Qiu, S. Shangary, W. Gao, D. Qin, J. Stuckey, and K. Krajewski. Structure-based design of spiro-oxindoles as potent, specific small-molecule inhibitors of the mdm2-p53 interaction. *Journal of Medicinal Chemistry*, 49(12):3432–3435, 2006.

[88] B. Yu, D.-Q. Yu, and H.-M. Liu. Spirooxindoles: Promising scaffolds for anticancer agents. *European Journal of Medicinal Chemistry*, pages 1–26, 2014.

[89] Y. Zhao, S. Yu, W. Sun, L. Liu, J. Lu, D. McEachern, S. Shargary, D. Bernard, X. Li, and T. Zhao. A potent small-molecule inhibitor of the mdm2-p53 interaction (mi-888) achieved complete and durable tumor regression in mice. *Journal of Medicinal Chemistry*, 56(13):5553–5561, 2013.

[90] A. M. Sosin, A. M. Burger, A. Siddiqi, J. Abrams, R. M. Mohammad, and A. M. Al-Katib. Hdm2 antagonist mi-219 (spiro-oxindole), but not nutlin-3 (cis-imidazoline), regulates p53 through enhanced hdm2 autoubiquitination and degradation in human malignant b-cell lymphomas. *J Hematol Oncol*, 5(57):1756–8722, 2012.

[91] M. Rottmann, C. McNamara, B. K. S. Yeung, M. C. S. Lee, B. Zou, B. Russell, P. Seitz, D. M. Plouffe, N. V. Dharia, and J. Tan. Spiroindolones, a potent compound class for the treatment of malaria. *Science*, 329(5996):1175–1180, 2010.

[92] Q. Ding, Z. Zhang, J.-J. Liu, N. Jiang, J. Zhang, T. M. Ross, X.-J. Chu, D. Bartkovitz, F. Podlaski, and C. Janson. Discovery of rg7388, a potent and selective p53-mdm2 inhibitor in clinical development. *Journal of Medicinal Chemistry*, 56(14):5979–5983, 2013.

[93] Z. Zhang, Q. Ding, J.-J. Liu, J. Zhang, N. Jiang, X.-J. Chu, D. Bartkovitz, K.-C. Luk, C. Janson, and C. Tovar. Discovery of potent and selective spiroindolinone mdm2 inhibitor, ro8994, for cancer therapy. *Bioorganic & Medicinal Chemistry*, 22(15):4001–4009, 2014.

[94] Y. Rew, D. Sun, F. Gonzalez-Lopez De Turiso, M. D. Bartberger, H. P. Beck, J. Canon, A. Chen, D. Chow, J. Deignan, and B.M. Fox. Structure-based design of novel inhibitors of the mdm2-p53 interaction. *Journal of Medicinal Chemistry*, 55(11):4936–4954, 2012.

[95] Y. Zhao, A. Aguilar, D. Bernard, and S. Wang. Small-molecule inhibitors of the mdm2p53 proteinprotein interaction (mdm2 inhibitors) in clinical trials for cancer treatment: Miniperspective. *Journal of Medicinal Chemistry*, 58(3):1038–1052, 2015.

[96] Brian S Lucas, Benjamin Fisher, Lawrence R McGee, Steven H Olson, Julio C Medina, and Eugene Cheung. An expeditious synthesis of the mdm2–p53 inhibitor am-8553. *Journal of the American Chemical Society*, 134(30):12855–12860, 2012.

[97] N. Issaeva, P. Bozko, M. Enge, M. Protopopova, L. G. G. C. Verhoef, M. Masucci, A. Pramanik, and G. Selivanova. Small molecule RITA Binds to p53, Blocks p53HDM2 Interaction and Activates p53 Function in Tumors. *Nature Medicine*, 10:1321–1328, 2004.

[98] K. L. Malloy, H. Choi, C. Fiorilla, F. A. Valeriote, T. Matainaho, and W. H. Gerwick. Hoiamide D, a Marine Cyanobacteria-Derived Inhibitor of p53/MDM2 Interaction. *Bioorganic & Medicinal Chemistry Letters*, 22(1):683–688.

[99] A. Vaupel, G. Bold, A. De Pover, T. Stachyra-Valat, J. Hergovich-Lisztwan, J. Kallen, K. Masuya, and P. Furet. Tetra-substituted imidazoles as a new class of inhibitors of the p53-mdm2 interaction. *Bioorganic & Medicinal Chemistry Letters*, 24(9):2110–2114, 2014.

[100] I. R. Hardcastle, S. U. Ahmed, H. Atkins, H. A. Calvert, N. J. Curtin, G. Farnie, B. T. Golding, R. J. Griffin, S. Guyenne, and C. Hutton. Isoindolinone-based inhibitors of the mdm2-p53 protein-protein interaction. *Bioorganic & Medicinal Chemistry Letters*, 15(5):1515–1520, 2005.

[101] B. L. Grasberger, T. Lu, C. Schubert, D. J. Parks, T. E. Carver, H. K. Koblish, M. D. Cummings, L. V. LaFrance, K. L. Milkiewicz, and R. R. Calvo. Discovery and cocrystal structure of benzodiazepinedione hdm2 antagonists that activate p53 in cells. *Journal of Medicinal Chemistry*, 48(4):909–912, 2005.

[102] H. K. Koblish, S. Zhao, C. F. Franks, R. R. Donatelli, R. M. Tominovich, L. V. LaFrance, K. A. Leonard, J. M. Gushue, D. J. Parks, and R. R. Calvo. Benzodiazepinedione inhibitors of the hdm2:p53 complex suppress human tumor cell proliferation in vitro and sensitize tumors to doxorubicin in vivo. *Molecular Cancer Therapeutics*, 5(1):160–169, 2006.

[103] D. J Parks, L. V. LaFrance, R. R. Calvo, K. L. Milkiewicz, V. Gupta, J. Lattanze, K. Ramachandren, T. E. Carver, E. C. Petrella, and M. D. Cummings. 1, 4-benzodiazepine-2, 5-diones as small molecule antagonists of the hdm2-p53 interaction: Discovery and sar. *Bioorganic & Medicinal Chemistry Letters*, 15(3):765–770, 2005.

[104] S. V. Ryabukhin, D. M. Panov, D. S. Granat, E. N. Ostapchuk, D. V. Kryvoruchko, and O. O. Grygorenko. Toward lead-oriented synthesis: One-pot version of castagnoli condensation with nonactivated alicyclic anhydrides. *ACS Combinatorial Science*, 16(3):146–153, 2014.

[105] M. Leão, S. Gomes, J. Pedraza-Chaverri, N. Machado, E. Sousa, M. Pinto, A. Inga, C. Pereira, and L. Saraiva. α-mangostin and gambogic acid as potential inhibitors of the p53–mdm2 interaction revealed by a yeast approach. *Journal of Natural Products*, 76(4):774–778, 2013.

[106] C. A. Sasiela, D. H. Stewart, J. Kitagaki, Y. J. Safiran, Y. Yang, A. M. Weissman, P. Oberoi, I. V. Davydov, E. Goncharova, J. A. Beutler, J. B. Mcmahon, and B. R. O'Keefe. Identification of Inhibitors for MDM2 Ubiquitin Ligase Activity from Natural Product Extracts by a Novel High-Throughput Electrochemiluminescent Screen. *Journal of Biomolecular Screening*, 13:229–237, 2008.

[107] Pascal Furet, Patrick Chène, Alain De Pover, Thérèse Stachyra Valat, Joanna Hergovich Lisztwan, Joerg Kallen, and Keiichi Masuya. The central valine concept provides an entry in a new class of non peptide inhibitors of the p53–mdm2 interaction. *Bioorganic & Medicinal Chemistry Letters*, 22(10):3498–3502, 2012.

[108] Anna L Bowman, Zaneta Nikolovska-Coleska, Haizhen Zhong, Shaomeng Wang, and Heather A Carlson. Small molecule inhibitors of the mdm2-p53 interaction discovered by ensemble-based receptor models. *Journal of the American Chemical Society*, 129(42):12809–12814, 2007.

[109] Tony Pawson and Piers Nash. Protein–protein interactions define specificity in signal transduction. *Genes & development*, 14(9):1027–1047, 2000.

[110] C. Garcia-Echeverria, P. Chène, M. J. J. Blommers, and P. Furet. Discovery of potent antagonists of the interaction between human double minute 2 and tumor suppressor p53. *Journal of Medicinal Chemistry*, 43(17):3205–3208, 2000.

[111] G. Flouret, T. Majewski, W. Brieher, and L. Wilson Jr. Systematic substitution of an oxytocin antagonist with d-amino acids; unexpected high antagonistic potency of the d-cys6-substituted analog. *Journal of Medicinal Chemistry*, 36(6):747–749, 1993.

[112] B. Hu, D. M. Gilkes, and J. Chen. Efficient p53 Activation and Apoptosis by Simultaneous Disruption of Binding to MDM2 and MDMX. *Cancer Research*, 67(18):8810–8817, 2007.

[113] J. A. Kritzer, J. D. Lear, M. E. Hodsdon, and A. Schepartz. Helical β-Peptide Inhibitors of the p53-hDM2 Interaction. *Journal of the American Chemical Society*, 126:9468–9469, 2004.

[114] Y.-W. Kim, T. N. Grossmann, and G. L. Verdine. Synthesis of all-hydrocarbon stapled α-helical peptides by ring-closing olefin metathesis. *Nature Protocols*, 6(6):761–771, 2011.

[115] F. Bernal, M. Wade, M. Godes, T. N. Davis, D. G. Whitehead, A. L. Kung, G. M. Wahl, and L. D. Walensky. A stapled p53 helix overcomes hdmx-mediated suppression of p53. *Cancer Cell*, 18(5):411–422, 2010.

[116] A. F. Bernal, F.and Tyler, S. J. Korsmeyer, L. D. Walensky, and G. L. Verdine. Reactivation of the p53 tumor suppressor pathway by a stapled p53 peptide. *Journal of the American Chemical Society*, 129(9):2456–2457, 2007.

[117] L. Chen, H. Yin, B. Farooqi, S. Sebti, A. D. Hamilton, and J. Chen. p53 α-helix mimetics antagonize p53/mdm2 interaction and activate p53. *Molecular Cancer Therapeutics*, 4(6):1019–1025, 2005.

[118] S. J. Duncan, S. Grüschow, D. H. Williams, C. McNicholas, R. Purewal, M. Hajek, M. Gerlitz, S. Martin, S. K. Wrigley, and M. Moore. Isolation and Structure Elucidation of Chlorofusin, a Novel p53-MDM2 Antagonist from a Fusarium sp. *Journal of The American Chemical Society*, 123:554–560, 2001.

[119] S. J. Duncan, M. A. Cooper, and D. H. Williams. Binding of an Inhibitor of the p53/MDM2 Interaction to MDM2. *Chemical Communications*, pages 316–317, 2003.

[120] S. Y. Lee and D. L. Boger. Synthesis of the Chlorofusin Cyclic Peptide. *Tetrahedron*, 65:3281–3284, 2009.

[121] P. Desai, S. S. Pfeiffer, and D. L. Boger. Synthesis of the Chlorofusin Cyclic Peptide: Assignment of the Asparagine Stereochemistry. *Organic Letters*, 5:5047–5050, 2003.

[122] W.-J. Qian, W.-G. Wei, Y.-X. Zhang, and Z.-J. Yao. Total Synthesis, Assignment of Absolute Stereochemistry, and Structural Revision of Chlorofusin. *Journal of The American Chemical Society*, 129:6400–6401, 2007.

[123] S. Y. Lee, R. C. Clark, and D. L. Boger. Total Synthesis, Stereochemical Reassignment, and Absolute Configuration of Chlorofusin. *Journal of The American Chemical Society*, 129:9860–9861, 2007.

[124] U. Rothweiler, A. Czarna, M. Krajewski, J. Ciombor, C. Kalinski, V. Khazak, G. Ross, N. Skobeleva, L. Weber, and T. A. Holak. Isoquinolin-1-one inhibitors of the mdm2-p53 interaction. *ChemMedChem*, 3(7):1118–1128, 2008.

[125] M. Cushman and N. Castagnoli Jr. The condensation of succinic anhydrides with schiff bases. scope and mechanism. *The Journal of Organic Chemistry*, 36(22):3404–3411, 1971.

[126] M. Cushman and N. Castagnoli Jr. Synthesis of pharmacologically active nitrogen analogs of the tetrahydrocannabinols. *The Journal of Organic Chemistry*, 39(11):1546–1550, 1974.

[127] D. Strumberg, Y. Pommier, K. Paull, M. Jayaraman, P. Nagafuji, and M. Cushman. Synthesis of cytotoxic indenoisoquinoline topoisomerase i poisons. *Journal of Medicinal Chemistry*, 42(3):446–457, 1999.

[128] M. Cushman and W. C. Wong. Total synthesis of (+/-)-corydalic acid methyl ester. *The Journal of Organic Chemistry*, 49(7):1278–1280, 1984.

[129] M. Cushman and N. Castagnoli Jr. Synthesis of trans-3'-methylnicotine. *The Journal of Organic Chemistry*, 37(8):1268–1271, 1972.

[130] M. M. D. Cominetti, S. A. Goffin, K. D. Raffel, E.and Turner, J. C. Ramoutar, M. A. OConnell, L. A. Howell, and M. Searcey. Identification of a new p53/mdm2 inhibitor motif inspired by studies of chlorofusin. *Bioorganic & Medicinal Chemistry Letters*, 2015.

[131] V. T. Kamble, V. S. Jamode, N. S. Joshi, A. V. Biradar, and R. Y. Deshmukh. An efficient method for the synthesis of acylals from aldehydes using silica-supported perchloric acid ($hclo_4$-sio_2). *Tetrahedron Letters*, 47(31):5573–5576, 2006.

[132] Y. Huang, S. Wolf, D. Koes, G. M. Popowicz, C. J. Camacho, T. A. Holak, and A. Dömling. Exhaustive fluorine scanning toward potent p53-mdm2 antagonists. *ChemMedChem*, 7(1):49–52, 2012.

[133] S. Wang, Y. Zhao, D. Bernard, A. Aguilar, and S. Kumar. Targeting the mdm2-p53 protein-protein interaction for new cancer therapeutics. In *Protein-Protein Interactions*, pages 57–79. Springer, 2012.

[134] C. A. G. Haasnoot, F. A. A. M. de Leeuw, and C. Altona. The relationship between proton-proton nmr coupling constants and substituent electronegativitiesi: an empirical generalization of the karplus equation. *Tetrahedron*, 36(19):2783–2792, 1980.

[135] J. C. Owicki. Fluorescence polarization and anisotropy in high throughput screening: Perspectives and primer. *Journal of Biomolecular Screening*, 5(5):297–306, 2000.

[136] A. Czarna, G. M. Popowicz, A. Pecak, S. Wolf, G. Dubin, and T. A. Holak. High affinity interaction of the p53 peptide-analogue with human mdm2 and mdmx. *Cell Cycle*, 8(8):1176–1184, 2009.

[137] R. B. Merrifield. Solid phase peptide synthesis. i. the synthesis of a tetrapeptide. *Journal of the American Chemical Society*, 85(14):2149–2154, 1963.

[138] W. C. Chan and P. D. White. *Fmoc Solid Phase Peptide Synthesis: A Practical Approach*, volume 222. Oxford University Press, 1999.

[139] E. Kaiser, R. L. Colescott, C. D. Bossinger, and P. I. Cook. Color test for detection of free terminal amino groups in the solid-phase synthesis of peptides. *Analytical Biochemistry*, 34(2):595–598, 1970.

[140] M. Friedman. Applications of the ninhydrin reaction for analysis of amino acids, peptides, and proteins to agricultural and biomedical sciences. *Journal of Agricultural and Food Chemistry*, 52(3):385–406, 2004.

[141] J.-H. Zhang, T. D. Y. Chung, and K. R. Oldenburg. A simple statistical parameter for use in evaluation and validation of high throughput screening assays. *Journal of Biomolecular Screening*, 4(2):67–73, 1999.

[142] P. Restorp, O. B. Berryman, A. C. Sather, D. Ajami, and J. Rebek Jr. A synthetic receptor for hydrogen-bonding to fluorines of trifluoroborates. *Chemical Communications*, pages 5692–5694, 2009.

[143] C. A. Lepre, J. M. Moore, and J. W. Peng. Theory and applications of nmr-based screening in pharmaceutical research. *Chemical Reviews*, 104(8):3641–3676, 2004.

[144] VV Krishnan. Ligand screening by saturation-transfer difference (std) nmr spectroscopy. *Current Analytical Chemistry*, 1(3):307–320, 2005.

[145] M. Mayer and B. Meyer. Characterization of ligand binding by saturation transfer difference nmr spectroscopy. *Angewandte Chemie International Edition*, 38(12):1784–1788, 1999.

[146] J. L. Wagstaff, S. L. Taylor, and M. J. Howard. Recent developments and applications of saturation transfer difference nuclear magnetic resonance (std nmr) spectroscopy. *Molecular BioSystems*, 9:571–577, 2013.

[147] A. Viegas, J. Manso, F. L. Nobrega, and E. J. Cabrita. Saturation-transfer difference (std) nmr: a simple and fast method for ligand screening and characterization of protein binding. *Journal of Chemical Education*, 88(7):990–994, 2011.

[148] Frances C Bernstein, Thomas F Koetzle, Graheme JB Williams, Edgar F Meyer, Michael D Brice, John R Rodgers, Olga Kennard, Takehiko Shimanouchi, and Mitsuo Tasumi. The protein data bank: A computer-based archival file for macromolecular structures. *Archives of Biochemistry and Biophysics*, 185(2):584–591, 1978.

[149] Alexander D MacKerell, Donald Bashford, MLDR Bellott, RL Dunbrack, JD Evanseck, Martin J Field, Stefan Fischer, Jiali Gao, H Guo, S a Ha, et al. All-atom empirical potential for molecular modelling and dynamics studies of proteins. *The Journal of Physical Chemistry B*, 102(18):3586–3616, 1998.

[150] K. Khoury, G. M. Popowicz, T. A. Holak, and A. Dömling. The p53-mdm2/mdmx axis–a chemotype perspective. *MedChemComm*, 2(4):246–260, 2011.

[151] M. Cushman and N. Castagnoli Jr. Novel approach to the synthesis of nitrogen analogs of the tetrahydrocannabinols. *The Journal of Organic Chemistry*, 38(3):440–448, 1973.

[152] R. C. Clark, S. Y. Lee, I. Hwang, M. Searcey, and D. L. Boger. Evaluation of chlorofusin, its seven chromophore diastereomers, and key analogues. *Tetrahedron Letters*, 50(26):3151–3153, 2009.

[153] R. J. Steel. *Targeting The Nrf2/Keap1 Interaction*. PhD thesis, University of East Anglia, Norwich Research Park, August 2015.

[154] J. S. Richardson. *The Anatomy and Taxonomy of Protein Structure*, volume 34. Academic Press, 1981.

[155] A. Isidro-Llobet, M. Alvarez, and F. Albericio. Amino acid-protecting groups. *Chemical Reviews*, 109(6):2455–2504, 2009.

[156] H. C. Kolb, M. G. Finn, and K. B. Sharpless. Click chemistry: Diverse chemical function from a few good reactions. *Angewandte Chemie International Edition*, 40(11):2004–2021, 2001.

[157] L. S. Campbell-Verduyn, W. Szymański, C. P. Postema, R. A. Dierckx, P. H. Elsinga, D. B. Janssen, and B. L. Feringa. One pot click reactions: Tandem enantioselective biocatalytic epoxide ring opening and [3 + 2] azide alkyne cycloaddition. *Chemical Communications*, 46(6):898–900, 2010.

[158] R. Franke, C. Doll, and J. Eichler. Peptide ligation through click chemistry for the generation of assembled and scaffolded peptides. *Tetrahedron Letters*, 46(26):4479–4482, 2005.

[159] S. Ulrich, D. Boturyn, A. Marra, O. Renaudet, and P. Dumy. Oxime ligation: A chemoselective click-type reaction for accessing multifunctional biomolecular constructs. *Chemistry-A European Journal*, 20(1):34–41, 2014.

[160] G. N. Grover, J. Lam, T. H. Nguyen, T. Segura, and H. D. Maynard. Biocompatible hydrogels by oxime click chemistry. *Biomacromolecules*, 13(10):3013–3017, 2012.

[161] A. Dondoni. The emergence of thiol-ene coupling as a click process for materials and bioorganic chemistry. *Angewandte Chemie International Edition*, 47(47):8995–8997, 2008.

[162] J. A. Johnson, M. G. Finn, J. T. Koberstein, and N. J. Turro. Construction of linear polymers, dendrimers, networks, and other polymeric architectures by copper-catalyzed azide-alkyne cycloaddition click chemistry. *Macromolecular Rapid Communications*, 29(12-13):1052–1072, 2008.

[163] G. C. Tron, T. Pirali, R. A. Billington, P. L. Canonico, G. Sorba, and A. A. Genazzani. Click chemistry reactions in medicinal chemistry: Applications of the 1, 3-dipolar cycloaddition between azides and alkynes. *Medicinal Research Reviews*, 28(2):278–308, 2008.

[164] A. Dumont, A. Malleron, M. Awwad, S. Dukan, and B. Vauzeilles. Click-mediated labeling of bacterial membranes through metabolic modification of the lipopolysaccharide inner core. *Angewandte Chemie International Edition*, 51(13):3143–3146, 2012.

[165] J. M. Baskin, J. A. Prescher, S. T. Laughlin, N. J. Agard, P. V. Chang, I. A. Miller, A. Lo, J. A. Codelli, and C. R. Bertozzi. Copper-free click chemistry for dynamic in vivo imaging. *Proceedings of the National Academy of Sciences*, 104(43):16793–16797, 2007.

[166] V. Hong, N. F. Steinmetz, M. Manchester, and M. G. Finn. Labeling live cells by copper-catalyzed alkyne- azide click chemistry. *Bioconjugate chemistry*, 21(10):1912–1916, 2010.

[167] Y. H. Lau, Y. Wu, P. de Andrade, W. R. J. D. Galloway, and D. R. Spring. A two-component'double-click'approach to peptide stapling. *Nature Protocols*, 10(4):585–594, 2015.

[168] Y. H. Lau, P. de Andrade, N. Sköld, G. J. McKenzie, A. R. Venkitaraman, C. Verma, D. P. Lane, and D. R. Spring. Investigating peptide sequence variations for double-click stapled p53 peptides. *Organic & Biomolecular Chemistry*, 12(24):4074–4077, 2014.

[169] L. K. Rasmussen, B. C. Boren, and V. V. Fokin. Ruthenium-catalyzed cycloaddition of aryl azides and alkynes. *Organic Letters*, 9(26):5337–5339, 2007.

[170] V. D. Bock, H. Hiemstra, and J. H. Van Maarseveen. Cui-catalyzed alkyne-azide click cycloadditions from a mechanistic and synthetic perspective. *European Journal of Organic Chemistry*, 2006(1):51–68, 2006.

[171] G. R. Abel, B. H. Cao, J. E. Hein, and T. Ye. Covalent, sequence-specific attachment of long dna molecules to a surface using dna-templated click chemistry. *Chemical Communications*, 50:8131–8133, 2014.

[172] D. T. S. Rijkers, H. H. R. van Vugt, H. J. F. Jacobs, and R. M. J. Liskamp. A convenient synthesis of azido peptides by post-assembly diazo transfer on the solid phase applicable to large peptides. *Tetrahedron Letters*, 43(20):3657–3660, 2002.

[173] Jeffrey Zaloom and David C Roberts. Preparation of azido derivatives from amino acids and peptides by diazo transfer. *The Journal of Organic Chemistry*, 46(25):5173–5176, 1981.

[174] S.-H. Hwang, M. A. Blaskovich, and H.-O. Kim. A convenient reduction of α-amino acids to 1, 2-amino alcohols with retention of optical purity. *Open Organic Chemistry Journal*, 2:107–109, 2008.

[175] Charles J M Stirling. Leaving groups and nucleofugality in elimination and other organic reactions. *Accounts of Chemical Research*, 12(6):198–203, 1979.

[176] G. A. Olah, S. C. Narang, B. G. B. Gupta, and R. Malhotra. Synthetic methods and reactions. 62. transformations with chlorotrimethylsilane/sodium iodide, a convenient in situ iodotrimethylsilane reagent. *The Journal of Organic Chemistry*, 44(8):1247–1251, 1979.

[177] J.-M. Gao, S.-X. Yang, and J.-C. Qin. Azaphilones: Chemistry and biology. *Chemical Reviews*, 113(7):4755–4811, 2013.

[178] I. R. Hardcastle, S. U. Ahmed, H. Atkins, G. Farnie, B. T. Golding, R. J. Griffin, S. Guyenne, C. Hutton, P. Källblad, and S. J. Kemp. Small-molecule inhibitors of the mdm2-p53 protein-protein interaction based on an isoindolinone scaffold. *Journal of Medicinal Chemistry*, 49(21):6209–6221, 2006.

[179] A. R. Germain, D. M. Bruggemeyer, J. Zhu, C. Genet, P. O'Brien, and J. A. Porco Jr. Synthesis of the azaphilones (+)-sclerotiorin and (+)-8-o-methylsclerotiorinamine utilizing (+)-sparteine surrogates in copper-mediated oxidative dearomatization. *The Journal of Organic Chemistry*, 76(8):2577–2584, 2011.

[180] M. J. Dearden, C. R. Firkin, J.-P. R. Hermet, and P. O'Brien. A readily-accessible (+)-sparteine surrogate. *Journal of the American Chemical Society*, 124(40):11870–11871, 2002.

[181] A. D. Somoza, K.-H. Lee, Y.-M. Chiang, B. R. Oakley, and C. C. C. Wang. Reengineering an azaphilone biosynthesis pathway in *aspergillus nidulans* to create lipoxygenase inhibitors. *Organic Letters*, 14(4):972–975, 2012.

[182] J. Zhu, A. R. Germain, and J. A. Porco. Synthesis of azaphilones and related molecules by employing cycloisomerization of o-alkynylbenzaldehydes. *Angewandte Chemie*, 116(10):1259–1263, 2004.

[183] F. Brucelle and P. Renaud. Synthesis of a leucomitosane via a diastereoselective radical cascade. *The Journal of Organic Chemistry*, 78(12):6245–6252, 2013.

[184] Z. Wang. *Menke Nitration*. John Wiley & Sons, Inc., 2010.

[185] H. G. O. Becker, W. Berger, G. Domschke, E. Fanghänel, J. Faust, M. Fischer, F. Gentz, K. Gewald, R. Gluch, and R. Mayer. Organikum-organisch-chemisches praktikum. *ChemInform*, 24(40), 1993.

[186] N. Miyaura and S. L. Buchwald. *Cross-Coupling Reactions: a Practical Guide*, volume 219. Springer Science & Business Media, 2002.

[187] K. Sonogashira, Y. Tohda, and N. Hagihara. A convenient synthesis of acetylenes: Catalytic substitutions of acetylenic hydrogen with bromoalkenes, iodoarenes and bromopyridines. *Tetrahedron Letters*, 16(50):4467–4470, 1975.

[188] QIAGEN Technical Services. Qiaprep miniprep handbook. In QIAGEN Technical Services, editor, *Sample and Assay Technologies (2nd edition)*. QIAGEN, Sample and Assay Technologies, 2012.

[189] Thermo Scientific. Nanodrop 1000 spectrophotometer users manual v 3.8. In Thermo Scientific Technical Resources, editor, *Thermo Scientific Technical Resources*. Thermo Scientific, Thermo Fisher, 2010.